MINIMIZATION OF NO EMISSIONS FROM MULTI-BURNER COAL-FIRED BOILERS

Final Report

For the Period:
October 1, 1997 – September 30, 2001

E.G. Eddings, A. Molina, D. W. Pershing, A. F. Sarofim
Dept. of Chemical and Fuels Engineering, University of Utah

T. H. Fletcher, H. Zhang
Dept. of Chemical Engineering, Brigham Young University

K. A. Davis, M. Denison, H. Shim
Reaction Engineering International

January 2002

U.S. Dept. of Energy Grant No. DE-FG26-97FT97275

University of Utah
Department of Chemical and Fuels Engineering
1495 East 100 South, 109 KENN B
Salt Lake City, Utah 84112-1114

Brigham Young University
Department of Chemical Engineering
350 CB
Provo, Utah 84602

Reaction Engineering International
77 West 200 South, Suite 210
Salt Lake City, Utah 84101

DISCLAIMER

ABSTRACT

The focus of this program is to provide insight into the formation and minimization of NOx in multi-burner arrays, such as those that would be found in a typical utility boiler. Most detailed studies are performed in single-burner test facilities, and may not capture significant burner-to-burner interactions that could influence NOx emissions. Thus, investigations of such interactions were made by performing a combination of single and multiple burner experiments in a pilot-scale coal-fired test facility at the University of Utah, and by the use of computational combustion simulations to evaluate full-scale utility boilers. In addition, fundamental studies on nitrogen release from coal were performed to develop greater understanding of the physical processes that control NO formation in pulverized coal flames - particularly under low NOx conditions.

A $CO/H_2/O_2/N_2$ flame was operated under fuel-rich conditions in a flat flame reactor to provide a high temperature, oxygen-free post-flame environment to study secondary reactions of coal volatiles. Effects of temperature, residence time and coal rank on nitrogen evolution and soot formation were examined. . Elemental compositions of the char, tar and soot were determined by elemental analysis, gas species distributions were determined using FTIR, and the chemical structure of the tar and soot was analyzed by solid-state ^{13}C NMR spectroscopy.

A laminar flow drop tube furnace was used to study char nitrogen conversion to NO. The experimental evidence and simulation results indicated that some of the nitrogen present in the char is converted to nitric oxide after direct attack of oxygen on the particle, while another portion of the nitrogen, present in more labile functionalities, is released as HCN and further reacts in the bulk gas. The reaction of HCN with NO in the bulk gas has a strong influence on the overall conversion of char-nitrogen to nitric oxide; therefore, any model that aims to predict the conversion of char-nitrogen to nitric oxide should allow for the conversion of char-nitrogen to HCN. The extent of the HCN conversion to NO or N_2 will depend on the composition of the atmosphere surrounding

the particle.

A pilot-scale testing campaign was carried out to evaluate the impact of multiburner firing on NOx emissions using a three-burner vertical array. In general, the results indicated that multiburner firing yielded higher NOx emissions than single burner firing at the same fuel rate and excess air. Mismatched burner operation, due to increases in the firing rate of the middle burner, generally demonstrated an increase in NOx over uniform firing. Biased firing, operating the middle burner fuel rich with the upper and lower burners fuel lean, demonstrated an overall reduction in NOx emissions; particularly when the middle burner was operated highly fuel rich.

Computational modeling indicated that operating the three burner array with the center burner swirl in a direction opposite to the other two resulted in a slight reduction in NOx.

TABLE OF CONTENTS

EXECUTIVE SUMMARY

INTRODUCTION

The focus of this program is to provide insight into the formation and minimization of NOx in multi-burner arrays, such as those that would be found in a typical utility boiler. Most detailed studies are performed in single-burner test facilities, and may not capture significant burner-to-burner interactions that could influence NOx emissions. Thus, investigations of such interactions were made by performing a combination of single and multiple burner experiments in a pilot-scale coal-fired test facility at the University of Utah, and by the use of computational combustion simulations to evaluate full-scale utility boilers. In addition, fundamental studies on nitrogen release from coal were performed to develop greater understanding of the physical processes that control NO formation in pulverized coal flames - particularly under low NOx conditions.

The following summarizes efforts and results obtained from four different aspects of this program. The first two sections describe the results of fundamental studies on nitrogen release during secondary pyrolysis and during char oxidation. The next section describes results of pilot-scale studies of multiburner arrays. The final section discusses computational modeling efforts including the incorporation of two fundamental submodels and simulations of the pilot-scale facility.

NITROGEN EVOLUTION DURING SECONDARY PYROLYSIS

Economical NO_x control techniques used in pulverized coal furnaces, such as air/fuel staging, promote secondary reactions of the primary coal volatiles. Secondary reactions significantly influence the nitrogen transformations among different combustion products and the ultimate NO_x production. The major objectives of this study were to investigate the nitrogen evolution and soot formation mechanisms at high temperature, high heating rate conditions.

A $CO/H_2/O_2/N_2$ flame was operated under fuel-rich conditions in a flat flame reactor to provide a high temperature, oxygen-free post-flame environment to study secondary reactions of coal volatiles. Effects of temperature, residence time and coal rank on nitrogen evolution and soot formation were examined. Elemental compositions of the char, tar and soot were determined by elemental analysis, gas species distributions were determined using FTIR, and the chemical structure of the tar and soot was analyzed by solid-state ^{13}C NMR spectroscopy.

Both temperature and residence time have a significant impact on the secondary reactions of tar. Coal-derived soot exhibited loss of aliphatic side chains and oxygen functional groups prior to significant growth in average aromatic ring size. Polymerization reactions accelerated at temperatures above 1400 K, leading to a larger and more interconnected cluster.

Experiments were performed on the model compounds of biphenyl and pyrene to study soot formation mechanisms for aromatic hydrocarbons. Ring opening reactions were shown to constitute the first step in the soot formation process for biphenyl, followed by ring size growth and cluster crosslinking. Little evidence of ring opening reactions was observed during the pyrolysis of pyrene. A simple model was devised to describe the secondary reactions of coal volatiles based on the chemical structure analysis.

During secondary pyrolysis, an enrichment of nitrogen in tar was first observed, followed by a subsequent fast nitrogen release, finally decreasing at a much slower rate at high temperatures. The decay of the nitrogen functionalities in the tar is similar for all the coals in this study, indicating that reactivity of the tar nitrogen functionalities show very little rank dependence. As pyrolysis proceeded, the clusters in soot became larger and more interconnected, which retarded the further release of nitrogen. Some types of quaternary nitrogen are thought to be responsible for the earlier release of NH_3 than HCN at low temperatures. However, additional NH_3 can be formed through the interactions of

HCN and other oxygen radicals in the gas phase or on a specific surface.

EVOLUTION OF NITROGEN DURING CHAR OXIDATION

Although much of the nitrogen present in coal evolves during devolatilization, a significant fraction is also released during the process of char oxidation, with some of that nitrogen being converted to nitrogen oxides. A detailed study of the mechanisms by which this process occurs was carried out under this program, and the study was comprised of several components.

In the first component, an experimental study was performed in order to evaluate the rate of nitric oxide reduction on the char surface, as shown in the following reaction:

$$C + NO \rightarrow \tfrac{1}{2} N_2 + CO \qquad \text{R-1}$$

Although this reaction has been subject of numerous studies, it has been found that most of the rate expressions reported in the literature tend to underestimate the amount of nitric oxide reduced during char oxidation. Some researchers have therefore proposed alternative values for this rate, considerably higher than ones reported previously. In contrast to these results, the experimental data obtained in this study show that the rate of nitric oxide reduction on the char surface is predicted within one order of magnitude by the values traditionally reported in the literature. There are, however, two processes that increase the rate of nitric oxide reduction on the char surface: 1) the reaction of HCN (formed from secondary devolatilization) with nitric oxide; and 2) the accumulation of nitrogen-containing surface complexes on the char surface at the beginning of the char-nitric oxide reaction. The first process is related to the conversion of volatile-nitrogen to nitric oxide and therefore should not affect the conversion of char-nitrogen to nitric oxide. The second one was found to be important only in the temperature range of

fluidized bed combustion (1123 – 1323 K), and thus has lesser influence on pulverized coal combustion.

The second part of the study tried to explain a steep reduction in the conversion of char-nitrogen to nitric oxide as the concentration of nitric oxide in the background is increased. This trend was observed in experiments conducted for three different fuels: coal; char previously produced under pulverized combustion conditions; and an activated carbon. The effect was more pronounced at a concentration of 4% O_2 than at 20% and was almost insensitive to variations in particle size.

The development of a mathematical model that used a traditional value for R-1 correctly predicted the trend of reduction in the conversion of char-nitrogen to nitric oxide as the nitric background concentration increased. However, it overestimates its magnitude, particularly for chars with low surface area. If the rate for R 1 is increased by two orders of magnitudes, the predicted value for the conversion of char-nitrogen to nitric oxide is close to the experimental results.

The detection of HCN during the process of char oxidation, particularly as the sample size increased, suggested that the homogeneous reaction of HCN and NO is an alternative route for the destruction of nitric oxide. An alternative model that considered homogeneous reactions in the boundary layer and in the bulk showed that the homogeneous reactions of HCN with the NO present in the background can explain the reduction in the conversion of char-nitrogen to nitric oxide as the background nitric oxide concentration is increased; in particular for the coal char. For the activated carbon with low nitrogen content and high surface area, the heterogeneous process can be dominant, but for the other chars the influence of the homogeneous reactions in the bulk is significant.

The experimental evidence and simulation results show that some of the nitrogen present in the char is converted to nitric oxide after direct attack of oxygen on the particle, while another fraction of nitrogen, present in more labile functionalities, is

released as HCN and further reacts in the bulk gas. The reaction of HCN with NO in the bulk gas has a strong influence on the overall conversion of char-nitrogen to nitric oxide; therefore, any model that aims to predict the conversion of char-nitrogen to nitric oxide should allow for the conversion of char-nitrogen to HCN. The extent of the HCN conversion to NO or N_2 will depend on the composition of the atmosphere surrounding the particle.

PILOT-SCALE STUDIES: MULTIBURNER FIRING OF PULVERIZED COAL

A pilot-scale testing campaign was carried out to evaluate the impact of multiburner firing on NOx emissions. Extensive data had been previously collected using a single pulverized-coal (PC) burner, and this data was thus available for comparison with NOx emissions obtained while firing three burners at the same overall load and operating conditions. A range of operating conditions were explored that were compatible with the single-burner data, and the emission trends as a function of air staging, burner swirl and other parameters were compared. In addition, a number of burner-to-burner operational variations were explored to provide insight on their potential impact on NOx emissions.

In general, the results indicated that multiburner firing yielded higher NOx emissions than single burner firing at the same fuel rate and excess air. At very fuel rich burner stoichiometries (SR < 0.75), the difference between multiple and single burners became indistinguishable. This result is consistent with previous single-burner data that showed that at very rich stoichiometries the NOx emissions became independent of burner settings such as air distributions, velocities and burner swirl.

Comparisons were made exploring a mismatch in individual burner firing rates to identify any positive or negative impact. Two different approaches to firing rate mismatch were used: 1) where individual burner stoichiometries were held constant (changing both coal and air flowrates); and 2) where individual burner stoichiometries were varied (changing coal feedrate only). In both approaches, the center

burner firing rate was increased up to as high as 3X that of baseline, and the upper and lower burner firing rates were decreased to maintain an overall constant firing rate. In general, a 3X increase in firing rate in the center burner resulted in a notable increase in NOx emissions for both staged and unstaged conditions. This effect was observed for both constant and variable burner stoichiometry conditions. Note that a 2X increase in firing rate in the center burner resulted in minimal differences from uniform operation.

Some conditions were identified where NOx emissions could be reduced in a multiburner firing scenario; specifically, through the use of burner biasing. If the middle burner was operated very fuel rich, with the outer burners operated at high excess air levels to compensate, the overall NOx emissions were lower than when all burners were operated with equal air/fuel flow rates. Burner parameters such as swirl had to be optimized, however, to achieve stable operation. This approach yielded NOx emissions that were slightly lower than the single burner data under unstaged conditions; however, the application of such severe biasing should be evaluated in the context of corrosion, deposition, or other potential adverse affects in the near burner region. A commercial application would be likely to demonstrate a greater effectiveness at less severe biasing due to the ability to bias in the direction of gas flow. In other words, a vertical staging effect could be accomplished without the use of overfire air.

COMPUTATIONAL MODELING

A comprehensive combustion code (*GLACIER*) was used to simulate the reacting flow of a pilot scale pulverized coal facility and a 500 MW utility opposed wall fired boiler. In addition, the Chemical Percolation Devolatilization (CPD) model was incorporated into the combustion code, along with a soot formation model.

The pilot scale furnace of the University of Utah, known as the L1500 furnace, was simulated and different burner arrangements were modeled: 1) all three burners rotating clockwise looking from the burners toward the exit; and 2) top and bottom burners rotating clockwise and the center burner rotating counterclockwise looking from the

burners toward the exit. The flames all looked similar with all the burners having equal direction of swirl. Changing the direction of the center burner swirl caused the bottom two flames to move slightly downward. Changing the direction of swirl of the center burner reduced the NOx by about 7.5%. The exit temperature, O_2, and CO where essentially unchanged. This reduction in NOx, though small, is the effect of changes in mixing between the burners. The temperatures, oxygen and NOx were in reasonable agreement with the measured data.

The Chemical Percolation Devolatilization (CPD) Model (Genetti, 1999) was incorporated into *GLACIER* and was used to predict coal particle volatile yields as compared to those of the original two-step devolatilization model in *GLACIER* (Kobayashi et al. 1976) for a simple simulation with Illinois #6 coal. Comparisons of volatile yield predicted by the CPD model and by *GLACIER* indicated that the times for onset of devolatilization and the overall volatile yields predicted by the two models were comparable; however, the initial devolatilization rate predicted by the CPD model is steeper than that predicted by *GLACIER* and the duration of devolatilization is longer.

The soot model for coal-fired system developed by Brown et al. (1998) was implemented into *GLACIER* and applied to the pilot-scale test furnace at the University of Utah Combustion Research Laboratory. The soot model is made of three transport equations for tar mass fraction, soot mass fraction, and the number of soot particles per unit mass. Tar evolution is calculated from the CPD model (Fletcher et al., 1992b). The simulation results illustrated some interesting behavior for the soot formation and oxidation. The model results predicted that tar starts to form due to coal devolatilization close to the burner and at the same location, soot volume fraction and number density increase as tar is being converted to soot. Soot volume fraction then decreases due to oxidation. Soot number density also decreases due to oxidation and agglomeration of soot particles. Upon additional air introduction at the staging port, complete soot oxidation occurs. Additional air input at the staging port completes soot oxidation.

1 NITROGEN EVOLUTION AND SOOT FORMATION DURING SECONDARY COAL PYROLYSIS

1.1 INTRODUCTION

The consumption of coal for power generation is projected to increase steadily into the new century. Coal combustion produces more NO_x per unit of energy than any other major combustion technology (Smoot, 1993). Therefore, pollutant emission associated with coal combustion will have a huge impact on the environment. NO_x (nitrogen oxides), a major pollutant from coal fired furnaces, can cause a variety of environmental and health problems such as stratospheric ozone depletion and urban smog. Consequently, the reduction of NO_x emissions is currently a major topic of coal research.

The major source of NO_x from coal combustion is the nitrogen present in the coal itself, since the production by the thermal mechanism (thermal NO_x) is effectively inhibited by regulating flame temperatures (Niksa, 1994). In commercial pulverized coal furnaces, coal nitrogen is released in three stages, as shown in Figure 1.1.1. Nitrogen is initially liberated with the volatiles during primary devolatilization. Primary devolatilization involves the thermal decomposition of the coal's organic structure and the release of low molecular weight volatiles. These volatiles can be divided into two parts: (a) light gases which *do not condense* at ambient temperature and pressure; and (b) tars which are comprised of relatively heavy, aromatic structures that *do condense* at ambient temperature and pressure. During primary devolatilization, nearly all the volatile-N is released with the tar (Chen and Niksa, 1992a). In the second stage of nitrogen transformation, the volatiles undergo secondary reactions (secondary pyrolysis) in hot, fuel-rich conditions that convert part of the nitrogen in the tar into HCN (Nelson, et al. 1990; Chen, 1991; Ledesma, 1998). Since tar has a strong propensity to form soot at high temperatures and long residence times, some of the nitrogen in the tar will be incorporated into the soot. At the same time, nitrogen trapped in the char, i.e., the organic solid remaining after the initial stage of devolatilization, is expelled by thermal dissociation induced

by higher particle temperatures. In the third stage, oxygen reacts with char, liberating all additional nitrogen by chemical conversion to NO_x (Pershing, 1977). All of the nitrogen released will end up in the combustion products. However, volatile-N, unlike char nitrogen, is amenable to reduction to N_2 through inexpensive techniques such as burner configuration modifications and aerodynamic control, which can reduce NO_x emission by 50-80% (Smoot, 1993).

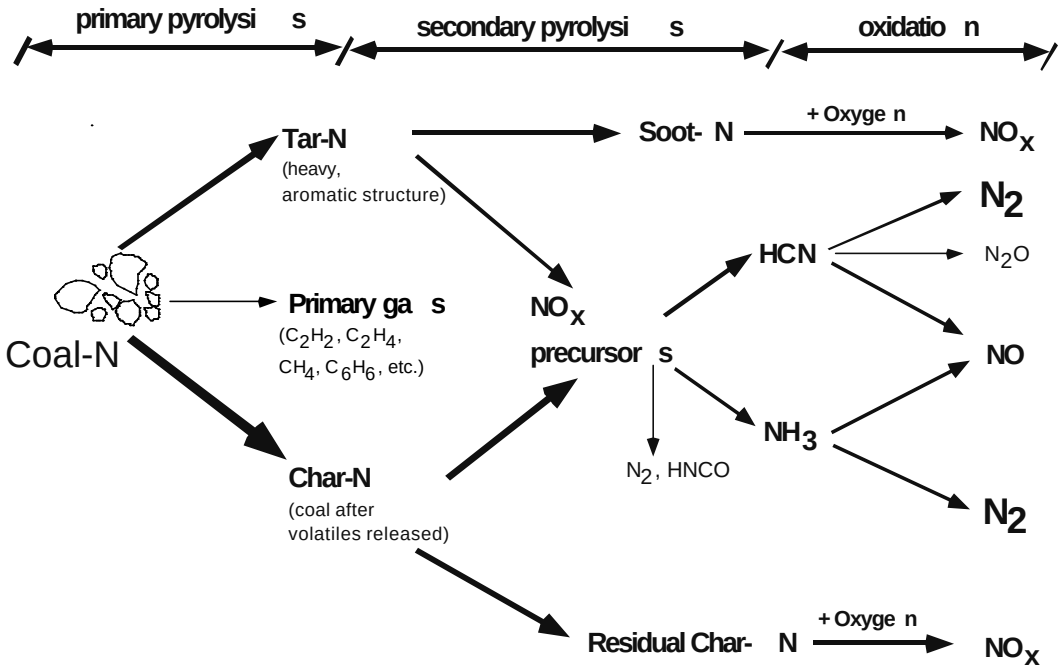

Figure 1.1.1. Three stages of nitrogen release during coal combustion.

The most economical combustion modification to reduce NO_x is air staging. In air staging, the combustion air is distributed at different elevations along the furnace wall to establish alternating fuel-rich and fuel-lean zones (Man, et al. 1998). Air staging promotes the conversion of volatile-N to N_2, hence minimizing NO_x formation by delaying the mixing of the air (oxygen) supply with volatile-N (Van der Lans, et al., 1997). Such delayed mixing therefore gives the primary coal volatiles (tar and light gas) ample time to undergo secondary reactions. Since

aerodynamic control methods such as air staging totally rely on the availability of volatile nitrogen in the gas phase, the incorporation of tar nitrogen into soot has an adverse effect on NO_x reduction. It is clear that secondary pyrolysis significantly influences the ultimate NO_x production in industrial furnaces. Consequently, a detailed investigation into the nitrogen transformations during secondary pyrolysis and the effects of the tar-soot transition on nitrogen release is critical for design and implementation of new pollution control strategies.

Current nitrogen release models, including the CPD model at BYU (Fletcher, et al. 1992c), only simulate the nitrogen release during primary pyrolysis, which occurs at relatively low temperatures (below 1200 K). However, the temperatures in the pyrolysis zones of industrial furnaces are usually much higher (1800 K). The form and partitioning of nitrogen species at high temperatures, after they are released from the char, directly determine the NO_x production in the furnace. This project intends to investigate the nitrogen transformations during secondary pyrolysis and to build a more extensive model that accounts for nitrogen release and transformations at conditions more relevant to industrial furnaces.

1.2 LITERATURE REVIEW

Previous studies on pulverized coal pyrolysis are reviewed here with emphasis on the secondary reactions of coal volatiles, the formation of NO_x precursors in the gas phase, and the effects of secondary reactions on nitrogen transformations.

1.1.1 General Mechanism of Coal Devolatilization

Coal pyrolysis is the first step in coal combustion and gasification. Although coal pyrolysis occurs on a time scale (up to several hundreds milliseconds) much shorter than the subsequent char oxidation process (0.5 to 2 seconds for pulverized coal), it has a huge impact on the overall combustion efficiency and pollutant production in industrial furnaces. Coal pyrolysis has been studied extensively for more than a century. However, no general mechanism is universally accepted, nor can all observations be accounted for by any single model (Chen, 1991). This is probably because of the numerous chemical and transport processes that occur simultaneously in

the coal flame, making them very difficult to distinguish and interpret. In addition, coal pyrolysis is very sensitive to specific properties of coal type, which vary substantially among coal rank. In this section, fundamentals needed to interpret pyrolysis experimental data are reviewed, starting with a brief description of the chemical structure of coal, and followed by a discussion of the sequence in coal pyrolysis. Finally, previous studies on secondary reactions of coal volatiles are reviewed in detail.

1.1.2 Chemical Structure of Coal

Coal is mainly composed of a variety of organic structures. Coal can be viewed as a complex organic polymer consisting of large polycyclic aromatic clusters of several fused rings linked together by assorted hydrocarbon chains and bridges of varying lengths. Modern analytical techniques (NMR, FTIR, etc.) have established four major structures in coal: aromatic clusters; aliphatic bridges and loops; side chains; and oxygen groups (Chen, 1991; Smith, et al. 1994). These structures are shown in Figure 1.2.1.

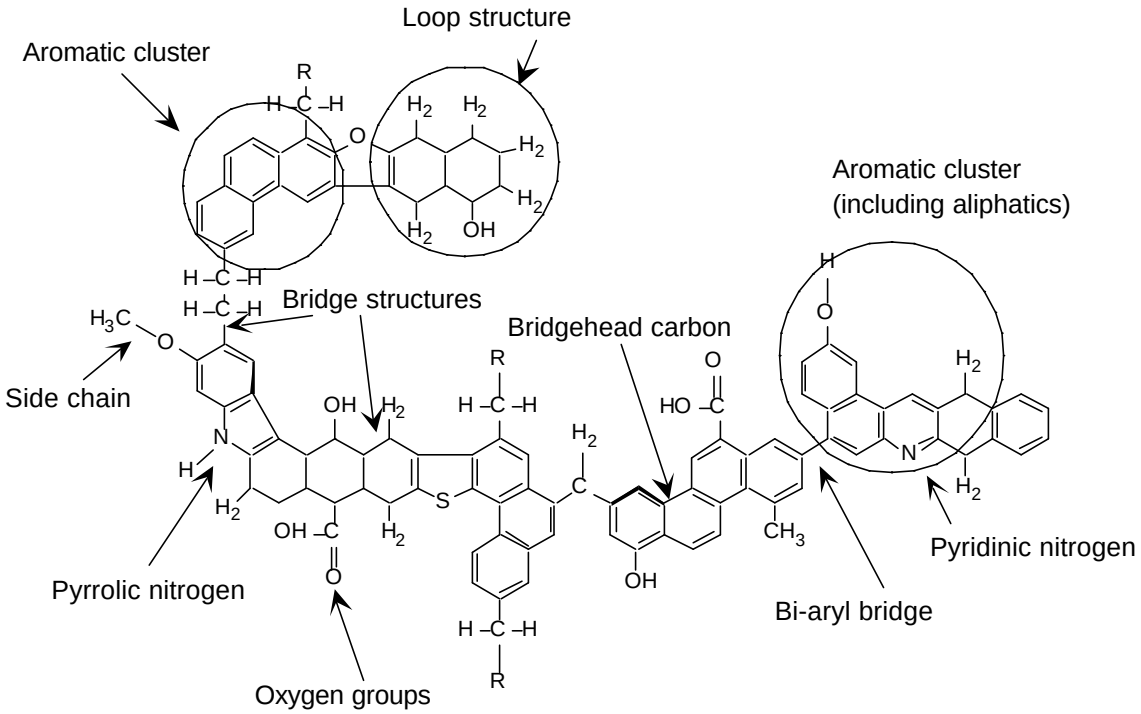

Figure 1.2.1. The structure of a hypothetical coal molecule (adapted from Solomon, et al. 1988).

^{13}C NMR analysis of coals has shown that the majority of the carbon in coal is aromatic (Solum, et al. 1989). The percentage of aromatic carbon (aromaticity) usually increases with coal rank. Aromatic carbons are incorporated into various sizes of condensed rings, ranging from one to three condensed rings for lignites and subbituminous coals to two to four condensed rings for bituminous coals (Pugmire, et al. 1990). There are also aliphatic side chains and oxygen-containing functional groups at the edges of these aromatic clusters. These aromatic clusters are linked together by the aliphatic bridges or ether bridges to make a large three-dimensional macromolecular network.

Other important heteroatoms in coal are sulfur and nitrogen. Those elements generally comprise a small fraction of the organic materials, but they account for almost all the pollutants formed during coal combustion. A detailed description of the nitrogen forms in coal is presented

in a later section.

1.1.3 Coal Pyrolysis

The observed phenomena during coal pyrolysis are not only determined by the chemical structure of the coal, but are also influenced by physical properties (particle size, moisture content) and operating conditions. Nevertheless, three main processes can be identified during coal devolatilization. (1) Upon heating, coal undergoes mild changes, including the disruption of hydrogen bonds, vaporization and release of certain noncovalently bonded molecules, and low temperature crosslinking (large aromatic fragments attaching together) in low rank coals with more than 10% oxygen (Solomon, et al. 1992). These early reactions usually occur at temperatures lower than 500 K, and are generally not very important in the whole pyrolysis process. (2) During primary pyrolysis at higher temperatures (500 K-1000 K), the weak aliphatic bridges connecting large aromatic clusters in the coal matrix are cleaved to produce molecular fragments. Those fragments containing one to several aromatic ring structures will be released as tar if their vapor pressure is sufficiently high to escape the coal matrix. The larger fragments, too large to vaporize, will eventually undergo moderate temperature "crosslinking" reactions to attach to the char. At the same time, release of some of the functional groups attached to the aromatic clusters and some labile bridges leads to the formation of light gases, including CO, CO_2 and light hydrocarbons. (3) Secondary pyrolysis initiates when the tar and certain light gases (such as benzene and acetylene) begin to undergo further reactions in the gas phase. There are ambiguous and contradictory definitions for secondary pyrolysis in the literature (Haussmann and Kruger, 1989; Chen, 1991; Solomon, et al. 1992). In this work, secondary pyrolysis is referred to as any reaction of volatiles after they leave the char particles. Figure 1.2.2 shows the major reaction pathways of coal during pyrolysis.

Tar is the major reactant in secondary reactions, although certain light hydrocarbons are also believed to participate in secondary pyrolysis at high temperatures. At temperatures from about 1000 K to1300 K, functional groups and side-chains attached to the aromatic rings in the tar will thermally decompose to release additional gases, usually comprising CO, CO_2, light

hydrocarbons, H_2 and heteroatom species (HCN, NH_3, SO_2, COS, etc.) (Doolan, et al. 1986; Serio, et al. 1987; Xu and Tomita, 1989; Bassilakis, et al. 1993). At temperatures higher than 1200 K and prolonged residence time, the aromatic rings in the tar will attach together to form larger clusters in a process similar to the crosslinking reactions in the char. The size of the clusters will continue to grow until the identifiable soot nuclei form in the flame. It is the generation of such nuclei from the initial gas-phase reactants that initiates the soot particle inception process. These nuclei will serve as seeds to form large soot particles through process of coagulation, agglomeration, and aggregation (Ma, 1996). The molecular weight of the final soot particles can be as high as several million amu. The hypothetical molecule of the parent coal and the succeeding pyrolysis stages from a molecular point of view are demonstrated in Figure 1.2.2.

1.1.4 Secondary Reactions of Coal Volatiles

As mentioned in the first chapter, secondary reactions play an important role in the overall coal combustion process. However, most of the previous research in the field has been devoted to primary pyrolysis. The limited studies on the secondary reactions of coal volatiles will be reviewed here in two parts: the first part discusses the formation and distribution of various gases from tar cracking reactions; the second part emphasizes soot formation in coal pyrolysis or combustion systems. Although these two parts are reviewed separately here, it should be pointed out that these two processes significantly overlap during secondary pyrolysis. It is believed that soot formation is favored at higher temperatures (Doolan, et al. 1986; Solomon, et al. 1992). The effects of secondary reactions on nitrogen release will be reviewed in the next section.

1.1.4.1 Gas Phase Cracking Reactions

The kinetics of vapor-phase secondary reactions for coal tar were studied by Serio and coworkers (Serio, et al. 1987). Their experiment consisted of two independently-heated tubular chambers connected in series. The first chamber was a fixed-bed reactor used to pyrolyze a Pittsburgh bituminous coal at a low heating rate (3^oC/min) to a maximum temperature of 550^oC.

The freshly generated tar and other volatiles were pyrolyzed in the second chamber at temperatures ranging from 500-900^{o}C and residence times ranging from 0.6-3.9 s. The major products from the tar cracking were light gases (CH_4, C_2H_4, C_2H_2, etc.), light oils and some transformed tar. Higher temperatures promoted higher conversion of the tar vapors in the second reactor. Kinetic parameters for the cracking reactions were reported based on the measured data.

In a similar study, tar was generated by a fluidized-bed flash pyrolyzer from an Australian coal (Doolan, et al. 1986). The tar vapor and other gases were then cracked in two reaction systems, one using tar vapor in tubular quartz reactors at 900-1400 K and residence

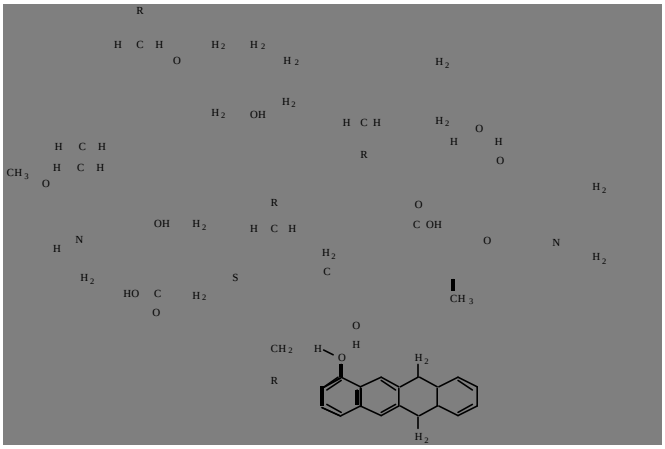

coal

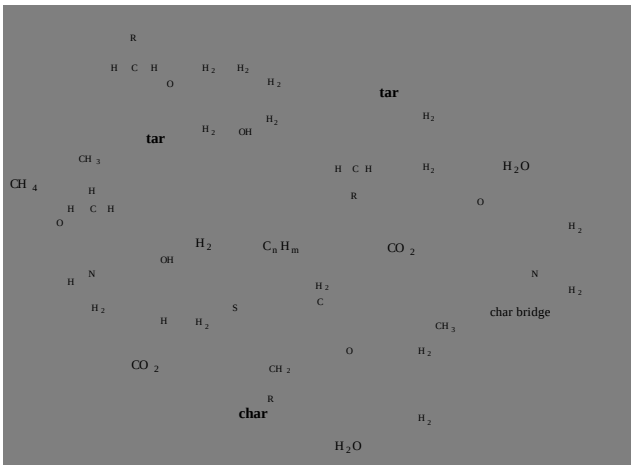

primary pyrolysis

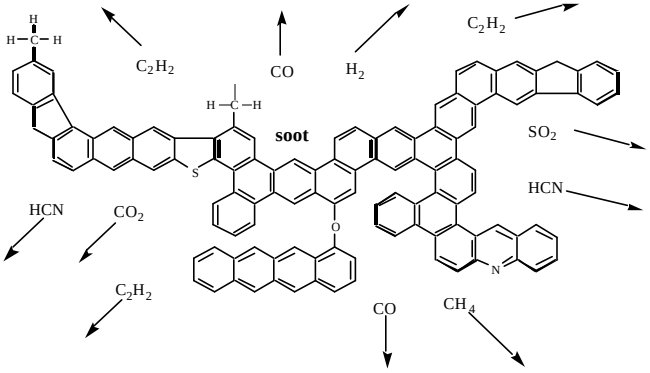

secondary pyrolysis

Figure 1.2.2. Stages of pyrolysis viewed at the molecular level (adapted from Solomon, et al.

1988).

times of ~0.2 and ~1 s, the other using tar aerosol in a shock tube at 1100-2000 K and a residence time of 1 ms. Yields of CO and light hydrocarbons including CH_4, C_3H_6, C_2H_2, C_6H_6, were determined as a function of temperature. All of the measured gases reached a maximum yield with temperature and then declined, with the exception of C_2H_2, which increased dramatically in the temperature range 1200 K-1400 K. Pyrolytic carbon (soot) was also identified starting at about 1300 K, which is coincident with the depletion of hydrogen in the tar.

Nelson et al. (1988) investigated the pyrolysis of coal at high temperatures in fluidized bed reactors and in a shock tube. The experiments were compared with results from an experiment where tar was produced at 600°C in a fluidized-bed reactor and where the tar subsequently flowed into a shock tube that operated between 600 and 800°C. The gaseous hydrocarbon yields observed from secondary cracking of the tar were similar to those observed for direct pyrolysis of the same coal in a fluidized-bed pyrolyzer at 600-800°C. The kinetic parameters obtained for the production of C_2H_4 and C_3H_6 from tar pyrolysis were similar to those obtained from model compounds like hexadecane. However, the activation energies obtained for the formation of these products by direct pyrolysis of coal were much lower than from the model compounds.

A more detailed study was carried out by Xu and Tomita (1989) who treated the effects of temperature and residence time on secondary reactions separately. The distributions of inorganic gases, hydrocarbon gases and liquids by pyrolyzing nascent volatiles were carefully measured using gas chromatography. It was found that temperature and residence time exerted the most influence on secondary reactions of volatiles. Tar started to decompose at 600°C, forming aliphatics, aromatics and coke, but the yield of CO_x remained constant. At 800°C, the nature of the secondary reactions changed considerably due to soot-forming reactions. The conversion of tar to aliphatics became negligible above 800°C. The decomposition of aliphatic hydrocarbons and small aromatic oils became significant at 900°C, resulting in a continuous increase of coke formation. At this high temperature, the reported coke and soot yields were not distinguished. The kinetic parameters derived from curve-fitting their experimental data showed agreement with those observed in the pyrolysis of coal itself or in the tar pyrolysis, implying that the

formation rates of hydrocarbons were similar in the above cases. This is in agreement with the findings of Nelson (1988).

The changes in molecular structure of flash pyrolysis tar generated from a subbituminous coal in a fluidized-bed reactor were analyzed by Field-Ionization Mass Spectrometry (FIMS) (Hayashi, et al. 1992). The extent of secondary reactions was regulated by an independent temperature-controlled freeboard zone in the reactor. The H/C ratio of tar was found to decrease with the increasing freeboard temperature, and the yields of CO, CO_2 and light hydrocarbons increased monotonically up to 800^{o}C. Analysis of the tar showed that the yields of pure aromatics and nitrogen-containing compounds increased monotonically with temperature, while hydroxyl compounds decreased.

1.1.4.2 Soot Formation Reactions

Soot can be found in almost all combustion and pyrolysis systems. Extensive research on soot formation demonstrated that soot is usually formed when the local environment is sufficiently fuel-rich to allow condensation or polymerization reactions of the fuel to compete with oxidation (Ma, 1996). In pulverized coal furnaces with staged combustion, the high temperature and the lack of oxygen by the delayed mixing promote the formation of soot. Soot impacts coal combustion in two ways. First, soot particles suspended in the combustion flame will significantly enhance radiative heat transfer due to their large surface area, small size (submicron for young soot and several hundred microns for the mature soot) and spectrally continuous radiation characteristics (Rigby, 1996). Calculations have shown that the near-burner flame temperature could be lowered up to 300 K due to the radiative heat transfer between the soot and the wall (Brown, 1998). It is therefore important to include the effects of soot in combustion models, since kinetic predictions are a strong function of temperature. Second, part of the nitrogen released from coal during devolatilization will be reincorporated into the soot, which complicates models of nitrogen transformation and NO_x production.

The limited studies on coal-derived soot are reviewed here, including the hypothesized

precursors, proposed soot formation mechanisms, and the influence of local combustion parameters on soot formation.

The formation of soot from electrically-heated entrained flow pyrolysis of different coal ranks was studied by Nenninger (1986). The aerosols from the collection system were analyzed for tar and condensed ash by both extraction with methylene chloride and neutron activation analysis. The soot yields were calculated by difference. The sum of tar plus soot was reported to be constant while the soot yield increased dramatically at temperatures above 1200 K (with an equally dramatic decline in tar yield). This was the first direct evidence that tar, whose main components are polycyclic aromatic hydrocarbons, or PAH, is the soot precursor in coal systems.

Wornat and coworkers (1988a) determined the comprehensive compositions of PAH from the pyrolysis of a high-volatile bituminous coal in a drop tube reactor under sooting conditions. The results suggested that ring size and the presence of attached functional groups determine the reactivities of the PAH. Compounds with more complex attachments were more reactive than compounds with simple or no attachments. In addition, it was found that the increases in soot yield occurred at the expense of PAH yield, suggesting that PAH serves as a precursor to soot. About 20 wt% of the coal (daf) was converted to soot at high temperatures and long residence times, which is comparable with the data reported by Nenniger (20 wt%, daf) at 2200 K for a high-volatile bituminous coal.

FTIR spectra of the tar produced at high temperatures in a fluidized bed reactor showed the existence of peaks characteristic of the stretching frequency of the carbon-carbon triple bond, suggesting that alkynes generated from tar cracking reactions may participate in soot formation during higher temperatures.

A systematic characterization of temperature-induced secondary reactions of coal volatiles from a subbituminous coal and a hva bituminous coal was carried out in a radiant entrained-flow reactor (Chen, 1991). The soot formation from secondary reactions of coal volatiles was examined under inert conditions. Again, the yields of tar/oils plus soot in the high temperature experiments were reported to be relatively constant with temperature. It was hypothesized that

the weight loss due to expelling CO and other gases from tars was compensated by the addition of light hydrocarbons.

Coal-derived soot was analyzed from entrained-flow pyrolysis in a post-flame environment by Ma (1996). The total soot yields decreased slightly with increased temperature for coals ranging from lignite to hva bituminous, which is inconsistent with the observations of other researchers (Nenniger, 1986; Wornat, et al. 1988a; Chen, 1991). It should be pointed out that the other three experiments were conducted in inert conditions (N_2 or argon). Certain types of oxygen-containing species in the post flame may have altered the soot yield in Ma's experiment. Because coal combustion in industrial furnaces does not occur under inert conditions, Ma's results may be more useful in evaluating soot formation mechanisms in coal systems. A more comprehensive review of soot in coal combustion systems was published by Fletcher et al. (1997), describing various experiments on coal-derived soot, measured optical properties of soot, and existing models of soot formation and oxidation.

1.1.5 Nitrogen Transformations during Pyrolysis

1.1.5.1 Nitrogen Functionalities in Coal

Coal-bound nitrogen resides principally in heterocyclic ring moieties (Smith, et al. 1994). The results of X-ray Photoelectron Spectroscopy (XPS) studies reveal that most coal-N is present in pyrrolic (five-membered ring) and pyridinic (6-membered ring) groups. It was observed that pyrrolic functionalities in coals are present in much higher concentrations than pyridinic forms, and that the proportion of pyridinic-N seems to increase with coal rank (Kelemen, et al. 1993). In the XPS studies, an additional component, corresponding to quaternary nitrogen (Kelemen, et al. 1994), was often found necessary to achieve an acceptable fit to the measured XPS spectra. However, the exact nature of this functionality is still poorly understood. The XPS analysis of Argonne Premium Coals showed that quaternary nitrogen is only a small fraction of the total coal-N, and that the quaternary nitrogen content seems to decrease with coal rank (Figure 1.2.3).

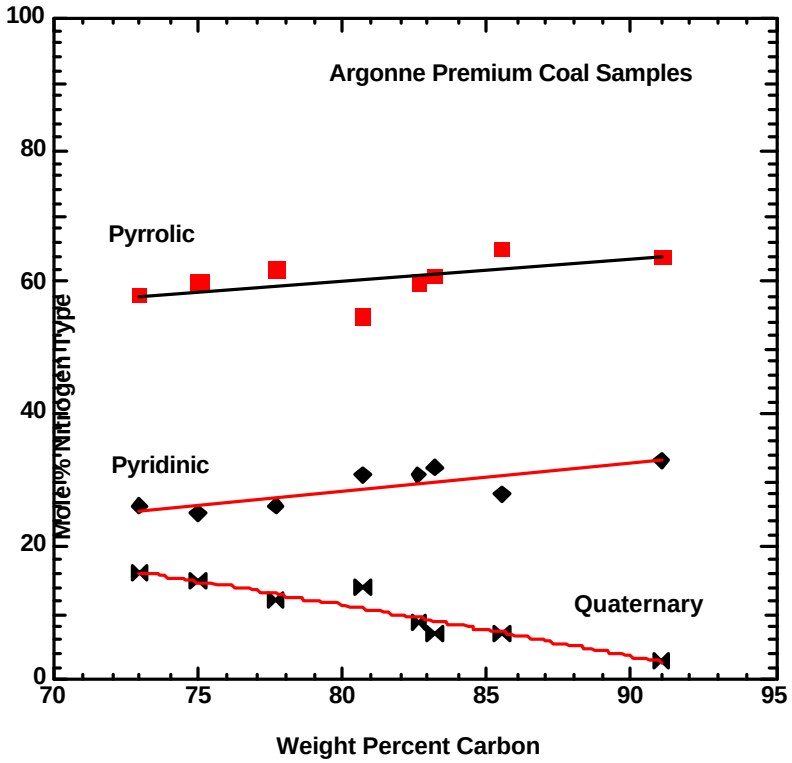

Figure 1.2.3. Nitrogen functional groups by XPS curve resolution analysis (adapted from Kelemen 1993).

It has been argued that quaternary nitrogen may be formed due to the oxidation of the pyridinic nitrogen to N-oxide (Nelson, et al. 1992). XPS analysis of the coal surfaces prepared by conventional wet polishing had been observed to produce an appreciable increase in the intensity of the quaternary nitrogen and a corresponding decrease in the intensity of the pyridinic nitrogen. Further studies are still required to verify the genuine structures of this class of nitrogen compounds.

1.1.5.2 Nitrogen Partitioning during Primary Pyrolysis

Primary pyrolysis is the first step during coal combustion, therefore the nitrogen release

during primary pyrolysis has a huge impact on the subsequent secondary reactions. The amount of coal nitrogen released as light gases is negligible at low temperatures (Freihaut, et al. 1993; Kelemen, et al. 1993). This is probably because nearly all forms of nitrogen in coal are incorporated into aromatic ring structures, which require higher energies to react. Pyrolysis studies on N-containing aromatic model compounds have demonstrated that significant thermal decomposition would only take place at temperatures higher than 800^{o}C.

Tar is the major transport mechanism for fuel nitrogen during the initial stage of pyrolysis (Solomon and Colket, 1978; Chen, 1991). Heated grid experiments on a lignite and 12 bituminous coals at a heating rate of 600 K/s showed that for temperatures up to 600^{o}C, no significant amount of nitrogen were released. The striking similarity between the tars and the corresponding parent coals by ^{13}C NMR and infrared analysis suggested that tar-N occurs in the same structures as in the parent coal in the initial stage of devolatilization.

The effects of heating rate on both tar yield and nitrogen partitioning between various products were examined on two bituminous coals without the interference of secondary reactions (Cai, et al. 1992). The tar-N fraction increased with heating rate, since the tar yield experienced a similar increase. This may suggest that the nitrogen content in the tar is independent of heating rate and that the nitrogen structure remains almost intact during primary pyrolysis.

A detailed study of primary nitrogen release in an entrained-flow system was conducted on four coals of different rank (Chen and Niksa, 1992b). It was found that the nitrogen was initially released almost entirely in the tar. His study also demonstrated the dependence of tar nitrogen release on coal type: high rank coal, with a higher tar yield, produced more tar-N than low rank coal.

Freihaut and coworkers (1993) used a heat grid reactor and an entrained-flow reactor to examine the influence of temperature, residence time, pressure, and particle size, on coal nitrogen release. In the entrained flow experiments, the low rank coal tar contained significantly less nitrogen on a mass fraction basis than the parent coal during the initial, primary tar evolution phases. Their results showed that the nitrogen evolution behavior of low rank coals differs from

that of bituminous coals both with respect to tar yield potential and intrinsic nitrogen concentration in the tar.

XPS analysis of the chars and tars obtained from pyrolyzing Argonne Premium coals showed some interesting results regarding nitrogen transformations. Pyrrolic and pyridinic species were the dominant nitrogen forms in chars and tars obtained from low temperature, low heating rate pyrolysis. However, an additional band corresponding to amino nitrogen or nitrile species was found necessary to obtain a good fit to the XPS nitrogen spectrum for low rank coals (Kelemen, et al. 1998). Pyrolysis studies in fluidized bed reactors reported significant amount of nitrile species in the high rank coal tar, but the tars generated from an entrained-flow system did not show a nitrile band. Because it is generally believed that amino species tend to form ammonia during thermal decomposition while nitrile compounds are the main source for HCN release, further studies on the genuine nature of this additional nitrogen form are needed.

1.1.5.3 Nitrogen Transformations during Secondary Reactions

At temperatures above 1000 K and at long residence times, the volatiles released during primary pyrolysis will undergo secondary reactions. Under fuel-rich conditions, thermal cracking of the tar molecules will cause ring opening reactions, leading to the release of nitrogen in the form of light gases such as HCN (Chen, 1991). When soot formation begins at 1300 K, a portion of the nitrogen in the tar is incorporated into the soot matrix. The nitrogen incorporated into the soot is not easily reduced by the aerodynamic technologies such as air/fuel staging. The study of soot nitrogen is complicated by the nitrogen released from char at similar temperatures. As mentioned earlier, the high temperature nitrogen release from the char is considered primary pyrolysis, since it has not reacted in the gas phase.

Experiments on a hv bituminous coal showed that the N/C ratio was quite different for the tar and soot, indicating that soot is not a simple accumulation of PAH's in the tar (Wornat, et al. 1988a). Incorporation of the N-containing PAH into the soot was faster than the non N-containing PAH during the initial soot formation process. The nitrogen content of the soot was found to decrease with increasing temperature. Two mechanisms were

suggested for such a decrease, including the liberation of N-containing gas species from the soot and the incorporation of PAH with successively lower nitrogen content during soot growth. The second aspect was suggested to have a larger effect on reducing the soot N/C ratio.

As much as 25% of the volatile-N was reported to be incorporated into soot for a hv bituminous coal and 10% for a subbituminous coal (Chen and Niksa, 1992b). It was also observed that nitrogen incorporation into soot occurred early during secondary pyrolysis, and that the fraction of coal nitrogen integrated into the soot remained constant, even though the soot yield increased steadily with increasing temperature. Consequently, the nitrogen content of the soot decreased throughout secondary reactions, which is consistent with Wornat's observation. The major N species in the gas phase was found to be HCN. Haussmann et al. (1989) also reported about 20-30% of volatile-N trapped in the soot for a bituminous coal. However, pyrolysis experiments in a flat flame burner showed much less nitrogen fraction trapped in the soot, and no significant changes of nitrogen composition in the soot with residence time were noticed (Rigby, 1996).

The nitrogen functionality of the tar was examined by pyrolyzing a German bituminous coal in a fluidized bed and performing size exclusion chromatography (SEC) on different molecular mass fractions (Li, et al. 1997). The nitrile group, not present in the raw coal and the tars produced at 600 and 700^{o}C, appeared in the SEC fractions of the tar produced at 800^{o}C, which coincides with the temperature at which N-containing model compounds begin to decompose. XPS analysis of the tars also indicated the conversion of pyridinic nitrogen to nitrile nitrogen in the range of 600-800^{o}C. The presence of reactive species and H was suggested as a reason for the earlier release of nitrogen gas species (HCN, NH_3, HNCO, etc.) from the coal than from the model compounds.

Heated grid experiments on some bituminous coals demonstrated the different nitrogen release patterns during high temperature pyrolysis (Man, et al. 1998). At relatively low temperatures (1000-1200^{o}C), volatile nitrogen (mostly contained in tar) fractional yields were approximately equal or slightly less than the total volatile yields. However, at higher temperatures (1400^{o}C above), there was additional release of nitrogen with very little

total mass loss. The "secondary" nitrogen release (defined by these authors to be any reactions occurring after the primary tar release) occurred at a much slower rate than the "primary" nitrogen release. This "secondary release" was associated with a reduction of hydrogen content in the char.

Ledesma's (1998) experiment on the thermal cracking of coal tars is the only study of nitrogen release from tars free from the effects of residual char and from transport effects from the coal surface. Primary tars were generated at 600°C in a fluidized reactor and subsequently thermally decomposed in a tubular reactor connected with the fluidized reactor. HCN was found to be the dominant nitrogen species from tar cracking. A considerable amount of NH_3 and HNCO was also identified. This is the only experiment where a significant amount of HNCO has been reported. The fraction of soot-N was not reported, but was likely less than 10% based on the nitrogen balance.

Recently, the N-containing PAH (NPAH) in the tars of a bituminous coal and a subbituminous coal were characterized according to their fused aromatic ring numbers using gas chromatography coupled with a chemiluminescence detector (Yu, et al. 1999). It was found that the initial depletion of N-containing species was mainly attributed to direct conversion to soot during the early stage of secondary pyrolysis. Neutralization and mass transformation of polar compounds (carboxyl-substituted NPAH) appear to be responsible for an observed increase of NPAC in the middle stage of secondary reactions. The decrease of NPAC, after reaching a maximum at the late stage of secondary pyrolysis, indicates the successive predominance of polymerization and ring rupture reactions, which lead to the release of HCN. Yu's results also confirm the findings of Axworthy (1978), in that the stability of NPAC does not necessarily correspond to the activation energy associated with a given pyrolysis condition. 2-ring NPAC (such as quinoline) in the coal tars, assumed to form from the reaction of pyridine and acetylene, appear to be the most stable species during severe secondary pyrolysis.

1.1.5.4 Noncondensible Nitrogen Gases

Secondary reactions of tar and thermal decomposition of char at high temperatures

will result in the release of nitrogen species into the gas phase. The major gas species are identified as HCN, NH_3, HNCO and N_2 (Xu and Tomita, 1989; Chen and Niksa, 1992b; Bassilakis, et al. 1993; Freihaut, et al. 1993; Li, et al. 1997; Ledesma, et al. 1998). HCN and NH_3 are by far the most important nitrogen species in pulverized coal burners and fluidized reactors, although some slow heating pyrolysis experiments on fixed bed did show N_2 as the dominant species (Axworthy, et al. 1978; Leppalahti, 1995; Takagi, et al. 1999). HNCO yields corresponding to 15% of the total volatile-N were reported in a fluidized bed pyrolysis experiment (Li, et al. 1997).

There is still controversy over the origins and interactions of HCN and NH_3 during coal pyrolysis. Some researchers believe HCN and NH_3 are generated from a similar source since the temperature of initial HCN and NH_3 formation is very close (Nelson, et al. 1992); others assume that NH_3 is converted to HCN under severe conditions (Chen 1991; Brill, et al. 1992). Recently, more and more researchers have begun to believe that HCN may be the primary nitrogen species during pyrolysis and that NH_3 is partly formed from HCN through hydrogenation (Bassilakis, et al. 1993; Leppalahti, 1995; Rudiger, et al. 1997; Ledesma, et al. 1998; Friebel and Kopsel, 1999; Schafer and Bonn, 2000). The absence of NH_3 from the decomposition products of N-containing model compounds was explained by the lack of donatable hydrogen atoms in these aromatic compounds (Mackie, et al. 1990; Mackie, et al. 1991). Enhanced HCN conversion to NH_3 by adding small amounts of water (hydrogen donor) was also reported (Schafer, 2000). The hydrogenation of HCN to NH_3 is further complicated by the fact that more NH_3 has been found in experiments with relatively high concentrations of oxygen-containing species (O_2, O, OH, etc.) (Van der Lans, et al. 1997). The relatively higher NH_3 yield associated with low rank coals under inert conditions may be somewhat correlated with the higher oxygen content in the parent coal.

The relative amounts of HCN and NH_3 can be affected by many factors such as coal rank, heating rate, temperature, local stoichiometry and even experimental apparatus. Table 1.2.1 shows the list of reported HCN and NH_3 yields from different coal pyrolysis experiments.

These results can be summarized as follows: HCN is predominant in high

temperature, high heating rate entrained-flow systems; however, in slow heating rate fixed bed experiments, more NH_3 is identified. Strong rank dependence of HCN and NH_3 release is demonstrated in entrained flow systems and fluidized bed experiments, with more NH_3 release for low rank coals than for high rank coals. The large variation in the reported HCN and NH_3 yields at various conditions shows that more understanding is needed. A simple correlation between the nitrogen functionalities in coal and the final nitrogen distributions in gas does not yet exist. Therefore, additional dedicated research is necessary on the release of HCN and NH_3 in industrially-relevant systems.

Table 1.2.1. Noncondensible Nitrogen Products under Pulverized Coal Combustion Conditions.

Nitrogen Products	Apparatus	Conditions
HCN is the dominant product	arc-jet fired entrained flow reactor (Haussmann, 1989)	900 ppm O_2, bit. and subbit. coal
	heated grid (Freihaut, et al. 1989)	in N_2, 14 coals
	radiant flow reactor (Chen, 1991)	inert atmosphere, 6 coals
	entrained flow reactor (Freihaut, et al. 1993)	inert atmosphere, 14 coals
	entrained flow reactor (Bassilakis, et al. 1993)	inert atmosphere, Argonne Premium coals
both HCN and NH_3 detected; HCN is the primary components with small amount of NH_3 for lower rank coals	entrained flow reactor (Blair, et al. 1976)	inert atmosphere, 20 coals
	laboratory-scale combustor (Rees, et al. 1981)	substoichiometric; bit. coals
	drop-tube reactor (Phong-Anant, et al. 1985)	in argon, subbit. and lignite
	fluidized bed (Nelson, et al. 1992)	inert atmosphere; 3 coals
	pyroprobe in an air-staged entrained flow furnace (Kambara, et al. 1995)	inert atmosphere, bit. and subbit. coals
	radiant flow reactor (Niksa,1996)	slightly oxidizing atmosphere, bit. and subbit. coals
	fluidized bed (Ledesma, et al. 1998)	inert atmosphere, bit. coal
more NH_3 is formed than HCN	electrically heated furnace (Kremer,1986)	oxidizing atmosphere; mv bit. coal

	flat-flame burner (Peck, et al. 1984)	Ar/O_2 flame, subbit. coal
	fixed bed (Leppalahti, 1995)	inert atmosphere; slow heating rate; Russian coal
	TG-FTIR (Bassilakis, et al. 1993)	inert atmosphere; Argonne Premium coals
more HCN is found in high rank coals, while the distribution of NH_3 increases towards lower rank coals, and can become larger than HCN	laboratory-scale combustor (Chen, et al. 1988)	$Ar/O_2/CO_2$; 48 coals; various stoichiometry
	fixed bed (Friebel, 1999)	inert atmosphere, low rank coals

1.1.6 Summary

Thorough understanding of the mechanisms of nitrogen evolution and transformation during the different stages of devolatilization is essential to the comprehension and prediction of the ultimate fate of coal nitrogen during coal combustion. As a result of this literature review, the following needs for the information of coal nitrogen release are identified in order to develop a generalized coal-dependent nitrogen release model:

1) Nitrogen partitioning among the gas, tar/soot and residual char during primary and secondary coal pyrolysis

2) Nitrogen evolution rates from tar, soot and char

3) Interactions of nitrogen species in the gas, tar/soot and char

Unfortunately, after several decades of dedicated studies on NO_x control, a satisfactory and complete solution for the above issues has not yet been obtained. Data on nitrogen release during secondary pyrolysis, which process predominates in novel air-staged coal furnaces, are insufficient. Disagreement still exists regarding which species are the primary NO_x precursors

during pyrolysis and combustion. Soot formation mechanisms in coal systems and the effects of soot on nitrogen transformation are not fully understood. And finally, the gas phase reactions involving nitrogen transformation still need improvement. Enhanced knowledge on the above topics is required in order to develop realistic models of nitrogen evolution in coal combustion, which are essential for further optimization of burner design and pollutant suppression.

1.3 OBJECTIVE AND APPROACH

The general objective of this research is to further investigate the secondary reactions of coal volatiles under conditions relevant to commercial pulverized coal furnaces, with emphasis on nitrogen transformations and soot formation. As the research proceeded, an opportunity arose to study a few pure hydrocarbon compounds that are found in coal tar and other fuels (such as jet fuel and diesel). Therefore, a secondary objective of this study was added: to study the solids produced in the early stages of soot formation from representative model compounds.

More specifically, the effects of temperature, residence time, and coal rank on the nitrogen partitioning in the gas, tar/soot and char at high temperature (1150 K-1850 K), high heating rate entrained flow system are examined. Since a complete reaction mechanism for the conversion of stable NO_x precursors (mainly HCN and NH_3) in the gas phase to NO_x is already available (Miller, 1989), special emphasis is placed on the studies of the release rate of these nitrogen precursors during secondary pyrolysis. Soot formation mechanisms are investigated using elemental analysis and ^{13}C NMR analysis on the tar and soot generated from both coal and model compounds. The effects of tar-soot transition on nitrogen transformations are also addressed, since soot retards the conversion of NO_x to N_2 by limiting the nitrogen in the gas phase.

Four coals ranging from lignite to hva bituminous were pyrolyzed in a post-flame environment in a flat-flame reactor. Eighty pyrolysis tests were performed at seven temperature settings and four residence times, which provide important data for deriving kinetic parameters for secondary reactions of coal volatiles. The condensed products (tar, soot and char) were collected and analyzed separately using various modern analytical techniques including elemental analysis, Inductively Coupled Plasma (ICP) and ^{13}C NMR spectroscopy. The gas phase compositions were analyzed using Fourier Transform Infrared (FTIR) Spectroscopy. The nitrogen evolution were examined both in the condensed phase and in the gas phase.

The main tasks in this project can be summarized as:

1) Determination of the tar/soot yields and mass release in coal pyrolysis under a broad

range of conditions.

2) Development of PPB-level gas analysis capability for N-containing and other relevant species using an FTIR system.

3) Examination of the soot formation process from coal and from model compounds. The mechanism of nitrogen evolution during tar-soot transition is proposed based on the analysis of tar and soot from these experiments.

4) Postulation of reaction mechanisms and derivation of kinetic parameters to explain tar reduction, soot formation and nitrogen evolution.

Chapter 4 presents the description of how the experiments were performed. Chapter 5 presents the results of experiments regarding the secondary reactions of coal volatiles, focusing on the hydrocarbon structures. This chapter also presents results of a modeling effort to describe the experimental observations. Chapter 6 presents results of the solid-state ^{13}C NMR analyses of tars and soots from coal and model compounds, showing changes in the chemical structures in the solid phase products during pyrolysis. Chapter 7 presents the nitrogen release and transformation data. Finally, in Chapter 8, a summary and lists of conclusions drawn from this study are presented, followed by limitations and recommendations for future work.

1.4 DESCRIPTION OF EXPERIMENTS

1.1.7 Flat Flame Burner

The flat flame burner (FFB) used in this study was described thoroughly by Ma (1996). An FTIR gas analysis system was added and used in connection with the suction probe in the FFB system to allow on-line gas measurement. Figure 1.4.1 shows the revised FFB system. A syringe-type particle feeder was used to provide a steady feed rate (~1 g/hr) and to allow an accurate measurement of the total amount of sample fed in each experiment. This flow rate ensured single particle behavior in the reactor. The particles from the feeder were entrained in N_2 and injected about 1 mm above the burner surface through a metal centerline tube. The temperature in the FFB can be adjusted by changing fuel type, the amount of dilution N_2, and the equivalence ratio. The calculated heating rate for pulverized coal particles can reach 10^5 K/s (Ma, 1996), which is close to particle heating rates in industrial furnaces. The entire reactor can be raised and lowered relative to the level of the sampling probe to accommodate desired residence times. All the reaction products were collected by a water-cooled probe with nitrogen quench jets at the probe tip. Nitrogen was also transpired though a porous inner wall of the probe in order to minimize soot deposition on the probe walls. A virtual impactor at the end of the suction probe was used to separate the large, dense char particles from the small and low-density soot particles. A cyclone connected behind the virtual impactor was used for char collection. The soot particles were collected on polycarbonate filters with a 1 μm pore

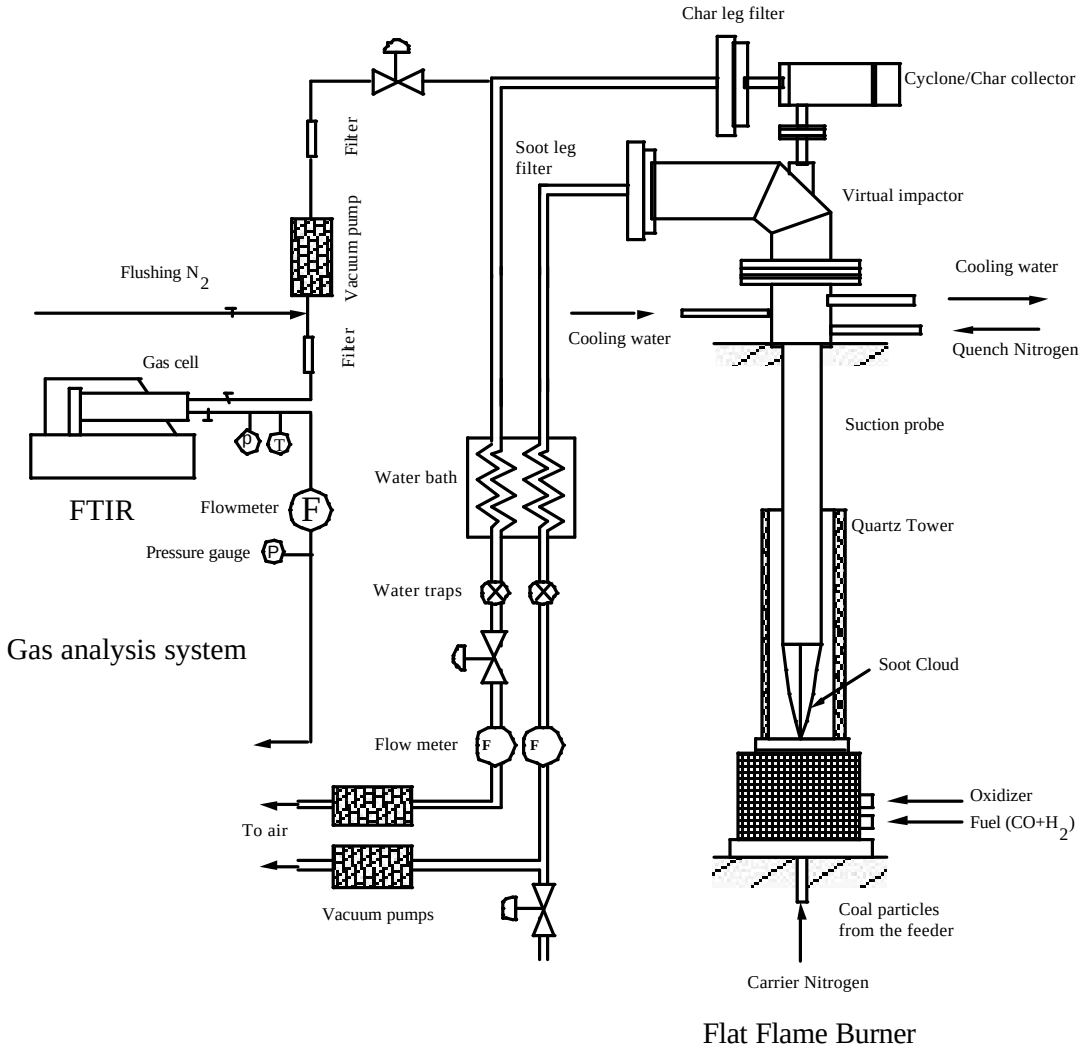

Figure 1.4.1. Schematic of the Flat Flame Burner (FFB) with the gas analysis system.

size, supported by a separate glass filter. Soot samples were carefully scraped from the filters to avoid the use of solvents. The reaction gas stream was collected after passing the filters and was analyzed by the FTIR to get the gas compositions. A detailed discussion on the gas phase FTIR measurement is presented in a later section.

1.1.8 Gas Temperature Control

Temperature is a critical parameter in coal pyrolysis. For many years, methane was used as the major fuel in the FFB to perform high temperature, high heating-rate experiments. Since the flammability limit of methane is very narrow (from 5% to 15%, volume in air), the lowest operating temperature of a fuel-rich methane flame is about 1600 K. However, significant secondary reactions usually start at a temperature as low as 1100 K for a coal system. A method was devised to lower the temperature to about 1100 K for the study of secondary pyrolysis. As a result of this study, it was found that carbon monoxide (CO) is an ideal fuel for low temperature experiments in the FFB. It has several advantages over other fuels (such as methane). First, because CO has much broader flammability limits (12.5%-75%, volume in air) than most of the common hydrocarbon fuels (2%-15%, volume in air for methane, ethane, propane etc.), the temperature of a stable CO flame can theoretically be maintained at about 1000 K even at very fuel-rich conditions. Such low temperatures can not be achieved using other hydrocarbon fuels. In practice, a small amount of hydrogen was also added to the fuel stream to enhance stability. Second, CO flames also minimize the steam production, which can greatly interfere with FTIR measurement of other weakly absorbed species. Using a CO flame, the temperature can be easily adjusted from 1100 K to 2000 K in the FFB to facilitate the pyrolysis experiments, with steam production less than 1% in the post-flame gases. A CO monitor was used in the lab for safety reasons when the CO flame was in operation. The experiment was also performed under a safety hood to prevent CO poisoning.

1.1.9 Coal Selection

Coal rank is an indicator of the coalification (maturation) of a coal from a variety of plant precursors. It is well established that coal rank is one of the most important factors that determine the behavior of coal devolatilization. Temperature sensitivity of tar evolution, the tar yields and compositions are strongly correlated with coal rank (Freihaut, et al. 1993). Since secondary reactions and the involved nitrogen chemistry are directly related to tar evolution, the secondary nitrogen release is also influenced by coal rank. For example, it has been demonstrated by most researchers that ammonia formation is usually associated with lower rank coals. Consequently, four coals covering a broad range of coal ranks were employed in this

study. These coals, namely Illinois #6 (Bituminous), Utah (Bituminous), Black Thunder (Subbituminous) and Knife River (Lignite), were obtained from the DOE/UCR program at the University of Utah and Brigham Young University. Figure 1.4.2 displays the sample positions on a coalification band plot. The O/C ratio varies from about 0.1 to 0.27, while the H/C ratio falls in a relative narrow range from 0.86 to 0.9.

1.1.10 Sample Preparation

All the coals were pulverized and sieved to 45-75 μm in an inert environment. Each coal sample was dried in an inert environment at 105°C for two hours prior to the experiment. Drying the samples helps to reduce the unpredictable effects of moisture on pyrolysis, and assists in achieving a steady and reproducible feed rate while avoiding agglomeration. The coal or char samples were separately evenly using a specifically designed rotating splitter to reduce the heterogeneity, a practice suggested by Perry (1999).

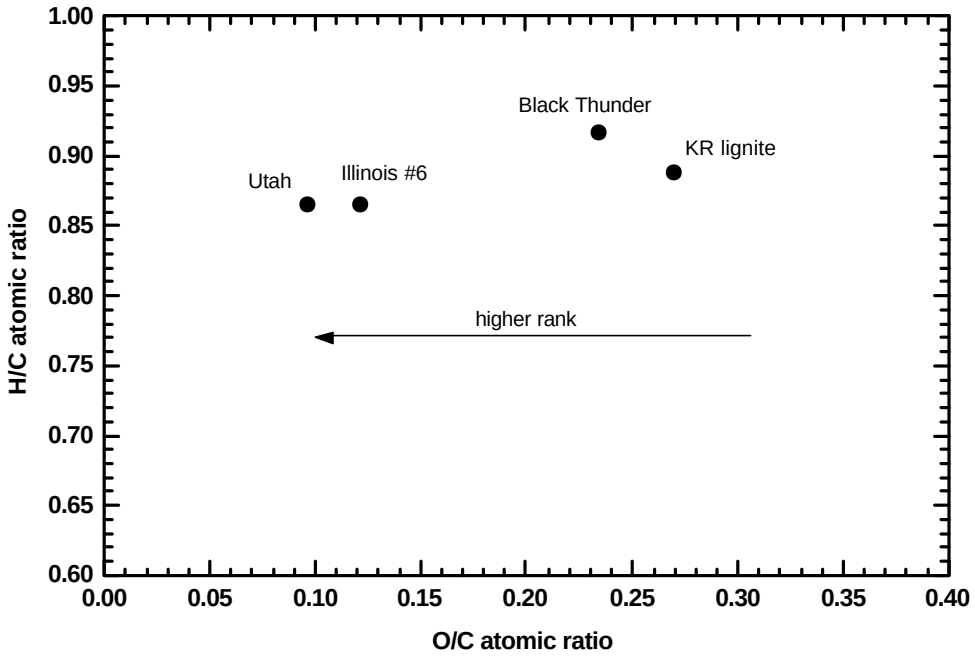

Figure 1.4.2. Coalification band plot of coal samples investigated.

1.1.11 Particle Feeder

The particle feeding system is the same one used by Ma (1996). Coal particles were contained in a 2.5 ml open-ended syringe. A syringe pump pushed the particles into a funnel, and then the entrained nitrogen flow carried the coal particles to the burner through a thin polyethylene tube (1mm I. D.). The feed rate was adjusted by changing the frequency or period of the pulse signal used for driving the step motor that operates the syringe pump. The stepping rate for all the experiments was set at 2 steps per second, which corresponded to a particle feed rate of about 1.2 gram/hour for coals. The feed rate was then calibrated by recording the weight of the coal fed during a certain period of time. Figure 1.4.3 shows the cumulative coal feed versus time for Knife River coal. The profiles for other coals are similar, indicating that an excellent feed rate can be maintained at a given step frequency. The slope of the line gives the actual particle feed rate. At this feed rate, single particle behavior was obtained in the reactor, as evidenced by measurements using a high speed camera (see Chapter 5).

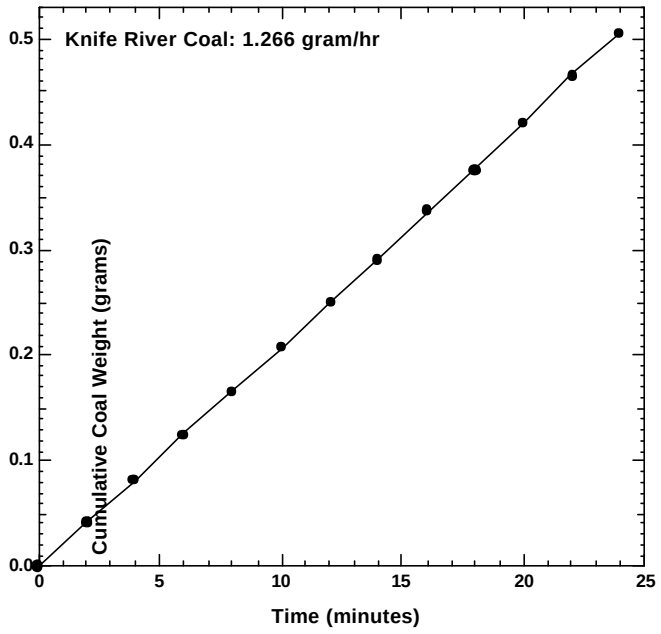

Figure 1.4.3. Cumulative feed of the Knife River coal.

1.1.12 Temperature Settings and the Corresponding Flow Rate

By shifting the fuel from methane to carbon monoxide, a much broader range of temperature settings can be achieved in the FFB simply through the manipulation of the equivalence ratio and the dilution nitrogen. Seven temperature conditions were devised in this study beginning from about 1100 K, where significant secondary reactions are believed to start, up to about 1900 K, where previous studies have shown that the mass release from coal will complete. The corresponding flow rates of carbon monoxide, air, hydrogen (enhancing the burning of CO), dilution nitrogen, carrier nitrogen and quench nitrogen are listed in Table 1.4.1, along with the peak temperature and equivalence ratio.

Table 1.4.1. Flow Rates in the Seven Temperature Settings.

Peak gas temperature (K)	Air (slpm*)	CO (slpm)	H_2 (slpm)	Dilution N_2 (slpm)	Carrier N_2 (slpm)	Quench N_2 (slpm)	Equivalence ratio
1159	9.25	9.75	0.3	6.5	0.0367	60	1.45
1281	11.25	9.75	0.3	6.5	0.0367	60	1.37
1411	13.5	9.75	0.3	6.5	0.0367	60	1.28
1534	19.5	12	0.35	10.2	0.0367	60	1.21
1618	24.5	12	0.4	8	0.0367	60	1.20
1752	23	12	0.32	6	0.0367	60	1.12
1858	24.25	12	0.32	3.5	0.0367	60	1.10

∗slpm: standard liters per minutes (at 1 atmosphere and 298 K)

Since nitrogen release during pyrolysis, not combustion, is studied, the equivalence ratio for each condition was maintained at a value greater than unity to ensure an oxygen-free

environment. The post-flame centerline temperatures were measured in the absence of particles using a thermocouple (OMEGA® type-B) with a small bead (about 0.9 mm in diameter) as a function of height above the flat flame burner surface. The thermocouple readings were then corrected for radiative heat loss using energy balance calculations. The detailed correction procedure is described by Zhang (2001). Because the actual coal loading is so light, the measured temperature profile is believed to sufficiently describe the temperature field the coal particles were subjected to during the experiments. Each condition is referred to by its peak gas temperature for the sake of convenience. The centerline temperature profiles for the seven conditions used in this investigation are presented in Figure 1.4.4.

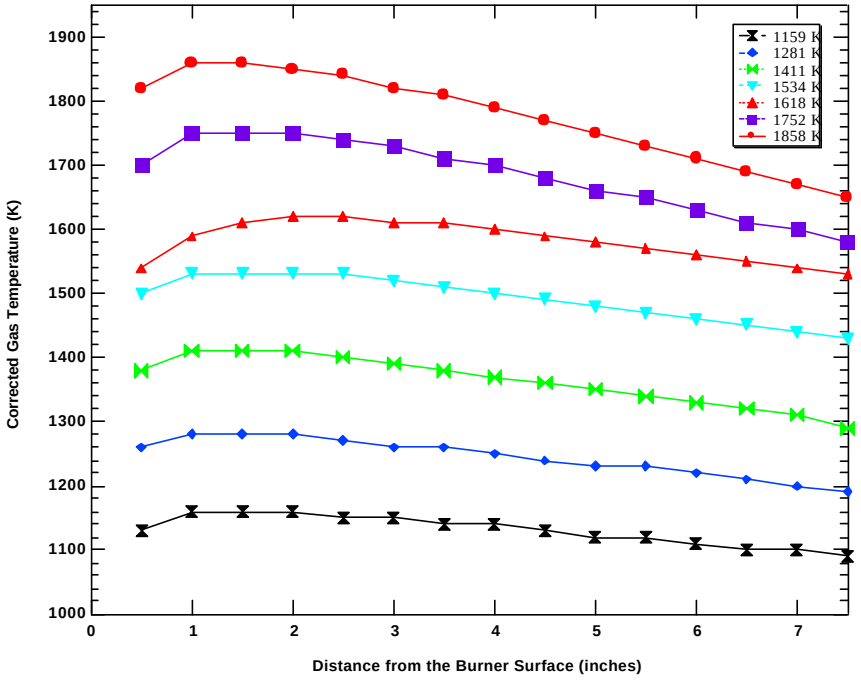

Figure 1.4.4. Centerline gas temperature profiles (after radiation correction).

1.1.13 Particle Residence Time Measurement

Product yields and compositions collected at different residence times are used to provide kinetic rates of nitrogen transformations during secondary pyrolysis. Accurate measurement of the residence time is critical in modeling the nitrogen release rate from the coal particles. For the bulk collection of the pyrolysis samples, residence time was varied by changing the position of the reactor relative to the stationary collection probe. For each temperature condition, reaction products were collected by the suction probe at four different elevations above the burner, namely 1, 3, 5 and 7 inches. However, even at the same elevation, the residence times vary for different temperature conditions, since the total mass flow rate and temperatures were changed. A high-speed video camera (Kodak EktaPro Imager) was used to record the trajectory of single coal particles at different temperature conditions. Three recording speeds were used in the measurement: 1000 frames per second; 500 frames per second and 250 frames per second. There is a trade-off when choosing the appropriate recording speed. Higher recording speeds will give a more precise time measurement (due to a smaller time increment for each frame), however, it also requires a much stronger light source. The video images of coal particles were first stored into a memory device (Kodak EktaPro EM Processor). These images were then played back on a TV monitor. Usually three distinct particles were identified and chosen for the measurement, and the three measured values were averaged. The video images can also be transferred to a regular VHS tape for further examination. The major limitation of the residence time measurement was that the resolution of the high-speed camera was not very high (256 pixels). Therefore, only coal particles with sufficient luminance could be identified and measured on the TV screen. At the two lowest temperature conditions of 1159 K and 1281 K, no trajectories of burning particles could be seen, regardless of the recording speed. Actually, the temperatures at these conditions were so low that the coal particles could not be recognized even with the naked eye. Consequently, the residence times at these two conditions were estimated through theoretical calculations. Even at higher temperature conditions, there was still a certain distance between the tip of the coal injection tube and the first luminescent point where the residence time could not be measured directly. The residence time for this distance was also estimated by theoretical calculations (see Chapter 5). The Illinois #6 coal was chosen as the representative sample to perform the residence time measurement. The measured residence times for this coal

were applied to all the other coals since it was demonstrated that the profiles of height versus residence time were similar for a broad range of coals (Ma, 1996), as long as the particle size was similar.

1.1.14 Experimental Test Matrix

Nitrogen evolution during the secondary coal pyrolysis is a very complicated process. Coal parameters, burner configurations and operation conditions can greatly affect the nitrogen release during coal combustion. In this study, temperature, residence time and coal rank were chosen as the test variables, since these factors exert most of the influence on the nitrogen transformation.

Temperature is one of the most important parameters that affect the nitrogen chemistry during pyrolysis, since kinetics are strongly dependent on local temperature. Previous study also showed that residence time has a significant influence on coal pyrolysis (Chen and Niksa, 1992a).

Coal rank is another important parameter to be addressed in this study. Tar evolution, its reactivity and the nitrogen release are strongly dependent on coal type (Freihaut, et al. 1989; Solomon, et al. 1990; Chen and Niksa, 1992b). The four coals used in this study have been well characterized previously and have been used extensively in industry. Therefore, the data obtained in this study can easily be compared with relevant data from the literature.

In this study, eighty pyrolysis experiments were performed in the FFB as outlined in Table 1.4.2. The four coals were pyrolyzed in seven different temperature conditions. Each condition is represented by its peak gas temperature after radiation correction. For the Illinois #6 and Utah coals in the 1534 K and 1618 K conditions, pyrolysis experiments were performed before the FTIR analysis was available (these experiments are represented by the symbol Δ in the table). The gas analyses for the two temperature conditions were performed a year later. Although special efforts were made to duplicate the experimental conditions, the data obtained in these two conditions are not so accurate as those obtained at other conditions where the pyrolysis experiments and gas analysis were performed at the same time.

Table 1.4.2. Testing Matrix for FFB Experiments.

Illinois #6	1 inch	3 inch	5 inch	7 inch
1858 K		s (NMR)		
1752 K	s			s
1618 K	Δ	Δ	Δ	Δ
1534 K	Δ	s (NMR)	Δ	Δ
1411 K	s	s (NMR)		s
1281 K	s	s (NMR)	s	s
1159 K	s (NMR)			s

Utah	1 inch	3 inch	5 inch	7 inch
1858 K		s		
1752 K	s			s
1618 K	Δ	Δ	Δ	Δ
1534 K	Δ	Δ	Δ	Δ
1411 K	s	s		s
1281 K	s	s	s	s
1159 K	s			s

Black Thunder	1 inch	3 inch	5 inch	7 inch
1858 K	s	s		s
1752 K	s	s		s
1618 K	s	s		s
1534 K	s	s	s	s
1411 K	s	s		s

1281 K	s	s	s	s
1159 K	s			s

Knife River	1 inch	3 inch	5 inch	7 inch
1858 K		s		
1752 K	s			s
1618 K				
1534 K	s	s	s	s
1411 K	s	s		s
1281 K	s	s	s	s
1159 K	s			s

s: normal test with on-line gas measurement at the same time

Δ: pyrolysis experiments were performed, and tar/char were collected and analyzed in 1998, gas measurement were performed a year later after adopting a reliable procedure.

NMR: tar and soot samples were analyzed by ^{13}C NMR at the University of Utah

Solid-state ^{13}C NMR analysis of the tar and char collected at different reaction severity has previously been performed to provide critical information regarding the chemical structure changes at various stages of devolatilization (Fletcher, et al. 1990; Hambly, 1998: Perry, 1999). It has been shown that nitrogen release during primary pyrolysis is directly associated with the chemical structures of the char (Perry, et al. 2000). Consequently, one would expect that the changes of chemical structures of the tar should also help us to better understand the mechanism governing the nitrogen liberation from tar during secondary pyrolysis. The tar and soot samples collected at five conditions using Illinois #6 coal were therefore analyzed by ^{13}C NMR at the University of Utah. A discussion of the NMR analysis will be presented in Chapter 6.

Because of the time required to perform experiments, sample collection was only repeated for the Illinois #6 coal at the 1 inch height for the 1159 K case and at the 3 inch height for the 1534 K case. However, repeat elemental analyses were performed on all the solid products. ICP analysis on the chars and FTIR analysis on the gas phase were also repeated to evaluate the variations of the results in this study. A detailed discussion of the repeatability of the current study is presented in the section of error analysis in Appendix E of Zhang (2001).

1.1.15 Pyrolysis of Model Compounds

Two aromatic model compounds, biphenyl and pyrene, were pyrolyzed in the FFB to generate tar and soot samples for subsequent ^{13}C NMR analysis. Of major importance in this study is the transformation of aromatic hydrocarbons to PAH to soot, and at what temperature this occurs for different soot precursors. The starting model compounds were obtained from the Aldrich Chemical Company.

During the experiment, it was found that the particle feed system, originally designed for feeding coal particles, could not handle the model compounds. The organic compounds, when ground to the approximate size of the coal particles (~50 μm), were almost impossible to inject directly into the reactor because the particles adhered to the wall of the funnel and to the polyethylene transport tubing connecting the funnel and the reactor. Coal particles can be

transported smoothly into the reactor because of the mineral matter in the coal. The mineral matter helps to reduce the surface tension or electrostatic forces between the particles and the wall. Pyrene and biphenyl particles become very sticky due to electrostatic forces when ground to small sizes. In this study, an inorganic compound was mixed with the model compounds and then ground to fine powders ranging from 45-75 μm to produce a mixture to be used in the existing particle feeding system. Several inorganic compounds were tested, and silica gel was found to work well. Silica gel (SiO_2, a major component in coal mineral matter) will not be pyrolyzed or vaporized under the desired temperature conditions (1160 K to 1470 K). The SiO_2 shows no color when injected into the hot flame, so there is no interference with the luminescent yellow cloud produced by soot particles. The luminosity caused by radiation from soot particles is the easiest way to identify the formation of soot in a combustion system. Other inorganic salts do exhibit colors because they contain certain glowing metals. The model compounds, when mixed with silica gel, were easily transported into the reactor through the connection line. In addition, silica gel has a much higher density than soot particles, therefore, it can be separated in a similar fashion as coal char by the virtual impactor and the cyclone.

However, some problems were also identified during the model compound experiments. It was found that the fraction of silica gel deposited with soot on the soot filters could be significant at certain conditions. A detailed discussion on this problem is presented in a later section. The elemental analyses of the soot samples from model compounds were performed at BYU, and a correction was made to account for ash contamination in the soot. The Illinois #6 coal and coal soots were also analyzed by Galbraith Laboratories in Knoxville, Tennessee, as a means of independent verification of the BYU analysis.

1.1.16 Sample Characterization

1.1.16.1 Separation of Soot from Char

In experiments conducted at the highest temperatures (>1752 K) and the longest residence times, significant amounts of black and low-density powders were found mixed with the char in

the cyclone of the collection system. By shaking the vial containing the samples in the cyclone, a totally dark layer was found sitting on top of a gray layer. The top layer was mainly soot particles, as evidenced by the elemental analysis (85-98% carbon) and certain physical characteristics such as density and strong electrostatic property. The bottom layer was mainly char particles, although sometimes nearly white ash-rich particles were also identified. The existence of soot particles in the cyclone was also reported by Ma (1996). The virtual impactor used for the char/soot separation in the FFB was designed based on the assumption that the soot particles should be smaller than 5 μm. Since the soot agglomerates generated in this system at high temperatures can be as large as 20 μm, it is not surprising that the virtual impactor failed to separate soot from char efficiently. A complete separation of soot from char is essential in order to get an accurate soot yield and elemental analysis of the final soot and char.

A gravity separation of soot from char simply by shaking the mixture in a vial was described by Ma. However, the soot particles near the interface of the two layers were very hard to remove, and a complete separation was almost impossible. A quantitative soot and char separation was also conducted on a fly ash sample containing certain amount of soot and char (Veranth, et al. 1998). The sample was dispersed in ethyl alcohol by ultrasonic agitation. Through a series process of settling and decanting with fresh ethyl alcohol, the carbon found in the final supernatant fraction was assumed to be soot and the carbon in the bottom fraction of the separation was assumed to be char. Since both soot and char are organic in nature, the use of organic solvents in the separation will inevitably introduce errors. The solvent can also change the physical and chemical properties of soot and char, so the subsequent analysis will not be accurate in reflecting the characteristics of the original samples.

A mini-cyclone was designed to accomplish the soot/char separation in the current experiments (Figure 1.4.5). First, the soot/char mixture was placed into the cyclone, which is closed on one end and open on the other end. Then the mixture was stratified by gravity using a vibrator. The upper part of the soot layer, which was usually pure soot particles, was carefully

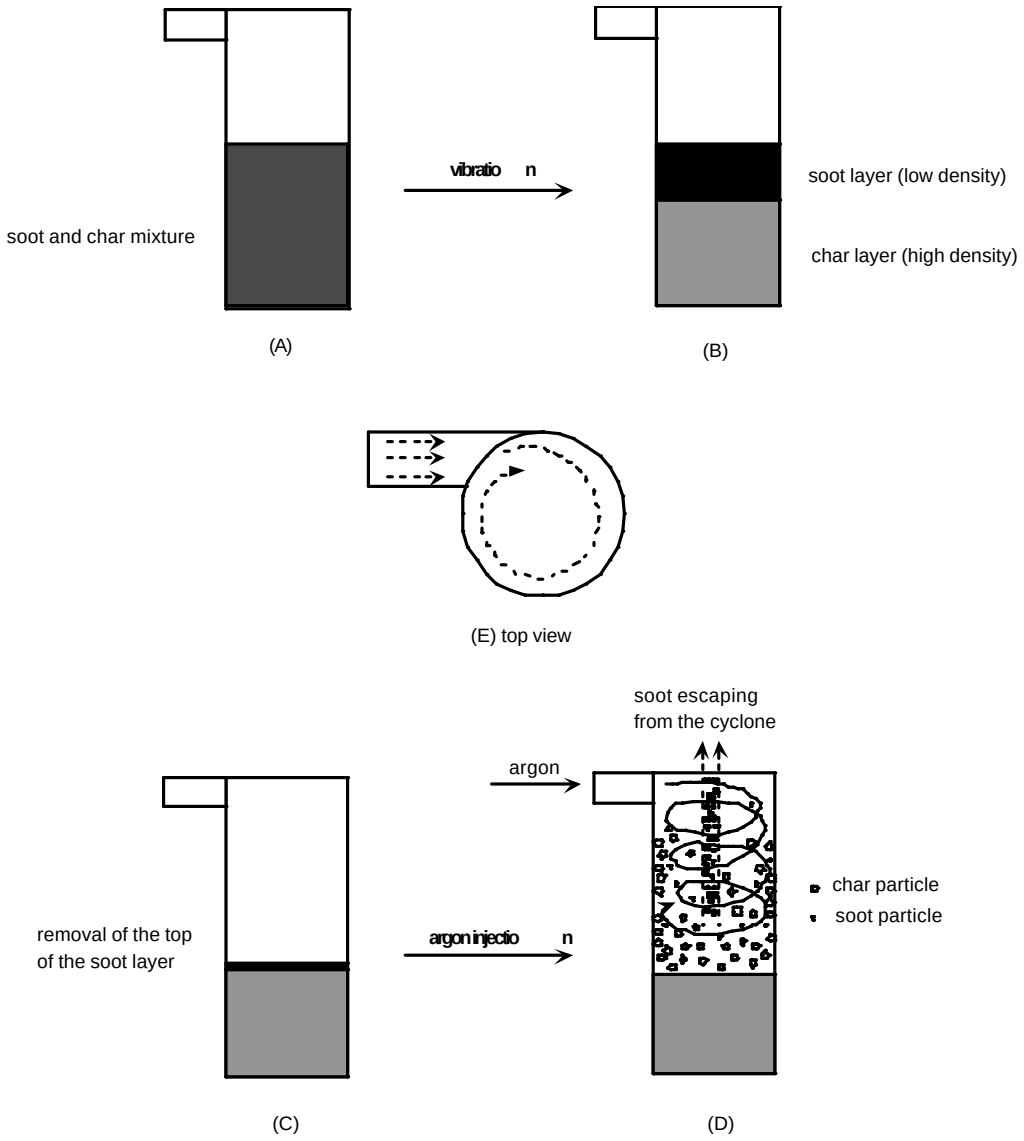

Figure 1.4.5. Soot/char separation using an aerodynamic method.

removed by a spatula. When there was little soot left on top of the char layer, tangential argon injection was introduced at the top of the cyclone. As expected in a cyclone, the low density soot particles were first entrained with the swirl flow created by the tangential argon flow. The soot particles were then easily removed by the outgoing argon flow, while the high density char particles remained in the cyclone. After a visual check, the remaining char was then weighted and used for further analysis. The mass fraction of soot in the mixture was estimated from a mass balance. Comparison of the elemental analysis on the separated soot and

those collected on the filters showed similar results, within experimental error. The carbon content of the separated char was never higher than 80%, indicating that soot contamination was negligible.

1.1.16.2 Tar and Soot Analysis

As explained in the first chapter, the heavy, aromatic volatiles released from the coal particles that condense at room temperature are collectively termed tar. The major components of tar are large polycyclic aromatic hydrocarbons and oils (Nelson, et al. 1986). Under conditions of high temperature and long residence time, the tar has a strong propensity to form soot (black, carbon-rich solids) (Chen and Niksa, 1992b; Ma, 1996). Although any further reactions of the tar are defined as secondary reactions, the study of the transition from tar to soot (which usually occurs at 1350-1450 K) is emphasized in this study.

During the experiments, the tar-soot transition can be qualitatively illustrated by examining the condensable solids collected on the filters from the gaseous pyrolysis products. At low temperatures (under 1200 K), the coal particles in the reactor were not luminescent. The solids collected were very sticky and light yellow in color. This is a characteristic of coal tar. As the temperature increased, the color of the solids became darker and darker (from yellow to brown, then to dark brown) but less and less sticky. Finally the solids turned into jet-black powder and were highly electrostatic in nature. These solids are usually considered to be soot.

Another interesting phenomenon observed during the experiments also clearly demonstrated the difference in the size of the tar and soot (see Figure 1.4.6). In this study, two filters were packed together in the filter holder to collect any condensable volatiles. A polycarbonate filter (Osmonics, Inc.) with a pore size of 1 μm was placed on top of a glass microfibre filter (Whatman International, Ltd.). The tar/soot samples were easily removed from the polycarbonate filters without the use of solvents, which must be used to obtain samples from the glass fiber filters. The polycarbonate filter is a thin film with a smooth surface, so the deposits were easily scraped off using a blade. The glass filter was used as both a support for the

polycarbonate filter and as a second filter to trap escaping aerosols from the first filter.

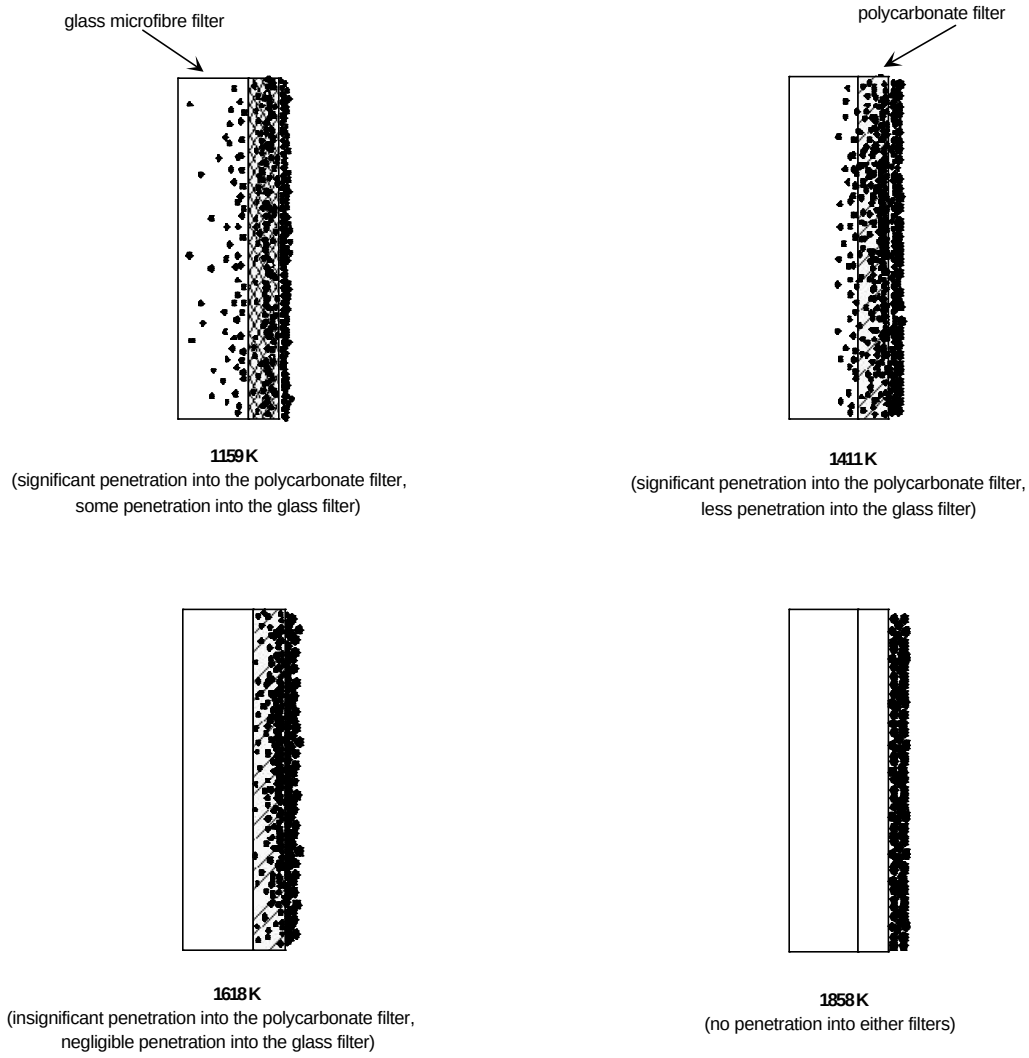

Figure 1.4.6. Tar/soot deposition on the filters at different temperatures.

By examining the deposits on the filters, it was found that at low temperatures (below 1411 K), the particles significantly penetrated through the polycarbonate filter, leaving some deposits even on the glass filter. The lower the temperature, the more deposits were found on the glass filter. This means that some of the tar or young soot molecules were much smaller than 1 μm, as expected. However, at high temperatures (above 1752 K), the amount of soot particles that penetrated through the polycarbonate filter became negligible. The glass filter was absolutely

clean at 1858 K, indicating that all the soot particles were larger than 1 μm in diameter. Scanning Electron Microscopy (SEM) analysis showed that soot agglomerates can grow as large as 20 μm in the FFB (Ma, 1996). Since large particles caused less clogging in the polycarbonate filters, longer run times were possible at high temperatures. The tar or soot yields were determined by weighing the two filters together before and after each experiment.

The density of the tar is also much higher than that of the soot. Because the transition from tar to soot is a gradual process, it is extremely hard to quantitatively determine the percentage of soot existing in the solids collected on the filters. Chen and coworkers defined soot as the residue remaining after the condensed volatiles were extracted with tetrahydrofuran (THF) in an ultrasonic bath (Chen and Niksa, 1992b). Pugmire suggested using methylene chloride to extract tar from the collected volatiles in order to determine the soot yield (Pugmire, 1999). However, both methods need large quantities of samples and are subject to errors in many aspects (temperature, extraction time, and polarity will all affect the results). In this study, the collected condensable volatiles are treated as mixtures to avoid using solvents. The volatiles deposited on the filters in this study are therefore collectively termed as tar/soot, and are analyzed together without separation. It is recommended separate examination of extracts and residues from soot/aerosol samples be included in future studies.

1.1.16.3 Ash Contamination in Tar and Soot

During the coal pyrolysis experiments, it was found that small amounts of char and ash particles were deposited with the tar and soot on the soot filters. The char particles were found on the soot filters when these particles were sufficiently small and could not be separated by the virtual impactor. The small char particles could have been formed from particle fragmentation. The ash in the tar and soot was likely caused by the recondensation of some volatile inorganics and ash, which vaporized from the char during pyrolysis (Nenniger, 1986). From the experiments of the model compounds, a significant amount of silica gel was found mixed with the tar or soot, making a reliable measurement of elemental analysis hard to achieve. The ash contents of the tar or soot samples were therefore determined in the same way as that for the

chars and the parent coals as presented in the "Sample Analysis" section.

The measured ash contents of the collected deposits on soot filters during pyrolysis of the coals and model compounds are presented in Appendix E of Zhang (2001). That work presents the measured ash content in the tars and soots obtained from coal and model compounds. As described by Zhang (2001), ash contamination for the coal tars or soots is only significant for the Knife River lignite, where about 10% ash was mixed with the tar or soot. A correction was therefore made to account for the ash contamination in the elemental analysis. For the other three coals, ash contamination was negligible. However, the impurities in the tars or soots of the model compounds were much more significant. For biphenyl, the ash content was as high as 77%. For pyrene, the ash content ranged from 7% to 35%. The small particle size (32-63 μm) of the silica gel used in this study is thought to be the major reason for the inefficiency of the virtual impactor in separating silica gel and soot. In addition, silica gel absorbs water (steam) very easily, and does not release the water until about 800^{o}C. Consequently, the absorbed water can interfere with the elemental analysis of the soot samples, especially the hydrogen content.

1.1.17 Sample Analysis

A number of modern analysis techniques were used to characterize the parent coal, char, tar, soot and gaseous samples produced in this study. A detailed discussion on each technique is given in the following sections.

1.1.17.1 Proximate Analysis

Proximate analysis refers to the determination of the moisture, volatile matter and ash content in a coal or char. Proximate analysis was performed following the standard practice for proximate analysis for coal and coke set by the American Society for Testing Materials (ASTM). Minor changes have been made to accommodate the analysis in our lab. An electrically-heated, programmable oven was used for the proximate analysis.

1.4.1.1.1 Moisture

About 0.4 gram of char or 1 gram of coal was weighed and added into a platinum crucible. Then the sample was dried at 105^{o}C in a hood for two hours. The difference in weight before and after the drying procedure gives the moisture content of the sample.

1.4.1.1.2 Ash

When the sample was dried, the crucible was placed back into the oven. The oven temperature was ramped up to 500^{o}C in one hour. The sample was flooded with air every 30 minutes by opening the oven door. This ensured the sample was burning well. The temperature was then ramped up to 750^{o}C in another hour. Finally, the sample was soaked at 750^{o}C for at least 12 hours before the sample was cooled down and weighed again. The weight loss was used to calculate the ash content of the sample.

1.4.1.1.3 Volatile Matter

Volatile matter of the parent coal was determined in a manner similar to the ASTM test method D3175. About 1 gram of coal was placed into a small ceramic crucible sitting inside of a larger ceramic crucible. The larger crucible was used because it is much easier to handle and it helps to preserve all of the carbon deposit even for sparking samples. The small crucible was covered with a loose fitting lid and put into the oven. The whole set was soaked in 950^{o}C for exactly seven minutes before it was cooled down and weighed. The percentage loss of weight minus the percentage moisture gives the volatile matter content.

1.1.17.2 Ultimate Analysis

A Leco CHNS-932 elemental analyzer was used to obtain the mass fraction of carbon, hydrogen, nitrogen and sulfur of the coal, char and tar/soot samples. Nitrogen and hydrogen content of samples are the most important data in elemental analysis because it is believed that the nitrogen release is directly associated with these two elements. Elemental analysis is also necessary to close the elemental mass balances in this study.

Each sample was weighed into a tared silver crucible before being totally burned by pure

oxygen in the oxidation furnace in the analyzer. The combustion gas was then swept through the non-dispersive infrared absorption detection system. H_2O, SO_2 and CO_2 were measured in sequence, and the signals were converted into weight-percent hydrogen, carbon and sulfur. These infrared sensitive gases were then removed by special reagents, leaving only N_2. The remaining N_2 was measured by thermal conductivity and was converted to the weight percent of nitrogen in the sample. Oxygen content was calculated by difference. Five replicates of each sample were analyzed in succession and the results were averaged.

For coals and chars with high ash content, the samples were first ground to fine powders to reduce heterogeneity using a wig-l-bug device. Several coal standards, one coke standard, and a pitch standard, all with known compositions, were used to calibrate the coal, char and tar samples. An appropriate standard was used between every four samples to account for the possible machine drift. It was observed that the measurements for carbon and hydrogen were very accurate, usually within 1% (relative). Nitrogen and sulfur analyses were also sufficiently accurate. A detailed discussion on the variations in elemental analysis is presented in Appendix E of Zhang (2001).

1.1.17.3 Determination of Dry, Ash-free Mass Release by the ICP Technique

Inductively Coupled Plasma (ICP) atomic emission spectroscopy was used to determine the total mass release of the parent coal using a tracer technique described by Fletcher (Fletcher and Hardesty, 1992a). It is based on the assumption that the tracer is preserved during the pyrolysis.

A balance on the tracer balance results in the following equations:

$$m_{coal} \cdot y_{t,coal} = m_{char} \cdot y_{t,char} \qquad (4.1)$$

$$\frac{m_{char}}{m_{coal}} = \frac{y_{t,coal}}{y_{t,char}} \quad \text{dry basis} \qquad (4.2)$$

Then

$$\frac{m_{char,daf}}{m_{coal,daf}} = \frac{m_{char,dry} \cdot (1 - x_{ash,char,dry})}{m_{coal,dry} \cdot (1 - x_{ash,coal,dry})} \qquad (4.3)$$

$$\frac{m_{char,daf}}{m_{coal,daf}} = \frac{y_{t,coal}}{y_{t,char}} \cdot \frac{(1 - x_{ash,char,dry})}{(1 - x_{ash,coal,dry})} \qquad (4.4)$$

By mathematical manipulation, the mass release on a dry, ash-free basis is obtained:

$$MR = 1 - \frac{m_{char,daf}}{m_{coal,daf}} = 1 - \frac{y_{t,coal}}{y_{t,char}} \cdot \frac{(1 - x_{ash,char,dry})}{(1 - x_{ash,coal,dry})} \qquad (4.5)$$

Several tracers including silicon, titanium, aluminum, barium and zinc were tried, with Ti and Al giving the most reliable results. The difference of the mass release data obtained from these two tracers is usually less than 5% (relative). The mass release determined by the Ti or Al tracer technique was also compared with that obtained using the ash as a tracer and with the overall mass balance (the mass of char collected, divided by the mass of coal fed into the reactor). The final mass release reported is the averaged value of the two measurements using the Ti tracer and the Al tracer.

1.1.17.4 Chemical Structure Analysis by ^{13}C NMR Spectroscopy

The average chemical features of the Illinois #6 coal and the tars or soots from both the coal and model compounds were characterized by solid-state ^{13}C NMR spectroscopic techniques at the University of Utah. Three different NMR experiments were used to determine the carbon skeletal structure of a sample, including a standard cross-polarization and magic angle spinning (CP/MAS) experiment, a variable contact time experiment, and a dipolar dephasing experiment (Solum, et al. 1989). Fourteen structure parameters can be directly derived from the NMR spectra, giving the aromaticity and the relative amount of different types of functional groups of a sample. These structure parameters can be used to calculate the lattice parameters which are used in the CPD model (Fletcher, et al. 1992c). The lattice parameters include the aromatic

cluster size, attachments per cluster, cluster molecular weight, and bridge mass. For an estimation of the cluster mass and bridge mass, the dry, ash-free carbon content in the sample obtained from elemental analysis is also required.

1.1.17.5 Quantitative Analysis of the Pyrolytic Gas using the Fourier Transform Infrared Spectroscopy (FTIR)

Analysis of the pyrolysis gases is critical for following the nitrogen species after they are released from the coal. It is also essential for the closure of the mass balance and tracking the effects of other gas species on the nitrogen transformations.

Accurate measurement of the nitrogen species in the product gas stream from the FFB was the biggest challenge in this study. A large amount of CO and H_2 are burned in order to maintain the high temperature, high heating rate environment in the FFB that is necessary for the study of secondary nitrogen release. On the other hand, the coal loading has to be kept very low (about 1 gram/hour) to facilitate single particle reactions (which provide easily interpretable data for computer simulation). In addition, large quantities of nitrogen used to quench the reaction stream further dilute the concentrations of the gas species. Consequently, the concentrations of the nitrogen species in the collection system fall in the range of parts per billions (PPB).

Quantification of the nitrogen precursors (HCN and NH_3) during pyrolysis was previously attempted using an industrial toxic gas monitor (Hambly, 1998; Perry, 1999; Zhang, 1999). However, it was shown that the monitor was not capable of accurately measuring HCN and NH_3 in the FFB because of a large drift in the measurement, sometimes resulting in a standard deviation as high as 500% (Zhang, 1998). This is probably due to the interference of steam. A high resolution gas chromatograph (HP 6890) was also tested, however, the detection limit of the GC is only up to high parts per million (PPM) level. In addition, since the pyrolyzed gases are a complicated mixture, different types of detectors would be needed for the complete gas analysis (Flame Ionization Detector for hydrocarbons; Thermal Conductivity Detector for N_2; .Electron Capture Detector for electronegative species such as HCN).

Application of FTIR on trace-gas analysis in combustion systems has been reported by several researchers (Kallonen, 1990; Breton, 1992; Kassman, 1995; Ledesma, 1998). The techniques in IR spectroscopy can be used for most common combustion gas measurements (except for diatomic gases such as N_2, H_2, etc.), and at the same time eliminate the complexity and reliability problems experienced with systems employing multiple individual gas analyzers, each with their own detectors. By choosing a proper resolution and a suitable gas cell, FTIR spectroscopy replaces the following traditional analyzers:

Chemiluminescence for NO and NO_2

U. V. absorption for ozone

Non-dispersive infrared for CO

Gas Chromatography for hydrocarbons

Flame photometry for sulfur-containing species

However, since the reported trace gas concentrations were usually in the range of PPM (from 5 PPM to several hundred PPM), accurate measurement of trace gases was difficult. In addition, the measurement was also complicated by the harsh environment, which contained about 15% CO_2, 25% CO and small amounts of H_2O experienced in this study. All of these gases are extremely strong infrared absorbers, which can greatly interfere with the measurement of other low-concentration and weakly-absorbing species (such as HCN, C_2H_4 and C_6H_6).

1.4.1.1.4 FTIR Analysis Procedure

A BOMEM® MB-155 FTIR coupled with a 10 m multi-reflection gas cell (Infrared Analysis, Inc.) was successfully used to perform the on-line measurements of the PPB-level HCN, NH_3, hydrocarbons and other significant species in the FFB. The schematic of the sampling system is shown in Figure 1.4.7. The IR beam produced from a Globar IR source was introduced into the gas cell by several reflecting mirrors. The beam was reflected between the two sets of gold-plated mirrors installed at the two ends of the gas cell. After passing

through the specified path length, the IR beam was directed out of the gas cell and was received by a liquid N_2-cooled MCT detector (EG&G, Inc.) with a detectivity (D*) of 10^{10}. The detailed description of the gas cell can be found in the next section.

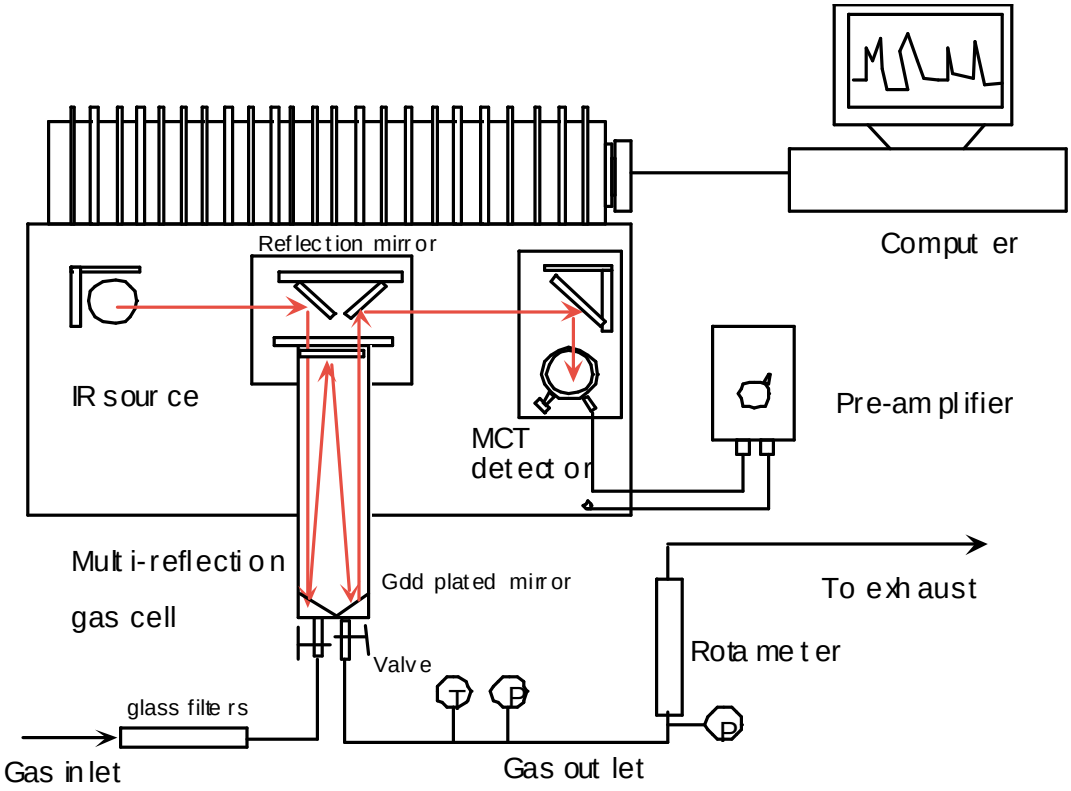

Figure 1.4.7. On-line FTIR gas analysis system.

The procedure for the gas cell purging and spectra collection can be summarized in the following steps. First, the gas cell was purged with pure nitrogen for 15 minutes to remove any possible contaminants. Next, the combustion gas without coal particles was pumped into the gas cell after passing several glass filters. The glass filters were used to remove any possible aerosols that might deposit on the gold-plated reflection mirrors. The reflection mirrors have to be kept extremely clean to ensure best results. After the gas cell was purged for 5 minutes (preliminary tests showed that 5 minutes was enough to totally purge the gas cell at the flow rates used in the gas sampling line), the single-beam background spectrum was collected by the

spectrometer. The gas cell was then purged again with pure nitrogen and refilled with the pyrolysis gas with coal particles flowing in the reactor. The sample was allowed to achieve thermal equilibrium for several seconds. Because the pyrolysis gas was quenched and water-cooled, the equilibrium was quickly reached in a few seconds within the gas cell as evidenced by the stability of the measured concentrations. A spectrum of the gas sample was collected, using the previously collected single-beam spectrum as the background for ratioing. The cell was then flushed with nitrogen to be made ready for the next sample. All the spectra were acquired with a resolution of 1 cm^{-1} and a spectral range of 500-4000 cm^{-1}. By using a liquid N_2-cooled MCT detector, the detection limit of the FTIR can be as low as 50 PPB for certain types of gases (including NH_3, C_2H_4 and C_2H_2). The detection limits for other gases are generally about 100 PPB. Figure 1.4.8 shows the existence of HCN and NH_3 in the coal pyrolysis spectra and a comparison with the corresponding reference spectra.

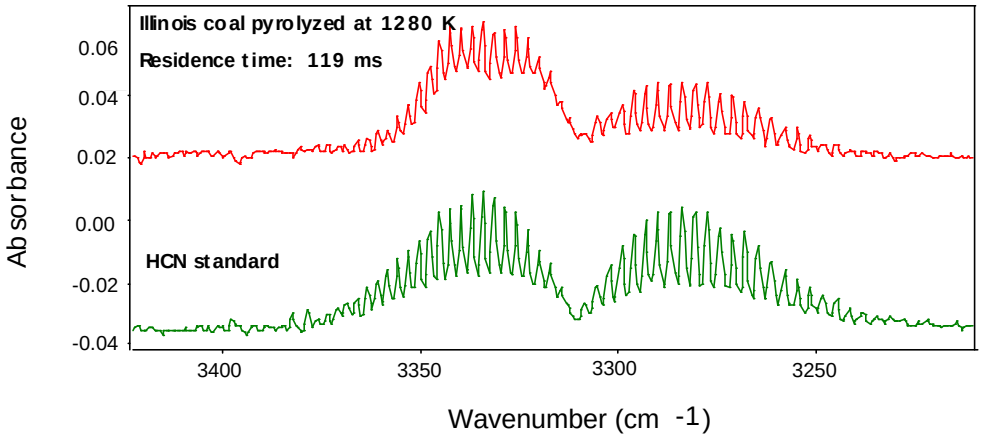

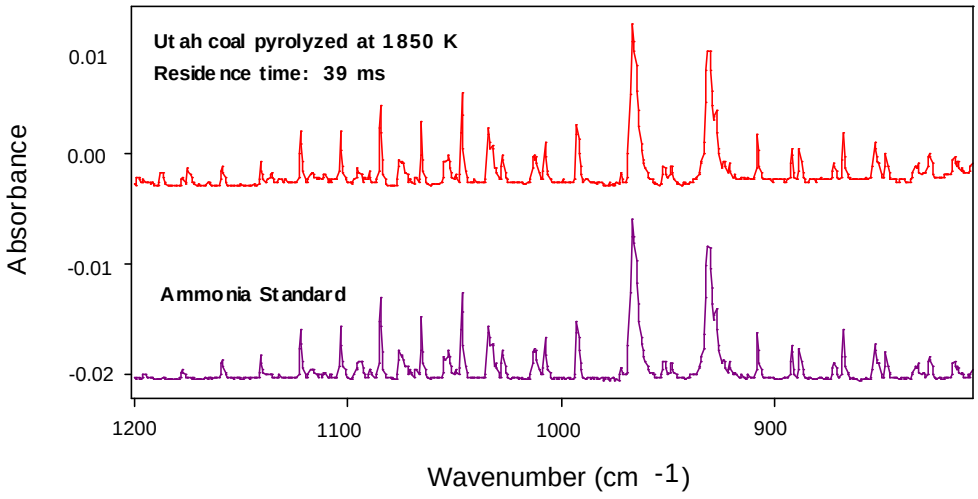

Figure 1.4.8. Identification of HCN and NH_3 in the coal spectra by comparison with the reference spectra.

1.4.1.1.5 Gas Cell Operation

The gas cell is a very important component in the FTIR measurement of the trace-gases in this study. It is impossible to measure low-ppb level trace gases without using a proper gas cell. The long-path heatable gas cell (type G-3-8-H-Ba-Au, Infrared Analysis, Inc.) used in this study was made of borosilicate glass, and therefore was resistant to most corrosive and reactive gases common in combustion systems.

The gas cell was constructed based on the original "White" cell design in which the basic three-mirror system is used to direct the IR beam within the gas cell (Hanst, 1999a). The basic set of four passes of the "White" cell is described as follows. The light from the source is directed into the gas cell. Initially, it is focused on to a real image in the entrance aperture of the cell. The beam then diverges and is collected by one of the two objective mirrors placed on one end of the gas cell. The objective mirror is a spherical mirror situated two focal lengths from the image so that it re-focuses the image, inverted, on the lower part of the opposite field mirror, which has the same focal length as the objective mirror. The field mirror is designed so that the reflected diverging beam falls entirely on the second objective mirror. When the beam is re-

focused and redirected out of the cell, there are four passes of the IR beam (see Fig. 4.9).

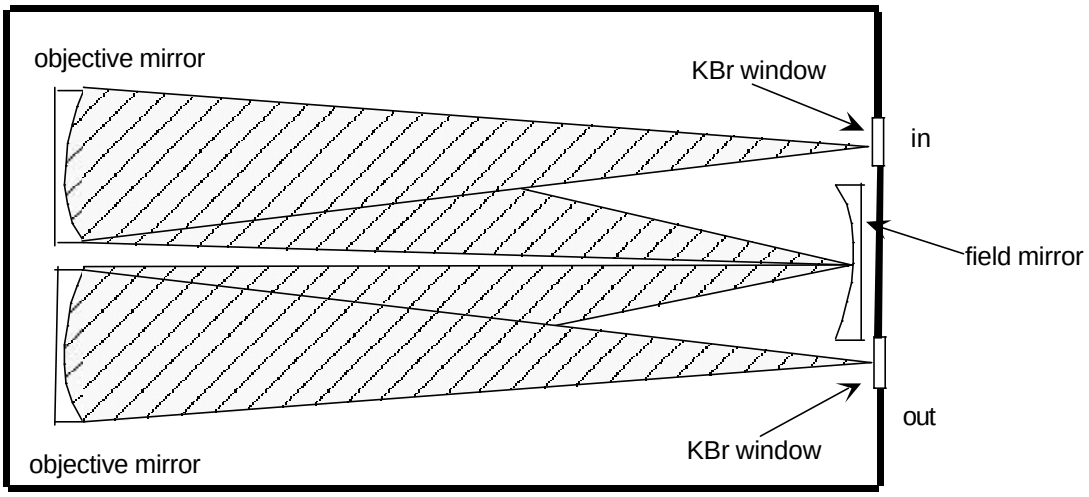

Figure 1.4.9. Three mirror optical system with a basic set of four passes (White, 1942).

By manipulating the position of the field mirror, different path lengths in multiples of four passes can be achieved. In the cases where more than four passes are achieved, there are two rows of images on the field mirror. The number of images on the lower part of the field mirror determines the path length. The number of images allowed in the row depends on the placement of the first image in the lower part of the field mirror. If it falls exactly on the centerline, no more than four passes are possible. The further to the right the first image falls, the greater the number of passes allowed. In practice, the number of passes is determined by counting the number of images in the bottom row of the field mirror and multiplying by four. In this study, 48 passes were used with 12 images in the bottom row (see Fig. 4.10). The total path length was calculated to be approximately 9.75 m.

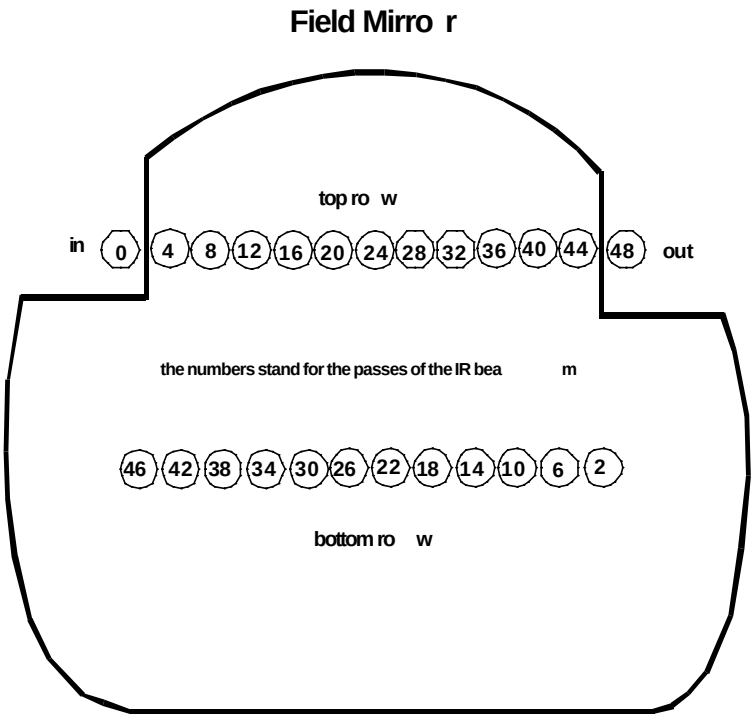

Figure 1.4.10. Placement of images on the field mirror in this study.

The determination of a proper path length is critical in accurate measurement of trace gases in a harsh environment encountered in the FFB. According to Beer's law, the absorbance of an IR beam is proportional to the concentration of the absorbing media and the path length it travels:

$$-\log\left(\frac{I}{I_0}\right) = A = a \cdot c \cdot L \qquad (4.6)$$

I: intensity I_o: incident intensity a: absorption coefficient

c: concentration of the absorber L: path length A: absorbance

The concentrations of the absorbing species at a certain experimental condition were fixed. Variation of the path length will result in a change of the absorbance. Increasing the path length

will raise the absorbance of a certain species, whose peak will be higher and much easier to identify. Since the concentrations of HCN and NH_3 are extremely low (low-ppb), increasing the path length will facilitate the accurate measurement of these species. However, because there are also large quantities of CO and CO_2 in the system, the increase of path length will simultaneously boost the absorbance of these strong IR absorbers, which results in serious interference with the measurement of other weakly-absorbed or low-concentration species. For example, the strongest absorption peak for HCN is at 712 cm^{-1}, but this peak cannot be used in the analysis, since a strong CO_2 peak absorbed at 680 cm^{-1} significantly overlaps with the HCN peak, making the measurement extremely difficult. Finally, it was found that a path length of 9.75 m would give the best results for most of the conditions used in this study.

1.4.1.1.6 Verification of the Reliability and Reproducibility

Obtaining reliable and repeatable gas measurement is critical in the FTIR analysis. The gas measurement can be affected by many factors.

1.4.1.1.6.1 Temperature and Pressure Effects

It is extremely important to carefully control both the temperature and pressure when performing any quantitative analysis on gas species. Absorption band intensities, widths, and areas are dependent upon both parameters. In this study, all the spectra (reference, background and sample spectra) were collected at room temperature ($23\pm1^{o}C$) and ambient pressure (12.4 psia, at the altitude of BYU). Therefore, the spectra were easily manipulated without worrying about the possible absorption band broadening and band shift caused by changes of temperature and pressure.

1.4.1.1.6.2 Memory Effects

The results from trace-component analysis in long-path gas cells can be adversely affected due to the selective adsorption or desorption of materials from the cell walls (Compton, 1993). Figure 1.4.11 shows the measured concentration of the major species in the gas phase when the Black Thunder coal was pyrolyzed at 1858 K. Those concentrations reported were acquired at

different residence times after the gas cell was flushed. These data demonstrate that negligible

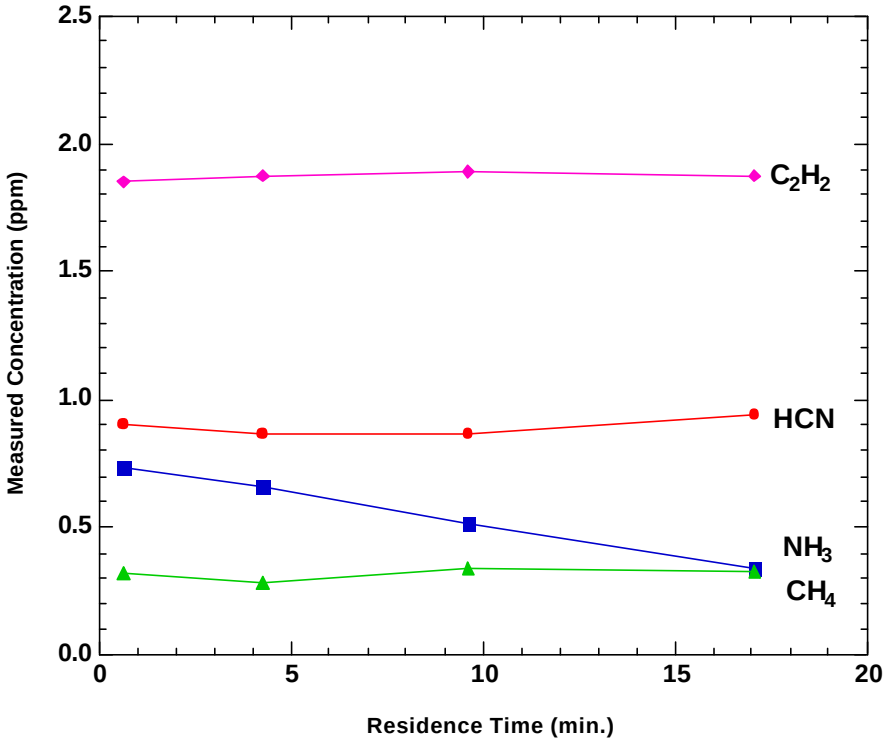

Figure 1.4.11. Measured concentration of major species at different residence times in the gas cell.

selective absorption occurred for all the gases except ammonia. Ammonia decays roughly linearly with residence time. In order to remove the cell "memory", the flushing of the gas cell by pure nitrogen was extended to 15 minutes and a spectrum was then collected to verify the absence of any species from the subsequent degassing. The spectra showed that the concentration of ammonia left in the gas cell after flushing was negligible. In order to minimize wall adsorption effects, NH_3 was measured immediately after the gas cell was filled, requiring about 40 seconds (10 scans). Other gases were measured using 144 scans to obtain a better signal to noise ratio, since the signal to noise ratio is proportional to the square root of the

number of scans (Ingle, 1988).

1.4.1.1.6.3 Coal Heterogeneity and Feed Rate

As indicated earlier, the coal samples were dried and split off evenly in order to reduce the heterogeneity. However, particle-to-particle variations in particle size, ash content and elemental composition cannot be totally eliminated. In addition, although the measured coal feed rate was fairly stable over a relative long time (several minutes), the amount of coal fed into the burner was not essentially constant at each instant. Therefore, the gas concentration also changed during the experiments. Since the coal feed rate was much more steady over a long period of time, the gas cell was allowed to be purged continuously for five minutes before a spectrum was collected. Repetitive measurements showed that the fluctuations in gas concentrations were not serious, as demonstrated in Figure 1.4.12. All of the concentration data for various species are tabulated in Appendix A of Zhang (2001).

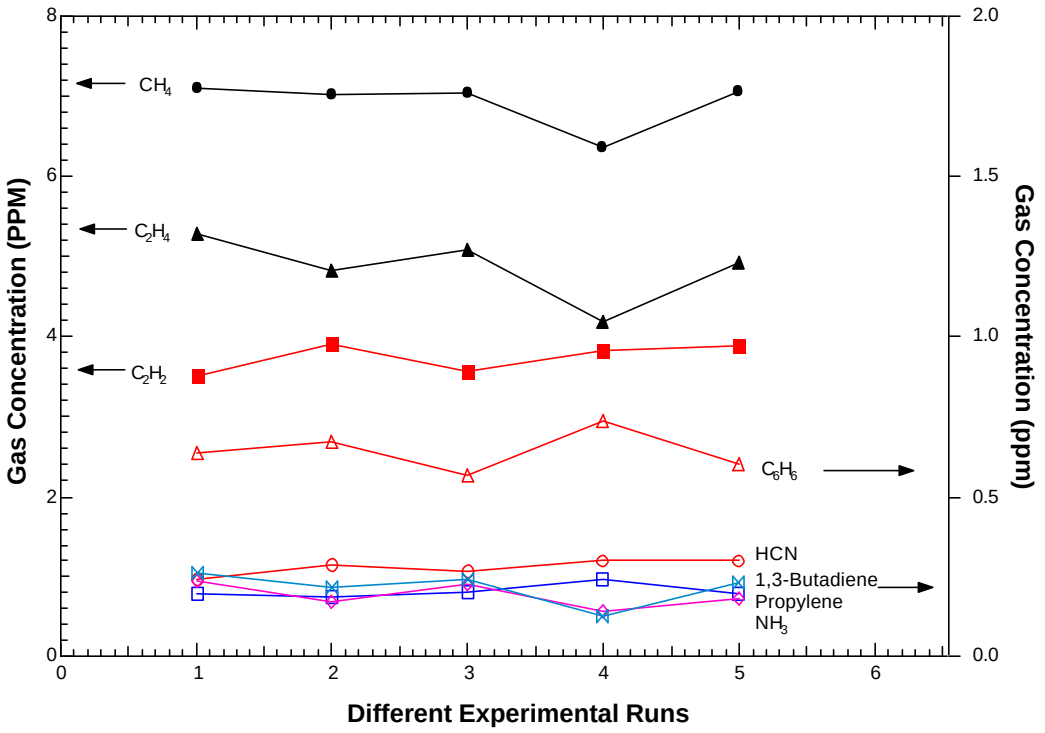

Figure 1.4.12. Duplicate FTIR measurements of major pyrolysis gas species (The Illinois #6 coal pyrolyzed at the 1 inch location at 1411 K).

1.4.1.1.7 Quantification of the Gas Species

Prior to the quantitative analysis, calibration gases of the major species found in the pyrolysis gas were purchased from different sources after being certified to the desired concentration (see Table 1.4.3).

These reference gases were then diluted to the appropriate range using nitrogen as diluent. The calibration curves were determined from each calibration gas at three different concentrations (roughly 1ppm, 5 ppm and 15 ppm) at the same temperature and pressure as the pyrolysis gas. These calibration curves were only used to check the extent of the linearity of the absorbance versus concentration for each reference gas. Special care was taken to ensure that the concentration range of each gas was within the dynamic range over which the analytical curve was linear. A linear calibration curve for each gas was used in this study in order to facilitate the detection of abnormalities and because of mathematical ease of use (easy subtraction, accurate ratioing). The exact concentrations of a reference gas were determined by a quantitative FTIR program called QASoft developed at Infrared Analysis, Inc (Hanst, 1999b). The corresponding standard gas spectrum (with known concentration) from a quantitative database was used to calibrate the reference gas. This practice ensures that a reference gas is always calibrated by the same standard gas spectrum, which is digitized in the database. Signal drift caused by the modification of the optical path and detector is unavoidable. Using a single, digitized standard spectrum introduces less error than the traditional calibration method which relies on the calibration curve established by dilution of a certified standard. One of the drawbacks of the traditional method is that the certified standard may decay in the container, resulting in additional uncertainties.

Table 1.4.3. Reference Gas Concentrations and Their Origin.

Reference gas	Concentration	Origin
Acetylene	99.8 ppm	SUPELCO
Ethylene	105 ppm	SUPELCO
Methane	97.8 ppm	SUPELCO
Hydrogen Cyanide	9.8 ppm	AGA Specialty Gas
Ammonia	44.5 ppm	AIRGAS
Propyne	98%	SIGMA ADRICH

These reference gases were then diluted to the appropriate range using nitrogen as diluent. The calibration curves were determined from each calibration gas at three different concentrations (roughly 1ppm, 5 ppm and 15 ppm) at the same temperature and pressure as the pyrolysis gas. These calibration curves were only used to check the extent of the linearity of the absorbance versus concentration for each reference gas. Special care was taken to ensure that the concentration range of each gas was within the dynamic range over which the analytical curve was linear. A linear calibration curve for each gas was used in this study in order to facilitate the detection of abnormalities and because of mathematical ease of use (easy subtraction, accurate ratioing). The exact concentrations of a reference gas were determined by a quantitative FTIR program called QASoft developed at Infrared Analysis, Inc (Hanst, 1999b). The corresponding standard gas spectrum (with known concentration) from a quantitative database was used to calibrate the reference gas. This practice ensures that a reference gas is always calibrated by the same standard gas spectrum, which is digitized in the database. Signal drift caused by the modification of the optical path and detector is unavoidable. Using a single, digitized standard spectrum introduces less error than the traditional calibration method which relies on the calibration curve established by dilution of a certified standard. One of the drawbacks of the traditional method is that the certified standard may decay in the container, resulting in additional uncertainties.

The reference gas was calibrated using a novel analytical technique called RIAS (Region Integration and Subtraction) developed by Philip Hanst. RIAS was originally developed to take advantage of fine structures (very small integration regions) in the spectra. However, in the reference gas calibration, the spectral range over which the integration was made was intentionally chosen to be broad. Because the standard spectra in the database were recorded by a different spectrometer and a different detector, differences of the fine structures in the standard spectra and the reference spectra are expected. A broad integration region covering many peaks helps to reduce such errors. For other species of less importance to this project, i.e., COS, SO_2 and CS_2, the corresponding standard gas spectra in the database were used directly to make the measurements.

After the reference gas was calibrated, the concentrations of the target compound were determined using GRAMS/32® (Galactic Industries Corporation) on the basis of the integrated area of a sample and a reference gas over the same spectral region (Figure 1.4.13). The integration region and the baseline in the spectra were determined beforehand for the integration using the characteristic absorption peak of each gas. Spectral regions used for quantitative analysis of each gas are given in Table 1.4.4.

The experimental data showed that the nitrogen is balanced within 10% for most cases. FTIR has proven to be a very effective way to measure the PPB-level gas species simultaneously and accurately in this study.

Table 1.4.4. Spectral Regions used in the Quantitative Analysis.

Compound	Spectral Region, cm^{-1}
HCN	3250-3400
NH_3	900-1000
C_2H_2	3200-3400

C_2H_4	900-1000
CH_4	2855-3185
C_6H_6	1000-1080
Propylene	800-1100
1,3-butadiene	800-1000
NO	1750-1970
SO_2	1300-1400
COS	2000-2100
CS_2	1480-1560

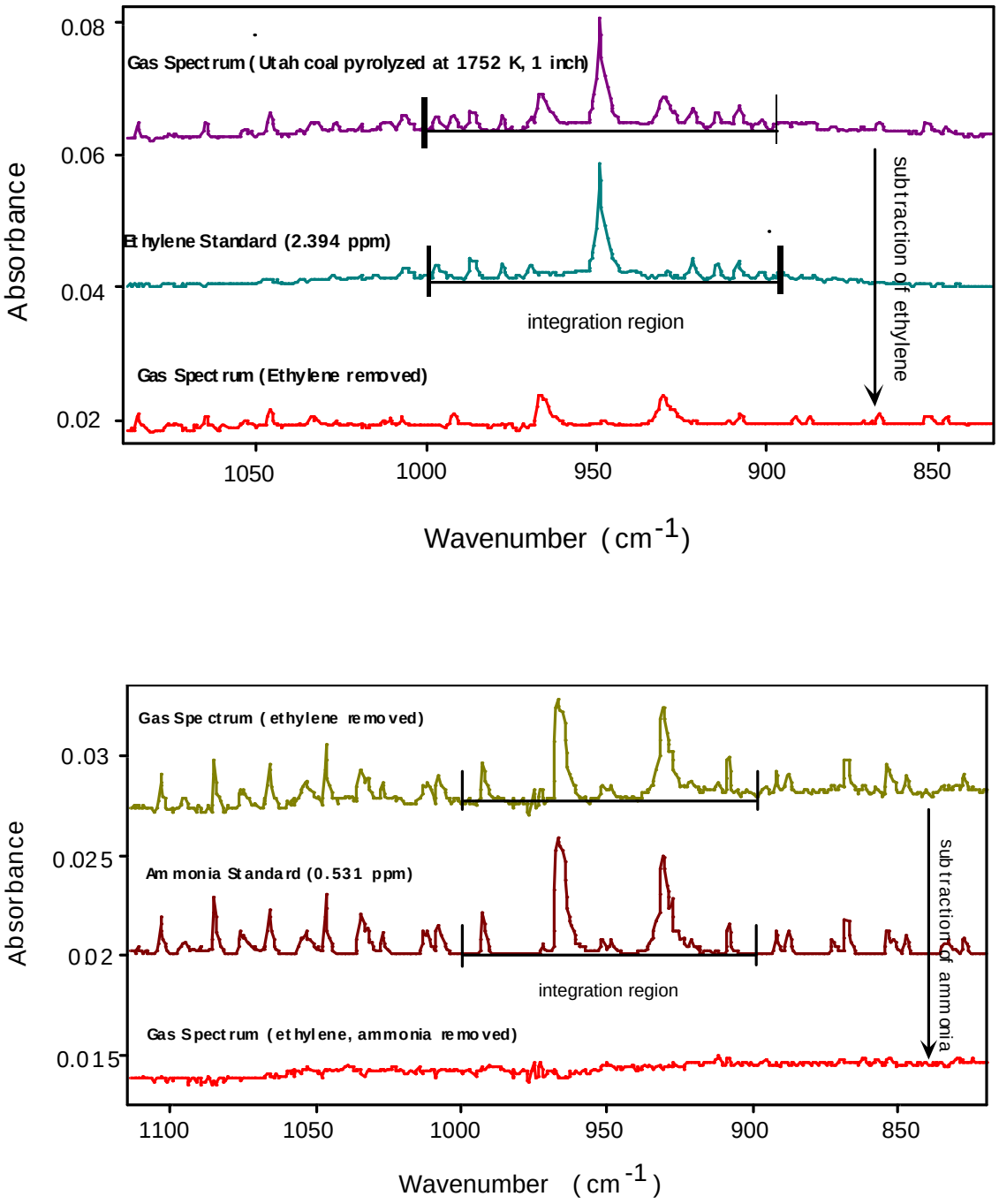

Figure 1.4.13. Demonstration showing the determination and subtraction of ethylene and

ammonia peaks from the coal spectra.

1.5 SECONDARY REACTIONS OF COAL VOLATILES

1.1.18 Coal Characterization

The proximate and ultimate analyses of the four coals, ranging from lignite to high-volatile bituminous, are summarized in Table 1.5.1. The experimental methods used to obtain these measurements are explained in Chapter 4. In the ultimate analysis, oxygen content was determined by subtracting out the summation of carbon, hydrogen, nitrogen and sulfur. Because the sulfur values as determined by the elemental analyzer include both organic and inorganic sulfur, the oxygen values are somewhat under-estimated.

1.1.19 Residence Time Determination

As described in Chapter 4, the residence times of a coal particle at certain collection locations were measured using a high-speed camera. However, the low-resolution camera can only track those particles with sufficient luminance reaching a certain height in the FFB. The residence time, used for a particle traveling from the tip of the injection tube to the first luminescent point where it can be recognized, has to be accurately estimated in order to obtain the total residence time. The final residence time reported is actually the summation of the time calculated during the non-luminous zone and the time measured after the first luminescent point.

The residence time over the non-luminous zone was calculated based on a particle momentum balance. The coal particles were carried upward by the carrier N_2 in the injection tube, as shown in Figure 1.5.1. Since the injection tube is about 300 mm long, the coal particle should reach its terminal velocity at the tip of the tube. This terminal velocity also served as the

Table 1.5.1. Proximate and Ultimate Analyses of the Coals Used.

Coal	Rank	Proximate Analysis (wt%)	Ultimate Analysis (wt%, daf)

		Ash	Volatile Matter (daf)	C	H	N	O$^{=}$	S
Illinois #6‡	hvCb	12.3	48.8	75.7	5.2	1.5	12.8	4.6
Utah	hvBb	9.8	49.3	81.4	5.9	1.6	10.5	0.5
Black Thunder ∅	subC	6.8	52.3	76.6	5.0	1.1	16.9	0.5
Knife River#	lignite	11.2	74.7	70.8	4.8	1.0	21.9	1.5

$^{=}$: O=100-(C+H+N+S)

‡: Ultimate analyses were obtained from Dr. Mark Solum of the University of Utah

∅: Ultimate analyses were obtained from the Commercial Testing and Engineering Company

#: Proximate and ultimate analysis for Knife River lignite were obtained from Dr. Eric Eddings of the University of Utah

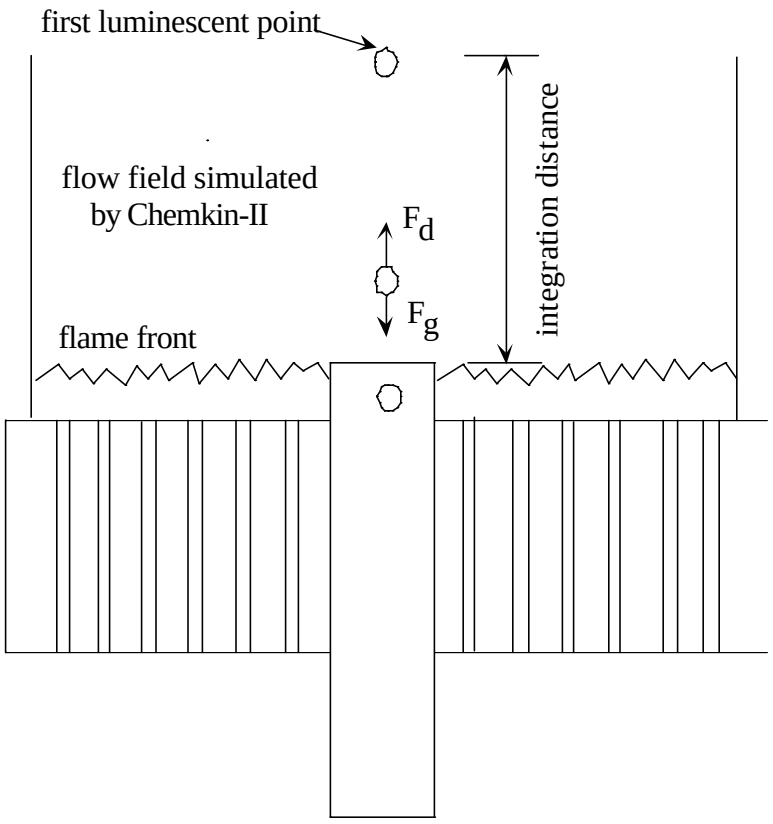

Figure 1.5.1. Illustration of the non-luminous zone in the Flat Flame Burner for the coal particle residence time calculations.

initial velocity in the calculations of the residence time. The two forces acting on a coal particle, namely the drag force and the force of gravity, can be modeled assuming the coal particle is a sphere with a diameter of D_p and density of ρ_p.

Since the particle size is on the order of microns, *Stokes Law* can be applied for the estimation of the drag force:

$$F_d = 3\pi\mu_g v_\infty \qquad (5.1)$$

$$v_\infty = v_p - v_g \qquad (5.2)$$

v_∞: slip velocity between the particle and the entraining gas

μ_g: gas viscosity

The gravitational force acting on the particle is

$$F_g = \frac{\pi}{6} D_p{}^3 (\rho_p - \rho_g) g \qquad (5.3)$$

Then, the acceleration of the particle can be expressed as

$$a = \frac{F_d - F_g}{m_p}$$

$$= \frac{3\pi\mu_g D_p v_\infty - \frac{\pi}{6} D_p{}^3 (\rho_p - \rho_g) g}{\frac{\pi}{6} D_p{}^3 \rho_p} \qquad (5.4)$$

$$= \frac{18\mu_g v_\infty}{D_p{}^2 \rho_p} - (1 - \frac{\rho_g}{\rho_p}) g$$

The terminal velocity of a coal particle can be calculated by setting the acceleration to zero.

$$v_{p,terminal} = \frac{(\rho_p - \rho_g) g D_p{}^2}{18\mu_g} \qquad (5.5)$$

For the Illinois #6 coal with a density of 1210 kg/m^3 and an average diameter of 60 μm, the terminal velocity is about 0.133 m/s. This particle velocity was used as the initial velocity for all

of the coals. The residence time was obtained by integrating over the height z of the following differential equation set:

$$\begin{cases} \dfrac{dz}{dt} = v_p \\ \dfrac{dv_p}{dt} = \left(\dfrac{18\mu_g (v_g - v_p)}{D_p{}^2 \rho_p} - \left(1 - \dfrac{\rho_g}{\rho_p}\right) g \right) \\ v_{p,o} = 0.133 \end{cases} \qquad (5.6)$$

In equation 5.6, the only unknowns are the density, viscosity and velocity of the gas. These values were estimated by simulations using the Chemkin-II premixed code (Kee, et al. 1985). The flame in the FFB was assumed as a premixed flame, although in reality it consists of dozens of tiny diffusion flames. This should be a valid assumption due to the rapid mixing of the fuel and oxidizer. Another assumption was that the flow is one-dimensional, since the premixed code can only handle one-dimensional flow. Although there are some boundary layer effects near the wall of the FFB, previous measurements had shown that the temperatures were almost uniform radially around the centerline (Ma, 1996). The total mass flow rate and measured centerline temperature profiles were used as input in the Chemkin simulation. A comprehensive $CO/H_2/O_2$ combustion mechanism was adapted from a published source (Yetter, et al. 1991). The mechanism was modified later into the Chemkin format (Austin, 1999) and was used throughout all the calculations. The final version of the mechanism can be found in Appendix B of Zhang (2001).

During the measurement, it was also found that the length of the non-luminous zone is dependent on the total flow rate and the temperature condition. The integration of the residence time was only made over that length. The calculated residence times, the total mass flow rates, and the peak temperatures for all the temperature settings are tabulated in Table 1.5.2.

Table 1.5.2. Calculated Residence Times in the Non-Luminous Zone.

Conditions	1858 K	1752 K	1618 K	1534 K	1411 K
total flow rate (g/cm^2-sec)	0.033	0.034	0.039	0.034	0.024
measured integration length (mm)	12.7	16.5	13.3	12.7	33.6
calculated residence time (ms)	11.9	15.2	12.1	14.7	42.2

The residence time after the first luminescent point, as measured by the high-speed camera, was then added to the calculated residence time in the non-luminous zone to obtain the total residence time for a given height. For the two lowest temperature conditions in this investigation, the residence times were calculated using a bulk gas velocity, since no visual particle velocity measurement could be made at these conditions. The 1411 K condition was used as a reference for the calculation.

$$\dot{m} = \rho v A \tag{5.7}$$

$$\frac{v_2}{v_1} = \frac{T_2}{T_1} \cdot \frac{\dot{m}_2}{\dot{m}_1} \cdot \frac{M_1}{M_2} \tag{5.8}$$

$$\Delta t = \frac{\Delta z}{v} \tag{5.9}$$

Where T, M, $\dot{m}$ and v stand for temperature, molecular weight, mass flow rate and gas velocity, respectively.

The mean molecular weight of the gas was estimated from an equilibrium calculation using

the NASA-Lewis code. Equation 5.8 was used to calculate the velocity of a particle in a new condition, and the residence time over a small step of height can be obtained from equation 5.9. The total residence time was obtained by adding all the small time steps together. The residence times for any given height at all the conditions are presented in Table 1.5.3. These values are also shown in Figure 1.5.2 with a residence time measurement at Sandia National Laboratories as a reference. The Sandia measurements were made at 1700 K in a similar reactor.

Table 1.5.3. Residence Time versus Height at All Conditions.

Height (in.)	1159 K (ms)	1281 K (ms)	1411 K (ms)	1534 K (ms)	1618 K (ms)	1752 K (ms)	1858 K (ms)
1	46	38	33	19	18	19	17
3	105	88	74	44	38	43	39
5	143	119	102	66	58	63	58
7	182	153	130	88	76	84	78

1.1.20 Mass Release

1.1.20.1 Results

The mass release data measured at selected collection elevations for all the coal types are shown in Figures 1.5.3 through 1.5.6. The mass release approached an asymptote at the most severe pyrolysis condition (highest temperature and longest residence time) for all cases in this study. That means the ultimate value of the mass release at the current heating rate was reached and the devolatilization reaction was essentially completed at the most severe condition. Since the

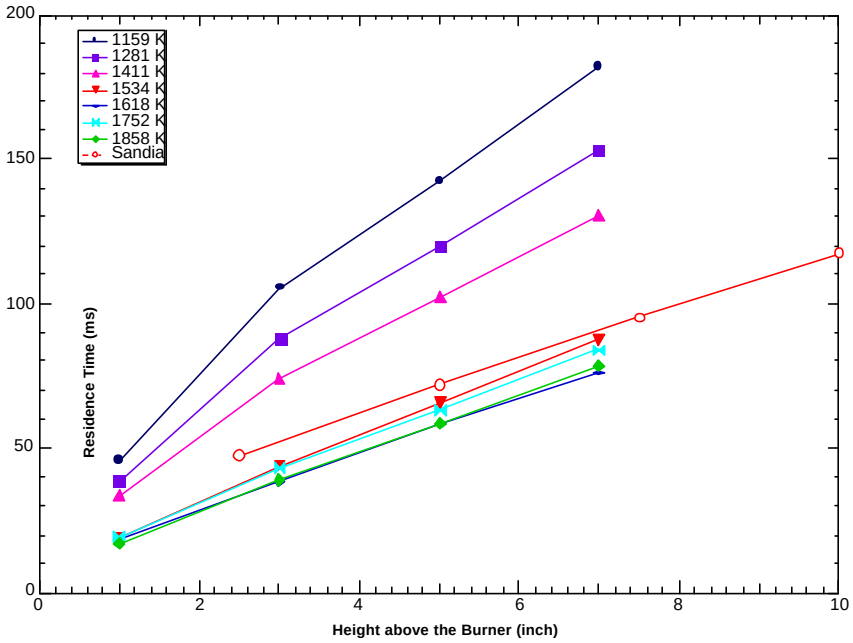

Figure 1.5.2. A plot of residence time versus height for all conditions (the dashed line represents residence times measured at the Sandia National Lab using a similar reactor at about 1700 K).

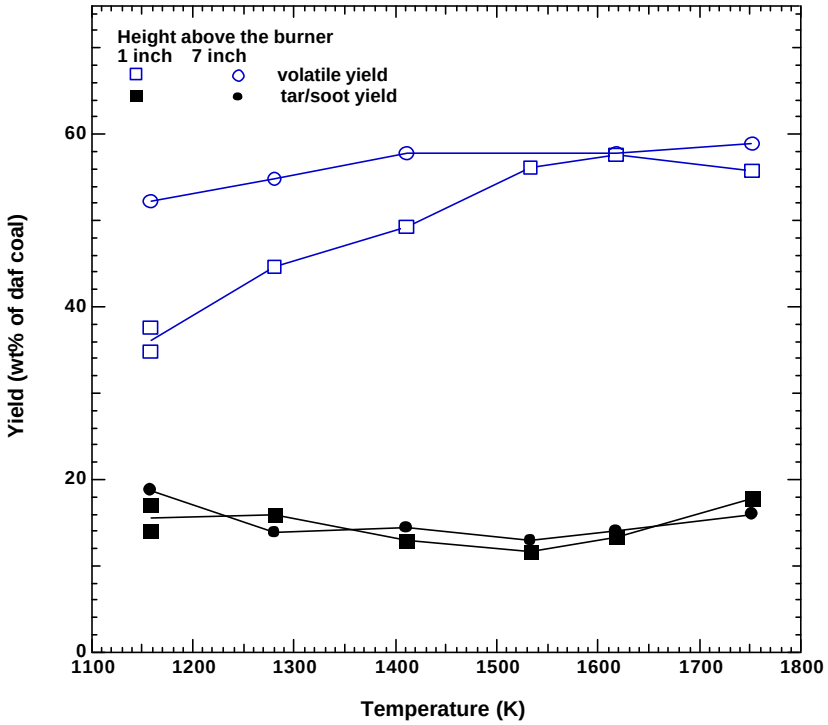

Figure 1.5.3. Volatile and tar/soot yields of the Illinois #6 coal at selected collection heights.

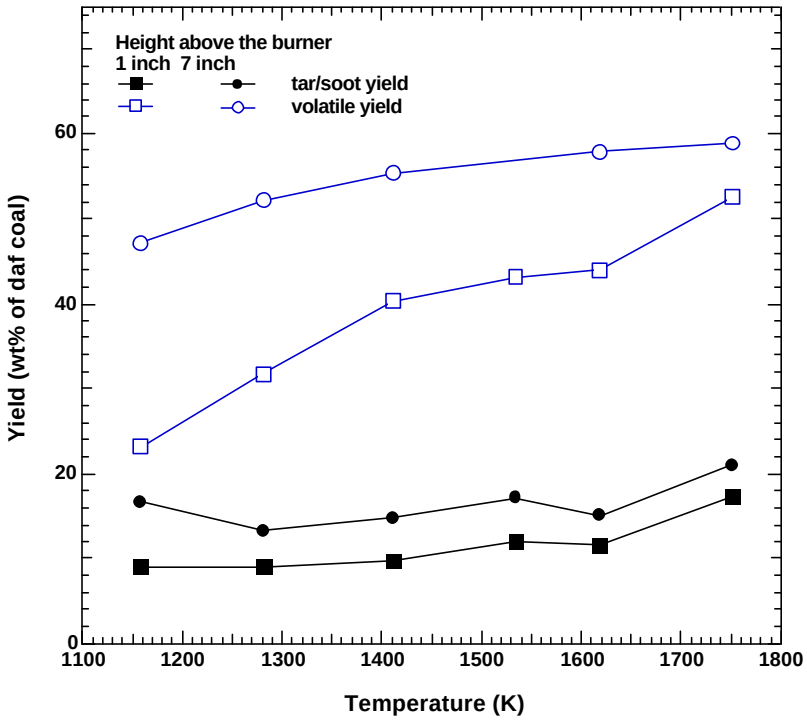

Figure 1.5.4. Volatile and tar/soot yields of the Utah coal at selected collection heights.

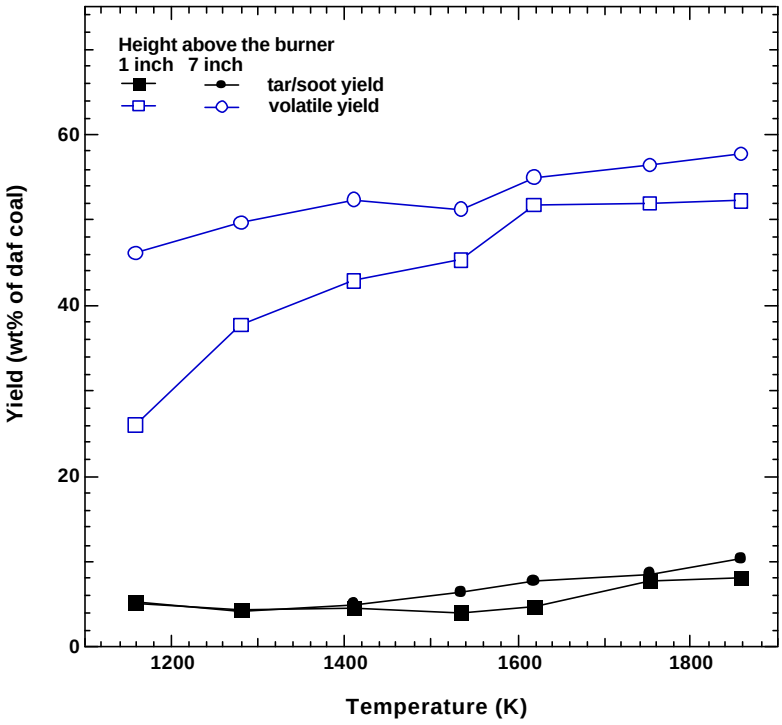

Figure 1.5.5. Volatile and tar/soot yields of the Black Thunder coal at selected collection heights.

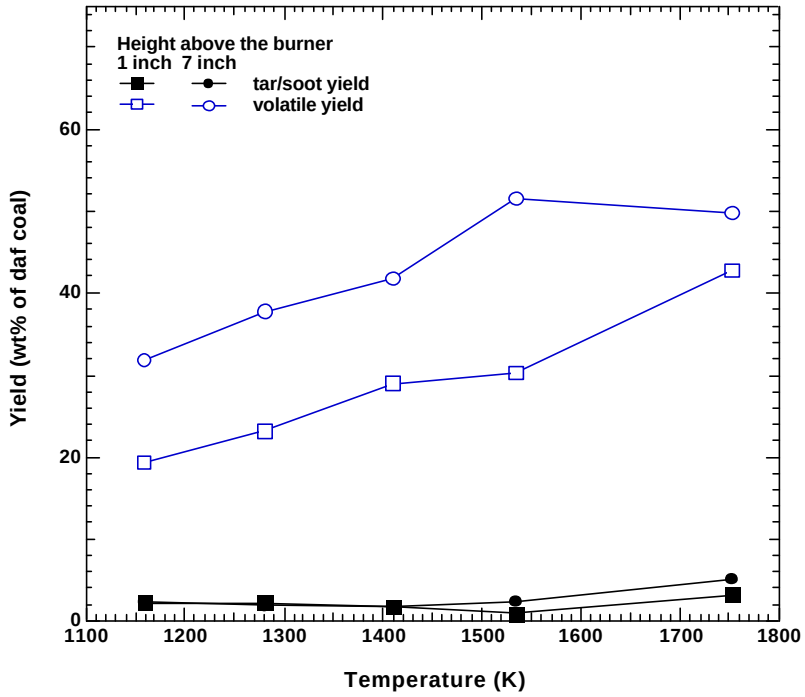

Figure 1.5.6. Volatile and tar/soot yields of the Knife River lignite at selected collection heights.

nitrogen released during the devolatilization is the focus of this study, the ultimate mass release will help to better understand the relationship between the nitrogen release and the total volatile yield.

As seen in these figures, a large difference in the total mass release was observed between the 1 inch and 7 inch data. It is interesting that the total mass release observed at 7 inches in the 1159 K condition is very close to that obtained at 1 inch in the 1858 K condition for all coals except lignite. This indicates that temperature and residence time both influence the total mass release. Such an effect was noticed in a previous study on primary tar yields (Chen, 1991). The data obtained in the current study indicate that secondary reactions are also strongly influenced by temperature *and* residence time.

1.1.20.2 Rank Dependence of Ultimate Mass Release

The ultimate mass release for the four coals used in this study are compared with the data reported by other researchers, as shown in Figure 1.5.7. The ultimate mass release refers to the asymptotic value achieved at the most severe condition for each coal in this study. The ultimate mass release for these experiments are remarkably consistent with Chen's data, showing that the ultimate mass release is approximately constant from high-volatile bituminous to subbituminous. However, the ultimate mass release decreases for lignites and low-volatile coals. The ultimate mass release data reported by Pugmire and coworkers are also comparable with the results in this study, showing that the ultimate mass release for a lignite is lower than that for a bituminous coal (Pugmire, et al. 1990).

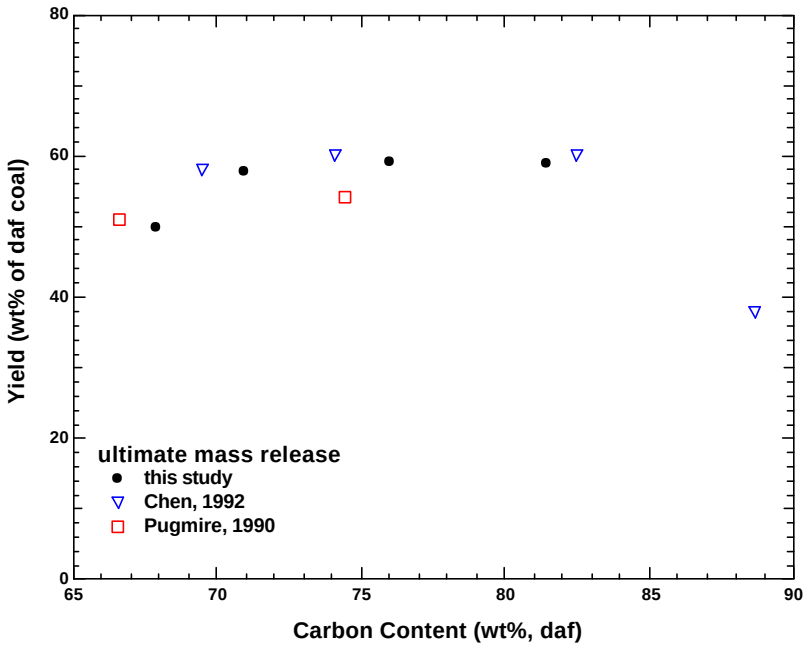

Figure 1.5.7. Rank dependence of the ultimate mass release.

1.1.21 Secondary Reactions of Coal Volatiles

This section of experimental results and discussion is grouped into three sub-sections. First, the results of measured tar and soot yields and the distributions of light hydrocarbons from the coal pyrolysis are presented. Second, a modeling effort to describe the secondary reactions of coal volatiles under high temperature, rapid-heating conditions is presented. Finally, a comparison and discussion of the results in this study with those reported in the literature is presented.

1.1.21.1 Results

1.5.1.1.1 Tar and Soot Yields

1.5.1.1.1.1 Temperature Effects

A graphical summary of the measured tar/soot yields at all conditions is plotted in Figure 1.5.8, so the trends can be clearly examined. Despite the scatter in the data, it is found that the "tar plus soot" yields first decrease with temperature, then increase at higher temperatures. This observation is different from the findings of Chen (1991) and Nenniger (1986) which showed that the sum of the tar and soot yield is constant during secondary pyrolysis.

The trend of the decrease of "tar plus soot" yield at low temperatures followed by an increase at high temperatures is especially true for the low rank coals. The tar/soot yields collected at the 7 inch location in the 1752 K condition for the Knife River and Black Thunder coals are 4.36% and 10.32%, respectively. At the 1281 K condition, these values are 1.79% and 4.17% respectively. The measured yields are more than doubled when the temperature was changed from 1281 K to 1752 K, which cannot be explained by experimental error. During the experiments, it was found that the color of the deposits collected on the filters started to become darker at 1281 K, which implies that soot began to form at that temperature. This is consistent

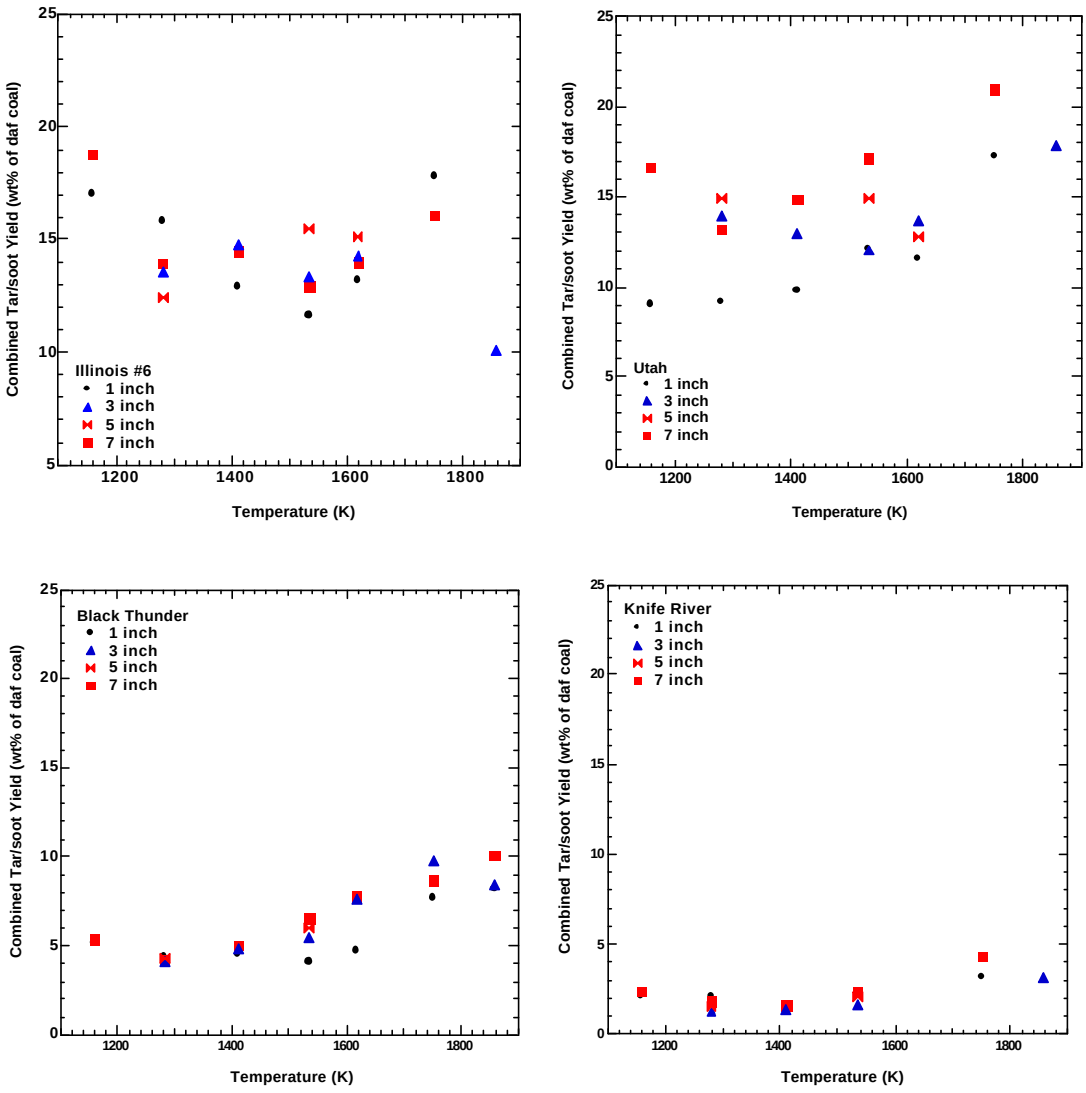

Figure 1.5.8. Measured tar/soot yields with temperature for the coals in this investigation.

with the soot inception temperature from the pyrolysis of the model compounds in this study and other research (Glassman, 2000). The primary tar usually starts to decline after reaching the ultimate yield at about 1000 K (Fletcher, et al. 1992). At low temperatures (1000-1300 K), the decline of the tar yield is due to thermal cracking reactions, which lead to the release of

secondary gases (light hydrocarbons, CO and CO_2) (Doolan, et al. 1986). At these temperatures, soot formation is still insignificant, causing the measured tar and soot yield to decrease with temperature. The high soot yield at high temperatures (>1800 K) cannot be explained by direct tar conversion alone; the light gas released from char seems to participate in the soot formation. It should be noted that the temperature at which the tar and soot yield starts to increase is different for different coal ranks. This means that the tar/soot yield not only depends on the secondary reactions of the tar but also strongly depends on the tar structure and reactivity.

1.5.1.1.1.2 Residence Time Effects

The tar and soot yields measured at different residence times can be used to understand the detailed secondary reaction kinetics of the tar. Since there is a certain portion of nitrogen trapped in the tar and soot, elemental analysis of the tar also reveals the nitrogen release during secondary reactions. Figures 1.5.9 and 1.5.10 show the variation of the measured tar and soot yields with residence time at different temperature conditions for the Illinois #6 and Black Thunder coals, respectively. At the 1281 K condition, the tar cracking reaction predominated, resulting in a net decline of the combined tar/soot yield. Significant soot formation from tar was observed at 1534 K, as seen by the rapid growth of the tar/soot yield in the figures. At the 1858 K condition, the soot growth was observed to occur at a slower rate. Such trends can be viewed more clearly by examining the slopes of the soot yield versus residence time curves at different temperatures as shown in Figure 1.5.10. These data indicate that the rate of soot growth was highest in the temperature range from 1500 K to 1700 K.

1.5.1.1.2 Gas-Phase Product Distributions

CO, CO_2 and H_2O are products of CO combustion in the FFB. Because the coal loading is very low (about 1 g/hr), the incremental amount of these gases released from the coal could not be measured accurately. The hydrocarbons released from the coal during pyrolysis were carefully measured and are presented here.

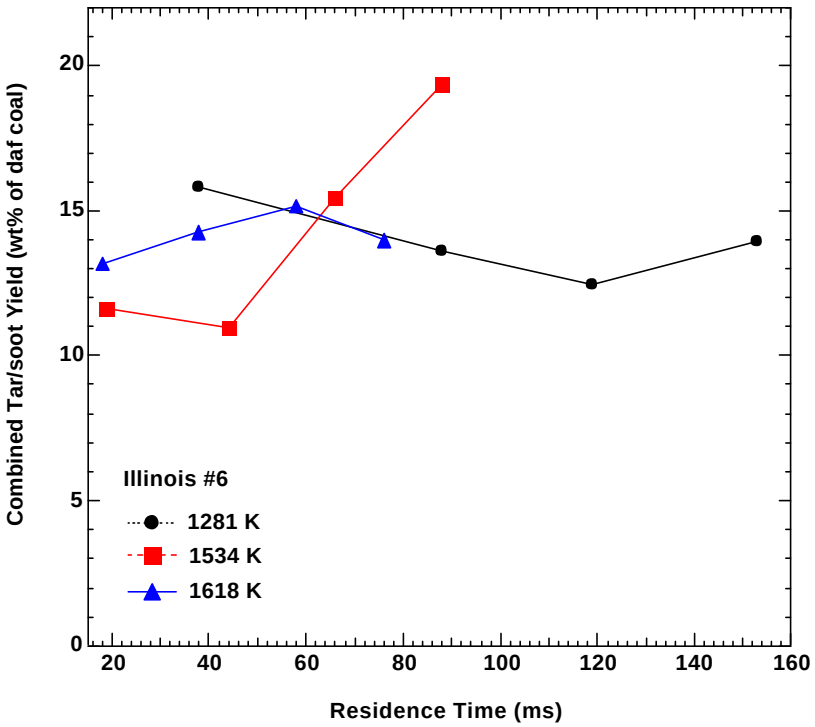

Figure 1.5.9. Tar / soot yield versus residence time for Illinois #6 at various temperatures.

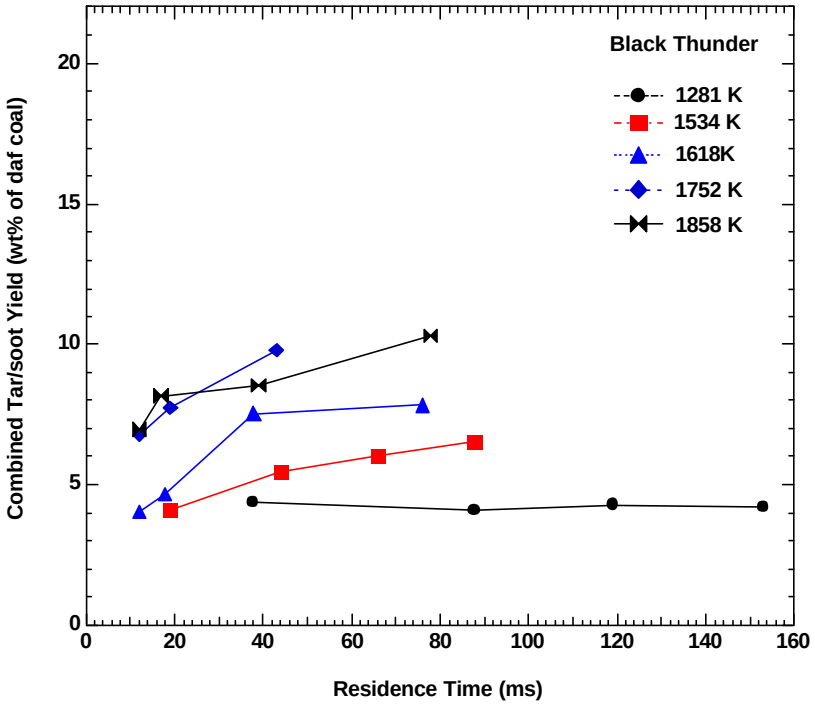

Figure 1.5.10. Tar / soot yield versus residence time for Black Thunder at various temperatures.

Previous studies have shown that homogeneous secondary reactions have a strong effect on the distributions of hydrocarbon gases. The hydrocarbon gases play an important role in soot chemistry at high temperatures. Also, the nitrogen transformations during secondary reactions can be greatly influenced by hydrocarbon gases, as suggested by the reburning mechanism (Smoot, 1993). In the practice of reburning, nitrogen oxides are converted to N_2 by injecting methane or natural gas into the coal flame. Some researchers have proposed detailed reaction mechanisms for the interaction of hydrocarbon radicals (CH, CH_2, etc.) with both NO_x and NO_x precursors such as HCN and NH_3 (Miller,1989; Glarborg, 1994; Miller, 1996). Therefore, the yields of individual hydrocarbons during secondary reactions must be examined in order to fully understand the nitrogen reaction pathways.

The yields of hydrocarbon gases reported here were calculated from the FTIR

measurements. There are two types of hydrocarbons that cannot be accurately quantified by the FTIR, so they are not reported here. One type is the alkynes in the spectral region 3300-3360 cm^{-1}. Careful examination revealed that this should be a mixture of propyne, 1-butyne, 1-pentyne and phenylacetylene. The large amount of overlap of these peaks made the identification and quantitative measurement of each individual species impossible. The total area (which is proportional to their concentrations) underneath these alkyne spectral peaks exhibited a temperature dependence similar to that of methane or benzene. By comparing the spectral area, it was found that these alkynes only accounted for less than 5% of the total hydrocarbons. Therefore their effects should be quite small. The other type of unidentified hydrocarbon fraction is the non-condensable light oils (gaseous hydrocarbons having more than six carbons) whose spectra overlap with the methane peak. Although FTIR spectroscopy offers far more accuracy and much lower detection limits for light hydrocarbons (less than six carbons) than the conventional analyzing instruments such as gas chromatography, it is not an ideal analyzer for differentiating hydrocarbons having more than six carbons. In this study, the individual species in these light oils were not measured. However, the measurement of the total spectral area of these light oils showed that their combined fraction never exceeded 5% of the total hydrocarbons in the gas phase.

1.5.1.1.2.1 Temperature Effects

Figures 1.5.11 to 1.5.14 shows the distribution of the non-condensible hydrocarbons with temperature for the four coals used in this study. These measurements were performed at the longest residence time at each temperature setting. The distributions at other residence times are similar to those presented here. The hydrocarbon release data exhibited a similar trend with temperature for all coal types. Propylene (C_3H_6) and 1,3-butadiene (C_4H_6), which only constitute a very small fraction of the light gases at the lowest temperature, decreased monotonically with temperature and were completely depleted at about 1400 K. Except for the lignite, the yields of all the other gas species increased with temperature, reached a maximum, then declined. Each individual species exhibited a characteristic maximum evolution temperature, which seemed to be independent of coal. However, different species exhibited different maximum evolution

temperatures. For instance, methane reached its peak at about 1400 K, ethylene at 1300 K and acetylene at a much higher temperature of 1550-1600 K.

It should be noted that the set of gas species measurements at the 1534 K condition for the Illinois #6, Utah and Knife River coals was performed before a reliable FTIR procedure was adopted. Therefore, the data reported for the 1534 K condition should be viewed with caution. However, reliable measurements on the Black Thunder coal covering the whole temperature spectrum showed a similar trend, indicating that the early measurements were reasonable.

The lignite demonstrated a different pattern of hydrocarbon release at long residence times. All the gases were found to decrease monotonically with temperature, except for C_2H_2. This may suggest an earlier release of light hydrocarbons for lignite than for other higher rank coals. Such observation is consistent with the ^{13}C NMR analysis of the coal, which shows a higher fraction of aliphatic side chains and bridges in lignites. The early release of light gases from low rank coals is also accounted for in the CPD model (Fletcher, et al. 1992).

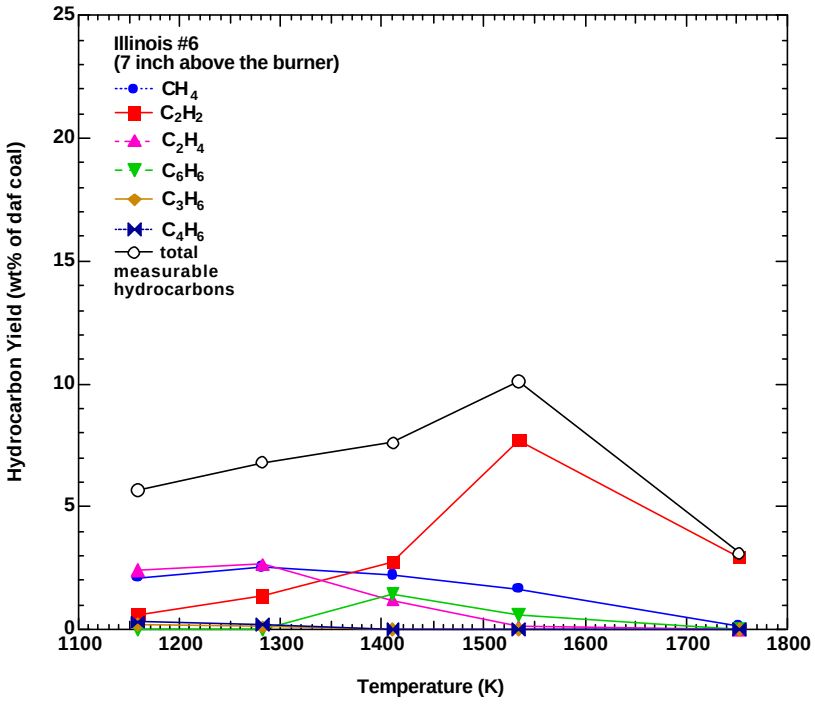

Figure 1.5.11. Temperature dependence of hydrocarbon yields for the Illinois #6 coal.

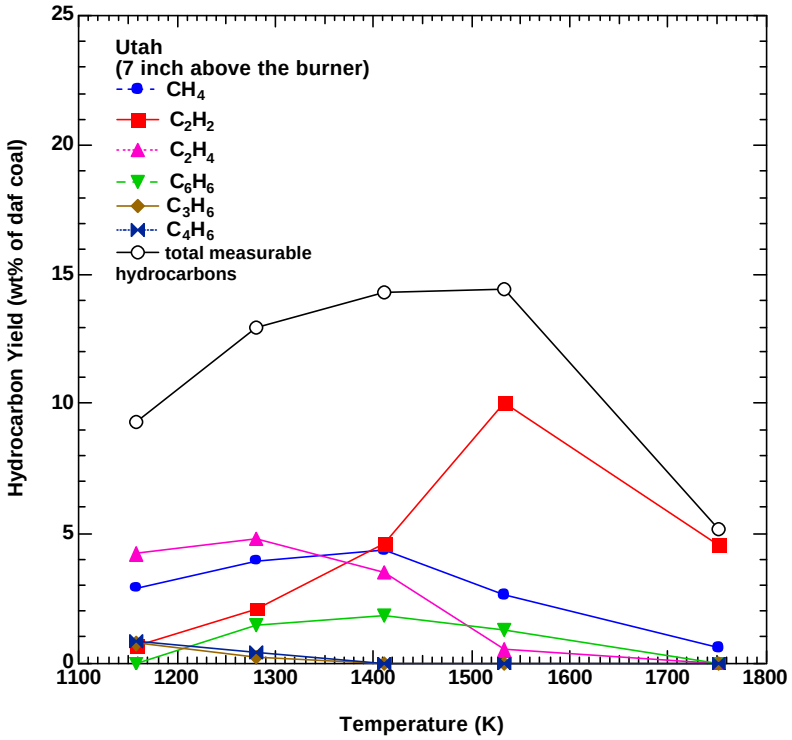

Figure 1.5.12. Temperature dependence of hydrocarbon yields for the Utah coal.

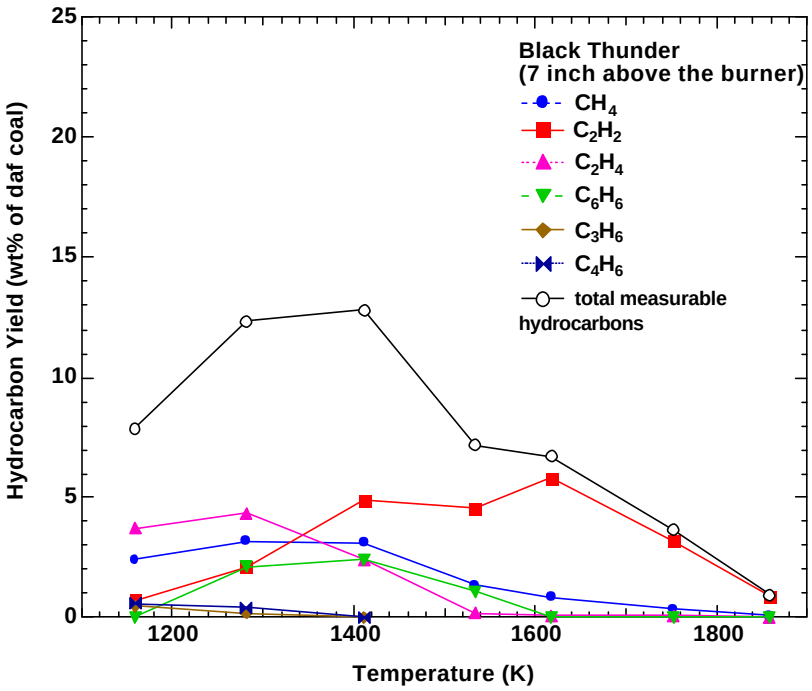

Figure 1.5.13. Temperature dependence of hydrocarbon yields for the Black Thunder coal.

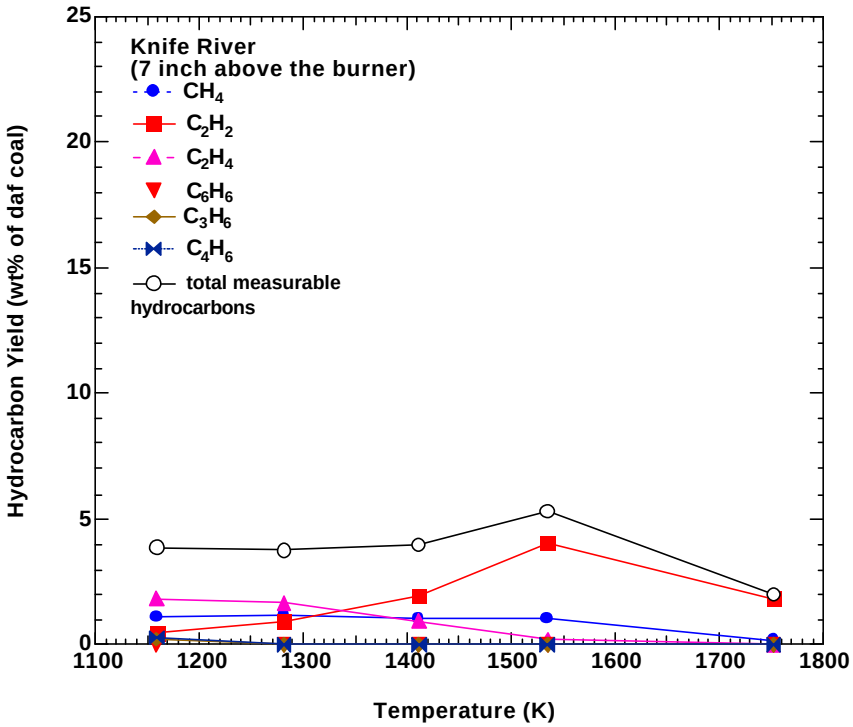

Figure 1.5.14. Temperature dependence of hydrocarbon yields for the Knife River coal.

Another interesting finding is that all the gases were consumed except for C_2H_2 at the most severe condition. The trend in the figures strongly implies that all of the light gases will eventually be depleted at even higher temperatures. Doolan and coworkers showed that the major carbon-containing species from coal volatiles are CO and soot at temperatures above 1800 K (Doolan, et al. 1986).

1.5.1.1.2.2 Residence Time Effects

The hydrocarbons are believed to form from two different sources during the coal pyrolysis. Some of the hydrocarbons are released during primary pyrolysis by breaking the bonds of the aliphatic attachments or bridges. The others are released through the secondary reactions of the tar and/or light oils. At high temperatures, these species (especially C_2H_2 and C_6H_6) may make significant contributions to the surface growth of the soot particles (Frenklach, et al. 1986).

Investigations of these hydrocarbons help to understand the mechanism governing the transition from tar to soot.

Figures 1.5.15 and 1.5.16 show the measured hydrocarbon yields for the Utah and Black Thunder coals as a function of residence time. The other two coals showed similar results. At the 1281 K condition, C_2H_4 and CH_4 were the major species. C_2H_2 only accounted for less than 20% of the light gases. The yields of all the gases increased with residence time at this temperature, then declined. The decline of the total hydrocarbon yields is consistent with the increase in soot yield. At the 1618 K condition (Figure 1.5.16), C_2H_2 became the most prevalent species in the pyrolysis products. The total hydrocarbons also dropped more rapidly with residence time at higher temperatures. Since C_2H_2 can play an important role in the early stage of soot formation (Glassman, 1988), the existence of high concentrations of C_2H_2 may indicate that significant soot formation has begun in the flame. This trend can be seen more clearly in Figure 1.5.17. Even at 1534 K, the growth of the soot yield seemed to be partially compensated by the decline of the C_2H_2 yield, indicating that C_2H_2 addition may be one of the primary sources

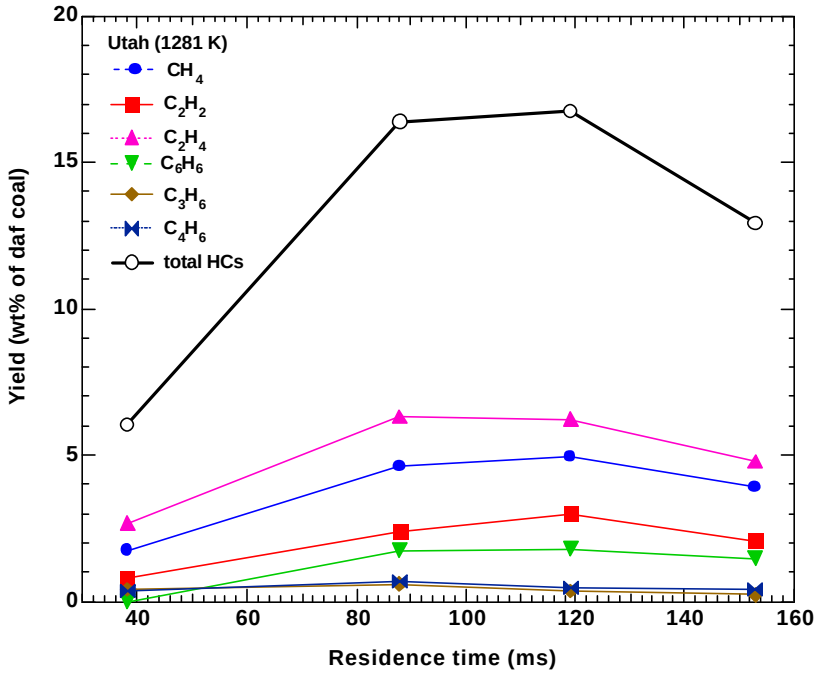

Figure 1.5.15. Yields of hydrocarbons for the Utah coal during pyrolysis at 1281 K.

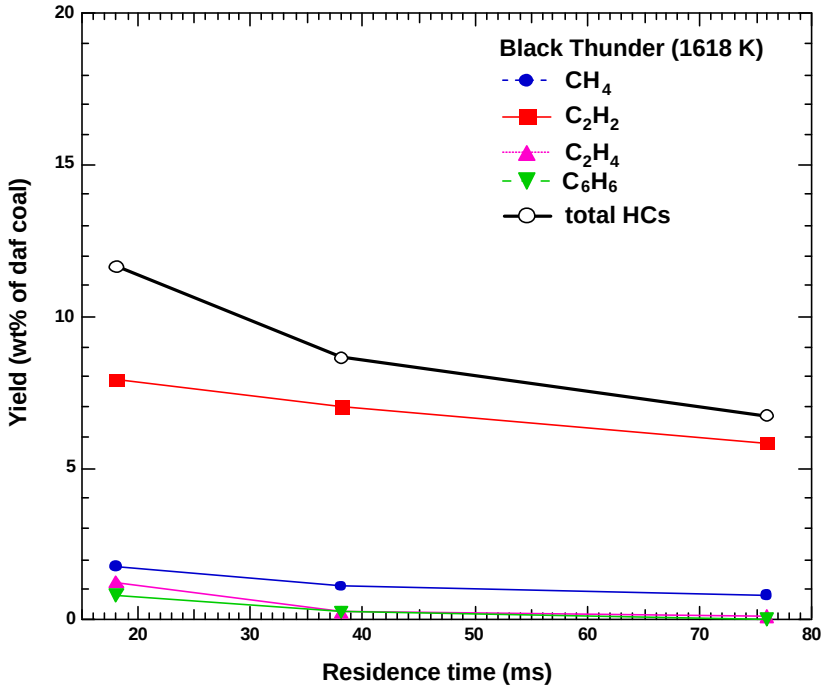

Figure 1.5.16. Yields of hydrocarbons from the Black Thunder coal during pyrolysis at 1618 K.

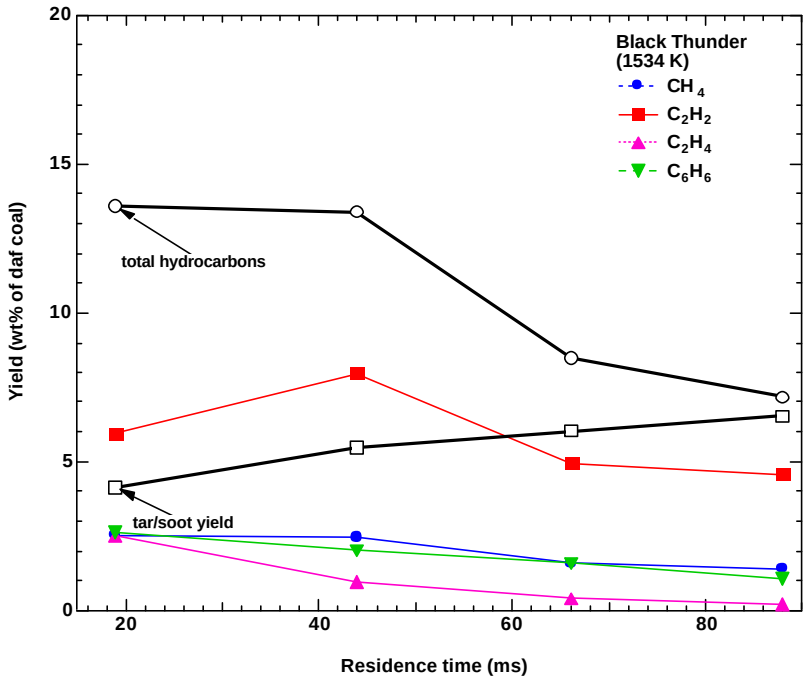

Figure 1.5.17. Yields of tar/soot and hydrocarbons from Black Thunder coal during pyrolysis at the 1534 K condition.

for soot growth. The proposed mechanism of soot addition from secondary light gases will be discussed in the next section.

1.1.21.2 Modeling

1.5.1.1.3 Simulation of the CO flame

In this study, the coals were pyrolyzed in a post-combustion environment, and the effects of the post-flame gases on secondary coal pyrolysis must be addressed. The flame structure of the CO flame was modeled by the Chemkin/Premix code using the measured centerline gas temperatures as input. The assumptions made in the simulation were given in the previous section. The profiles of the major molecular species in the CO flame at the 1159 K and 1858 K conditions are plotted in Figure 1.5.18. It can be seen that the steam production never exceeds

1% for either case, as originally designed, to facilitate the FTIR analysis in the gas phase. At the 1159 K condition, CO is dominant and its mole fraction is much higher than that of CO_2. However, at the 1858 K condition, the reverse trend is observed. Large quantities of CO_2 in the post-flame have the potential to reduce the soot yield, according to the following gasification reaction:

$$CO_2 + C = 2CO \qquad (5.10)$$

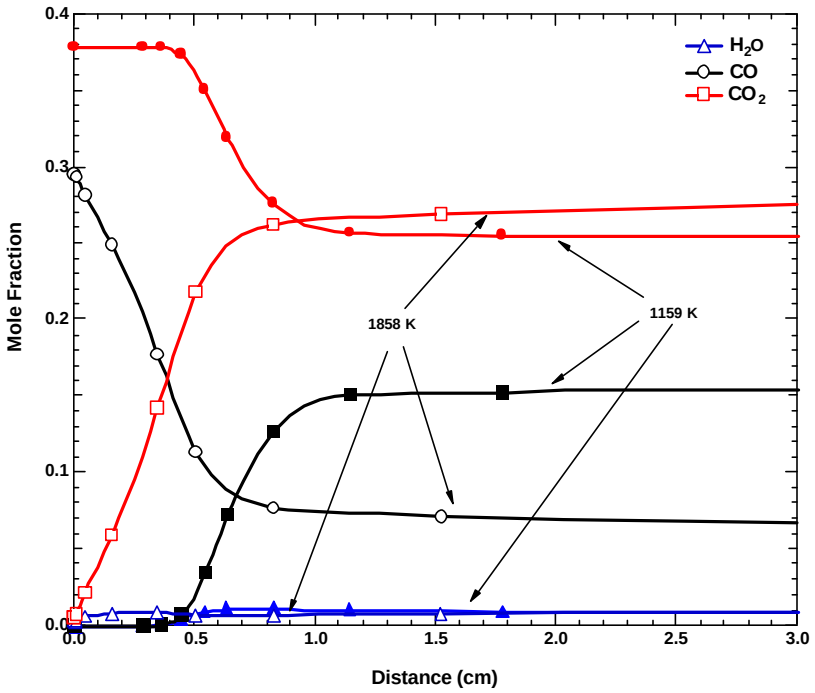

Figure 1.5.18. Calculated mole fractions of the municipal molecular species versus distance in the FFB with a CO flame.

Oxygen-containing radicals are of special interest, due to their high reactivity in a flame. Calculations have shown that five major species exist in the flame, including O_2, O, OH, HO_2, and H_2O_2. HO_2 and H_2O_2 are not considered in the discussion because their molar fractions

never exceed 10^{-5}. The calculated concentrations of the other three species, O_2, O and OH, at 1159 K and 1858 K are shown respectively in Figure 1.5.19. The profiles at other temperatures are similar. Several trends are observed from the plot. First, the mole fractions of molecular oxygen at high temperatures are higher than those at low temperatures. This is partly due to the lower equivalence ratio in the high temperature condition (see Table 1.4.2). Second, the mole fractions of O and OH radicals are only significant at the flame front and decay rapidly thereafter. This suggests that the influence of oxygen-containing radicals on coal pyrolysis is only appreciable at the flame front, which is only about 1 cm thick, as seen from the oxygen concentration profiles. Third, the mole fractions of OH and O radicals at 1858 K are much higher than those at 1159 K. This is not surprising since a high temperature can provide enough energy to initiate bond scission to produce more radicals. Finally, it is interesting that the mole fractions of O radical are much higher than those of OH radical at all cases in the CO flame. However, in a methane flame, the calculations showed more OH than O, as shown in Figure 1.5.20. The higher OH concentration in the methane flame may have important implications on the trend of the measured soot yields versus temperature in a CO flame versus a methane flame.

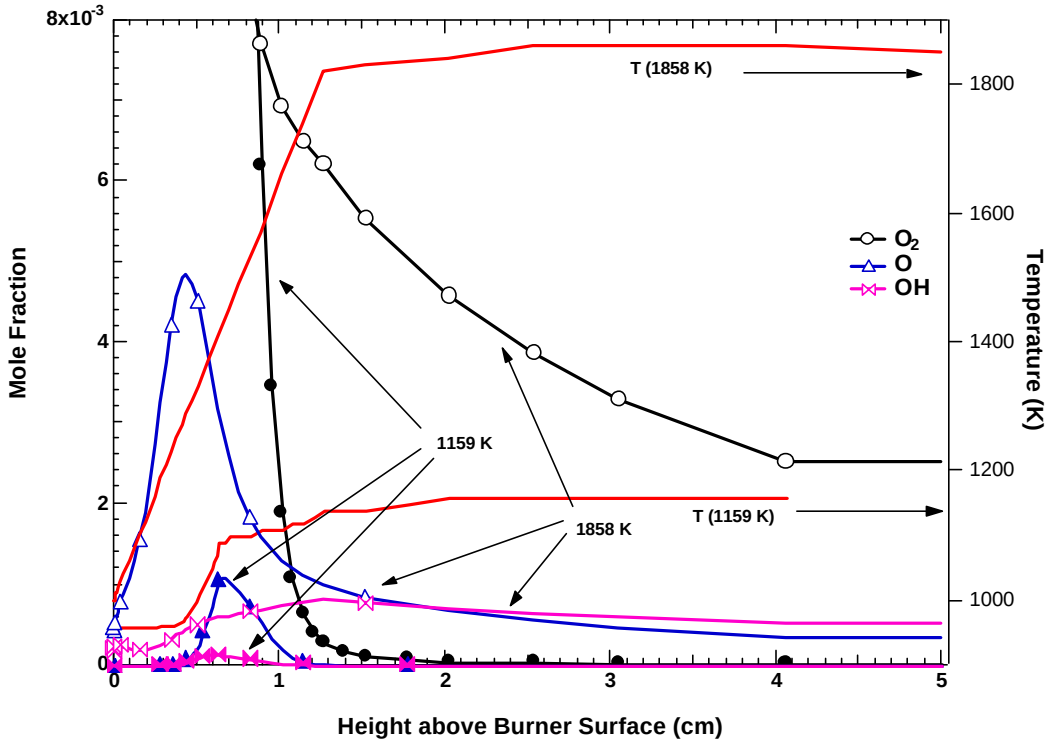

Figure 1.5.19. Calculated mole fractions of the major oxygen-containing species versus distance in the FFB with a CO flame.

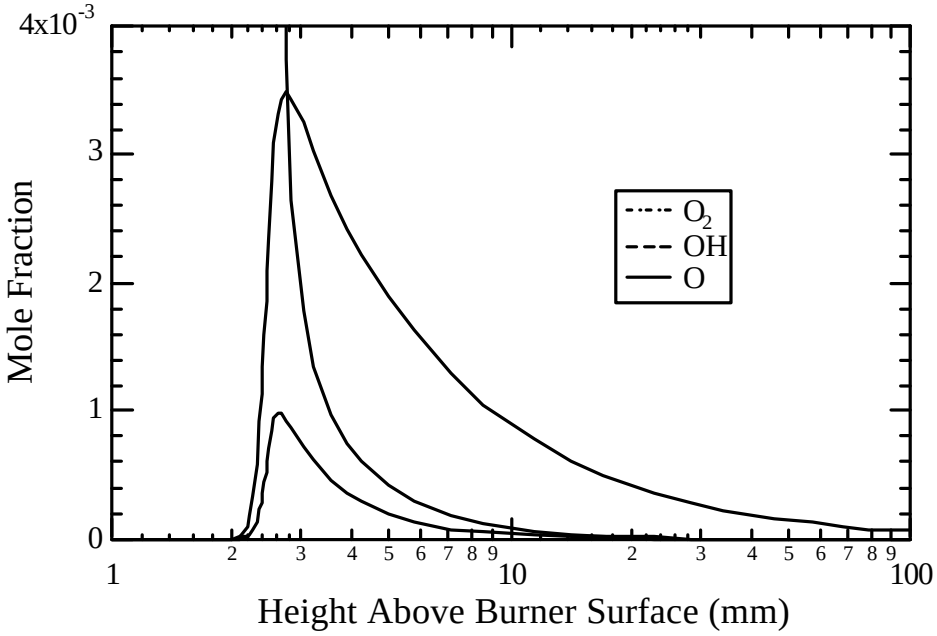

Figure 1.5.20. Mole fractions of the major oxygen-containing species in the FFB with a methane flame at 1900 K (adapted from Ma, 1996).

Fletcher and coworkers (1997) reported a slight decrease in soot yields with increasing temperature (above 1650 K) when coal was pyrolyzed in a methane flame. However, in contrast, soot yields were found to increase with increasing temperature for all the coals in the current study (see Figure 1.5.8). These coal pyrolysis experiments were performed in the same reactor; the only difference is the fuel. The slight decrease in soot yields at high temperatures in the methane flame was thought to be due to two major reasons. First, the much higher steam production in a methane flame could reduce the soot yields by steam gasification, as shown in equation 5.11. Second, the higher fractions of OH in a methane flame could react with soot precursors such as PAH in the tar, resulting in lower soot yields.

$$H_2O + C = CO + H_2 \qquad (5.11)$$

Bittner and Howard have suggested that the addition of OH to the ring may be responsible for the destruction of benzene in a sooting flame (Bittner and Howard, 1981). Haynes also pointed out that OH radicals appear to be the chief oxidant of the PAH formed from a coal or liquid fuels (Haynes, 1991). Therefore, it is logical to believe that OH radicals could play a more important role than other radicals in the destruction of tar molecules before soot formation. At 1860 K, the peak mole fraction of OH is about 8×10^{-4} in the CO flame, while the peak mole fraction of OH in the methane is about 3.5×10^{-3}, which is more than four times higher at a similar temperature condition. It is possible that the larger concentration of OH radicals in the methane flame that causes the decline of soot yield with increasing temperature at temperatures above 1600 K.

Since radicals are very reactive, the destruction of soot precursors by radicals is very plausible. The fact that the methane flame has higher mole fractions of OH is therefore consistent with the observed decrease in soot yields in that flame.

1.5.1.1.4 Modeling of Tar and Soot Yields

As explained in the first chapter, there are three stages in coal combustion including primary pyrolysis, secondary pyrolysis and char oxidation. Among these three processes, the primary pyrolysis is the most sensitive to the chemical structures of different coal types (Niksa, 1994). Based on the measured chemical structure parameters, the CPD model (Fletcher, et al. 1992) can describe the early stage of devolatilization with adequate accuracy. However, secondary reactions of volatiles from primary pyrolysis are not treated in the CPD model.

A simple mechanism is proposed here based on previous studies to describe the major reaction pathways during secondary coal pyrolysis. Only secondary reactions are modeled here, with three major reaction routes illustrated in Figure 1.5.21. It is assumed that there are two competitive reactions, cracking (r_c) and polymerization (r_p), for primary tars. At temperatures below 1200 K, the cracking reaction is dominant, causing the release of aliphatic materials and

carbon oxides. These secondary gases are mainly formed from the side chains and oxygen-containing functional groups in the tar molecules. At more severe pyrolysis conditions, secondary reactions cause ring opening reactions, preferentially those aromatic structures with heteroatoms such as oxygen and nitrogen, to release HCN (Chen, 1991) and CO (Ledesma, 1998). Beginning at 1400 K, ring structures will undergo polymerization to form soot after stripping off the functional groups. It is further assumed that only a certain fraction of primary tar can be directly converted to soot. This assumption is based on the fact that the secondary gas production from primary tar reaches an asymptote at high temperatures. The fraction of primary tar that can be directly transformed to soot is assumed constant for each coal and dependent on coal rank (correlated with coal oxygen content). In order to simplify the problem, another assumption is made that the cracking and polymerization reaction, which are very complicated and involving hundreds of elemental steps, can be lumped into a set of first-order reactions.

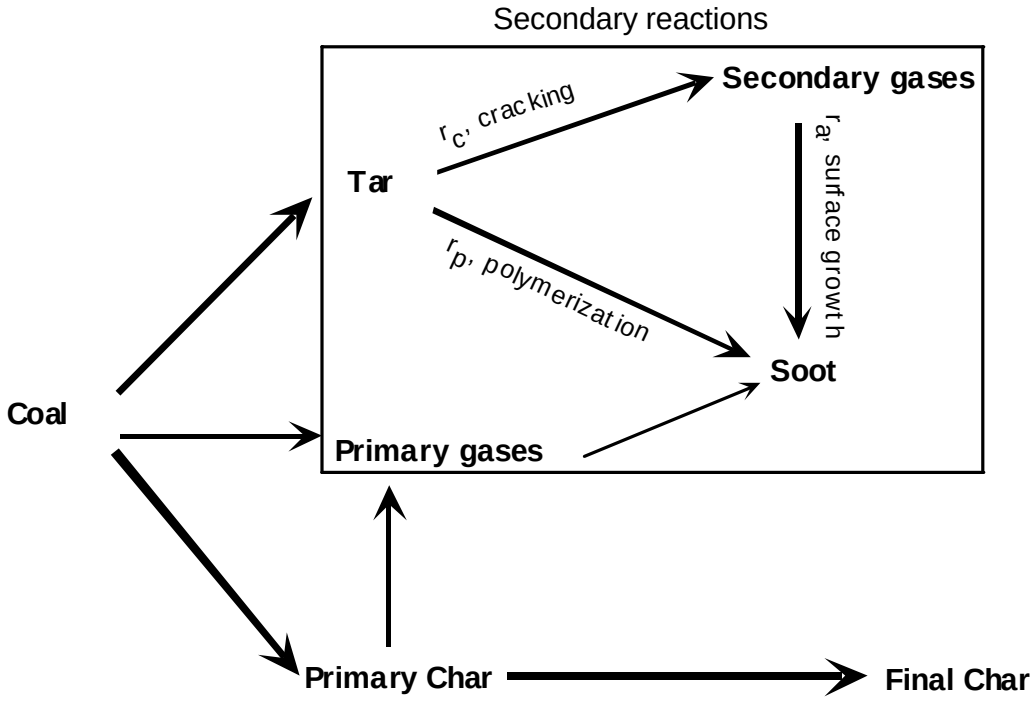

Figure 1.5.21. Proposed reaction mechanism in modeling the secondary pyrolysis.

During the construction of the model, it was also found necessary to include a secondary soot growth mechanism to best fit the experimental data. The soot addition (r_a) is also modeled as a first-order reaction by the attachment of hydrocarbons in the flame to the primary soot. Previous studies show that the surface of hot soot particles readily accepts hydrocarbons from the gas phase (Homann and Wagner, 1967). Pyrolysis experiments on coals also demonstrated that certain hydrocarbon gases (such as C_2H_2 and C_6H_6) may participate in soot formation at high temperatures (Haussmann and Kruger, 1989; Chen, 1991). Chen suggested that only the light hydrocarbons released from tar cracking (i.e., secondary gases) may participate in the soot addition. However, it seems more reasonable to include the hydrocarbons released during the early stage of devolatilization *and* the additional gases from thermal cracking of char (primary gases) as sources for soot growth. In this simulation, no differentiation was made between soot addition from the primary gases and from the secondary gases.

It should be noted that no chemical structure parameters were used in the simulation. The FTIR and GC analysis showed a distinct similarity in the major components for primary tars from various coal types (Freihaut, et al. 1989; Nelson, et al. 1990). The cracking reactions of tars from different coals also showed similar kinetic parameters (Doolan, et al. 1986; Serio, et al. 1987). Therefore, secondary reactions may be less influenced by the chemical structure than the local environment, such as temperature and stoichiometry. However, the chemical structure of the nascent tar is still important. It is well established that more aromatic structures exist in the tars of high rank coals, which implies a higher sooting tendency under pyrolysis conditions. However, for simplicity, the chemical structure of tar is omitted in this model development. The description of the rates for tar cracking, polymerization and gas-phase soot addition are as follows.

$$r_c = \frac{df_{tar,c}}{dt} = k_c(f^*_{tar,c} - f_{tar,c}) \qquad (5.12)$$

$$r_p = \frac{df_{tar,p}}{dt} = k_p(f^*_{tar,p} - f_{tar,p}) \quad (5.13)$$

$$r_a = \frac{df_{soot,a}}{dt} = k_a(f^*_{soot,a} - f_{soot,a}) \quad (5.14)$$

$$\frac{df_{tar}}{dt} = -(r_c + r_p) \quad (5.15)$$

$$f^*_{tar,c} + f^*_{tar,p} = 1 \quad (5.16)$$

where $f_{tar,c}$ stands for the mass fraction of primary tar that participates in tar cracking; $f_{tar,p}$ stands for the mass fraction of primary tar that participates in tar polymerization, and $f_{soot,a}$ stands for the mass fraction of the total additional soot (as dry, ash free coal) from hydrocarbons in the gas. The asterisk means the asymptotic solution (i.e., ultimate yield) for a specific fraction of primary tar or soot. For example, $f_{tar,c}^*$ stands for the ultimate mass fraction of primary tar that is eventually gasified to secondary gases; $f_{tar,p}^*$ stands for the ultimate mass fraction of primary tar that is eventually converted to soot, and $f_{soot,a}^*$ stands for the ultimate mass fraction of additional soot from hydrocarbons. It should be pointed out that it is the fraction of primary tar or the fraction of the ultimate soot growth from hydrocarbons that was modeled, not the coal mass fraction. The residual tar and soot yield based on the dry, ash-free coal can be calculated by the following equations:

$$y_{tar}(t) = y^0_{tar} \cdot f_{tar}(t) \quad (5.17)$$

$$y_{soot}(t) = y^0_{tar} \cdot f_{tar,p}(t) + f_{soot,a}^* \cdot f_{soot,a}(t) \quad (5.18)$$

where t, f and y are residence time, fraction of the ultimate products (tar or soot) and fraction as dry, ash-free coal, respectively.

1.5.1.1.4.1 Calculation of Kinetic Parameters

The tar cracking reaction was assumed to have an activation energy of 100 kJ/mol, obtained from the vapor-phase secondary cracking of nascent tars from a Pittsburgh #8 coal as reported by Serio et al. (1987). A comparable activation energy was also derived by fitting the tar cracking data for a subbituminous coal (Doolan, et al. 1986) and a bituminous coal respectively (Ledesma, 1998).

For the Illinois #6 coal, the primary tar yield was calculated from the CPD model using the measured ^{13}C NMR data. For the other coals, the primary tar yields were first calculated by the CPD model using a correlation of the structure parameters based on the elemental composition of the parent coal (Genetti, 1999). The first data point of tar yield in the current study is much lower than the "CPD-predicted" tar yield. The kinetic parameters presented here are the best fit for the data measured in the FFB. However, the tar decay rate using these parameters cannot explain the decay from the "CPD-predicted" tar yield to the first data point measured in this study. The "CPD-predicted" tar yield is too high to allow development of a reasonable tar decay model to fit the data in the current study. The low tar yields measured in the present work were probably due to the post-flame environment in which the coals were pyrolyzed; the short residence times in the FFB may be another reason. Determination of the exact reason for the low tar yields is beyond the scope of the present work.

The activation energy for soot formation from tar (E_p) was assumed to be 230 kJ/mol and the activation energy for soot addition from hydrocarbons (E_a) was assumed to be 320 kJ/mol. E_p is based on the result of previous studies (Ma, 1996) and is modified to better fit the experimental data. E_a is the best-fit parameter for this study. The activation energy for soot formation from tar is lower, because the tar has a higher sooting tendency since it contains PAH. With the activation energy fixed, the experimental data were used to fit the pre-exponential factor for different coals. The ultimate fraction of primary tar that can be converted to soot was also assumed based on the oxygen content of the coal.

A summary of the coal-dependent kinetic parameters by fitting the experimental data is

shown in Table 1.5.4. The values of $f_{tar,c}^*$, $f_{tar,p}^*$ and $f_{soot,a}^*$ are presented in Table 1.5.5. These numbers have no specific physical meaning, but represent the best values to fit the experimental data. However, this does not mean these values are only random numbers. CO and CO_2 are the major secondary gases from tar cracking. It was found that yields of CO and CO_2 are much higher for low rank coals than for high rank coals (Cliff, et al. 1984; Doolan, et al. 1986; Chen, 1991). The higher yield of secondary gases from tar implies an accordingly lower soot yield. Therefore, values of the ultimate tar fraction in Table 1.6.2 that can be directly converted to soot (f_p^*) were adjusted according to the coal rank. It is believed that secondary gas production from tar is somewhat associated with the oxygen content of the parent coal, but the exact nature of this relationship is still unclear. The measured and calculated profiles of the tar plus soot for the four coals are presented in Figures 1.5.22 to 1.5.25. It must be emphasized that these kinetic parameters are not expected to extrapolate to temperatures or conditions significantly different from those in the current experiments. The results, however, do provide insight into the rate of homogeneous (cracking) and heterogeneous (soot formation) tar secondary reactions for coals of different ranks.

Table 1.5.4. Summary of the Best-Fit Kinetic Parameters for Secondary Reactions of Coal Volatiles.

	A_c (sec^{-1})	E_c (kJ/mol)	A_p (sec^{-1})	E_c (kJ/mol)	A_a (sec^{-1})	E_a (kJ/mol)
Illinois #6	2.5E5	100	2.0E9	230	5.0E10	320
Utah	5.0E5	100	2.0E9	230	8.0E10	320
Black Thunder	1.0E6	100	2.0E9	230	3.0E11	320
Knife River	4.0E5	100	2.0E9	230	5.0E11	320

Table 1.5.5. Values of $f_{tar,p}^*$, $f_{tar,c}^*$ and $f_{soot,a}^*$ Used in the Simulation.

	ultimate tar fraction to soot ($f_{tar,p}^*$)	ultimate tar fraction to secondary gas ($f_{tar,c}^*$)	ultimate additional soot from hydrocarbons ($f_{soot,a}^*$)
Illinois #6	0.7	0.3	0.04
Utah	0.78	0.22	0.04
Black Thunder	0.63	0.37	0.04
Knife River	0.4	0.6	0.02

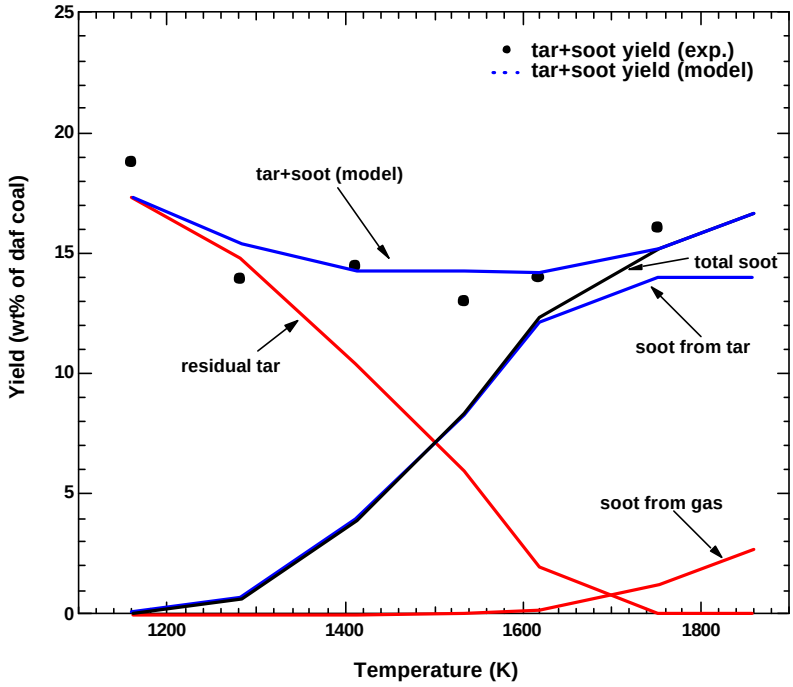

Figure 1.5.22. Calculated tar and soot yield for the Illinois #6 coal.

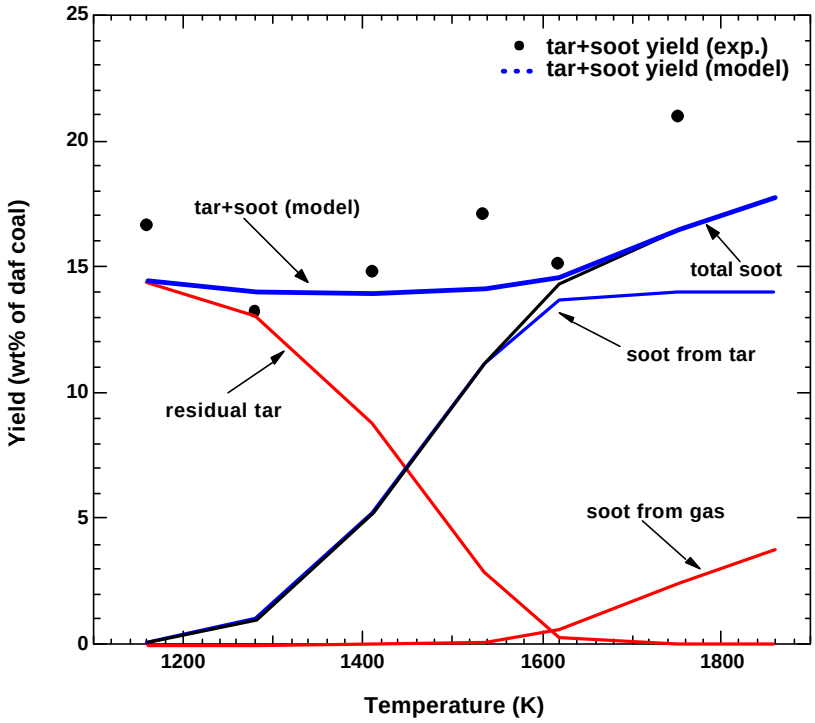

Figure 1.5.23. Calculated tar and soot yield for the Utah coal.

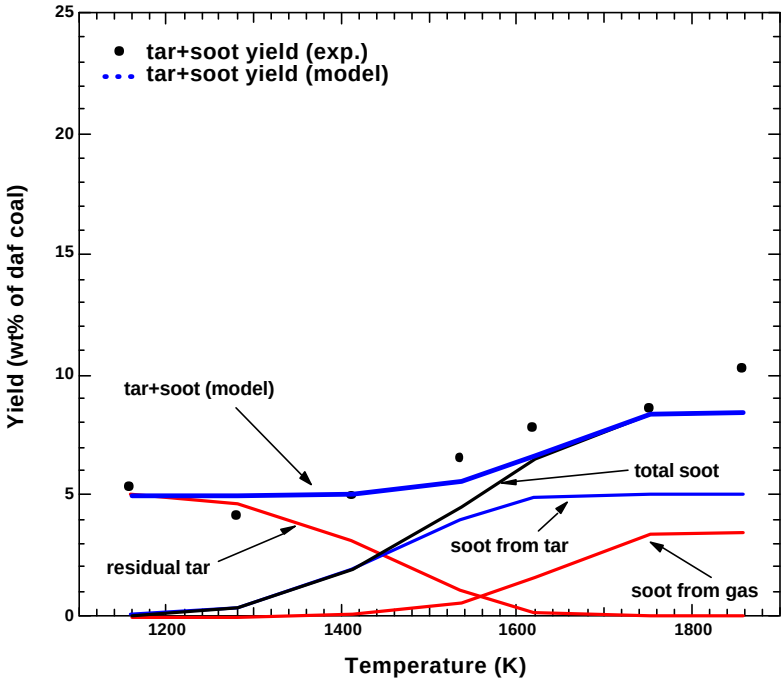

Figure 1.5.24. Calculated tar and soot yield for the Black Thunder coal.

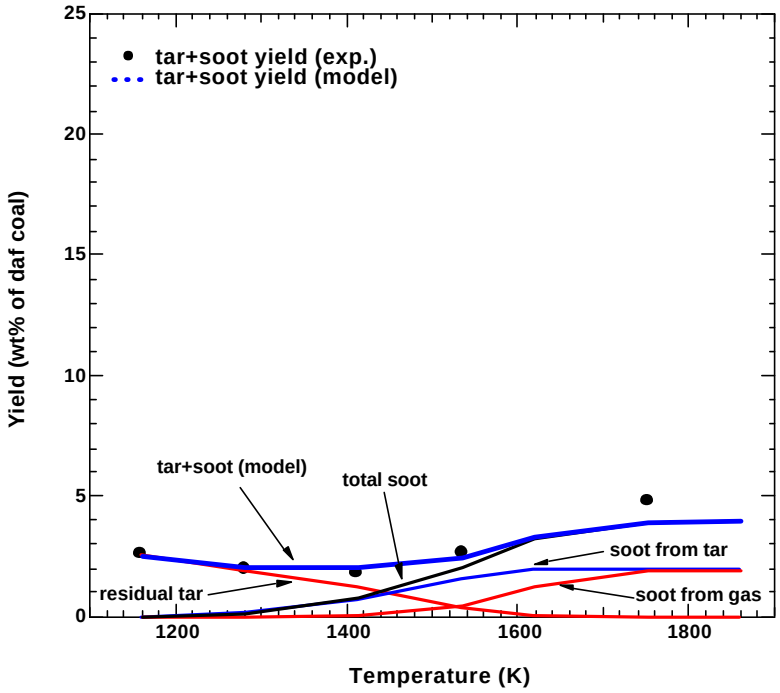

Figure 1.5.25. Calculated tar and soot yield for the Knife River lignite.

1.1.21.3 Discussion

1.5.1.1.5 Tar and Soot Yields

The Illinois #6 coals have been extensively studied, so a comparison of tar or soot yields with previous work can be made, as shown in Figure 1.5.26. The tar yields of Hambly (1998) and Watt (1996) were obtained by pyrolyzing the coal in a drop-tube reactor in an inert environment. Their data show a similar trend to that found in this study: the yields of tar plus soot decreased

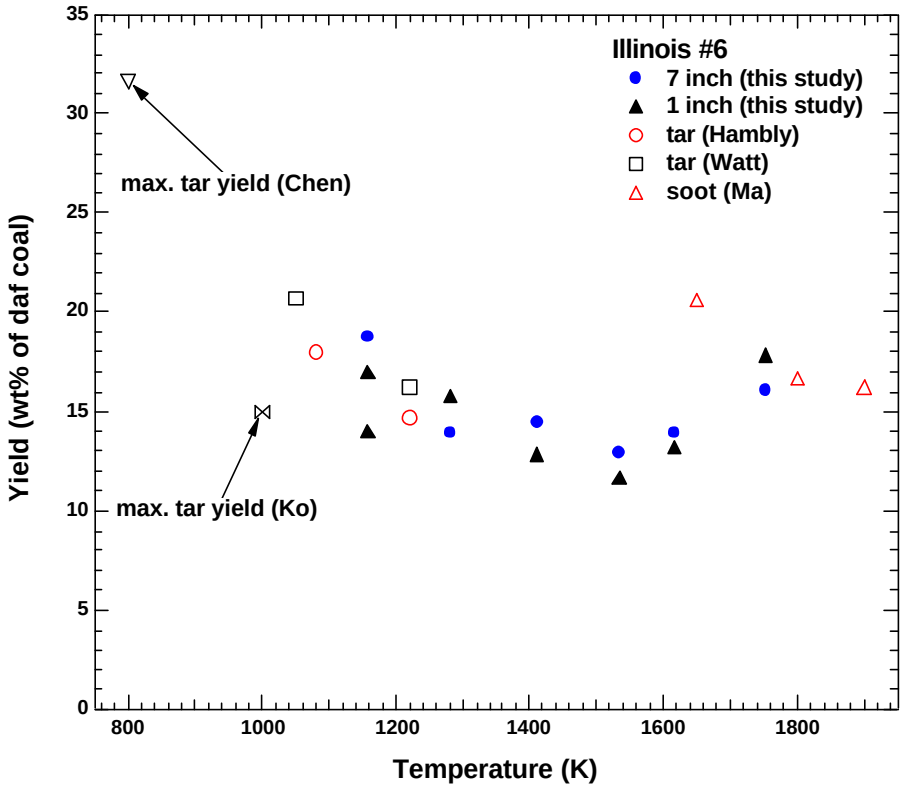

Figure 1.5.26. Comparison of tar and soot yields for Illinois #6 coal (the temperature is the particle temperature for Chen and peak gas temperature for others).

first at temperatures below 1400 K, due to secondary reactions. At high temperatures, the soot yields in this study agree well with Ma's data except the one point at 1650 K. Also shown in the figure is the maximum tar yield from primary pyrolysis reported by Chen (1991). The tar yield is more than 60% higher than the highest tar/soot yield obtained in this study. This cannot be solely attributed to secondary reactions. In Chen's experiment, the collected tar was extracted from glass filters by a solvent (THF). The pure tar sample was then weighed after evaporation of the solvent. The tar yield measured this way could be subject to the following errors: incomplete evaporation of the solvent arising from a partial miscibility between the solvent and the tar and possible residues from the solvent itself. Both can result in a higher value than the actual tar

yield. The maximum tar yield obtained in a heated grid reactor (Ko, et al. 1988) is lower than that in this study. There are probably two reasons for the difference. First, the low temperature and low heating rate used in the heated grid reactor may result in a lower tar yield. Second, tar collection may be incomplete due to recondensation of tar to the remaining char and deposition of tar on the trap wall, as reported by the author.

A comparison of the tar and soot yields of Utah seam coals is presented in Figure 1.5.27. It should be noted that the yields reported by Freihaut and coworkers (Freihaut and Seery, 1981) were obtained under vacuum pyrolysis and on a dry coal basis. It is clear that the tar and soot yields collected at the 1 inch location in this study are much lower than those collected at the 7 inch location. By examining the mass release data at 1159 K, it was found that mass release at the 7 inch location is 25% (absolute) higher than that measured at the 1 inch location, while the difference is about 10-15% for other coals. That means the lower tar and soot yields are probably due to the incomplete devolatilization process at short residence times. The tar and soot yields collected at the 7 inch location are comparable with those reported by Friehaut and Ma at temperatures below 1650 K. However, at temperatures higher than 1650 K, a different trend is observed. In this study, the soot yields continued to increase with increasing temperature, while the tar or soot yields declined with increasing temperature in the case of Freihaut and Ma. In Freihaut's experiment, tar was generated on a heated metal screen. Since the tar quickly escaped the hot screen once it was released, it had no chance to form soot. The systematic decrease of tar yields was totally due to the intra-particle or extra-particle thermal cracking of the tar. In Ma's case, the decrease of the soot yield is thought to be due to the existence of large quantities of OH radicals in the methane flame front that may destroy the soot precursors such as tar and PAH, as explained in the previous section.

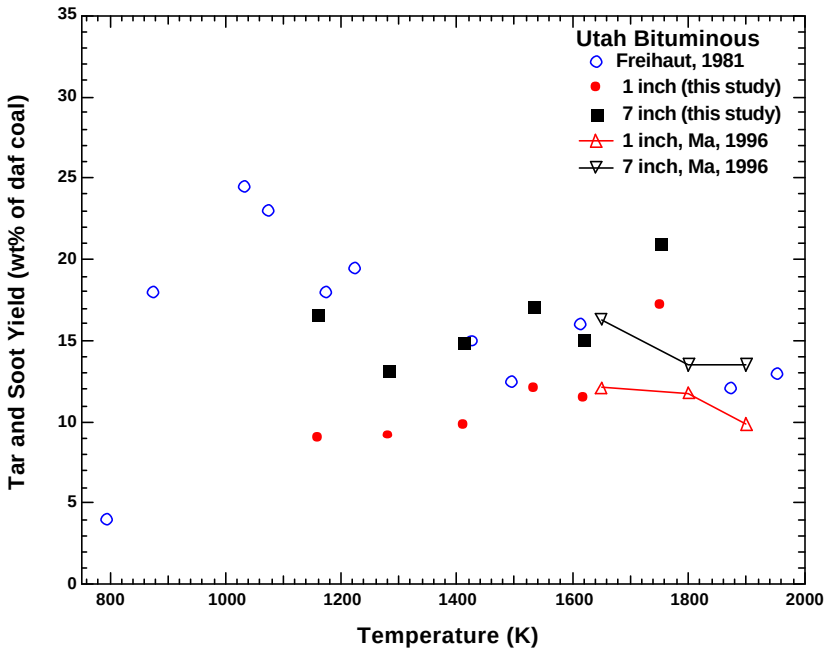

Figure 1.5.27. Comparison of tar and soot yields for Utah coal (Freihaut's data were on the dry coal basis).

For Black Thunder and Knife River coals, a similar comparison cannot be made due to a scarcity of data. The only tar yield for a Wyodak coal (which comes from the same seam as Black Thunder) was reported by Ko. Under 0.1 M Pa, the maximum tar yield was 19.3% (daf).

Finally, the rank dependence of tar and soot yields is compared to those from the literature (see Figure 1.5.28). The maximum tar yield defined in this study is the highest collectable tar at the lowest temperature setting, 1159 K. Xu and Tomita determined the maximum tar yield by pyrolyzing 17 coals at 1037 K in a Curie-point pyrolyzer (Xu and Tomita, 1986). The heating rate was approximately 3000 K/s. Tyler's data are exclusively for Australian bituminous coals pyrolyzed in a fluidized bed reactor (Tyler, 1979). The data reported by Chen (1992 a) are the maximum tar yields during primary pyrolysis. The maximum tar yields obtained in the BYU drop tube reactor are also shown. From the figure, several trends of the dependence

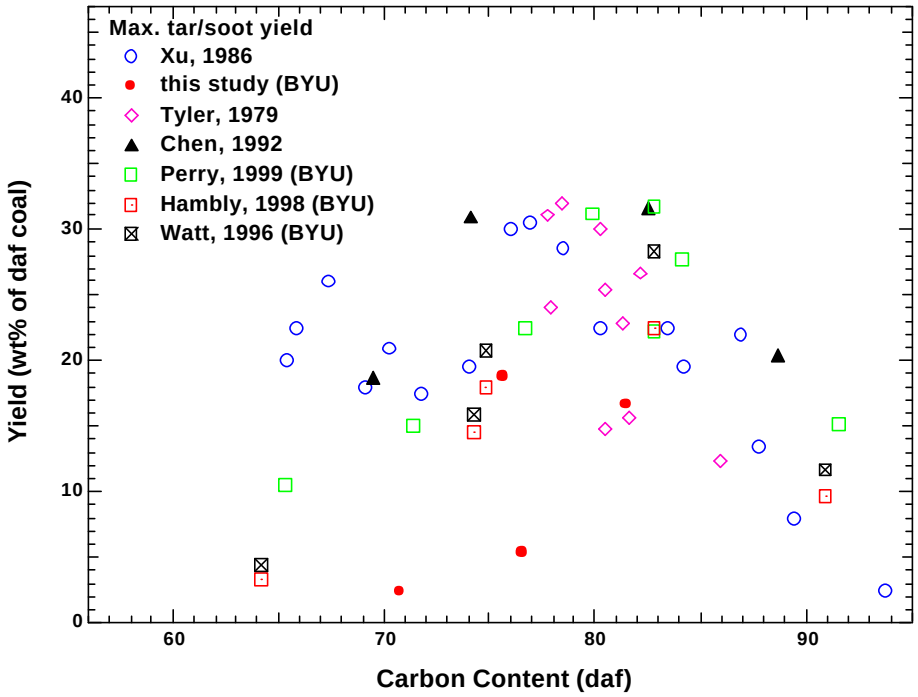

Figure 1.5.28. Comparison of rank dependence of tar and soot yields.

of tar/soot yield on coal type can be observed. First, there is no distinct relationship between carbon content and the maximum tar yield, as seen by the large scatter in the data. From Tyler's data, even for similar bituminous coals, the tar yield of one coal can be twice as much as another coal. The general rule of thumb is that the tar yield is highest for bituminous coals, but drops for lower rank coals such as subbituminous and lignite and higher rank coals such as anthracite. Second, for low rank coals, the yields reported at BYU are much lower than those of Xu. This is probably because Xu's tar yields were calculated by difference from the gas analysis and the weight loss, making them susceptible to over-estimation (Perry, 1999).

The tar/soot yields obtained in this study are much lower than those by other researchers, especially for low rank coals. Several factors may be responsible for such a difference. First, the data reported in this study are not the actual maximum tar yields. Significant secondary reactions have already occurred before the first sampling location in the FFB, leading to a lower

tar yield. The measured tar/soot yields declined monotonically with temperature below 1500 K. Second, it is possible that tar was trapped inside the filters instead of on the surface at low temperatures (Figure 1.4.6). However, the filters were weighed together to determine the tar yield. A yellowish deposit was found on the glass wool installed downstream before the gas cell. However, this amount was insignificant. Therefore, the low tar yield is not thought to be caused by the tar filters. Third, semivolatile species of molecular weight 100 to 200 amu may be another reason. They do not fit clearly into either the tar or gas categories (Solomon, et al. 1992). These species are too volatile to remain condensed on tar collection surfaces, but are not volatile enough to stay in the gas phase. This sometimes can result in 5-10% loss in materials. Fourth, the post-combustion environment used in this study may also contribute to the lower tar and soot yield. The combustion products, such as CO, CO_2 and H_2O, readily react with the highly active nascent tar molecules, resulting in a lower tar yield. The influence of the oxygen-containing species in the flame should be insignificant at low temperatures, due to the low concentrations. However, they may have a substantial effect on high temperature soot yields.

It was found that the secondary reactions of the tar before the first collection point in the FFB and the interactions of the post-combustion environment with the tar are likely the reasons for the observed low tar and soot yields in this study.

1.5.1.1.6 Secondary Reactions of Nascent Coal Volatiles

When heated, tar and light gases will be released from coal particles during primary pyrolysis. Primary pyrolysis is a fast reaction, usually occurring in a few milliseconds under a typical pulverized coal firing condition. The tar quickly reaches its maximum yield at about 1000 K. Under high temperature and fuel-rich conditions, the primary tar will undergo two competitive reactions: thermal cracking and soot formation.

1.5.1.1.6.1 Gas-phase Thermal Cracking Reactions

The chemical structure analysis by ^{13}C NMR methods clearly demonstrates that thermal cracking is dominant at low temperatures, leading to the release of secondary gases (Solum, et

al., 2000). Serio et al. (1987) investigated kinetics of the thermal cracking of fresh coal tars generated from fixed-bed pyrolysis at 500-900^{o}C. Tar conversion was found to be insignificant below 600^{o}C. At higher temperatures, the major products were light gases, oils and some transformed tar. The formation of char from secondary reactions of tar was also identified. There is certainly a possibility that the primary tar will redeposit onto the char surface to participate in the crosslinking reaction. However, under the high temperature, high heating rate conditions encountered in an industrial furnace, such reactions should be minimal.

Secondary reactions of primary tar were examined more clearly in Doolan's experiment (Doolan, et al. 1986). The primary tar was obtained by pyrolyzing an Australian subbituminous coal in a flash pyrolyzer operated at 870 K. The tar was then cracked in a quartz tube reactor at 870-1370 K and in a shock tube reactor at 1100-2000 K. The yields of various products in the quartz tube reactor are shown in Figure 1.5.29. Below 1300 K, the major products were various hydrocarbon gases, CO, H_2O and possibly some light oils. It is clear that thermal cracking of tar is a major source of hydrocarbon gases during pyrolysis. The release of light hydrocarbons increased with temperature up to 1300 K, then started to decline slightly after reaching the maximum yield. Soot formation commenced at 1300 K by direct conversion from tar, as evidenced by the sharp decrease of the remaining tar.

It is also interesting to find that the combined yields of light hydrocarbons, CO and H_2O reached an asymptote at 1200-1370 K. That is to say, the ultimate yield of secondary gases from primary tar is somewhat constant at high temperatures. Although the highest temperature used by Doolan in the quartz reactor was 1370 K, it is most likely that this trend will remain valid at even higher temperatures. The dashed line in Figure 1.5.29 represents the model prediction of the production of secondary gases from tar during secondary reactions using the kinetic parameters in the Tables 1.5.4 and 1.5.5. Only the cracking mechanism was included in the model prediction; no soot formation was included. An excellent agreement is reached between the data points and model predictions regarding the remaining tar below 1300 K, before the onset of soot formation.

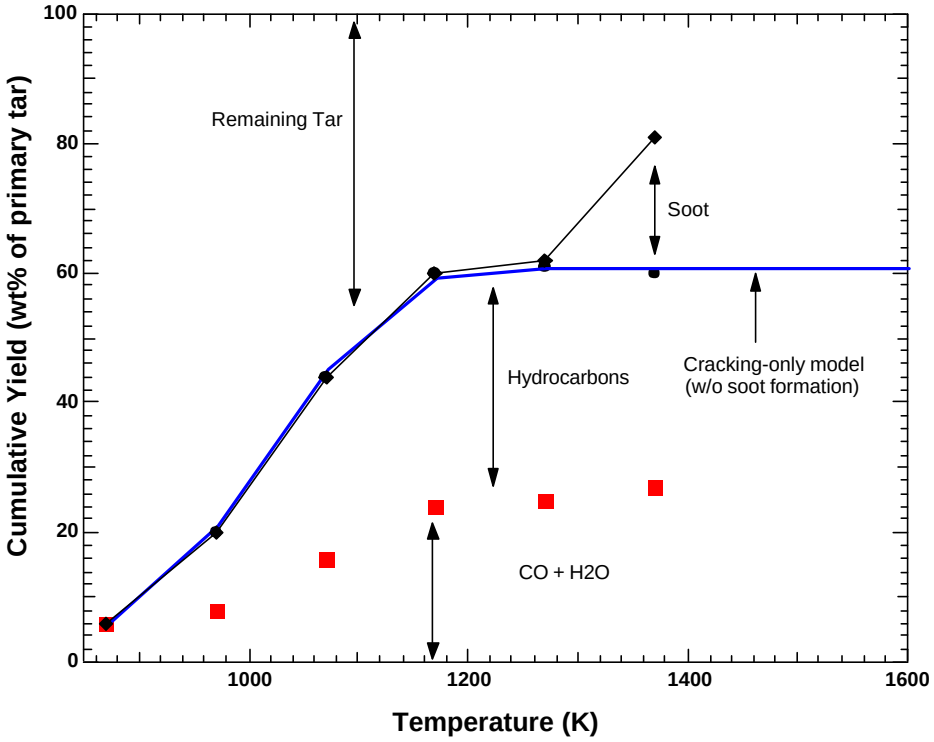

Figure 1.5.29. Cumulative product yields of the primary tar as a function of reactor temperature (adapted from Doolan, et al. 1986).

The hypothesis of constant gas production from the tar at higher temperatures (>1300 K) is supported by the following observations. First, in Doolan's high temperature shock tube experiment where a temperature as high as 2000 K was achieved, the yield of CO reached an asymptotic value of 18% (wt% of primary tar) at temperatures higher than 1600 K. The amount of oxygen in the CO produced from the tar was equal to the original oxygen in the tar. Second, the tar yields obtained at different final temperatures for various coal types reported by Freihaut (1981) also confirmed a constant ultimate gas release from primary tar at temperatures higher than 1400 K (see Figure 1.5.30). The tars were generated in a heated grid reactor operated at different temperatures. Despite the scatter in the data, a general trend can be identified for each coal: the tar yield quickly rises to its maximum during primary pyrolysis then decays slowly to

an asymptote which is coal-dependent. The decay of the tar was solely due to thermal cracking reactions, since no soot was present even at 1800 K. Once released from the coal, the tar was quenched immediately by the surrounding cold gas. Therefore, the tar had no chance to transform to soot, which is favored at high temperatures. The constant tar yields at high temperatures in Freihaut's study suggest a constant gas production from primary tar.

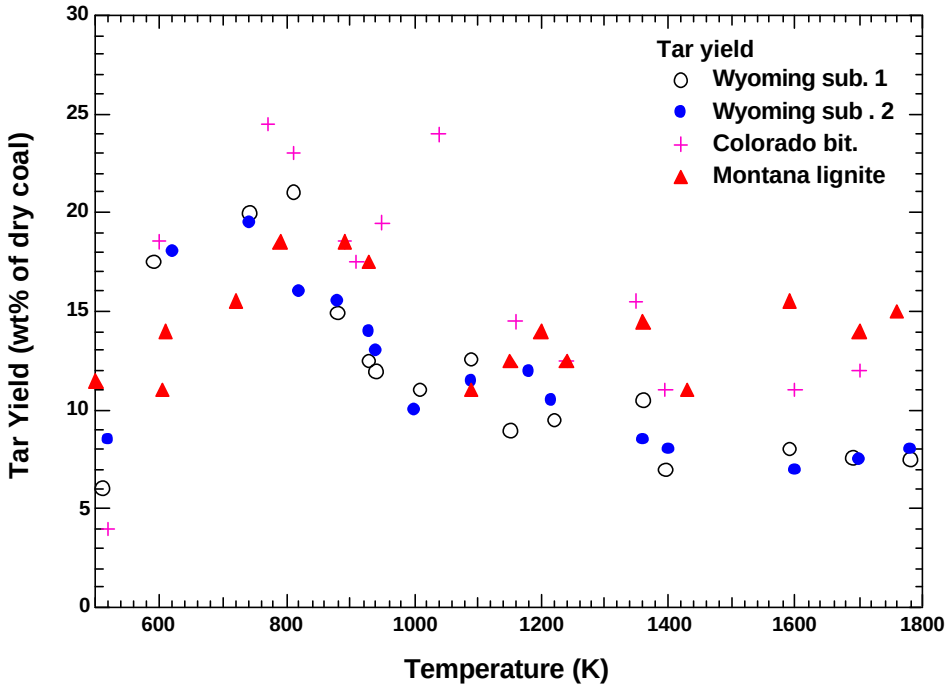

Figure 1.5.30. Tar yields as a function of final temperature for different coal types (adapted from Freihaut, et al. 1981).

It is well established that the fresh tar is comprised of polycyclic aromatic clusters with various attachments. On the other hand, soot is composed of much larger aromatic clusters and/or polymerized PAH's. The fraction of hydrogen and other heteroatoms in soot is very small. In order to form soot that is relatively free of hydrogen, oxygen and nitrogen, the tar must first shed the attachments or even open the aromatic rings to release those elements. The oxygen

will be converted to CO or, to a lesser extent, CO_2. Aliphatic side chains will be converted to light hydrocarbons. The nitrogen will be released mainly in the form of HCN.

In the simulation of the secondary reactions of tar in the modeling section, it was also assumed that the mass fraction of primary tar, which is eventually converted to gas, is also coal dependent, with lower rank coals producing more secondary gases. This hypothesis can be justified by the chemical structure data reported by Perry (1999).

In Table 1.5.6, the structural parameters derived from ^{13}C NMR for two coals and their corresponding tars and soots are presented. South Banko lignite and Pittsburgh #8 hv bituminous coal represent the two different coal types. Previous measurements have shown that the fresh tar released from coal usually has a similar chemical structure to that of the coal (Pugmire, et al. 1990). Therefore, here the coal parameters are used for the primary tar.

Table 1.5.6. Structural Parameters Derived from ^{13}C NMR Analysis for Tars

(adapted from Perry, 1999)[#].

sample	condition	χ_b	C_{cl}	σ+1	P_0	B. L.	S. C.	M_{cl}	M_δ
South Banko	coal	0.278	13	5.3	0.55	2.9	2.4	410	47
(lignite)	1250 K	0.255	12	2.7	0.95	2.6	0.1	164	5
Pittsburgh #8	coal	0.314	15	4.5	0.62	2.9	1.6	311	28
(hv bituminous)	1250 K	0.341	17	4.2	0.95	4.0	0.2	249	9
	1650 K (soot)	0.429	21	4.8	0.89	4.3	0.5	316	12

[#]see Nomenclature for the definition of the parameters.

There are 30% more side chains per cluster (2.4) in South Banko parent coal than in the Pittsburgh #8 coal (1.6). These side chains are usually aliphatic in nature and are released as

light hydrocarbons during pyrolysis (see Figure 1.2.2). At 1250 K, the side chains for the two coal tars are similar (0.1 and 0.2 respectively), indicating that more side chains are lost for the lignite tar. This can be viewed more clearly by comparing the total attachments per cluster (σ+1) and the average molecular weight per attachment (M_δ). For the Pittsburgh #8 coal, the number of total attachments per cluster for the primary tar (4.5) and the tar at 1250 K (4.2) are similar. However, σ+1 drops substantially from 5.3 to 2.7 for the South Banko coal tar over this same temperature range. The corresponding average molecular weight per attachment drops from 28 to 9 for the Pittsburgh #8 coal tar for this temperature range and from 47 to 5 for the South Banko tar. This means that low rank coal tars not only lose more attachments, but also lose more mass per attachment. This is direct evidence that low rank coal tars lose more mass than high rank coal tars during secondary reactions. However, a quantitative correlation of such rank dependence cannot be established from the limited data in this study.

1.5.1.1.6.2 Soot Formation

Soot formation from coal tar usually commences between 1350 and 1400 K, as indicated by the significant change of the tar structure during that temperature range (Solum, et al. 2000). Ring opening may be the first step in soot formation. Pyrolysis experiments on biphenyl (see Chapter 6) showed that ring opening is the first step to soot formation for some model compounds. Ring opening releases the heteroatoms and other aliphatic materials and creates free radicals. These radicals will then undergo a series of reactions to form larger clusters through such reactions as condensation and polymerization. The coal tar has a higher sooting tendency than aromatic model compounds and light hydrocarbons, since the soot incipient temperature for coal tar is much lower. This can be explained in two aspects. First, the coal tar can produce more radicals and is more reactive because it has more attachments per cluster (σ+1). Second, the larger ring structure in coal tar has a higher stabilizing effect during polymerization (Badger, et al. 1964).

The sooting potential of different coal types was studied in an inert pyrolysis environment in a drop-tube reactor (Nenniger, 1986). It was found that the soot yield increased while the tar and

hydrocarbon gas yield decreased as the pyrolysis temperature was raised. The soot yield reached an asymptote at high temperatures, which is dependent on coal rank. Wornat et al. (1988a) investigated changes in the composition of PAH during the tar evolution from the pyrolysis of high-volatile bituminous coal in argon. The compounds with more complex attachments were found to be more reactive than compounds with simple or no attachments. This is consistent with the previous discussion claiming that coal tar has a higher sooting tendency than the model compounds. PAH serves as a soot precursor, since the increase of soot yield was nearly offset by the decrease of PAH. In another pyrolysis experiment, Chen and co-workers (Chen and Niksa, 1992b) reported that the yields of tar/oils plus soot during secondary pyrolysis were constant and were equal to the maximum tar-plus-oil yields obtained during primary pyrolysis.

All of these pyrolysis experiments conducted in inert environments reported that the sum of tar plus soot remained constant during pyrolysis. The soot yields increased monotonically with temperature or reached an asymptotic value at high temperatures. However, the sum of tar plus soot in this study follows a different pattern: the soot yield first decreased and then increased with temperature. The sum of tar plus soot at 1858 K is almost two times the value at 1159 K for Knife River and Black Thunder coals, although the soot yields are small.

It is possible that the soot yield at high temperatures is susceptible to overestimation by ash contamination. Ash in the parent coal may vaporize during pyrolysis, then recondense with soot on the filters. Analysis of the high temperature soot samples showed about 10% ash in the Knife River soot and minimal amounts in the soots from the other three coals. Therefore, ash contamination of soot was not a major factor in these experiments, and cannot explain the increase in soot yields.

The chemical structure analysis facilitates the investigation of the major changes of tar during secondary pyrolysis, which can, in turn, be used to explain the measured tar and soot yields measured in this study. At 1159-1411 K, the thermal cracking reaction predominated, which is characterized by two distinct processes. First, the tar lost most of the aliphatic side chains and oxygen functional groups. Next, ring opening reactions also commenced to produce more light hydrocarbons and to release heteroatoms. Since soot formation is

negligible at this temperature range, a net decline of the yield of tar plus soot was observed. From 1411 K, direct conversion of soot from tar began, as evidenced by the increase of aromatic carbon per cluster. As secondary reactions proceeded, both ring rupture and polymerization became significant. As the cluster size became larger, polymerization of PAH was accelerated. The rate of soot formation surpassed the rate of tar decay, therefore, the sum of tar plus soot increased steadily from 1411-1618 K. The continuous growth of soot yield after 1618 K can only be explained by the addition of hydrocarbon species released from primary pyrolysis and the subsequent secondary cracking reactions. Eventually, these hydrocarbons were depleted at high temperatures (probably higher than 1900 K), and the soot yield reached an asymptotic value which is dependent on coal type.

Strong evidence has shown that direct addition of certain hydrocarbon species to the soot surface is a major soot growth mechanism at high temperatures. Soot formation from hydrocarbon fuels has been studied extensively. However, the effects of light hydrocarbons during the soot formation in a coal system are still unclear.

The participation of hydrocarbons in the growth of coal-derived soot was first noticed by Chen based on a carbon balance (Chen, 1991). In his experiment, the carbon fraction (total carbon in the coal) incorporated into the sum of tar/oils and soot was found to increase with increasing severity of secondary reactions. Since the carbon fraction released as CO during pyrolysis was negligible (less than 1%), the only source of carbon that contributed to soot growth would be hydrocarbons in the gas phase. Char is another possible carbon donor. However, the carbon in char (solid phase) cannot directly participate in soot growth, since carbons must be released as hydrocarbons first.

In this study, a similar phenomenon was also identified. The carbon fractions in the tars or soots are plotted in Figure 1.5.31 for the four coals in this study. As seen from the figure, at temperatures higher than 1500 K, the fraction of coal carbon incorporated into tar/soot increased substantially on a relative basis with increasing temperature. During secondary pyrolysis,

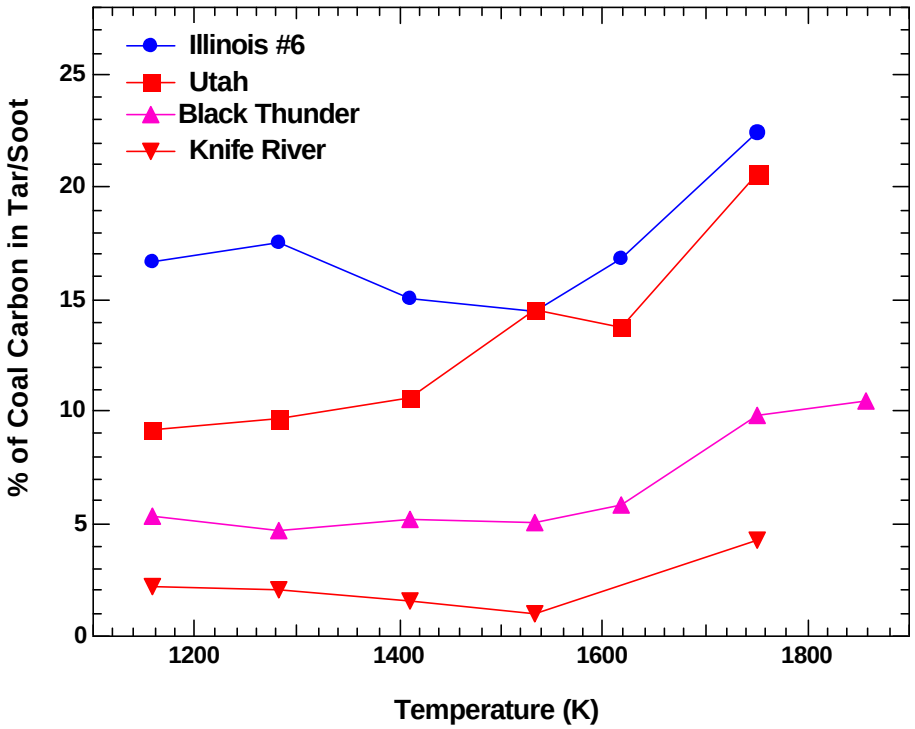

Figure 1.5.31. Fraction of coal carbon incorporated into tar and soot (collected at 1 inch above the burner surface).

primary tar will lose carbons due to the release of light hydrocarbons. When heteroatoms (mainly oxygen) in tar are expelled during ring opening reactions, additional carbons are lost since oxygen is released from tar as CO (Nenniger, 1986) and nitrogen as HCN (Chen, 1991). In Figure 1.5.31, the fraction of coal carbon in the sum of tar plus soot at 1858 K is much higher than that at 1159 K. That means the carbon loss during tar decomposition was compensated by gains in carbon from other sources. Previous studies showed that the CO yield always increases with increasing temperature during secondary reactions (Doolan, et al. 1986; Ledesma, et al. 1998), CO is therefore not considered to be a carbon source for the soot growth. The decline of measured total hydrocarbon yields at temperatures higher than 1500 K (Figures 1.5.11 to 1.5.14) conclusively demonstrates that hydrocarbons in the gas phase contribute significantly to the soot growth in a coal system.

Gas analysis in this study showed that C_2H_2 became the predominant species in hydrocarbons at temperatures higher than 1600 K (see Figure 1.5.16). Therefore, C_2H_2 should be the main species participating in the soot surface growth at high temperatures. Other researchers also reported that C_2H_2 is the only hydrocarbon that survives at temperatures above 1800 K (Doolan, et al. 1986). Direct C_2H_2 addition to the soot surface was modeled in a premixed hydrocarbon flame (Frenklach and Wang, 1990). It is most likely that this reaction is also important in coal pyrolysis. Benzene, claimed to be another important species in surface growth, seems to make much less contribution than C_2H_2, since benzene was consumed quickly at temperatures higher than 1600 K (Figure 1.5.16). The addition of hydrocarbons was modeled as a separate route for soot growth at high temperatures. The activation energy obtained for hydrocarbon addition is 320 kJ/mol, which is much higher than the activation energy for the direct tar conversion (230 kJ/mol). In other words, soot formation from tar is rapid compared to soot growth through hydrocarbon addition.

1.6 CHEMICAL STRUCTURE ANALYSIS

1.1.22 Chemical Structure Results

Solid-state ^{13}C NMR analysis gives insight into a variety of average chemical structural features in solid organic samples, such as coal, tar or soot. The NMR analyses were performed at the University of Utah for the tars and soots from the Illinois #6 coal and two model compounds. All the tar and soot samples used in the ^{13}C NMR analysis were collected at the 3 inch location in the FFB, except one tar sample was collected at the 1 inch location in the 1159 K condition from the Illinois #6 coal. A summary of these NMR analyses is given in Tables 1.6.1 and 1.6.2 respectively. In each table, the structural parameters derived directly from the NMR spectra are presented, followed by the lattice parameters calculated from the structural parameters. The elemental compositions of each sample are also shown. This is the first set of solid-state ^{13}C NMR analyses on tars from aromatic *model* compounds. These data, together with those previously reported on coal tars and soots (Hambly, 1998; Perry, 1999), give substantial insight into the transition from tar to soot. These data provide the basis for developing reliable soot mechanisms from aromatic compounds.

1.1.23 Analysis of Chemical Structure Data

Figure 1.6.1 shows the chemical structure of the two starting model compounds: biphenyl and pyrene. Biphenyl is made of two benzene rings connected with a single bond. Pyrene has a structure containing four fused benzene rings. These two compounds are pure aromatic

Table 1.6.1. Structural and Lattice Parameters for Tars/Soots from Illinois #6 Coal. (samples obtained at the 1 inch location at 1160 K, at the 3 inch location at other temperatures)

Structural Parameters[a]														
sample	f_a	f_a^C	f_a^O	$f_{a_O}^O$	$f_{a'}$	f_a^H	f_a^N	f_a^P	f_a^S	f_a^B	f_{al}	f_{al}^H	f_{al}^*	f_{al}^O
coal	0.72	0.05	0.02	0.03	0.67	0.21	0.46	0.08	0.18	0.20	0.28	0.19	0.09	0.05
1160 K	0.85	0.04	0.02	0.02	0.81	0.33	0.48	0.08	0.19	0.21	0.15	0.09	0.06	0.02
1280 K	0.92	0.02	0.005	0.015	0.90	0.42	0.48	0.04	0.19	0.25	0.08	0.05	0.03	0.02
1410 K	0.97	–	–	–	0.97	0.33	0.64	0.00?	0.19	0.45	0.03	0.03	0.00	–
1530 K	1.00	–	–	–	1.00	0.26	0.74			0.74	0.00	0.00	0.00	–

Lattice Parameters[b]								
	χ_b	C_{cl}	$\sigma+1$	P_0	B. L.	S. C.	M. W.	M_δ
coal	0.299	15	5.8	0.65	3.8	2.0	355	30
1160 K	0.259	12	4.0	0.78	3.1	0.9	227	21
1280 K	0.278	13	3.3	0.87	2.9	0.4	203	14
1410 K	0.464	23	4.5	1.00	4.5	0.0	319	9
1530 K	0.74	89		1.00			1186	

Elemental Analysis (daf)[c]				
	C (%)	H (%)	N (%)	O (%)
coal	75.68	5.16	1.50	12.78
1159 K	78.23	5.02	1.75	11.28
1281 K	85.61	4.00	1.89	4.22
1411 K	89.37	3.19	1.36	2.69
1534 K	90.15	1.73	0.6	3.37
1858 K	90.07	1.18	0.56	3.11

[a]Structural parameters:

Percent carbon: f_a-total sp^2-hybridized carbon; f_a^C-carbonyl, d>165 ppm; $f_{a'}$-

aromatic carbon; f_a^H-aromatic with proton attachment; f_a^N-nonprotonated aromatic; f_a^P-phenolic or phenolic ether; f_a^S-alkylated aromatic d=135-150 ppm; f_a^B-aromatic bridgehead; f_{al}-aliphatic carbon; f_{al}^H-CH or CH_2; f_{al}^*-CH_3 or nonprotonated; f_{al}^O-bonded to oxygen, d=50-90 ppm

[b]Lattice parameters:

χ_b: fraction of bridgehead carbons; C_{cl}: aromatic carbons per cluster; σ+1: total attachments per cluster; P_0: fraction of attachments that are bridges; B. L.: bridges and loops per cluster; S. C.: side chains per cluster; M_{cl}: the average molecular weight of an aromatic cluster; M_δ: the average molecular weight of the cluster attachments

[c]Elemental analyses were performed by Galbraith Laboratories in Knoxville, Tennessee

Table 1.6.2. Structural and Lattice Parameters for Model Compound Soots.

(samples obtained at the 3 inch location)

Structural Parameters													
	f_a	f_a^C	f_a^O	$f_{a\,O}^{O}$	$f_{a'}$	f_a^H	f_a^N	f_a^P	f_a^S	f_a^B	f_{al}	f_{al}^H	f_{al}^*
Biphenyl 1365 K	0.91	0.00	0.00	0.00	0.91	0.54	0.37	0.03	0.20	0.14	0.09	0.08	0.01
Biphenyl 1410 K	0.93	0.00	0.00	0.00	0.93	0.50	0.43	0.02	0.19	0.22	0.07	0.07	0.00
Biphenyl 1470 K	0.98				0.98	0.36	0.62	0.04	0.19	0.39	0.02	0.02	0.00
Pyrene 1410 K	0.98	0.02		0.02	0.96	0.47	0.49	0.02	0.12	0.35	0.02	0.02	0.00
Pyrene (1)[d] 1460 K	0.99				0.99	0.36	0.63		0.05	0.58	0.01	0.01	0.00
Pyrene (2)[e] 1460 K	0.99				0.99	0.36	0.63	0.03	0.13	0.47	0.01	0.01	0.00

Lattice Parameters								
	χ_b	C_{cl}	$\sigma+1$	P_0	B. L.	S. C.	M. W.	M_δ
Biphenyl 1365 K	0.154	9	2.3	0.96	2.2	0.1	–	–
Biphenyl 1410 K	0.237	11	2.5	1.00	2.5	0.0	–	–
Biphenyl 1470 K	0.398	20	4.7	1.00	4.7	0.0	–	–
Pyrene 1410 K	0.365	18	2.6	1.00	2.6	0.0	–	–
Pyrene (1)[d] 1460 K	0.586	35	1.8	1.00	1.8	0.0	–	–
Pyrene (2)[e] 1460 K	0.475	23	3.7	1.00	3.7	0.0	–	–

[d]Determined by deconvolution of the CP/MAS spectra.
[e]Determined by chemical shift range normally used in data analysis

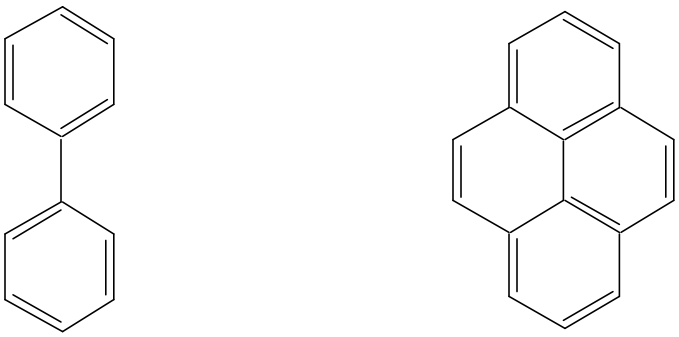

Biphenyl Pyrene

Figure 1.6.1. Chemical structure of biphenyl and pyrene.

compounds and found extensively in coal tars. Analysis of the chemical structure data of the tars from model compounds helps to reveal the important reaction pathways during soot formation from hydrocarbons. The tar/soot samples were generated at a temperature range where the transition from tar to soot is highlighted. During the experiment, it was found that no particles were observed in the reactor at temperatures lower than 1300 K. The deposits collected on the filters were yellowish and sticky, which is typical of tar. Only when the pyrolysis temperature was raised sufficiently high was luminosity noticed in the flame. The luminosity is due to the radiation emitted from the solid soot particles formed from tar. The soot incipient temperature varies for different starting compounds. In this study, the temperature was found to vary from 1350 to 1400 K for solid aromatic compounds.

The data in Tables 1.6.1 and 1.6.2 compare the chemical structures of the pyrolysis products at various stages of tar-soot transition. The numbers of side chains per aromatic cluster are plotted in Figure 1.6.2. For the coal tar sample at 1159 K, the number of side chains per cluster has been reduced by over 50% from that in the parent coal. Perry (1999) showed that the

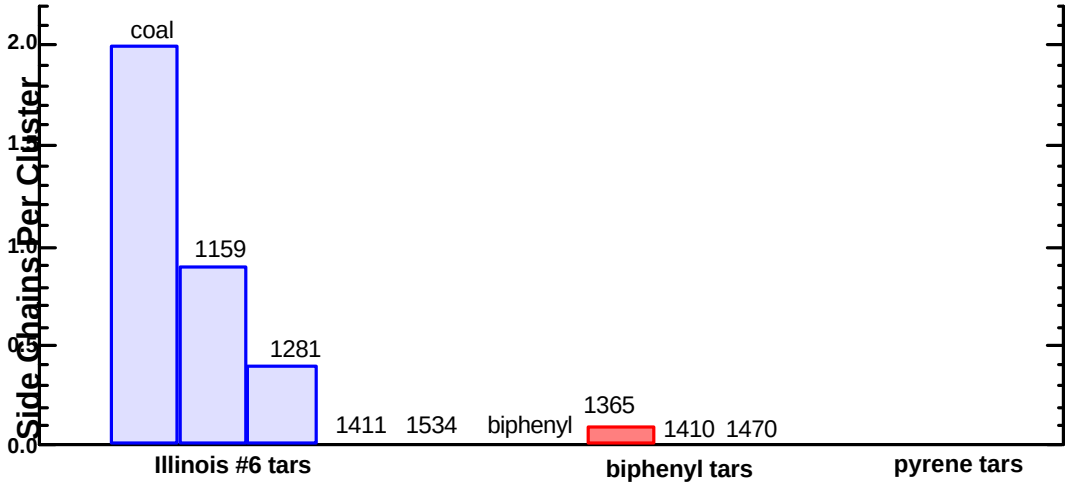

Figure 1.6.2. Changes of side chains per cluster with temperature for tars from Illinois #6 coal and two model compounds.

number of side chains per cluster in primary tars generated at 900 K in a drop-tube reactor were only 11% less than in the parent coal. This is a strong indication that significant secondary reactions had already occurred for the first tar samples collected in this study, resulting in a substantial loss of side chains. When the reaction severity increases, the tar continues to lose side chains, which are the source of the secondary gases such as light hydrocarbons, CO and H_2O. At 1411 K, no side chains were found in the coal tar. All the clusters were connected together by bridges or loops. In the case of biphenyl, there are no side chains in biphenyl itself. However, a small number of side chains was detected in the biphenyl tar at 1365 K. No side chains were found in pyrene tars, probably due to the high stability of the fused ring structure.

The number of bridges or loops can also be compared throughout the transition from tar to soot (see Figure 1.6.3). At 1159 K and 1281 K, the coal tar had fewer bridges or loops per cluster than the parent coal. This is consistent with the previous notion that tar is formed from

bond-breaking of the large coal network and is small enough to be vaporized into the gas phase. At 1411 K, the number of bridges and loops increased and was even higher than that in the parent coal. This means that the clusters in the tar are more interconnected, a sign of soot initiation. A similar finding was also reported by Hambly (1998) and by Perry (1999), but at a much lower temperature, 1080 K for Hambly and 1250 K for Perry.

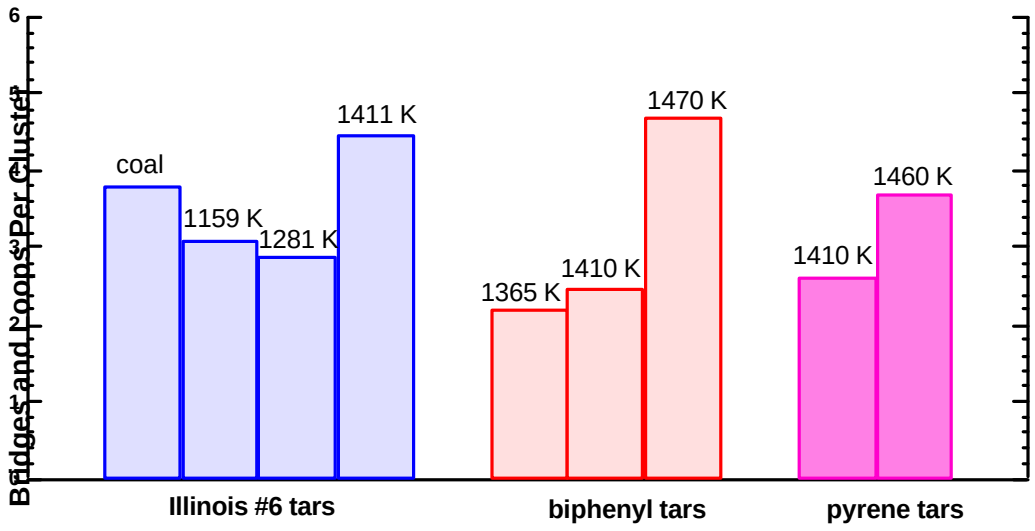

Figure 1.6.3. Changes of bridges and loops per cluster with temperature for tars from Illinois #6 and two model compounds.

The residence time at 1411 K in this study is about 74 ms, while the residence time is about 210 ms in Hambly's experiment and 300 ms in Perry's experiment. As explained previously, residence time also has an important effect on secondary reactions. The short residence time in this study may be responsible for the difference in the starting temperature of crosslinking in the tar.

The initiation of soot formation from tar can be best viewed from the number of aromatic carbons per cluster represented in Figure 1.6.4. The early coal tars have less aromatic carbons

per cluster than the parent coal, consistent with the findings of previous studies (Watt, et al. 1996; Perry, 1999). One explanation is that the clusters have to be sufficiently small in order to escape the coal matrix to form tar. Beginning at 1411 K, the number of aromatic carbons per cluster was higher than that in the parent coal. At the same time, the number of side chains decreased sharply. The only possible explanation is that the tar molecules began to undergo polymerization reactions (like crosslinking reaction in the char) after stripping off the side chains at this temperature. At 1534 K, the number of aromatic carbons per cluster is almost four times higher than that at 1411 K. However, for the tars from model compounds, the change is more gradual, but is comparable at temperatures below 1500 K.

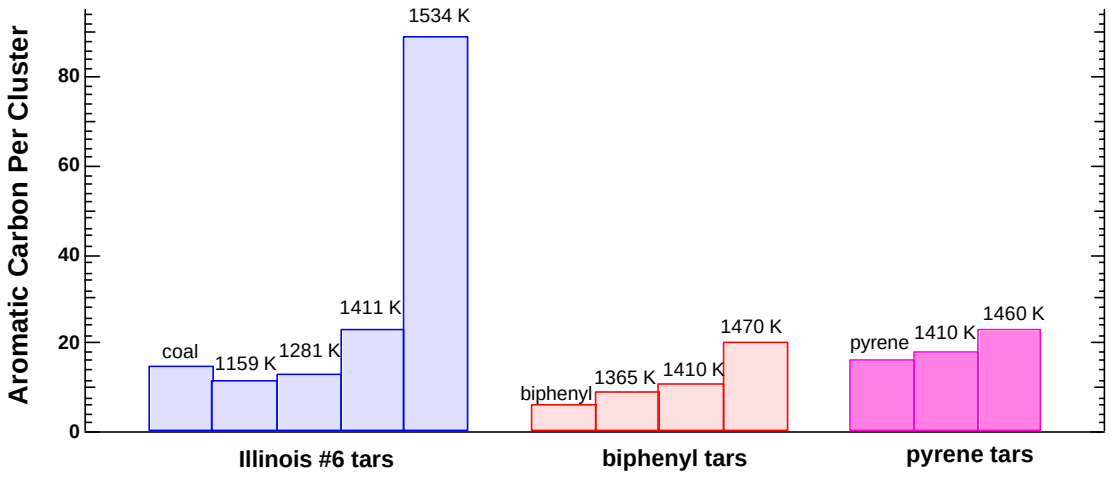

Figure 1.6.4. Changes of aromatic carbon per cluster with temperature for tars from Illinois #6 and two model compounds.

The average molecular weight of coal tar is shown in Figure 1.6.5. It is found that during

the transition from tar to soot, the size of the aromatic cluster grows substantially, consistent with the increase in the number of aromatic carbons per cluster. The molecular weight of soot samples from the two model compounds is not available due to the erroneous elemental analysis. However, the calculations showed that the increase (relative) of molecular weight of soots from the model compounds was much smaller than that for the coal tar, which indicates that coal tars have a higher sooting tendency than the model compounds.

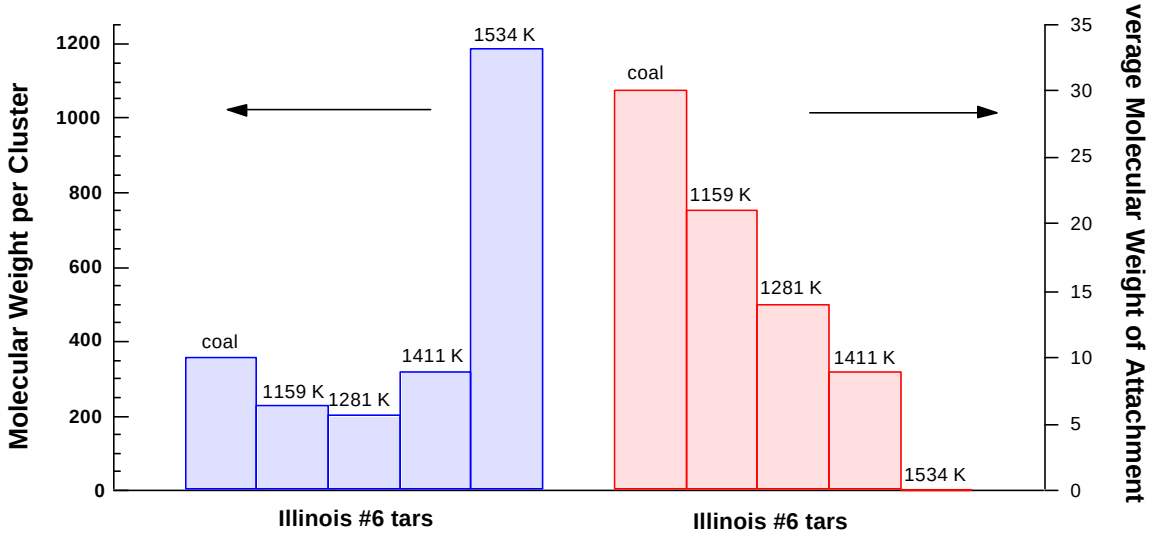

Figure 1.6.5. Changes of average molecular weight per cluster and average molecular weight per attachment with temperature for tars from Illinois #6 and two model compounds.

There is a striking similarity between the changes in aromatic carbons per cluster and the average molecular weight per cluster in the coal tars (compare Figures 1.6.4 and 1.6.5). The increase of the cluster size is almost entirely due to the increase in aromatic carbon. This is confirmed by the carbon aromaticity data (percent of carbon that is aromatic) in Figure 1.6.6.

The portion of the aliphatic carbon (side chains in this case) continued to decrease with the severity of the secondary reaction. Above 1400 K, almost all the carbons are aromatic, which means that ring growth reactions were dominant over ring opening reactions in the early stage of tar evolution. These aromatic clusters will continue to grow to form a large network of fused rings. A possible reaction pathway for the cluster growth is shown in Figure 1.6.7.

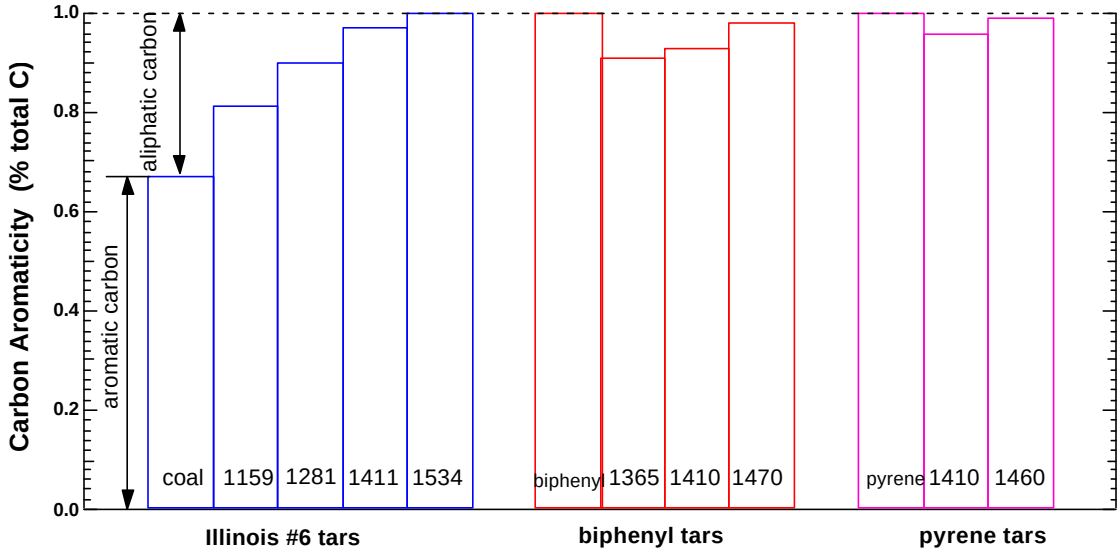

Figure 1.6.6. Changes of aromaticity with temperature for tars from Illinois #6 and two model compounds.

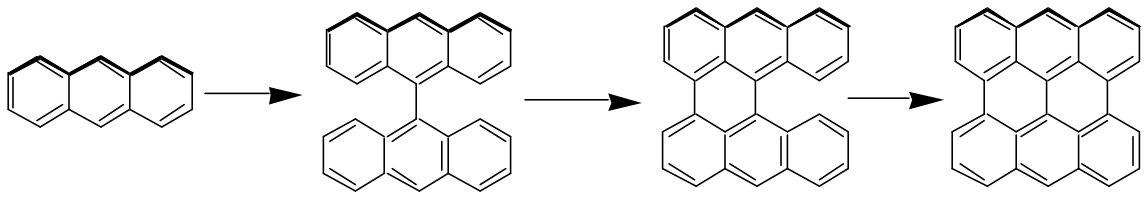

Figure 1.6.7. Hypothetical ring growth reaction in anthracene pyrolysis (adapted from Badger, et al. 1964).

In the case of coal, the primary tar, released from the coal matrix by breaking the labile bridges connecting the aromatic clusters, will first lose side chains or functional groups attached to the ring structure (see Figure 1.6.2). This will cause the release of secondary gases, which are seen in low temperature tar cracking studies. The side chain loss is also confirmed by the decrease in average molecular weight per attachment seen in Figure 1.6.5. From 1159 K, the molecular weight per attachment for the coal tar dropped quickly due to the mass release to the gas phase. At higher temperatures (1300-1500 K), the tar molecules undergo ring opening reactions. PAH with oxygen functional groups seem to have a higher reaction rate than non-polar PAH, as evidenced by the quick decline of f_a^O from 1159 K to 1411 K. Analysis of nitrogen-containing PAH from coal pyrolysis also indicated the preferential reaction of polar PAH in secondary reactions (Wornat, et al. 1988b). At temperatures higher than 1400 K, PAH undergoes polymerization to form larger clusters. This reaction is sensitive to temperature and becomes very fast at elevated temperatures, as evidenced by the marked increase in molecular weight per cluster seen in Figure 1.6.5, where the molecular weight increased by a factor of three between 1411 K and 1534 K. At this stage, the clusters are getting larger *and* more aromatic. At 1534 K, the aromaticity is very close to unity for the coal tar/soot. The higher number of bridges and loops for this sample also showed that the clusters are more interconnected. At the final stage, the cluster size (number of carbons per cluster) of the soot sample can be quite large (e.g. greater than 200 at 1858 K), suggesting that the polymerization reactions are dominant from 1600-1800 K. This is also consistent with the previous conclusion that soot formation is favored at high temperatures.

The data obtained for the biphenyl samples exhibit a different pathway for pyrolysis and soot growth. First, ring opening reactions have occurred during early pyrolysis, which is clearly evident by the aliphatic carbon present in the samples (see Table 1.6.2). FTIR analysis of the gas phase during the model compound pyrolysis also showed the existence of small hydrocarbon molecules including CH_4, C_2H_2 and benzene. Therefore, it is believed that a ring opening reaction occurs early in the soot formation process for biphenyl. The decrease of the fraction of

aliphatic carbon with increasing temperature (e.g., 0.09, 0.07 and 0.02) indicates that major structural rearrangements are occurring following the initial ring opening reactions. The number of bridges and loops per cluster, which is 1.0 in unreacted biphenyl, doubles to 2.2 and 2.5 at 1365 K and 1410 K and then doubles again to 4.7 at 1470 K. The cluster size, which starts at 6 in the parent molecule, grows to 9, 11 and 20 aromatic carbons respectively. Hence, the ring size not only grows significantly but the number of bridges and loops per cluster also increases from a value of 1 to nearly 5 over the relevant temperature range. This suggests that soot growth in biphenyl soot consists not only of ring size growth but also cluster crosslinking which could result in the formation of large crosslinked structures. Although NMR analyses for model compound samples at higher temperatures are not available, it is most likely that they will follow a trend of soot growth similar to that of the coal tar.

The evolution of pyrene soot follows still another path. First, little evidence is noted for ring opening reactions. Only approximately 1% of the carbon appears as sp^3 hybridized species, indicating that very little ring opening occurs, unless stable alicyclic molecular species are formed following ring opening. The smaller amount of aliphatic carbon in pyrene tar/soot samples is probably due to the high stability of fused ring structure in pyrene. Second, ring growth of only approximately 10% has occurred at 1410 K compared to nearly 100% in the case of the corresponding biphenyl soot. However, data on this 1410 K soot sample indicate that the relatively small cluster size has been augmented by an average of 2.6 crosslinking sites per cluster. The data obtained from this study are inconclusive regarding the exact mechanism for ring growth in the pyrene soots between 1410 K and 1460 K, since different analysis methods on the broadened aromatic band of pyrene soots generated different results.

1.7 NITROGEN RELEASE DURING COAL PYROLYSIS

1.1.24 Nitrogen Distribution

Temperature is a critical factor in determining the extent of secondary reactions. In this study, the temperature range was carefully selected in order to highlight the nitrogen release during secondary pyrolysis. The cumulative distributions of the coal nitrogen at various temperatures are presented in Figures 1.7.1 to 1.7.4. At the lowest temperature (1159 K), the secondary reactions just began as indicated by the initiation of HCN release. It is suggested that the initiation of HCN could be considered as a sign for the start of the gas-phase secondary reactions of the primary tar (Freihaut, et al. 1993). At the highest temperature (1858 K), the secondary reactions of the tar were near completion, as evidenced by the H/C ratio of the soot.

The distribution of the nitrogen from the parent coal was determined from the char and tar/soot yields coupled with elemental analysis. Gaseous nitrogen species were determined independently from the results of FTIR measurement. Except for the Illinois #6 coal, the nitrogen balance is within 10% at temperatures higher than 1500 K, but deteriorates at low temperatures. Below 1300 K, 10-20% of the nitrogen in the parent coal is not accounted for in the measurements. A similar trend was also observed in Chen's experiment, where about 10% of the coal nitrogen is not accounted for in the early phase of secondary pyrolysis (Chen, 1991). Haussmann also reported a nitrogen balance of 90% when pyrolyzing a Pittsburgh #8 coal in an arc-jet fired entrained-flow reactor (Haussmann, 1989). However, the missing nitrogen remained constant over the temperature range in his study (1200-1600 K). Therefore, Haussman labeled the missing nitrogen as N_2.

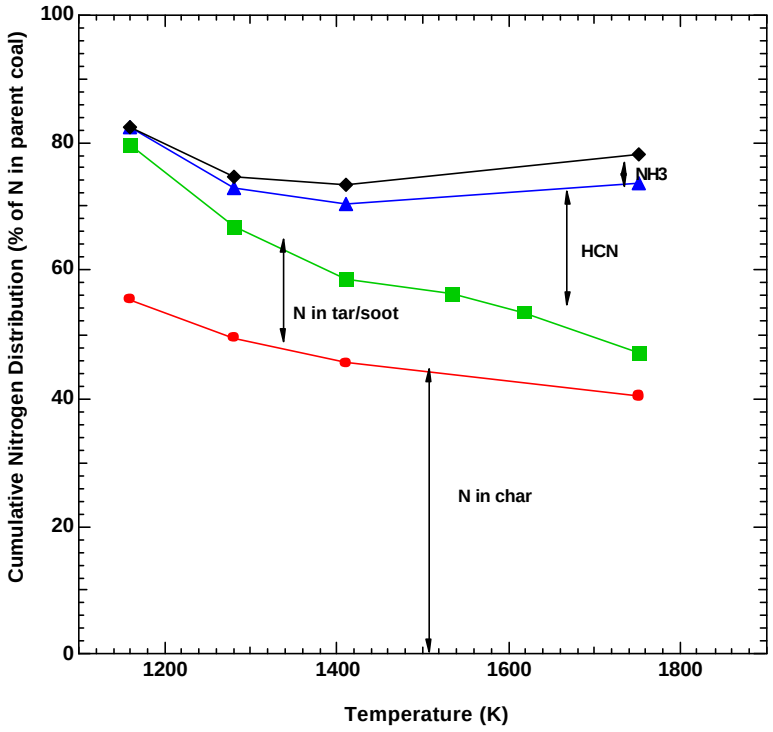

Figure 1.7.1. Cumulative distribution of the coal nitrogen for the Illinois #6 coal at the 7 inch location.

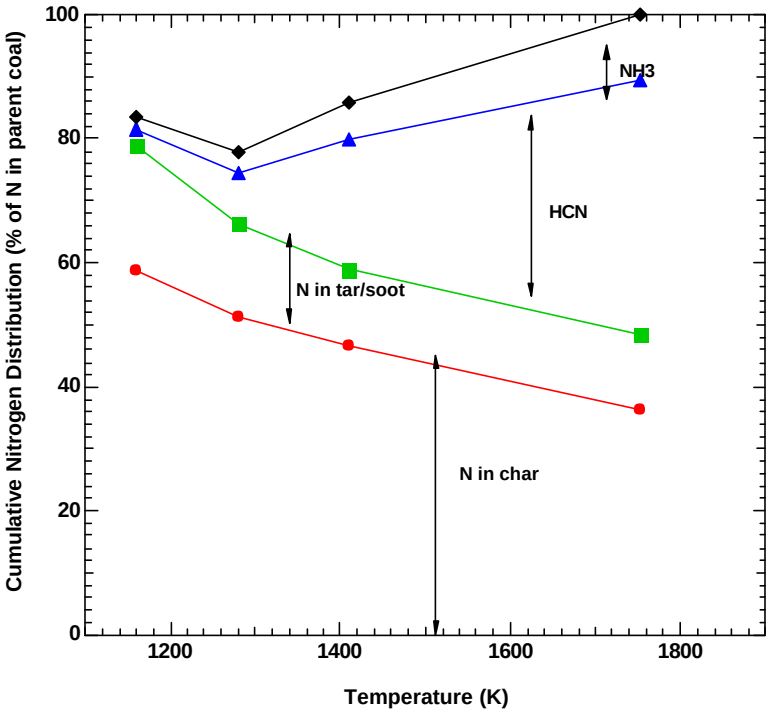

Figure 1.7.2. Cumulative distribution of the coal nitrogen for the Utah coal at the 7 inch location.

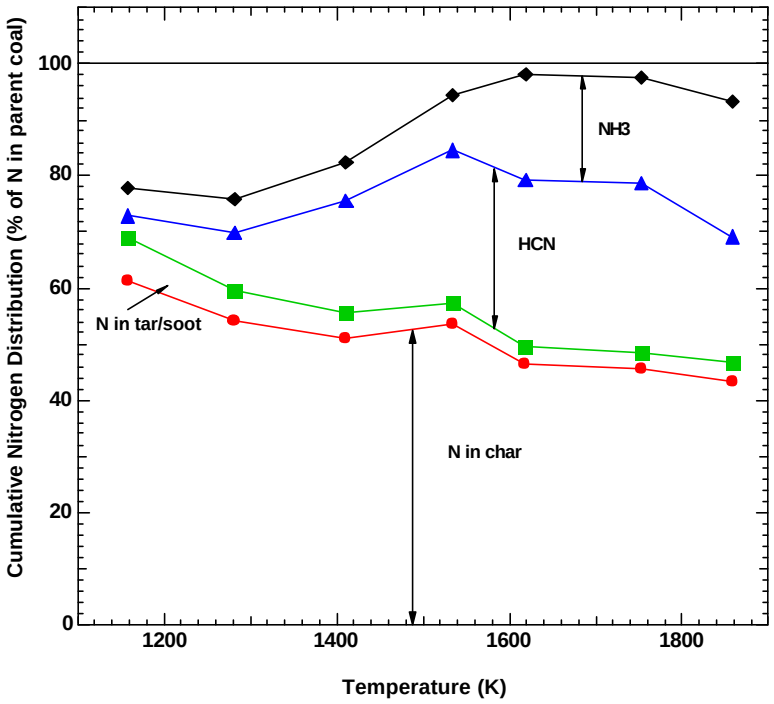

Figure 1.7.3. Cumulative distribution of the coal nitrogen for the Black Thunder coal at the 7 inch location.

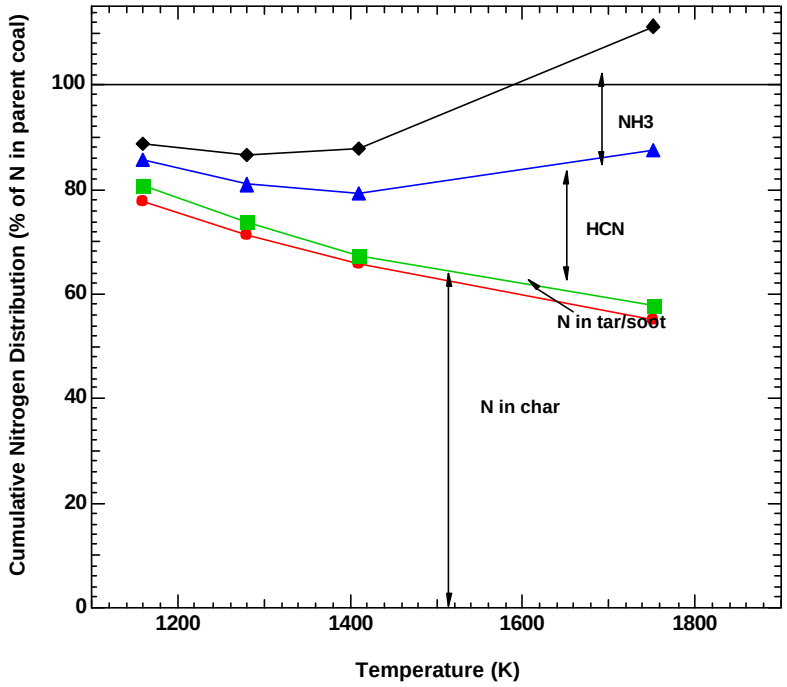

Figure 1.7.4. Cumulative distribution of the coal nitrogen for the Knife River coal at the 7 inch location.

Repeated FTIR analysis in the gas phase showed that the release of HCN and NH_3 at temperatures below 1300 K was insignificant. The small nitrogen-containing aromatics (1-2 rings) commonly found in coal tar (Nelson, et al. 1990) could possibly account for the missing nitrogen. However, no significant peaks associated with these nitrogen-containing species are identified in FTIR spectra. These species are also never reported in substantial amount in previous studies. Molecular nitrogen (N_2) may be responsible for the missing nitrogen during the pyrolysis of the Illinois #6 coal, possibly caused by reburning type reactions. However, it should not be a significant source of error for the other three coals, since the nitrogen balance improved and was close to 100% at high temperatures. Therefore, the gap in nitrogen balance is most likely due to inaccuracy of the nitrogen fraction in the solid phase and perhaps some unknown nitrogen species not mentioned above.

In Chapter 5, the tar and soot yields measured in this study are compared with those reported from literature. For coals of similar rank, systematic lower tar yields were observed in this

study, especially at low temperatures. This may partially reconcile the failure of the nitrogen closure at low temperatures. For Illinois #6, the missing nitrogen (as much as 20%) even at high temperatures is unclear.

1.1.25 Modeling of Nitrogen Evolution during Secondary Reactions

Nitrogen evolution is the major topic in this study. Two major processes of nitrogen evolution have been identified during secondary pyrolysis. First, thermal cracking of tar causes ring opening reactions, releasing nitrogen as HCN (Chen, 1991).

Second, at high temperatures, when polymerization reactions of tar are sufficiently rapid, certain portions of the tar nitrogen will be integrated into soot. However, nitrogen can also be released directly from char at elevated temperatures. The measured HCN and NH_3 were the sum of those released from tar and those released directly from char. No distinction can be made between these two mechanisms in the current study. In addition, some researchers believe that NH_3 maybe a secondary product formed from HCN. This makes the model of HCN and NH_3 even more complicated, since the reaction pathways for HCN-NH_3 conversion are not fully understood.

In this study, only the nitrogen evolution in the tar and soot was modeled. Nitrogen release from char has already been modeled using the revised CPD model with adequate accuracy for high temperature, high heating rate pyrolysis (Perry, 1999). The fraction of the coal-N incorporated in tar or soot can be calculated by

$$N_{tar} = \frac{m_{N,tar}}{m_{N,coal}} = \frac{[N]_{tar} m_{tar}}{[N]_{coal} m_{coal}} \qquad (7.1)$$

where [N] and m are the nitrogen content and mass of tar or coal, respectively. It should be noted that the mass of tar over the mass of coal gives the tar yield, as in (6.10)

$$\frac{m_{tar}}{m_{coal}} = y_{tar} \qquad (7.2)$$

then

$$N_{tar} = \frac{[N]_{tar}}{[N]_{coal}} y_{tar} = R_N \cdot y_{tar} \qquad (7.3)$$

Since the tar and soot yield can be calculated using the model in the previous section, only the nitrogen ratio needs to be modeled. By careful examination of the experimental data, it was found that the ratio of the nitrogen content in tar or soot over that in the parent coal (daf) follows a similar trend for all the coals at long residence times (Figure 1.7.5). The nitrogen ratio drops very quickly between 1300–1500 K, then decreases at a much slower rate at temperatures higher than 1600 K. An empirical first-order reaction mechanism was devised to fit the data in this study (also shown in Figure 1.7.5).

$$\frac{dR_N}{dt} = -A_N \exp(-\frac{E_N}{RT})(R_N - R_\infty) \qquad (7.4)$$

where A_N, E_N and R_∞ are the empirical pre-exponential factor, activation energy and ultimate nitrogen ratio, respectively. The coal-independent (for the coals in this study) kinetic parameters are shown in Table 1.7.1. The calculated amounts of coal nitrogen incorporated into tar and soot versus temperature using these parameters are shown in Figure 1.7.6. There is generally excellent agreement between the data and model predictions. The model does not agree with the data from the high temperature experiments on the Utah and Knife River coals (1752 K); these two points are thought to be in error, since nitrogen addition to soot is unlikely at this temperature.

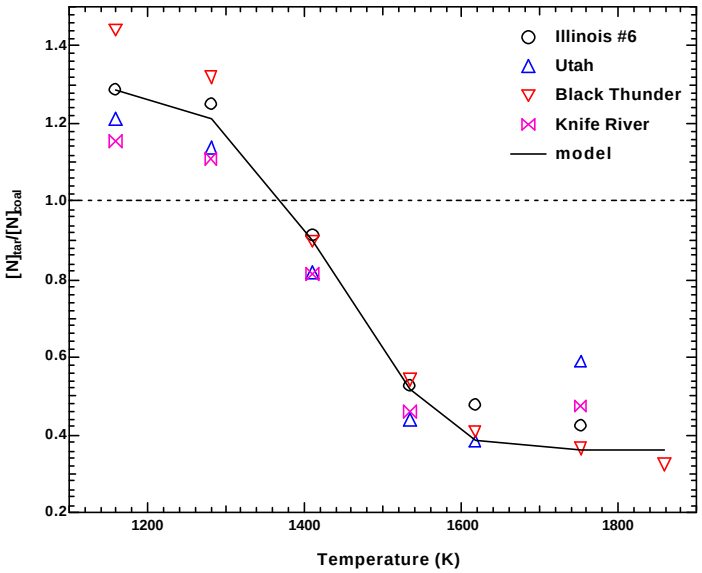

Figure 1.7.5. $[N]_{tar}/[N]_{coal}$ versus temperature for all the coals in this study. The line is the model prediction using the best-fit parameters in Table 1.7.1.

Table 1.7.1. Best-Fit Kinetic Parameters Used in the Simulation.

A_N (sec^{-1})	E_N (kJ/mol)	R_∞ (unitless)
5.90E8	220	0.36

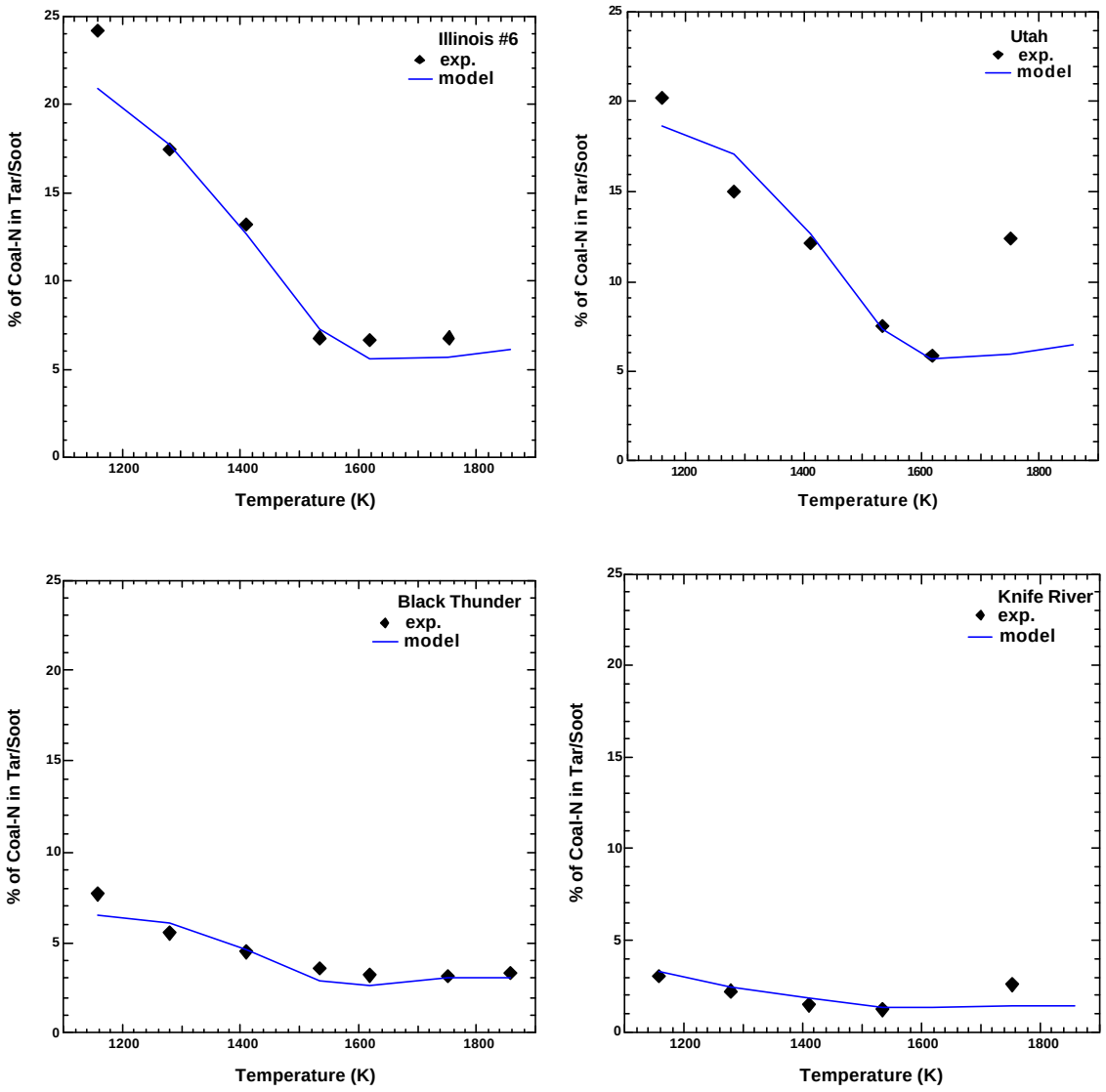

Figure 1.7.6. Predicted decay of the fraction of coal nitrogen in the tar and soot (N_{tar}) compared with the measured values (for the longest residence time at each temperature condition).

1.1.26 Nitrogen Release during Coal Pyrolysis

1.1.26.1 Total Nitrogen Release

As discussed in Chapter 1, only the nitrogen released to the gas phase can be reduced by effective methods such as air staging. Therefore, the fraction of volatile nitrogen somewhat determines the overall NO_x reduction efficiency for coal combustion. Figures 1.7.1 to 1.7.4 showed that about 40% of the coal nitrogen was released rapidly during the primary pyrolysis at 1159 K. However, the nitrogen release during secondary pyrolysis was at a much slower rate. At least 40% of the coal nitrogen remained in the char even at the most severe conditions. Pohl and Sarofim (1977) showed that all of the nitrogen in the char would be released if treated at 2100 K for 20 minutes. However, since typical residence times in industrial furnaces are about 2 s for pulverized coal, significant nitrogen remains in the char after pyrolysis.

During the pyrolysis process, nitrogen release is inherently related to mass release. In Figure 1.7.7a, the total nitrogen release versus mass release data obtained in this study are compared with the results reported by Baxter (1996) for an Illinois #6 coal and by Haussmann (1989) for a Pittsburgh #8 coal. This figure shows that the results in the current study are comparable with those in the literature. For bituminous coals, the nitrogen release is comparable with the mass release during the early stage of pyrolysis (0-30% mass release), followed by a slower nitrogen release than mass release in the 30-55% mass release stage. In the final stage (higher than 55% mass release), the nitrogen release was found to continue when the mass release was nearly completed.

The nitrogen release pattern for low rank coals is shown in Figure 1.7.7b and exhibits a different pattern from that observed for the bituminous coals in Figure 1.7.7a. In Figure 1.7.7b, the total nitrogen release versus mass release data for the Black Thunder coal and Knife River lignite are compared with the results from Haussmann (1989) for a Montana subbituminous coal and from Baxter (1996) for a Beulah lignite. In the early phase of devolatilization, the fractional nitrogen release rates for the low rank coals are much slower than the normalized overall mass

release. The slower nitrogen release during early pyrolysis is even more significant for the Montana subbituminous and the Beulah lignite operated in entrained-flow systems. As the pyrolysis proceeds, the particle temperatures rise and the nitrogen is released when the aromatic ring structures are volatilized or ruptured. During the late stages of pyrolysis, the nitrogen release catches up with the mass release. The continued slow nitrogen release after the completion of the mass release is less pronounced for low rank coals.

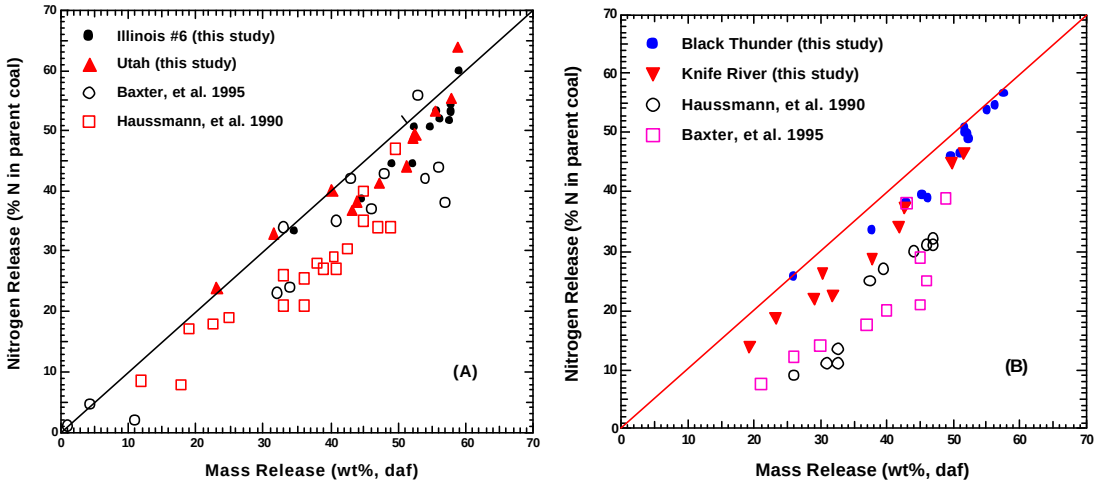

Figure 1.7.7. (A) Nitrogen release vs. mass release for the bituminous coals. Also shown are values reported by Baxter for an illinois #6 coal and by Haussmann for a Pittsburgh #8 coal; (B) nitrogen release vs. mass release for low rank coals. Also shown are values reported by Haussmann for a Montana subbituminous coal and by Baxter for a Beulah lignite.

1.1.26.2 Nitrogen Evolution in Tar and Soot

Under rapid heating conditions, tar is virtually the only carrier for nitrogen release when secondary reactions are eliminated. Almost all the nitrogen in coal exists in tightly bound aromatic ring structures, which are among the most thermally stable structures in the coal. These ring structures are transported essentially intact to form tar during primary pyrolysis. However,

different types of coals are observed to exhibit different patterns of primary nitrogen release, indicating a strong rank dependence.

The nitrogen ratio in tar, defined as the nitrogen content in the tar or soot divided by the nitrogen content in the parent coal (daf), is a convenient gauge to monitor the rank dependence of nitrogen release:

$$R_N = \frac{[N]_{tar/soot}}{[N]_{coal,daf}} \qquad (7.5)$$

Since the nitrogen content in the parent coal is a constant, the ratio actually reflects the change of nitrogen evolution in tar or soot. Freihaut et al. (1993) reported that bituminous coal tars display an almost constant R_N, irrespective of extent of tar evolution during the early phase of devolatilization. Values of R_N close to unity suggest that tar is a collection of random samples from the coal. This is also observed by Solomon and coworkers (1978) in a pyrolysis experiment involving 12 bituminous coals. They found that the amount of nitrogen released was proportional to the amount of tar released during the initial stage of devolatilization. However, low rank coal tars have a much smaller R_N, and R_N was found to increase with increasing temperature. The smaller R_N in low rank coal tars means the non-polar PAH are *preferentially* released as tar during pyrolysis of low rank coals. This is confirmed by the greater char nitrogen fraction in the Knife River lignite than other coals at 1159 K in this study. The exact nature of the delayed nitrogen release in low rank coal tars is not obvious, but it may be related to the early crosslinking reaction that occurs only in low rank coals. Some nitrogen-containing PAH (PAHN) are trapped in the large clusters during the early crosslinking, making them too large to vaporize as tar during pyrolysis.

After the tar escapes the coal matrix, nitrogen release will take different routes of release in the tar and in the remaining char. The tar nitrogen evolution is presented in the following discussion. Further nitrogen release from char will be discussed in the next section.

Figure 1.7.5 shows the nitrogen ratio (R_N) versus temperature for the four coals used in this

study. A similar trend is observed for all coals: the nitrogen ratios were higher than unity below 1300 K, followed by a rapid decay between 1300-1600 K, finally decreasing at a much slower rate at temperatures above 1600 K. The striking similarity of the nitrogen release from tars of different coal types indicates that reactivity of the tar nitrogen functionalities during secondary pyrolysis is largely rank independent.

It is interesting that the nitrogen content in tar is initially higher than the nitrogen content in coal, i.e., R_N is higher than unity, at the early stage of secondary pyrolysis. Such enrichment of nitrogen at the early phase of secondary pyrolysis can be explained by examining the chemical structure data of the tar and soot. From the chemical structure analysis, it was found that the first set of secondary reactions of tar was loss of side chains and functional groups (relatively free of nitrogen). The tar nitrogen release is delayed since nitrogen usually exists in aromatic ring structures that react at higher temperatures. Therefore, since the tar releases carbon, hydrogen and oxygen but not nitrogen, high nitrogen ratios are observed during the early stages of secondary pyrolysis. At later stages of secondary pyrolysis, ring opening reactions became significant, where the tightly bound nitrogen in aromatic rings was released (usually as HCN). The nitrogen ratio, R_N, therefore dropped due to the nitrogen loss from tar.

1.7.1.1.1 Nitrogen in Soot

Polymerization of the ring structures in tar becomes more pronounced at more severe pyrolysis conditions. A portion of the nitrogen is incorporated into the young soot particles. Recently, the evolution of the nitrogen-containing compounds in tar during secondary pyrolysis was examined. It was found that the initial depletion of nitrogen in tar is mainly attributed to direct conversion into soot (Yu, et al. 1999). This implies that the young soot should have a higher nitrogen ratio than the primary tar, which is confirmed by examining Chen's (1991) soot data. Figure 1.7.8 shows Chen's nitrogen ratio (R_N) data for tar and soot during the secondary pyrolysis for a Pittsburgh #8 coal. In his experiment, the aerosols collected on the glass filters were first extracted with tetrahydrofuran (THF), followed by filtration through a Teflon membrane. The membrane residue was denoted as soot and the sample going through the membrane was deemed tar. As seen from the figure, nitrogen is concentrated in the

soot during the early stage of secondary pyrolysis. However, the nitrogen ratio decreased rapidly due to the fast soot growth at more severe conditions. Haussmann and Chen reported that the fraction of coal nitrogen incorporated into the soot is constant during secondary pyrolysis, even though soot

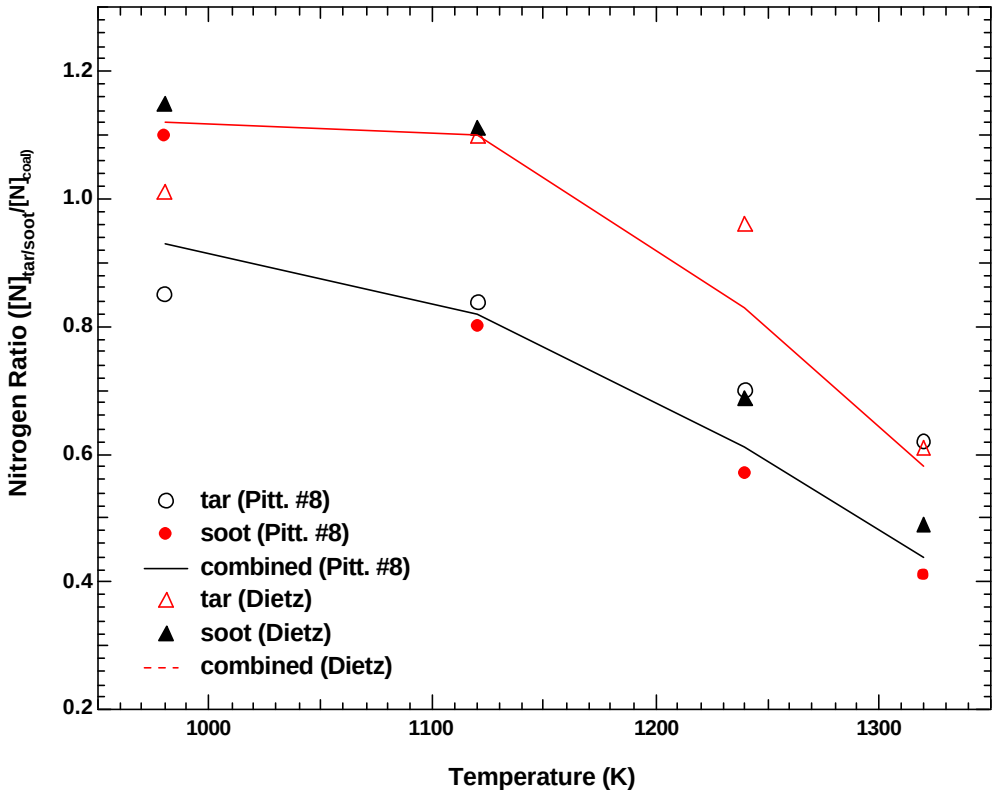

Figure 1.7.8. Nitrogen ratio of a Pittsburgh #8 tar and soot during secondary pyrolysis (adapted from Chen, 1991). Temperatures in the figure denote the maximum particle temperatures.

yields increase dramatically at the same time. The nitrogen analysis in this study supports this idea. In Figure 1.7.6, the fraction of coal nitrogen in tar and soot versus the temperature was shown. At temperatures above 1600 K, the nitrogen fraction in soot (there is almost no tar at these conditions) reaches an asymptotic value which is coal-dependent. The observed constant

nitrogen fraction in soot can be reconciled by the following arguments. As Yu pointed out, the incorporation of tar nitrogen into soot occurs during the early stages of secondary pyrolysis. As pyrolysis proceeds, the clusters in the soot become larger and more interconnected (see Figures 1.6.3 and 1.6.4), which serve as a barrier that hinders the further release of nitrogen by ring rupture. Direct addition of nitrogen-free hydrocarbons is an important soot growth mechanism at high temperatures, as discussed earlier. Soot growth by hydrocarbon addition lowers the nitrogen ratio in soot. Therefore, the amount of coal nitrogen integrated into soot in largely determined by the early soot formation process.

1.7.1.1.2 Reactivity of Nitrogen Functionalities in Tar

The decay in the nitrogen ratio is similar for all the coals in this study. Therefore, it is reasonable to suspect that the reactivity of the tar nitrogen shows little rank dependence. Analysis already showed that the nitrogen functionalities in coal tar are very similar for coals ranging from brown to bituminous (Nelson, et al. 1990). One or two ring nitrogen-containing aromatics such as pyrrole, pyridine, quinoline, indole and some nitriles are the major components. The observed nitrogen decay in tar would reflect the combined effect of all these compounds. As a homogeneous gas reaction, the nitrogen decay in tar is expected to be less dependent on the original coal properties.

1.1.26.3 Nitrogen in the Gas Phase

FTIR measurements in this study showed that HCN and NH_3 are the dominant nitrogen-containing gas species evolved during secondary pyrolysis (Figure 1.7.1 to 1.7.4). This is consistent with previous studies on coal nitrogen release under rapid heating conditions. Other important nitrogen species, reported previously in literature, were also examined. HNCO, found in fluidized-bed experiments (Ledesma, 1998), was not measured due to the significant overlap of the CO_2 and CO peaks in the spectral range 2200-2400 cm^{-1}. Scoping pyrolysis experiments were performed on a South Banko lignite in pure N_2 at 1000 K in the BYU drop tube reactor (Perry, 1999). No HNCO was detected in the gas phase. It is possible that HNCO formed

through interaction with the fluidized particles. Therefore, measurements were focused on HCN and NH_3.

The relative amount of HCN and NH_3 formed during coal pyrolysis is very important in determining the final fuel-N conversion. While NH_3 is mainly converted to NO, HCN can either be converted to NO or N_2O (Schafer, 2000). The nitrogen partitioning in the gas phase during pyrolysis is therefore important in predicting NO_x formation in coal-fired furnaces. However, it is still not clear whether HCN and NH_3 are released independently from different functionalities in the coal, or whether, and to what degree, NH_3 is a secondary product of HCN hydrogenation (Ledesma, 1998).

By examining the nitrogen distribution in this study, it was found that the sum of HCN and NH_3 at 1858 K is much higher than the fraction of coal nitrogen incorporated in the early tar. This observation indicates that secondary reaction of tar is not the only source of nitrogen release into the gas phase. Actually, the fraction of nitrogen released as tar is almost insignificant for low rank coals. The coal nitrogen in the early tars is only 8% for Black Thunder and 3% for Knife River. In contrast, the final amounts of HCN plus NH_3 can account for as much as 50% of the parent coal nitrogen. Thermal decomposition of char plays a significant role in nitrogen release during coal pyrolysis. Although XPS analysis showed that similar nitrogen functionalities are found in both tar and char (Kelemen, et al. 1998), the rate and mechanism of nitrogen release from these two sources are quite different. However, it was impossible to distinguish the separate contribution of char vs. tar to the HCN and NH_3 formation in the current study.

Thermal cracking of tar vapor without the interference of char was conducted in a tubular flow reactor from 600-1000^oC (Ledesma, 1998). HCN was found to be dominant in the gas phase, with a small amount of NH_3 and HNCO. The source of HCN is thought to be the nitriles found in coal tar. Nitrile functionality, absent in the parent coal and primary tar (at 600^oC), was identified in coal tar at high temperatures (800^oC) using XPS (Li, et al. 1997). However, amino nitrogen peaks, rather than nitriles, were found in low rank coal tars in another study (Kelemen, et al. 1998). It should be pointed out that it is difficult to distinguish these two

functionalities, due to the overlap of these peaks in the XPS spectra. Model compounds studies showed that the release of HCN from coal through nitriles is more plausible. Laskin and coworkers (1997) studied the decomposition of indole and quinoline (two nitrogen functionalities common found in coal tar) in a shock-tube reactor. Four major species were identified in the reaction system: acetylene, HCN, benzene and nitriles. Nitriles were formed by breaking the carbon-nitrogen bond in the compounds (Figures 1.7.9 and 1.7.10). HCN can be formed by breaking the weak carbon-carbon bond from nitriles, confirming that ring opening is the major mechanism for nitrogen release from coal tar. No NH_3 was detected in their analysis. Actually, HCN is the only nitrogen species reported in model compound studies, except that reported by Axworthy where a small amount (less than 5%) of NH_3 was detected (Axworthy, et al. 1978). Coal tar contains the same nitrogen compounds that have been examined in model compounds studies. In addition, tar cracking is also a homogeneous gas phase reaction. Therefore, it is reasonable to believe that the amount of NH_3 formed *directly* from coal tar is small.

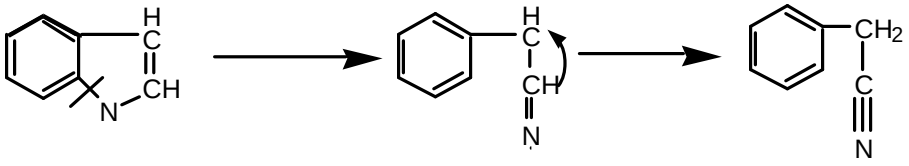

Figure 1.7.9. The reaction scheme of the formation of nitrile from indole (adapted from Laskin, 1997).

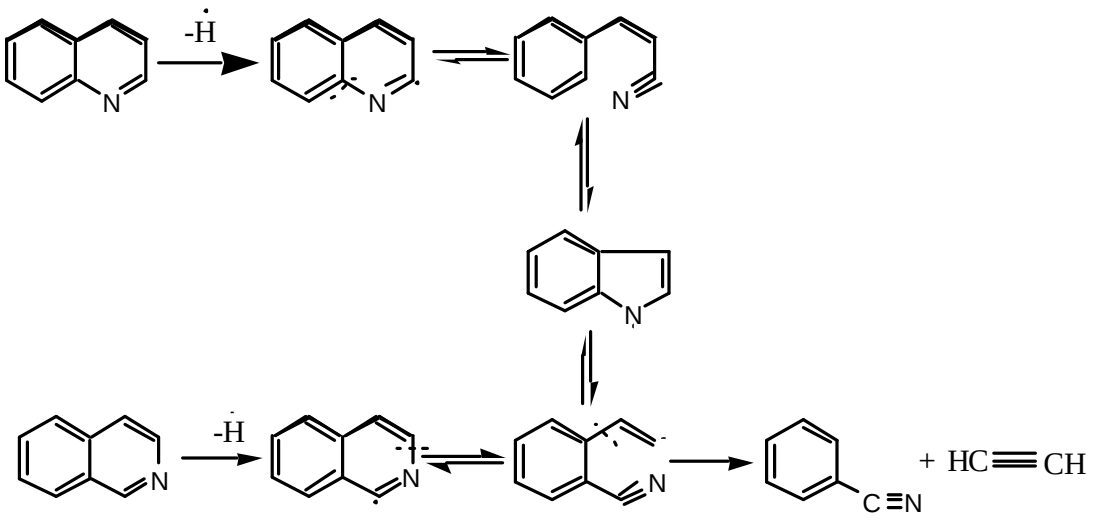

Figure 1.7.10. The reaction scheme of the formation of nitrile from quinoline and isoquinoline (adapted from Laskin, 1998).

Coal tar is not merely a mixture of pure aromatic nitrogen-containing compounds. It is more complex and contains aliphatic side chains and oxygen functional groups. It is believed that these attachments play an important role in tar nitrogen release. First, these side chains, when detached to form radicals (having lower selectivity and activation energy), tend to attack the ring structures, resulting in an early release of nitrogen. Previous studies show that HCN usually emerges between 1250-1350 K for model compounds such as pyrrole (Mackie, et al. 1991), pyridine (Mackie, et al. 1990), indole (Laskin, 1997), quinoline (Laskin, 1998) and 2-picoline (Terentis, et al. 1992). However, HCN release in coal pyrolysis occurs at about 1000 K, which is much lower. Second, the existence of oxygen in coal tar makes the conversion from HCN to NH_3 possible. Van der Lans and co-workers suggested that NH_3 is formed from other nitrogen compounds (like HCN) by reaction with oxygen-derived radicals, since more NH_3 has been found in experiments with larger amounts of oxygen (Van der Lans, et al. 1997). The higher NH_3 formation in pyrolysis of low rank coals is also attributed to the higher oxygen content. In addition, more NH_3 was always detected in peat (having a higher oxygen and hydrogen content) than in coal in the same pyrolysis condition (Aho, et al. 1993; Leppalahti, 1995). The current

study, to a certain degree, also seems to support this idea. Figures 1.7.1 to 7.4 show that the NH_3 yield increased with increasing temperature. However, as temperature increased in the current experiments, the equivalence ratio became lower (see Table 1.4.2). The equivalence ratio is 1.45 at 1159 K but only 1.09 at 1858 K condition. The higher concentration of oxygen-derived radicals (resulting from both the high temperature and initial high oxygen concentration) may be *partially* responsible for the observed increase of NH_3 in the current study.

The main reaction pathway for the conversion of HCN to NH_3 can be summarized as (adapted from Van der Lans, et al. 1997):

$$HCN / CN \xrightarrow{oxygen} NCO \xrightarrow{H} NH_i \qquad (7.5)$$

The oxygen can be O_2, OH or O radicals. In a post flame environment, OH is more important (Fenimore, 1979). However, NCO seems to be the intermediate for the conversion at all cases.

NH_3 can also be formed directly from coal pyrolysis. Figures 1.7.11 and 1.7.12 show the HCN and NH_3 yields as a function of temperature, collected at 1 inch above the burner. For bituminous coals, the formation of NH_3 commenced at the same temperature as HCN. For low rank coals, NH_3 was released at a lower temperature than HCN. It is unlikely that the NH_3 was formed from HCN, due to the low temperature and the high equivalence ratio. The early occurrence of NH_3 from low rank coals strongly suggests a unique source of NH_3 that is significant only in low rank coals.

Two types of nitrogen functionalities are possible origins for NH_3. One type is the amine-containing functional groups. Amine is thought to be the source of NH_3 in coal pyrolysis by many researchers (Leppalahti, 1995; Kelemen 1998). However, amines only exist in very small amounts in coal and usually thermally decompose between 500 and 600^oC, a temperature

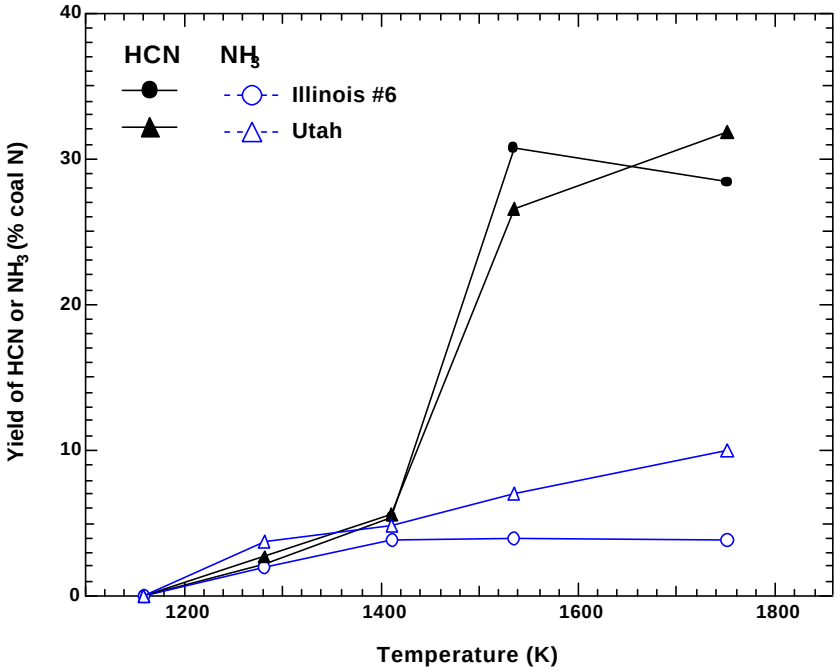

Figure 1.7.11. Yields of HCN and NH_3 versus temperature for high rank coals (collected at 1 inch above the burner).

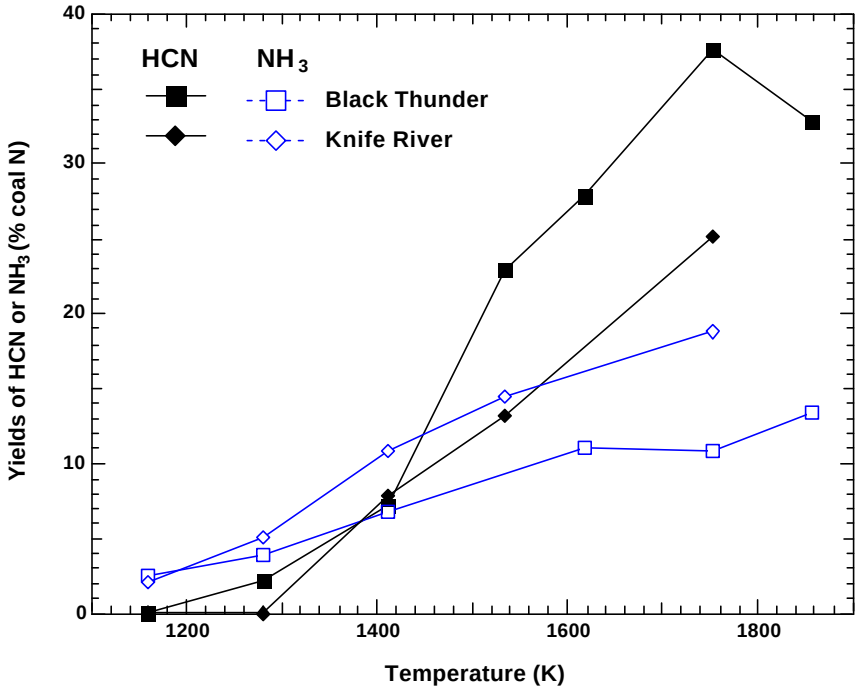

Figure 1.7.12. Yields of HCN and NH_3 versus temperature for low rank coals (collected at 1 inch above the burner).

range much lower than the lowest temperature in the current study. The other type is quaternary nitrogen. The exact nature of quaternary nitrogen is still controversial. Some investigators think quaternary nitrogen is a distinct nitrogen functionality. Others believethat quaternary nitrogen is formed due to the oxidation of pyridinic nitrogen (Nelson, et al. 1992) or association with nearby or adjacent hydroxyl groups (Kelemen, et al. 1994). Quaternary nitrogen is more likely to be the source for the early release of NH_3 in this study, since quaternary nitrogen shows strong rank dependence and can only be found in significant amount in low rank coals. It should be emphasized that quaternary nitrogen may only be responsible for the early release of NH_3 seen in many studies. It is unlikely that quaternary nitrogen is the source of the large quantities of NH_3 formed at more severe conditions.

Previous studies show that nitrogen release during coal pyrolysis is a complicated process. The relative amount of HCN and NH_3 formed is not only determined by coal properties, but also dependent strongly on reactor configuration and local environment. Therefore, more data are needed before an attempt can be made to correlate the release of HCN and NH_3 with coal properties (i.e., certain functional groups or elemental compositions).

1.1.26.4 Nitrogen in Char

Nitrogen release from char is quite different from that of tar, although the nitrogen functionalities in the tar and char are similar. Figure 1.7.13 shows the corrected N/C ratio versus temperature for the coals in this study. The corrected N/C ratio is obtained from the N/C ratio in tar or char divided by the N/C ratio in the parent coal. A striking similarity of the profiles of the nitrogen decay for the four coals is noticed in both tar and char. However, the N/C ratio in the char only decreased slightly from 1159 K to 1858 K. Chen (1991) suggested that the extensive, aromatic ring structures built up in char retarded the release of heteroatoms at elevated temperatures, a similar mechanism to that previously discussed for tar at the late stage of secondary reaction. A recent ^{13}C NMR analysis on the tar-char pair collected at increasingly

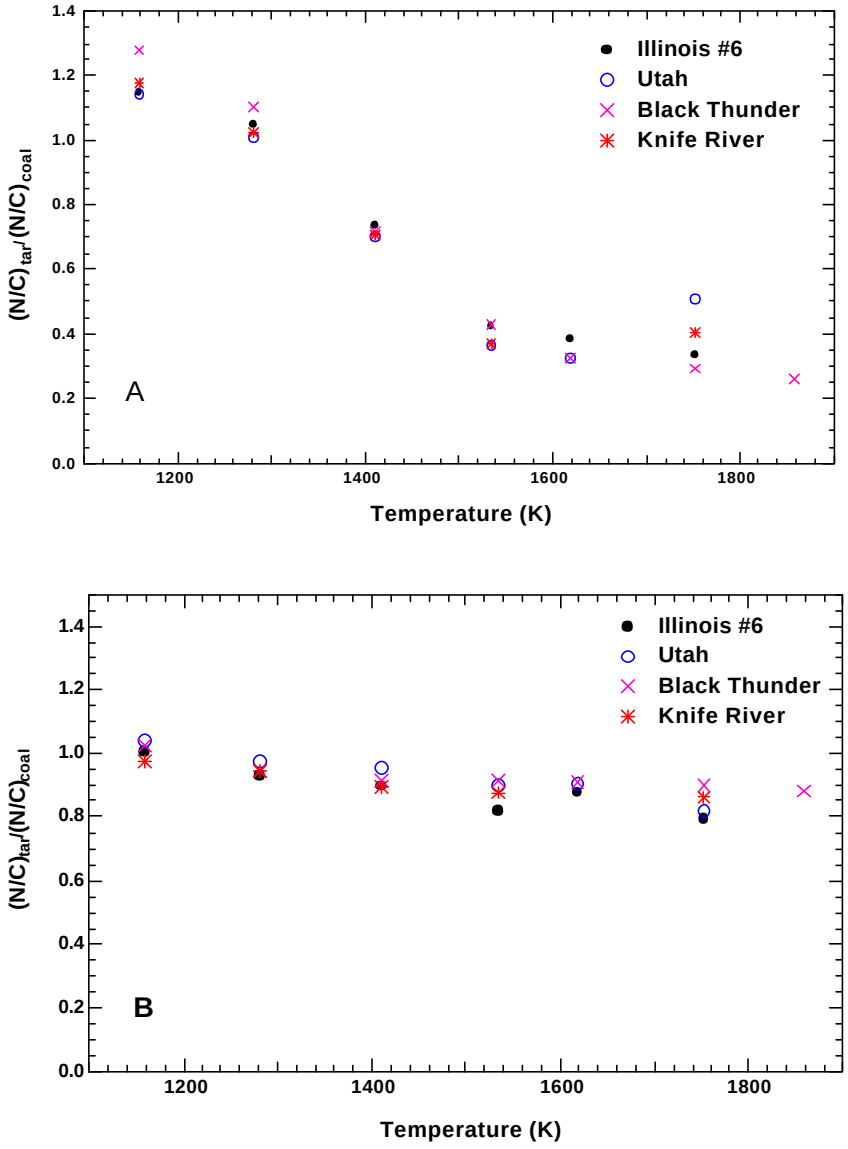

Figure 1.7.13. Corrected nitrogen/carbon ratio versus temperature (A) for the tar and soot and (B) for the char for the four coals in this study (collected at 7 inch above the burner).

severe conditions indicated that the ring buildup reaction rate is comparable in the tar and in

the char (Perry, 1999). Therefore, the much slower rate of nitrogen release from char cannot be solely attributed to the chemical structure change during coal pyrolysis. The large difference of nitrogen release rate from char and tar makes it reasonable to believe that differences in reactivity for the nitrogen functionalities in the char and tar may be also responsible. That is to say, the nitrogen functionalities trapped in char are less reactive than their counterparts in tar. These functionalities may either be transformed to more refractory types induced by heat during pyrolysis or stabilized by nearby functional groups, making them extremely resistant to thermal decomposition. More research is needed to verify the validity of this hypothesis.

It is thought that both HCN and NH_3 can be evolved from char during pyrolysis (Li, et al, 1996; Leppalahti, 1995). They may be released independently from different functionalities in char, or else NH_3 may be formed from HCN in the pores and surfaces of

the char (Bassilakis, et al. 1993). Unfortunately, the exact reaction mechanism of char nitrogen cannot be examined due to the limits of the current study. In this study, the contributions to the total HCN and NH_3 release from the char and the tar cannot be distinguished. More research on high temperature char pyrolysis is needed to clarify the exact contribution of each mechanism.

1.8 SUMMARY AND CONCLUSIONS

The major objective of this study is to investigate the mechanisms of secondary reactions of coal volatiles, including nitrogen evolution and distributions among different products. Furthermore, soot formation during secondary pyrolysis was examined, and its effect on nitrogen chemistry was evaluated. These information help understand the nitrogen transformations at typical coal firing conditions, and is essential to the development of a comprehensive nitrogen release model for the coal-utilization processes.

1.1.27 Accomplishments

A $CO/H_2/O_2/N_2$ flame was operated under fuel-rich conditions in a flat flame reactor to provide a high temperature, oxygen-free post-flame environment to study secondary reactions of coal volatiles. Temperature, residence time, and coal rank were chosen as the major test variables to examine the nitrogen evolution and soot formation mechanism during secondary pyrolysis. Temperatures in the reactor were adjusted from 1159 K to 1858 K, where secondary reactions were highlighted. Four coals, ranging from high volatile bituminous to lignite, were used to study the influence of coal properties on nitrogen release. The results were reasonable, repeatable and comparable with published data from the literature.

The major accomplishments achieved in this study can be summarized as:

1) Low temperatures in a post-combustion environment were achieved using a CO flame, which facilitated the study of secondary pyrolysis.

2) A set of eighty pyrolysis experiments, including four coals, seven temperature conditions, and four residence times was completed. The resulting char and tar/soot samples were analyzed to provide the elemental compositions, mass release and product yields for each test.

3) Noncondensible gases produced during pyrolysis were accurately quantified by FTIR

coupled with a multi-reflection, long-path gas cell. The results were reliable and reproducible, representing the first extensive gas analysis data of coal pyrolysis in a post-combustion environment. A detection limit as low as 50 ppb was achieved for some gases.

4) The chemical structure changes of tar and soot samples from a coal and two aromatic model compounds were derived from ^{13}C NMR analysis. This is the first data set of ^{13}C NMR analysis on tars and soots from model compounds.

5) A hypothetical secondary reaction mechanism of coal volatiles was developed. Three major processes were identified and modeled using first-order reactions. The nitrogen evolution from tar was also modeled as a first-order reaction and the corresponding rate expression was derived.

1.1.28 Summary of Results

1.1.28.1 Mass Release and Tar/Soot Yield

The ultimate mass release from coal pyrolysis in this study exhibited strong rank dependence and showed similar trends to those reported by other investigators. The tar and soot yields measured in this study are much lower than those reported in the literature at similar temperatures and heating rates, especially for low rank coals. Two major reasons may be responsible for the observed lower tar/soot yields including A) unaccounted semivolatile species; and B) gasification of the nascent tar by the oxidizing species in the post flame environment. Of these two reasons, gasification is thought to be more important.

1.1.28.2 Chemical Structures of Tar and Soot

Changes in the chemical structure of tars and soots from an Illinois #6 coal and two model compounds, biphenyl and pyrene, were analyzed using solid state ^{13}C NMR spectroscopy. This is the first time tars and soots from coals pyrolyzed at increasingly severe conditions from 1250 K to 1600 K have been analyzed by ^{13}C NMR. Since transition from tar to soot usually occurs

between 1300 K and 1450 K, this study provided a unique opportunity to examine the early soot formation mechanisms. This is also the first data set containing chemical structure analysis where two model compounds have been included, which gives insight into the evolution of soot from hydrocarbons.

The coal-derived soots exhibited loss of aliphatic and oxygen functional groups prior to significant growth in average aromatic ring size. This is evidenced by the dramatic loss of side chains per cluster at temperatures from 1160 K to 1280 K, while the aromatic carbons per cluster as well as bridges and loops per cluster remained roughly constant. Ring opening reactions started to dominate beginning at 1280 K. PAH containing oxygen functional groups seems to have a higher reaction rate than the non-polar PAH, as seen by the early disappearance of oxygen attached functional groups (carbonyl carbon, phenolic carbon and oxygen bonded to aliphatic or aromatic carbon) at 1400 K. At 1400 K, no aliphatic side chains were evident, but the number of bridges and loops increased dramatically, suggesting that ring polymerization reactions may have begun. Between 1411 K and 1534 K, polymerization reactions accelerated and became dominant; the clusters grew bigger and were more aromatic as well. The molecular weight per cluster increased more than three times and the aromaticity was very close to unity at 1534 K. Finally, at 1858 K, an extraordinarily large cluster size (greater than 100 carbons) was observed, indicating that soot growth is favored at high temperatures.

The data obtained for the model compounds exhibit a different pathway for pyrolysis and soot growth from that for the coal. For biphenyl, aliphatic carbon was absent in the starting compound, but was observed in the pyrolyzed samples. Therefore, it is believed that ring opening reaction is an early step in the soot formation process for biphenyl. Next, the decrease of the fraction of aliphatic carbon (from 0.09 to 0.02) with increasing temperature indicates that major structural rearrangements were occurring following the initial ring opening reactions. The number of bridges and loops, which is 1 in unreacted biphenyl, doubled to 2.2 and 2.5 at 1365 K and 1410 K and then doubled again to 4.7 at 1470 K. The cluster size, which started at 6 in the parent molecule, grew to 9, 11, 20 aromatic carbon, respectively. Hence, soot growth consists not only the ring size growth but also cluster crosslinking which results in the formation of large,

interconnected structures.

The evolution of pyrene soot follows another path. First, little evidence is observed for ring opening reactions. Second, ring growth of only approximately 10% has occurred at 1410 K compared to nearly 100% in the case of the corresponding biphenyl soot. However, data on this 1410 K soot sample indicate that the relatively small cluster size has been augmented by an average of 2.6 crosslinking sites per cluster. The data obtained from this study is inconclusive regarding the exact mechanism for ring growth in the pyrene soots between 1410 K and 1460 K, since different analysis methods on the broadened aromatic band of pyrene soots generated different results. Clearly, this is an area for future work.

1.1.28.3 Mechanism of Secondary Reactions of Coal Volatiles

A simple reaction mechanism of secondary reactions of nascent coal volatiles was proposed based on the tar/soot yields and chemical structure data. Two competitive reactions, cracking and polymerization, were assumed for primary tars. At low temperatures (below 1300 K), the cracking reaction is predominant, causing the release of secondary gases. At high temperatures, ring polymerization reaction accelerated, leading to substantial soot growth. It is further assumed that the fraction of primary tar that can be directly converted to soot is constant and dependent on coal rank. At temperatures higher than 1600 K, an additional soot growth mechanism from gas-phase hydrocarbon addition was also included.

The three reaction pathways were modeled as first-order reactions. Kinetic parameters were obtained by fitting the experimental data in the current study and those reported in literature. By using a single activation energy for each reaction, very good agreement was achieved between calculated tar/soot yields and measured yields. The early decrease of the tar plus soot yield with temperature, due to fast tar decay and slow soot growth, is clearly shown in the simulation.

1.1.28.4 Nitrogen Release during Coal Pyrolysis

Nitrogen release is inherently related to mass release during the early stage of

devolatilization. In addition, a strong rank dependence of the total nitrogen release is also observed. For bituminous coals, nitrogen release is proportional to mass release at first, followed by a delay during the middle stage, and then proceeding at a slow rate even after mass release is largely completed. For low rank coals, the fractional nitrogen release rates are much slower than the fractional release of overall mass during the early stage of pyrolysis. A delayed nitrogen release during the middle stage and a much slower nitrogen release from char after the majority of mass release ceases (at a prolonged time scale) is also observed.

Tar is virtually the only carrier of coal nitrogen during the early phase of pyrolysis. For bituminous coals, these ring structures in coal are transported essentially intact to tar during the early pyrolysis. Non-polar PAH are preferentially released as tar during the early pyrolysis for low rank coals, probably due to the early crosslinking in coal.

During secondary pyrolysis, an enrichment of nitrogen in tar is first observed, followed by a subsequent fast nitrogen release. The fraction of coal nitrogen in tar/soot reaches an asymptote during the late stages of pyrolysis. The enrichment of nitrogen in tar clearly shows that nitrogen exists in tightly-bound ring structures, which only react at more severe conditions. Subsequent nitrogen release, in the form of HCN, is caused by ring rupture at high temperatures. Incorporation of a portion of nitrogen into soot occurs during the early stages of soot formation. As pyrolysis proceeds, the clusters in soot become larger and more interconnected, which retard the further release of nitrogen. Therefore, the fraction of coal nitrogen incorporated into the soot remains constant while the soot yield increases rapidly. In addition, the nitrogen functionalities in tar seem to have a higher reactivity than their counterparts in the char.

It is thought that tar nitrogen is exclusively released as HCN from nitriles. NH_3 can be formed through the interactions of HCN and other oxygen radicals in the gas phase or on a specific surface. Direct release of nitrogen in char as both HCN and NH_3 is possible. The data in the current study by themselves are not conclusive regarding the complicated reaction pathways among the nitrogen species during coal pyrolysis. However, it proves that the relative amount of HCN and NH_3 formed is strongly dependent on reactor configuration and local

environment.

1.1.29 Principal Conclusions

This study of nitrogen evolution during secondary coal pyrolysis and soot formation mechanism from coal tar and model compounds at high temperature, high heating rate conditions has given rise to the following conclusions:

1) Both temperature and residence time have significant effects on volatile release from coal during secondary coal pyrolysis.

2) Secondary reactions of coal tar are influenced more by thermal history than by chemical structure, based on similar behavior of tar decay from a broad range of coal types.

3) Addition of gas phase hydrocarbons to existing soot particles is necessary to explain the slight increase in soot yield at temperatures above 1600 K, but is not the principal soot formation mechanism in a coal system. C_2H_2 is the major species participating in the soot surface growth, while benzene and other species make much less contribution.

4) The sooting mechanism was dependent on the chemical structure of the parent aromatic molecules. For coal tar, loss of aliphatic side chains and oxygen functional groups was the first step in soot formation, followed by rapid ring growth above 1400 K. For biphenyl, significant ring opening reactions occurred prior to ring growth. For pyrene, little evidence of ring opening reactions was found.

5) The reactivity of nitrogen functionalities in coal tar shows little rank dependence.

6) For low rank coals, NH_3 is released earlier than HCN; for high rank coals, NH_3 is released at the same time as HCN. Some types of quaternary nitrogen are responsible for the earlier release of NH_3 than HCN at low temperatures. However, quaternary nitrogen is not the source of the large quantities of NH_3 formed at more severe conditions.

7) Tar nitrogen is exclusively released as HCN. NH_3 can subsequently be formed from

HCN and other nitrogen species.

1.1.29.1 Limitations and Recommendations

The current study offered a unique opportunity to examine the secondary reactions of coal volatiles, with an emphasis on nitrogen species. The results confirm much of what has been reported in previous studies. At the same time, new phenomena have been observed and new ideas have been developed. Unfortunately, it is not possible to address all the questions regarding nitrogen evolution during secondary pyrolysis due to the limitations of the current study. The limitations in this study are presented and recommendations are proposed here which would be valuable for future work in this area.

1) The current tar and soot collection system should be reconstructed to improve the collection efficiency. Significant amounts of tar or soot (10-15%) were deposited on the walls of the collection system, which is hard to collect and measure. Although a correction is made to the tar/soot yields by weighing those deposits after wiping them off using kimwipes, a more accurate method is needed because the tar/soot yields are one of the most important measurements. Perhaps a porous wall could be used throughout the collection system to minimize tar or soot deposition.

2) Products collected at different residence times provide the detailed kinetics for secondary pyrolysis. However, the residence times in the current study are not long enough to further examine the additional soot formation from hydrocarbons and nitrogen evolution from soot, especially at high temperatures. Using a longer reactor is an option to obtain longer residence times.

4) A better closure on the nitrogen balance is desired, especially at low temperatures in this study. A further investigation is needed to resolve this problem. Since the nitrogen balance is very good at high temperatures, it is possible that some nitrogen species that are significant at low temperatures but converted to other species at more severe conditions were not measured.

3) N_2 and oxygen containing species (CO, CO_2, H_2O etc.) could not be measured in the current study. Accurate quantification of N_2 could help secure a better nitrogen balance and shed light on another possible pathway of nitrogen evolution during secondary pyrolysis. If air was replaced by pure oxygen and dilution/quench nitrogen was replaced by an inert gas such as argon or helium, N_2 could be measured using a high resolution gas chromatograph.

4) The collected tar and soot deposits should be split and examined separately. The soot percentage in the total deposit is a convenient gauge for the extent of secondary reactions of tar. It is essential to track the soot formation rate from tar and nitrogen evolution during different stages of secondary pyrolysis. It is also useful to test the validity of the current secondary reaction mechanism of tar.

5) The secondary reactions of coal volatiles and nitrogen release are modeled as empirical, first-order reactions in this study. All the kinetic data are derived from experimental data. No chemical structure data are involved in the model, therefore, it is not expected to be valid for conditions too far away from those adopted in the current study. A detailed, "intrinsic" model that incorporates changes of chemical structure and nitrogen functionalities is desirable in order to predict accurately the nitrogen release for coals from different origins and at a broad range of conditions.

6) It is demonstrated in the current study that nitrogen decay from tar is roughly independent of coal rank. Pyrolysis of nitrogen-containing model compounds (such as pyridine, pyrrole, quinoline, nitriles, etc.) in the flat flame reactor will provide useful clues regarding the nitrogen transformations within tar and the subsequent release as gas species. The gas phase should be carefully examined to verify the interactions of the nitrogen species with other species in the gas phase. The chemical structure analysis of the resulting soot will help understand the nitrogen evolution from soot at elevated temperatures.

7) The secondary reaction model should be incorporated into a general devolatilization model (such as the CPD model) so that the whole process of coal pyrolysis can be evaluated.

2 EVOLUTION OF NITROGEN DURING CHAR OXIDATION

2.1 INTRODUCTION

The three most common nitrogen oxides produced during coal combustion are air pollutants. Nitric oxide (NO) and nitrogen dioxide (NO_2) are acid rain and photochemical oxidant precursors. Nitrous oxide (N_2O) is a contributor of global warming and to the destruction of ozone layer. In order to control the production of these oxides is fundamental to understand all significant mechanisms for nitrogen oxidation during coal combustion.

This dissertation studied one of these mechanisms: the conversion of the nitrogen present in the char to nitrogen oxides. This section describes the present understanding of the process of char-N oxidation during coal combustion and identifies several research areas where numerous uncertainties are yet to be resolved. The main objective of this study is to provide insight into these areas by experimental and computational analysis.

2.1.1 Description of the Process of Char-N Conversion to Nitrogen Oxides

The conversion of char-N to nitrogen oxide can be described as the results of two competing processes: The release of the nitrogen present in the organic matrix of the char and the reactions that the formed nitrogen-containing species can have on the char surface or with the additional gaseous molecules present inside the char pores or in the boundary layer. The first sections of the introduction describe these processes as if one was independent from the other one. This thought experiment helps to understand the complete processes and to identify what areas need more study.

2.1.2 Release of Char-N to Produce Nitrogen-Containing Species

In the hypothetical case that any nitrogen-containing species released from the char does not react during its diffusion path in the char pores and in the boundary layer, the problem of the

conversion of char-N to nitric oxides reduces to identifying the nature and production rate of the nitrogen-containing species produced during char oxidation.

The nitrogen in the char can be converted to gaseous species through three major mechanisms: *a)* Temperature treatment; *b)* Direct reaction with oxygen and *c)* Reaction with nitric oxide. All these processes present different characteristics. However, all have the same starting point, the nitrogen in the char. The next section describes how the nitrogen atoms occur in the char organic matrix.

2.1.2.1 Nitrogen-containing functionalities in coal and char

XPS (X-ray Photoelectron Spectroscopy) of coal, chars, and synthetic chars has been widely used to study the nature of the nitrogen-containing groups in the char (Kambara et al., 1993, Pels et al., 1995, Kelement et al., 1994 Pels et al., 1993, Wójtowicz, 1995 Kelemen et al., 1998, Ashman et al., 1998, Stajczyk, 1999, Kelement et al., 1999Jones et al., 1999a). Some conclusions of these studies are presented by Thomas (1997) and may be summarized as follows:

1. Nitrogen functionalities in coal are basically pyrrolic (50-80%), pyridinic (20-40%) and quaternary nitrogen (0 - 20%). Small amounts (<10%) of amino groups may be present in low rank coals. The nature of the quaternary nitrogen is not clear. Pels et al. (1995) suggested that it may represent a N-oxide of pyridinic-N or protonated pyridinic-N. Kelemen et al. (1998) assigned this peak to pyridinic or basic nitrogen species associated with hydroxyl groups from carboxylic acids or phenols. Figure 2.1 presents a representation of these functionalities and their typical distribution in coal.

2. After mild pyrolysis (T < 923 K) there is an increase of pyridine groups, as the concentration of pyrrole and quaternary nitrogen is reduced.

3. More severe pyrolysis conditions (higher temperature and longer residence times) tend to reduce pyrrole concentration, whereas pyridine concentration remains constant or tends to increase due to the transformation of pyrrolic nitrogen to pyridinic nitrogen, and the conversion

of some pyridinic nitrogen to quaternary nitrogen. This quaternary nitrogen is not represented by the structures shown in Figure 2.1, but rather by incorporation of nitrogen in graphene layers (Pels et al., 1995).

4. The heating rate used for the formation of the chars also affects the distribution of nitrogen functionalities (Kelemen et al., 1998). High heating rates (10^4 K/s up to 923 K) prevent the formation of quaternary nitrogen so that pyrrolic and pyridinic structures will be favored.

The similar conclusions obtained from different groups and for different carbonaceous materials suggest that the nature of the nitrogen compounds present in coal is well understood. The question that arises now is how this information may be related to the production of nitrogen-containing gaseous species.

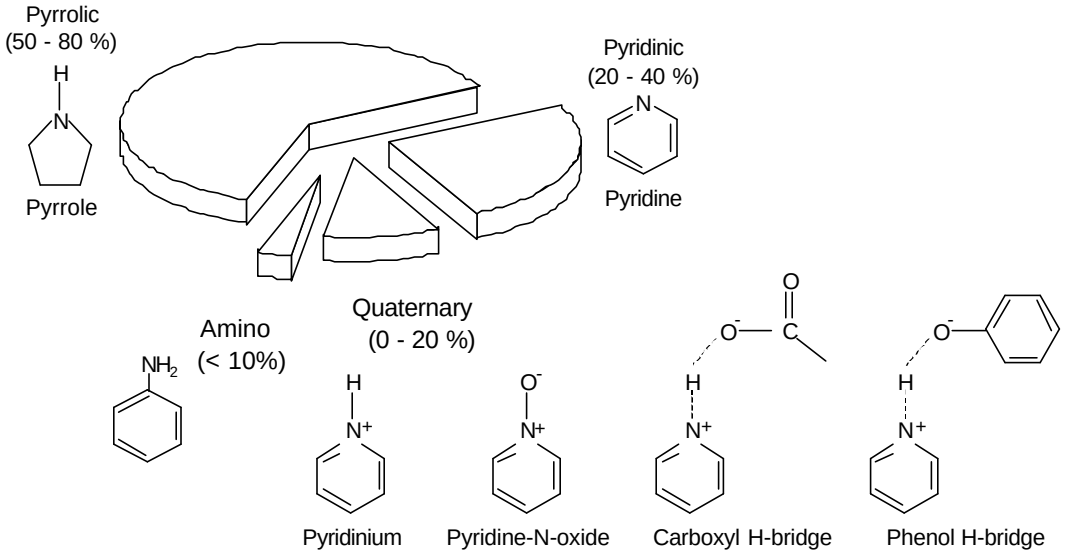

Figure 2.3. Distribution of nitrogen-containing functionalities in coal (Pels et al., 1993, , Stajczyk, 1999)

Two different answers are possible depending on whether the release of nitrogen compounds is studied during pyrolysis or during oxidation. Kambara et al. (1993) analyzed 20 coals and their respective chars by XPS as well as composition of the gases evolved during pyrolysis by GC and

concluded that the variation of the nitrogen functionalities in chars during pyrolysis can be qualitatively related with the yield of nitrogen-containing species. Quaternary nitrogen converts finally to NH_3 and some fraction of pyrrolic and pyridinic nitrogen converts to HCN. Their experiments were in an oxygen free environment. In contrast to the results for pyrolysis, when coals and chars have been oxidized no correlation has been found between the evolved gases and the nitrogen functionalities of coal and chars (Wójtowicz, 1995, Stajczyk, 1999, Jones et al., 1999a. Wójtowicz et al. (1995) and Stanczyk (1999) did not find any correlation between nitrogen functionality and coal or char-N conversion to NO, N_2O or N_2 during low temperature char oxidation. The reason for this lack of correlation may be that most final nitrogen functionalities after severe pyrolysis correspond to nitrogen present in six-membered rings (quaternary and pyridinic) and no matter what groups are present in the original coal the influence of them on the final NOx production is minor (Pels et al., 1995). Stanczyk (1999) states that the relation between nitrogen containing species and nitrogen functionalities in char is negligible when compared to other factors such as surface area of chars, porosity, or reactivity for NOx destruction.

Most studies agree with the conclusion that the functional form of nitrogen present in the char has a secondary effect compared to those of other parameters such as catalysts, char surface area, and pore size distribution, when considering char-N conversion to nitrogen oxides. However, the knowledge of how nitrogen atoms are bonded to the char structure is the first step when trying to explain the evolution of the nitrogen present in the char.

2.1.2.2 Evolution of nitrogen-containing species due to char heat treatment

When coal is submitted to high temperatures it decomposes into a gaseous phase formed by tars and gases and termed volatiles, and a solid residue called char. The amount of coal mass released as volatiles depends on the coal rank, heating rate and peak temperature. Under inert atmosphere, the coal mass loss increases with temperature until an asymptote is reached.

Contrary to what happens to the carbon mass, the mass fraction of nitrogen in the char decreases with temperature, and at temperatures of more than 2000 K the char nitrogen

concentration becomes zero (Pohl and Sarofim, 1976). This nitrogen depletion under inert atmosphere occurs at time scales in the order of hours. These results illustrate the low thermal stability of the nitrogen containing molecules in the char. The presence of heteroatoms in an aromatic cluster reduces the stabilization energy by about 41 – 67 kJ/mol (Baxter et al., 1996). It is possible then to expect that as the temperature is increased, aromatic clusters with pyridinic or pyrrolic nitrogen will decompose, while the main bulk of the carbon will condense to form graphite-like structures. In fact N_2 and solid carbon are the species favored from a thermodynamic point of view at these temperatures (see Appendix A of Molina, 2002).

The hour time scales needed for complete nitrogen depletion are far from the typical second (fluidized bed combustion) or millisecond (pulverized combustion) time scales of coal devolatilization at conventional industrial conditions. For the shorter time scales, the data available are more confusing and suggest a complex dependence on coal rank, heating rate and time of exposure at high temperatures.

In their seminal work, Pohl and Sarofim (1976) found a continuous reduction on the nitrogen retained in the char as exposure time increased at temperatures ranging from 1000 K to 2100 K for a lignite and a bituminous coal. Only at the lower temperatures (< 1500 K) an asymptote seemed to occur at retentions close to 50 % and for residence times longer than 1 second.

The results of Fletcher and Hardesty (1992) as presented by Genetti and Fletcher (1999) and in more detailed in Genetti (1999) show that at the temperatures typical of fluidized bed combustion (1000 – 1300 K), the nitrogen content of the aromatic clusters in the char slowly decreases until it reaches an asymptote after 100 to 250 ms. Gibbins and Williamson (1998) studied nitrogen evolution during char devolatilization at a higher temperature range (1723 – 2073 K). Their results show that as peak temperature increases, the residence time required to obtaining an asymptotic value on the nitrogen char content decreases. In this way at 1873 K a residence time of 2 seconds is necessary to reach the asymptote, whereas at 2073 K, only 0.15 seconds are necessary.

The discussion above has two major implications in the study on the conversion of char nitrogen to nitrogen oxides. The first one is that in a typical pulverized coal boiler (temperatures

1700 – 2200 K), where the devolatilization occurs in a time scale of the order of few milliseconds, the amount of char nitrogen released just due to thermal treatment is low when compared to other mechanisms. Only after long residence times, in the order of minutes, it is possible to deplete considerable nitrogen from the char just by thermal treatment (Pohl and Sarofim, 1976). Although the results of Fletcher and Hardesty (1992) and Gibbins and Williamson (1998) show a slow decrease on char-N with residence time at a high temperature, this decrease is too low and the rate of nitrogen evolution too slow when compared to that of total mass released in an oxidizing environment. Higher nitrogen releases would require higher temperatures, and might be achieved with high air preheat or oxygen enrichment of the oxidant stream. At fluidized bed conditions (temperatures 1000 – 1300 K) the competition between nitrogen release due to an increase of temperature and due to oxidation may be more important. In this case, a compound as HCN can be released due to the increase in char temperature that occurs at the first stages of char oxidation.

The second consequence of the release of nitrogen by heat treatment is that it will affect the determination of the nitrogen content initially present in the char. The most common approach when calculating the conversion of char nitrogen to nitrogen oxides is presented in E 2.2.1, where (N/C) represents the atomic ratio of nitrogen to carbon in the char.

$$\text{Conversion to } N_X O_Y = \frac{\text{atoms of N produced as } N_X O_Y}{\frac{N}{C} \times (\text{atoms of carbon released})} \qquad \text{E 2.2.1}$$

Any error on the evaluation of (N/C) has a direct impact on the conversion. Chars produced at a specific gas temperature and oxidized at the same gas temperature will have a temperature overshoot due to the exothermicity of the carbon-oxygen reaction. Some char nitrogen can evolve due to thermal decomposition during this period and the value for (N/C) of the original chars will be higher than the one of the char during the actual char oxidation process. This produces an under-prediction of the char nitrogen conversion to $N_X O_Y$. This observation is

particularly true when N_2 is not measured in the exhaust gases, since it is not possible to close the nitrogen balance in the system.

2.1.2.3 Evolution of nitrogen by reaction with oxygen

During char oxidation, the nitrogen present in the char can react with oxygen to produce nitrogen oxides. As important as this reaction is, the detailed kinetics of the reaction of char nitrogen with oxygen has not been studied, at least not in the refereed literature. This is not surprising considering that the reaction of carbon atoms with oxygen, arguably the most important reaction known Walker et al., 1991 is still subject of strong debate in issues as fundamental as reaction order with respect to O_2 and product distribution (Shaddix, 2001, Hurt and Calo, 2001, Haynes, 2001).

Due to the numerous experimental difficulties associated with the evaluation of the details of the carbon-oxygen reactions, alternative techniques as computational chemistry are used. This technique has become more common and sophisticated in the analysis of the carbon-oxygen system. First studies that used semiempirical calculations (Moulijn and Kapteijn, 1995) have been replaced by more robust Ab Initio computations (Montoya et al., 2001). The results do not only give information about the mechanism of the reaction (Chen and Yang, 1998) but also in the reaction rates (Montoya and Truong, 2001). It is possible that in the future the combination of these techniques with more comprehensive methods that consider a balance of complex sites on the char surface (Haynes, 2001) can be used to explain the process of char-oxidation and by analogy the reaction of the nitrogen in the char with oxygen (Sarofim et al., 1999). However, in the mean time it is reasonable to consider that the rate of abstraction of a nitrogen atom from the char matrix by reaction with oxygen should be similar to the rate of carbon abstraction by reaction with oxygen.

This does not mean that the rates of total carbon and nitrogen released are the same, but that the rate of nitrogen and carbon abstraction from the char matrix by oxygen should be similar. It is possible though that through alternative processes the total rate of nitrogen and carbon release will be different, as was suggested by Molina et al. (2000). These authors considered that the rate

of nitrogen release is not proportional to the rate of carbon release in two cases. At high temperatures, nitrogen release through heat decomposition is important at the first stages of char oxidation, as suggested from the experimental results of Baxter et al (1996). At moderate temperatures (700 – 900 K), the nitrogen oxide formed from nitrogen oxidation can be re-adsorbed in the char surface through reaction R 2.2.1, where C(_) represents a carbon active site.

$$2C(\_) + NO \rightarrow C(N) + C(O) \qquad \text{R 2.2.1}$$

These two processes affect the rate of nitrogen release. It will be higher than the rate of carbon release for the case when nitrogen is released due to a heat effect, and lower for the case when nitrogen oxide is re-adsorbed on the char surface. However, this does not imply that the rate for the reaction nitrogen-oxygen is different from the rate of the reaction carbon-oxygen, but that additional processes need to be considered when predicting the global results.

In summary, the present understanding of the reaction of char nitrogen with oxygen is limited. The best approximation is to consider it proportional to the rate of carbon reaction with oxygen and that the product is nitric oxide, as suggested by reaction R 2.2.2.

$$C(N) + O_2 \rightarrow C(O) + NO \qquad \text{R 2.2.2}$$

2.1.2.4 Evolution of nitrogen by reaction with nitric oxide

Nitric oxide can react with char to produce N_2, HCN and N_2O. In all these reactions, the nitrogen in the char evolves to the gaseous phase; therefore these reactions are mechanisms of char nitrogen evolution and are mentioned in this section of release of nitrogen containing species from the char. But since these reactions also destroy nitrogen oxides on the char surface, they are discussed in the next sections.

2.1.3 Reaction of Nitrogen-Containing Species on the Char Surface

Among the nitrogen-containing species that can be formed directly during char oxidation, nitric oxide and nitrous oxide can react on the char surface. The most studied reactions are the reduction of NO and N_2O on the char surface to produce N_2. They are discussed in the next two sections. The less known reaction of NO with char nitrogen to produce N_2O and HCN is analyzed in the last part.

2.1.3.1 Reduction of NO on the char surface

The non-catalytic and catalytic reduction of nitrogen oxides on char surfaces has been extensively investigated and can be classified into three main groups: *1)* those, carried out at low temperatures (< 573 K), that pursue a better understanding of the NO reduction phenomenon in order to develop materials suitable for the destruction of NO at post-combustion conditions (Rubel et al., 1995, Lizzio et al., 1997 García-García et al., 1997, Illán-Gómez et al., 1998, García-García et al., 1999, Xia et al., 1999 , Ciambelli et al., 1999) *2)* those focused on the mechanism of nitrogen oxides reduction on char surface (Madley and Strickland-Constable, 1953, Smith et al., 1959,Teng et al., 1992, Illán-Gómez et al., 1993, Chu and Schmidt, 1993, Teng and Suuberg, 1993a, 1993b, Rodríguez-Mirasol et al., 1994, Suzuki et al., 1994, Illán-Gómez et al., 1995a, 1995b, 1995c, 1996a, 1996b, Orikasa, H. et al., 1995, Chambrion et al., 1996, 1997a, 1997b., 1998a., 1998b., Guo and Hecker, 1996, Suuberg et al., 1996, Teng et al., 1997, Carabineiro et al., 1997, Aarna and Suuberg, 1998, 1999, Kyotani and Tomita, 1999, Zhonghua et al., 1999, Noda et al., 1999, Tomita, 2001); and those that search for a kinetic expression for this reaction suitable for modeling and design purposes (Furusawa et al., 1980, Levy et al., 1981, Song et al., 1981, Chan et al., 1983 Schuler et al., 1987, Jensen et al., 2000, Molina et al., 2001). Comprehensive reviews on these reactions can be found in the literature (Aarna and Suuberg, 1997, Li et al., 1998). This section describes the mechanism of the reaction and the most frequent kinetic parameters used to explain it.

Molina et al. (2000) reviewed the different mechanisms proposed for the reaction of nitrogen on the char surface. They concluded that at the conditions where most of the mechanistic studies have been conducted (temperatures between 800 and 1200 K and oxygen concentration lower than 0.2%) the mechanism suggested by Tomita and coworkers and summarized in reference (Tomita, 2001) is the one that better explains the experimental results. The first reaction in this mechanism is the dissociative chemisorption of NO represented by reaction R 2.2.1. Once chemisorbed, the active surface sites will react with incoming NO molecules to produce N_2 and CO according to R 2.2.3. Reactions R 2.2.4 and R 2.2.5 can also occur but in lesser magnitude.

$$C(N) + NO \rightarrow N_2 + C(O) \text{ or } CO \qquad \text{R 2.2.3}$$

$$2C(N) \rightarrow N_2 \qquad \text{R 2.2.4}$$

$$2NO + 2CO \rightarrow N_2 + 2CO_2 \qquad \text{R 2.2.5}$$

Even though the mechanism proposed by Tomita and coworkers (Tomita, 2001) explains most of the experimental observation on the reduction of NO in char, it does not give information on the kinetic parameters for the reaction. And this is probably one of the areas where there are more uncertainties in the study of the conversion of char nitrogen to nitrogen oxides. Most of the controversy originates from the failure of most rate kinetic parameters on predicting the conversion of char nitrogen to NO at pulverized coal combustion conditions. Visona and Stanmore (1996) found that only the kinetic parameters of Chan et al. (1983), the ones for which highest rate of NO reduction on char surface is calculated, were able to predict in a reasonable way the conversion of char nitrogen to nitric oxide. The other three kinetic expressions used (Levy et al., 1981, Song et al., 1981, de Soete, 1990[)] over-predicted the conversion. In a more recent study, Jensen et al. (2000) compared the rates of NO destruction on the char surface reported in the literature, with one evaluated under slightly oxidizing atmosphere, from chars prepared in situ and guaranteeing that the influence from particle-particle

reactions was minimum. These authors found that the rate of NO/char reaction was almost two orders of magnitude higher than the common values reported in the literature.

The kinetic parameters for the reduction of NO on the char surface are still unknown, particularly at pulverized coal combustion temperatures. This study evaluates the rate of NO reduction on the char surface for different carbonaceous materials and analyzes how the rate parameters influence the prediction of the conversion of char nitrogen to nitrogen oxides.

It also addresses the effect that an increase in the nitric oxide concentration in the boundary layer has on the conversion of char nitrogen to nitrogen oxides. The experimental study by Spinti (1997) and the calculations by Visona and Stanmore (1996) and Coda et al. (Coda et al., 1998) suggest that an increase in nitric oxide reduces the char nitrogen conversion to nitric oxide. This effect is related to the reduction of nitric oxide on the char surface as Molina et al. (2001) suggested. This dissertation presents a more detailed explanation of this phenomenon.

2.1.3.2 Reduction of N_2O on the char surface

Madley and Strickland-Constable (1953) postulated in 1953 the most important step on the mechanism of N_2O reduction on the char surface (R 2.2.6).

$$C(\_) + N_2O \rightarrow C(O) + N_2 \qquad \text{R 2.2.6}$$

More recently Noda et al. (1999) provided experimental evidence that supports R 2.2.6 as the main pathway for the reduction of N_2O on the char surface. Molecular Ab Initio calculations also support this conclusion (Kyotany and Tomita, 1999). This reaction mechanism is not surprising considering the strength of the nitrogen-nitrogen bond present in the N_2O molecule.

Contrary to the agreement on the mechanism, there is uncertainty regarding the values for the kinetics of N_2O reduction on char surfaces. Furthermore, the number of kinetic studies on the

reduction of N_2O on carbonaceous materials is less than for those of NO. Li et al. (1998) present a review of kinetic parameters for this reaction. The reported activation energy varied from 65 to 115 kJ/mol. Teng et al. (1997) suggest the existence of a two kinetic regime as that reported for NO(Aarna and Suuberg, 1997). At low temperatures (<748 K) the activation energy for the reduction of N_2O on a phenol-formaldehyde resin char increases with burn-off from 57 to 66 kJ/mol. At high temperatures (>748 K) the activation energy increases with burnout, from 170 to 230 kJ/mol. This divergence in results suggests the need of further research in determining the apparent kinetics for the reduction of N_2O on char surfaces.

This dissertation does not evaluate the parameters for this reaction since it considers that an approximate value for the rate of N_2O destruction on the char surface does not have a first order effect on the evaluation of the char nitrogen conversion to nitrogen oxides.

2.1.3.3 Other reactions of NO on the char surface

Although less studied than the previous two reactions, nitric oxide can react on the char surface to produce HCN as reported by de Soete (1992) and quoted by Åmand and Leckner (1993). It can also react with the nitrogen in the char to produce N_2O, according to the mechanism described in Figure 2.2 and suggested by Goel et al. (1994). This mechanism is currently subject of strong debate considering the importance of an alternative route where N_2O is produced from the homogeneous oxidation of HCN Winter et al. (1996). However, Montoya et al. (2000) found that the reaction of NO with the nitrogen present in the char in the presence of oxygen is possible from a thermodynamic point of view.

These additional reactions for the system of nitric oxide/char are important since they provide different pathways that can affect the final product distribution.

2.1.4 Homogeneous Reactions of Nitrogen-Containing Species in the Char Pores and in the Boundary Layer

Studies in the last five years have found that the homogeneous reactions occurring in the char boundary layer are important in the prediction of the char nitrogen conversion to nitrogen oxides. Particularly at fluidized bed conditions some researchers (Ashman et al., 1998, Winter et al., 1996, 1999 argue that homogeneous reactions in the boundary layer are necessary to explain the formation of N_2O during char oxidation.

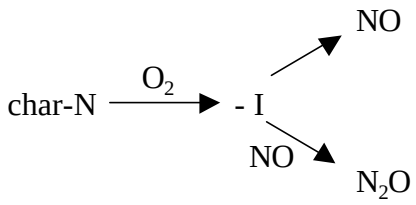

Figure 2.4. Mechanism proposed for N_2O formation.

After Goel et al. (1994)

Figure 2.3 (Molina et al., 2002) illustrates the effect that homogeneous reactions can have in the conversion of HCN to NO and N_2O at conditions similar to fluidized bed combustion. The model that predicts the results in Figure 2.3 follows the approach by Kramlich et al. (Kramlich et al., 1989) where char combustion is approximated by methane oxidation in a CSTR reactor with a residence time of 1 ms, and a PFR with a cooling rate of 275 K/s represents the reactions in the boundary layer. The equivalence ratio in the CSTR reactor and the temperature of injection of 1%w HCN to the system are varied. At low temperatures (900 K), HCN escapes the system of reactors without oxidation. At high temperatures (1700 K) HCN is completely oxidized to NO. And there is an intermediate region (1100 – 1300 K) where HCN is converted to N_2O and other species like N_2 and HNCO that are not presented in the figure. A similar effect occurs when the equivalence ratio is varied from 0.01 (highly oxidizing conditions) to 1.4. At low equivalence ratios, HCN is converted to NO, while at high values it escapes the reactors without oxidation. However, there is a region of intermediate equivalence ratios where N_2O is produced from HCN oxidation, particularly in the temperature range between 1100 and 1300 K.

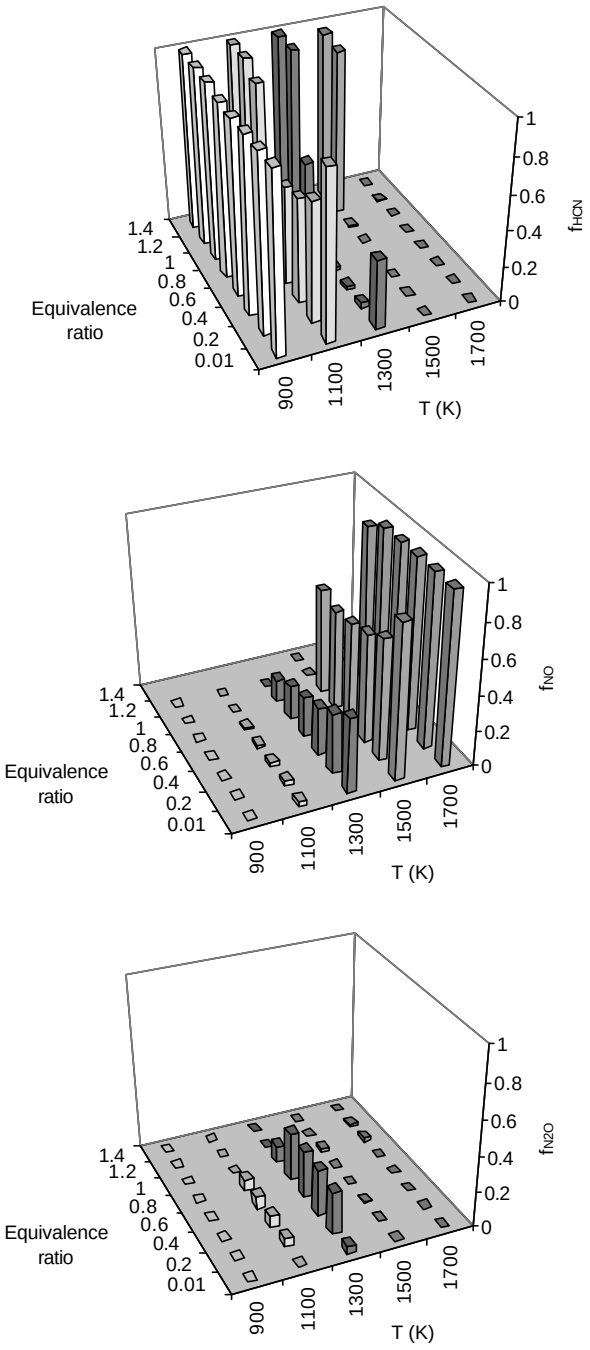

Figure 2.5. Predicted conversion of HCN to N_2O and NO when HCN is injected to a system of CSTR (1ms) and PFR (cooling rate 275 K/s) at different temperatures and equivalence ratios (After Molina et al. 2002).

Although analysis as the one in Figure 2.3 are frequent for the conditions of fluidized bed combustion (Ren et al., 2002, Molina et al., 2002 , the effect of homogeneous reactions on the conversion of char nitrogen to nitrogen oxides in the char pores and in the boundary layer at pulverized combustion conditions has normally been neglected. The studies of Mitchell et al. (1990), Lee et al. (1995) and Goel et al. (1996a) coupled homogeneous and heterogeneous reactions during char combustion, but they focused on the prediction of the CO/CO_2 ratio rather than on the nitrogen-containing species.

The homogeneous nitrogen reactions during combustion have been extensively studied (Miller and Bowman, 1989) and there are several mechanisms developed to predict most of the homogeneous reactions occurring at combustion conditions (e.g. Smith et al.). This dissertation make use of these mechanisms to study from a computational point of view the effect that homogeneous reactions may have at pulverized combustion conditions on the conversion of the nitrogen containing species generated during oxidation.

2.1.5 Prediction of Char Nitrogen Conversion to Nitrogen Oxides

The two previous sections discussed the conversion of char nitrogen to gaseous species and the reaction of those species on the char surface and in the boundary layer as separate processes. But during char oxidation all these processes occur at the same time. It is desirable though, to understand their separate effects. From an experimental point of view it is easy to study reactions of NO or N_2O on the char surface under inert atmosphere, but it is extremely difficult to isolate all these processes when oxygen is present due to the high velocity of the oxygen/char reaction. The release of nitrogen species, the reaction of these species on the char surface and in the boundary layer, all occur at the same time in most experimental setups.

At fluidized bed combustion conditions Winter et al. (1996, 1999) have successfully used a technique that employs iodine injection to suppress the radial reactions and in this way the effect of gas phase reactions. Jones et al. (1995) and Ashman et al. (1998, 2000) placed probes close to chars reacting at low temperatures (< 900 K) and were able to detect HCN and other species that suggest that they reduced the influence of boundary layer reactions.

These studies suppressed to a certain extension the reactions in the boundary layer, but the reaction of gaseous products with the char still occur. The difficulty of isolating these effects during experiments has made the use of models for the study of char nitrogen conversion to nitrogen oxides a common practice. Through models it is possible to separate all these process and to address their influence. This section describes how these models are used in the literature.

Molina et al. (2000) reviewed the single particle models used to predict the conversion of char nitrogen to nitrogen oxides. They identified four fundamental steps in the process of modeling char nitrogen conversion to nitrogen oxides.

2.1.5.1 Carbon oxidation

This part refers to the process of char oxidation itself. Char nitrogen conversion occurs in a system where the most important event is the oxidation of the carbon in the char to carbon monoxide and carbon dioxide. As Domino and Smith (1999) suggest, if this major process is not modeled in the right way, it is impossible to obtain a good prediction of the conversion of char nitrogen. Therefore, the models developed during this study try to apply most of the current understanding of char oxidation, despite of the various uncertainties that remain in the process (Shaddix, 2001, Hurt and Calo, 2001). However, it is important to stress that the main objective of the dissertation is to study the conversion of char nitrogen to nitrogen oxides, and not char oxidation itself. The effect that any simplification in the char oxidation model may have in the conversion of char nitrogen to nitrogen oxides should be considered during the analysis of the results of char nitrogen conversion to nitrogen oxides.

2.1.5.2 HCN formation

As discussed in section 2.2.1.4, HCN has been considered an important intermediate in the conversion of char nitrogen to nitrous oxide at fluidized bed combustion conditions. Modeling the conversion of HCN to nitrogen oxides during char oxidation presents a problem since the only published rate expressions that describe the release of HCN are the one that only consider HCN release due to heat treatment (Fletcher and Hardesty, 1992, Genetti and Fletcher, 1999, Genetti, 1999, Perry et al., 2000). To avoid this problem, Visonna and Stanmore (1996) used an empirically defined parameter that determines the amount of char nitrogen that is evolved as HCN. Ren et al. (2002) followed a similar approach. The empirical value they used was similar to the experimental conversion of char nitrogen to nitrogen cyanide species, as reported by Ashman et al. (2000) Although this is an approximation, it is an alternative way to understand the effect that the evolution of char nitrogen as HCN can have on the final formation of nitrogen oxides.

2.1.5.3 NO formation

Except from the values reported by Goel et al. (1994) and de Soete et al. (1999) that have specific expressions for the oxidation of char nitrogen to nitric oxide, most of the models assume that the rate of NO evolution is proportional to the rate of carbon oxidation from the char. As was discussed in section 2.2.1.2.3 this is a reasonable approximation if other processes that may change the rate of NO evolution, as for example NO chemisorption on the char surface, are considered.

The kinetic constants of the models like the one of Goel et al.(1994) and de Soete et al. (1999) were found after fitting the experimental results to complex heterogeneous mechanisms. For example, the model of Goel et al (1994) had thirteen constants fitted through a least square approximation of the experimental results obtained in a laboratory scale fluidized bed (Tulllin et al., 1993a, 1993b). Although these parameters predicted most of the experimental trends of char nitrogen conversion to nitrous oxide (Goel et al., 1994, 1996c) they failed to predict the trend for char nitrogen conversion to nitrogen oxides when the temperature increased (Kilpinen et al., 2001). The mechanism of de Soete et al. (1999) chas twenty-five coal-dependent constants.

Although there is nothing wrong on fitting experimental results to comprehensive mechanistic models, it is important to recognize that sometimes the use of multiple empirically derived constants from one set of experiment makes the model solely valid for the conditions at which the constant were evaluated.

The approach in this dissertation, when there are not universally accepted rate constants is to use values defined between theoretical limits and to analyze any possible implications that the uncertainty of this constants may have in the prediction of the final results.

2.1.5.4 NO reduction

In their pioneering study Wendt and Schulze (1976) considered the homogeneous reduction of NO as the only mechanism for nitrogen oxide destruction. However, most of the present models apply the rate of NO reduction on the char surface as the main pathway for NO destruction (Sarofim et al., 1999, Jensen et al., 2000, Visona and Stanmore, 1996, Goel et al., 1994, de Soete, 1999, Wendt and Schulze, 1976). In addition to the heterogeneous mechanism of NO destruction, this dissertation studies the effect that any homogeneous reaction will have in the conversion of char nitrogen to nitrogen oxides.

2.1.5.5 N_2O production

In the four main points defined by Molina et al (2000) they did not discuss the formation of N_2O. However, nitrous oxide is an important pollutant nitrogen pollutant at fluidized bed conditions. Most of the models developed for studying the conversion of char nitrogen to nitrogen oxides at fluidized bed conditions consider N_2O formation (Goel et al., 1994, de Soete, 1999). Those designed for pulverized combustion conditions do not (Sarofim et al., 1999, Molina et al., 2001, Visona and Stanmore, 1996, Wendt and Schulze, 1976, Shimizu et al., 1992). The reason is that nitrous oxide is not detected at typical pulverized coal conditions.

The fact that N_2O is not detected at pulverized combustion conditions does not mean that it is not produced from the char or in the boundary layer and then oxidized to NO or reduced to N_2 in the gaseous phase before it exhausts the boiler.

A thermodynamic calculation (see Appendix A of Molina, 2000 for details on equilibrium calculations) shows that at the conditions of pulverized bed combustion, all nitrous oxide will be converted to nitric oxide and molecular nitrogen. This dissertation considers the possible production of nitrous oxide during char oxidation even at pulverized coal combustion conditions. Homogeneous reactions in the boiler before gas exhaust simulate N_2O conversion to NO or N_2.

2.1.6 Implication for Coal-Fired Utility Boilers

It is unlikely that the development of a single particle model that describes the conversion of char nitrogen to nitrogen oxides in a comprehensive way will by itself reduce NOx emissions from utility boilers. However, the incorporation of such a model into computational fluid dynamic codes (CFD) can be used to understand how in the global picture of coal combustion, the char contributes to the total nitrogen oxide emission.

The most common approach for modeling the conversion of char nitrogen in CFD codes is the one proposed by Smith et al. (1982). According to this model, the release of nitrogen from the char is proportional to the mass consumption during char combustion. All fuel nitrogen is converted to HCN, which is then either oxidized to nitrogen oxide or reduced to molecular nitrogen according to the kinetic rates of de Soete (de Soete, 1975). This model has been extensively used in the literature (Jang and Acharya, 1991 with some variations to include empirical constants to account for the partitioning between volatile nitrogen and char nitrogen (Eddings et al., 1994Xu et al., 2000) or to consider additional heterogeneous reactions or NH_3 formation (Lockwood and Romo-Millares, 1992, Visona and Stanmore, 1998).

These models are applied as post-processors of the data generated by the main comprehensive CFD model. These post-processors use the temperature, flow field and

concentrations obtained from the main combustion model calculations and the NO production model is thus decoupled from these calculations. This is a reasonable approach since due to their low concentrations, the nitrogen-containing species have a negligible influence on the mass, heat and momentum balances of the complete furnace.

Sarofim et al. (1999) used a simplified single particle model that simplified the process of char nitrogen oxidation as the combination of the rate of NO destruction on char and the direct char nitrogen oxidation to produce nitrogen oxides as a postprocessor of the CFD data obtained from the simulation of a 500 MW coal utility boiler. These authors compared the results for one boiler before and after the implementation of a NOx control strategy (low NOx burners with over-fire air). The results suggested that the total conversion of char nitrogen to nitric oxide was in the order of 13% for both cases. Char nitrogen conversion to nitric oxide was not affected by the application of the NOx control technique that reduced the total NO emissions from 803 to 351 ppm. Sarofim et al. (1999) explained this invariability in char nitrogen conversion to NO by a combined effect of two competing processes. The lower nitric oxide concentration in the background tends to increase the char nitrogen conversion to nitric oxide (as discussed in section 2.2.1.3.1), however the NOx reduction strategy also reduced the oxygen concentration on the boundary layer of the char. This reduction on oxygen concentration increased the char burnout time, which consequently increased the amount of NO reduced on the char surfaces.

Following the lead by Sarofim et al. (1999), this dissertation uses a more comprehensive model to discuss the effect that variations in the surrounding gas composition and temperatures can have on the conversion of char nitrogen to nitrogen oxides.

2.1.7 Summary

Figure 2.4 shows in a very simplified way the process of char nitrogen conversion to nitrogen oxides and molecular nitrogen. The figure does not address the importance of the

mechanisms, but recognizes the existence of them. One of the objectives of this dissertation is to provide an insight into how important these mechanisms are at different conditions.

The left section of the diagram represents the heterogeneous processes. Through these processes the char nitrogen is converted from the solid phase to the gaseous phase. The most probable species to be released due to thermal decomposition is HCN. This mechanism of char nitrogen release competes with the direct attack of oxygen to produce NO. There are additional heterogeneous reactions that consider the reaction of NO on the char surface to produce N_2, HCN and N_2O. These reactions at the same time destroy NO.

All these three reactions only occur in the presence of oxygen. The heat necessary for HCN evolution is only produced when oxygen is present in the system. Oxygen is necessary for the production of NO. And without NO, the reactions leading to the production of N_2, HCN and N_2O do not occur.

Once these species leave the char surface, they can react in the char pores and in the boundary layer with all the gaseous species present in it. Nitric oxide and molecular nitrogen survive these reactions and are usually detected in the boundary layer in almost any reacting environment. N_2O is only detected at fluidized bed conditions, and HCN is only detected when the oxidation in the boundary layer is unimportant or has been suppressed. These species continue to react homogeneously in the bulk and at the exit of the boiler. Only NO, NO_2 and N_2 are detected at the exit of pulverized boilers. At fluidized bed combustion conditions, N_2O is also detected.

With few experimental exceptions, all these processes occur at the same time, making it difficult to evaluate their contribution to the conversion of char nitrogen to nitrogen oxides. However, the use of char oxidation models permit to identify what process are dominant at specific conditions.

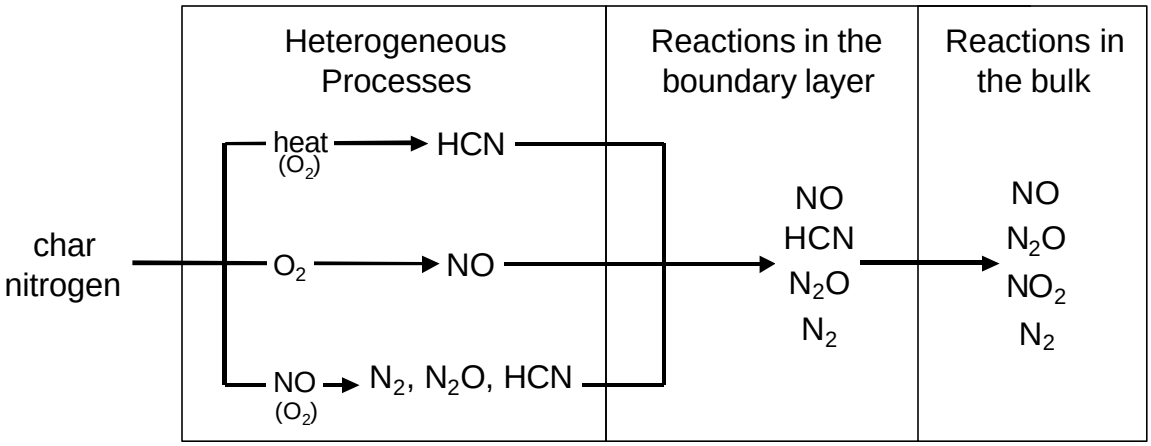

Figure 2.6. Simplified description of char nitrogen conversion

to nitrogen oxides

2.2 OBJECTIVES AND APPROACH

The main objective of this dissertation is study the conversion of the nitrogen present in the char to gaseous species. To this end, experimental and computational analyses of the system were performed.

The experiments had two specific objectives. *1)* To estimate the rate of NO destruction on the char surface and *2)* To evaluate the effect that nitric oxide concentration in the bulk, char particle size and oxygen concentration have in the conversion of the char nitrogen to nitric oxide.

Two carbonaceous materials were used during the study: a bituminous coal, the char produced from this coal and a commercial activated carbon. The difference between the nitrogen content of both materials facilitated the understanding of the phenomenon of char nitrogen conversion to nitric oxides.

The computational analysis part also focused on two objectives. *1)* To develop a single particle model that could be implemented in a CFD code to be used in the design of processes for the reduction of nitrogen oxides emissions during coal combustion and *2)* To evaluate with the use of a more comprehensive single particle model the relative importance of the different phenomena occurring during the conversion of char nitrogen to nitrogen oxides.

The experiments were carried out at temperatures that simulate pulverized coal combustion (1500 - 2300 K) since this is the region where less experimental information exists. The computational analysis though, not only considered pulverized combustion conditions, but also fluidized bed combustion. The idea was to develop a mechanistic model capable of describing the phenomena occurring during char combustion, over the temperature regime encompassing both fluidized bed and pulverized coal combustion.

2.3 EXPERIMENTAL SETUP

2.3.1 Horizontal Furnace

The experiments were carried out in an electrically heated, laminar-flow, drop-tube reactor with a diameter of 5.08×10^{-2} m that allowed a maximum continuous operating temperature of 1750 K. The conventional setup of the drop-tube was modified to allow the implementation of batch experiments with in situ char formation. Figure 2.5 presents a schematic of the experimental setup.

During the experiments, a specified amount of solid was introduced to the reactor by means of a custom-built distributor part. This distributor part is composed of a disk located in front of the char injection tube. The purpose of the disk is to generate a turbulent zone that spreads the coal uniformly over the entire cross-sectional area of the drop tube reactor, minimizing the chance of particle-particle interactions. To prevent the deposition of coal on the walls of the distributor, a radial gas stream is flown through the walls of the distributor that are in contact with the coal stream in the turbulent zone. After the disk, laminar flow develops before the gases enter the drop tube reaction zone and the coal stream is dispersed over the entire cross sectional area. Since the flow inside the reacting section is laminar, no deposition of coal on the reactor walls occurs. The solid stream is then collected over an alumina/silica non-woven fabric that was placed in the medium of the reacting zone. A quartz window on the top of the drop tube allowed visual examination of the particles.

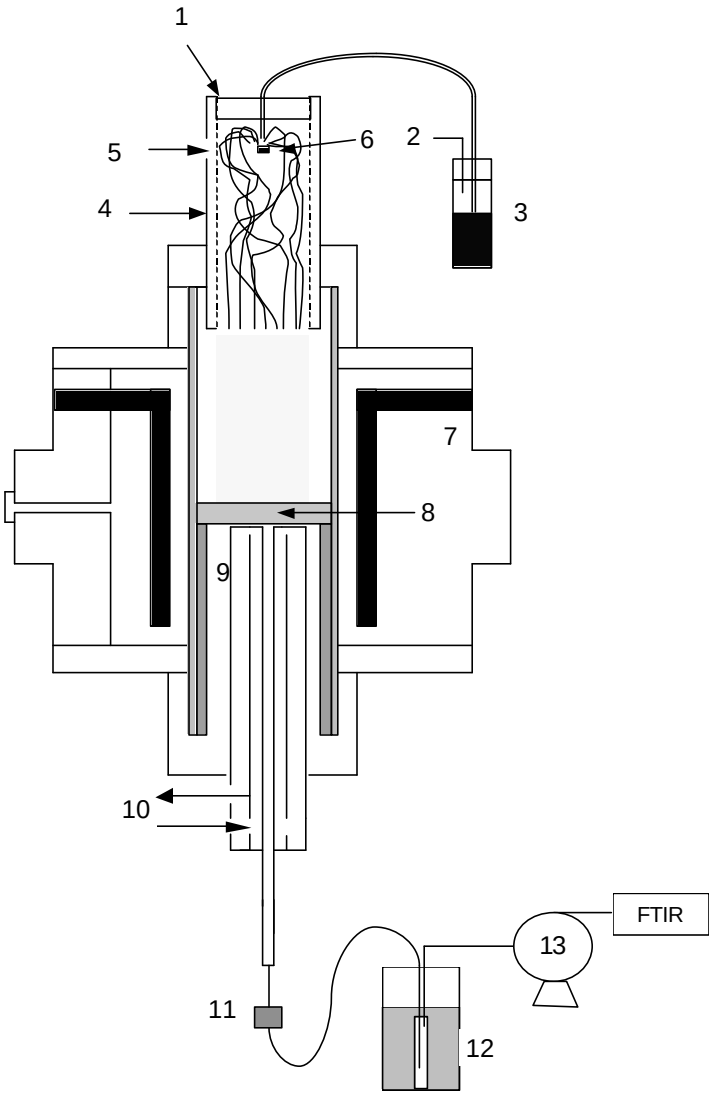

Figure 2.7. Experimental setup for the batch experiment: ***1.*** **Quartz window,** ***2.*** **Carrier gas input,** ***3.*** **Char feeding system,** ***4.*** **Distributor,** ***5.*** **Distributor radial gas,** ***6.*** **Disk input;** ***7.*** **Graphite heating element , 8. Alumina / silica non-woven fabric,** ***9.*** **Collection Probe,** ***10.*** **Cooling Water*11.* Filter,** ***12.*** **Cold trap,** ***13.*** **Diaphragm vacuum pump**

2.3.2 Gas Analysis

During char or coal oxidation at temperatures above 1200 K, the most abundant gaseous species are CO_2, O_2, N_2, NO and SO_2. Other species such as CO, NO_2, N_2O, HCN, C_2H_2 and CH_4 are also detected at lower concentrations that depend on experimental conditions. All the species in the first group except SO_2 are of relevance for the present study; therefore the gas analysis technique was focused on the correct quantification of CO_2 and NO (O_2 and N_2 could be deduced from a mass balance). The concentration of these four species was evaluated by FTIR analysis and double-checked with a NDIR analyzer for CO_2 and a chemiluminescent analyzer for NO. The use of the FTIR also allowed measurement of CO, NO_2, HCN, N_2O, SO_2, C_2H_2 and CH_4. However, the concentration of these species was not corroborated by an additional technique and therefore should be understood to be less precise.

2.3.2.1 FTIR

The use of FTIR for the analysis of the gases produced during coal combustion in experimental setups has become a common practice. For a detailed description of the method of calibration and of the analysis-regions used during these experiments the reader is referred to the theses by Spinti (1997), Sirdeshpande (1999) and Tullin (1995). This discussion focuses on the most critical aspects of the application of FTIR gas analysis that are specific to the experimental setup of this study.

2.3.2.1.1 Description of the FTIR gas analysis protocol

The FTIR used in the experiments was a Nicolet Model 550 Magna-IR Spectrometer equipped with a 254 cm^3 gas analysis cell with a path of 7.25 m. The software packages Omnic 5.2 and TQ Analyst 6.0 from Nicolet Instrument Corporation were used to define the method for gas analysis quantification. For the calibration, metered flows of standards of NO, NO_2, N_2O, CO and CO_2 of known concentration were mixed with He to obtain

different mixture concentrations that simulated the typical values expected during the experiments. Appendix B of Molina (2002) presents a summary of the standards and their concentration. With the standards as input, a Partial Least Square (PSL) algorithm implemented in the software package was applied to evaluate the species concentration.

Table 2.1 shows the spectral regions used to evaluate the concentration, the concentration range and the estimated error of the measurements for the most common species. In the definition of the absorption region, extreme care was taken to avoid any water interference. The errors are less than 6% for all the species excepting CO and CO_2. For these two species the error is slightly higher due to the broad range of concentrations measured.

Table 2.1. FTIR analysis spectral regions and detection limits

Gas	NO	CO	N_2O	CO_2	NO_2
Region (cm^{-1})	1959.3 – 1789.9	2058.9 – 2046.9	1259.8 – 1245.3	772.4 – 726.1	1600.4 – 1597.0
Concentration range	5 – 1540 ppm	30 ppm – 4.8 %	7 – 100 ppm	0.06 – 12.1 %	5 – 190 ppm
Estimated Error (%)	- 5.7 + 5.7	- 15.0 + 7.0	- 2.0 – + 10.0	- 12.3 + 3.3	- 6.0 5.7

Before every experiment, a background reading on Ultra High Purity (UHP) helium flowing directly through the FTIR at 4000 cm^3/min (298K, 101325 Pa) was taken. These background conditions were also used while collection the spectra of the standards and during the experiments. This allowed comparison between backgrounds on differentdates. There was no detectable variation in the background during the time the experiments were carried out. This indicates a negligible decay of FTIR sensitivity with time.

2.3.2.1.2 Effect of water condensation

The water produced during coal combustion condensates in the collection probe and cold trap. Water is known to affect the evaluation of nitrogen oxide concentration due its absorption of nitrogen dioxide and ammonia (Evans et al., 1993). However, due to the small sample size and the low hydrogen content of the samples water condensation, was not observed in the cold trap. Any loss of nitrogen oxides in the cooling system was therefore negligible.

2.3.2.1.3 Time resolution

Coal and char oxidation at temperatures above 1200 K is a rapid process. At 1700 K, the reaction time is ~ 100 ms. Since collection time for one spectra in the FTIR used in this study was close to 3 seconds, it is important to guarantee that despite the differences in time scale, the FTIR was able to detect enough data to evaluate the conversion of the nitrogen in the sample to nitrogen oxides.

In order to estimate the influence of time resolution, two different evaluations of the data collected with the FTIR were performed. In the first one, the data from the FTIR was compared to that obtained with a NDIR analyzer for CO_2 and a chemiluminescent analyzer for NO. These two instruments have response data in the order of 0.25 seconds. The results are described in the next section, but the conclusion is that despite the low time resolution of the FTIR, it captures the concentration of gases evolved during the oxidation experiments.

The second evaluation considered the determination of the Residence Time Distribution (RTD) in the reactor. The complete description is presented in Appendix C of Molina (2002). The conclusion of this evaluation is that the FTIR does not resolve in time the event of char or coal oxidation in the drop tube, since the dispersion of the products in the reactor volume and in the analysis system produced a broad RTD. However, the FTIR detects the total amount of gases produced during coal combustion.

2.3.2.2 NDIR and chemiluminescent analyzers

In order to improve the confidence in the experimental results, a complementary technique for the evaluation of the concentration of the main gases was implemented. A Non Dispersive Infrared (NDIR Nova Model 4280RM Dual Range CO and CO_2) analyzer was used to evaluate the concentration of CO_2 and a chemiluminescent analyzer (Thermo Environmental Model 10A Chemiluminescent NO-NO_x Gas analyzer) to evaluate the concentration of NOx. These two instruments were connected to an OPTO 22 I/O system for data acquisition and control, so that time vs. concentration profiles could be logged.

Both instruments were calibrated at concentrations of zero given by He (background gas) and those given by to different mixtures of standard gases. The calibration was checked every day during the experiments. Spinti (1997) presented a more detailed description of the instruments and of the calibration procedure.

Figure 2.6 presents a comparison of the profile of CO_2 and NO concentration as calculated from the FTIR and the NDIR and chemiluminescent analyzers respectively during the oxidation of 6 mg of coal Illinois No. 6 (particle size = 58 μm) at 1698 K in a mixture of 4% O_2/He. The figure shows that despite the difference in time resolution between the two analysis techniques, the calculated results for CO_2 and NO are very similar in magnitude and in shape. Similar plots were obtained for several other experiments. The differences between the results from the FTIR and the NDIR and chemiluminescent analyzers for the area under the curve were always lower than 10% for CO_2 and 20% for NO. This was considered a reasonable difference taking into account that the experiments do not occur simultaneously, the low concentration of the species involved and the short duration of the event.

After confirmation that the FTIR gave reasonable gas concentration, most experiments were analyzed exclusively with FTIR. To guarantee the continuous

calibration of the FTIR, the background of He was tested every day and the carbon mass balances was checked for every experiment.

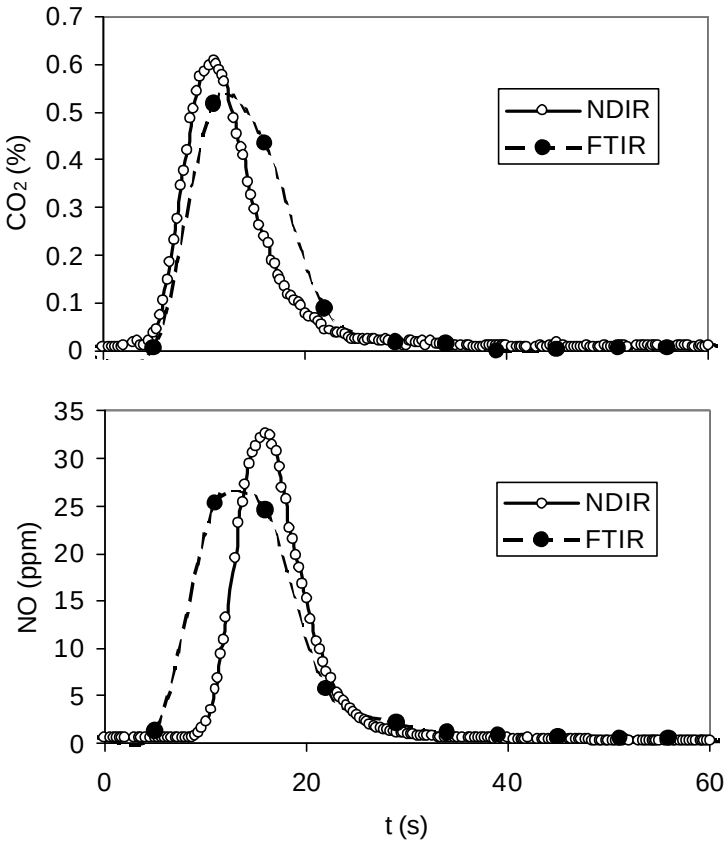

Figure 2.8. Comparison of the concentration vs. time profiles as calculated with the FTIR and with the NDIR and chemiluminescent analyzerz. Illinois No. 6. T_g = 1698, O_2 = 4%, D_p = 58 μm. Sample size = 6 mg

2.3.2.3 Collection probe

The collection probe was made of stainless steel, with an inner diameter of 0.0127 m (0.5 in). It had two entrances for cooling water. Contrary to the previous studies in the

drop tube (e.g. Graham, 1991), the collection probe did not use a quench gas. The reason for this is that a quenching stream dilutes the combustion gases to concentrations beyond detection limits for the gas analysis system. Nevertheless, with the use of a water-cooled probe it is possible to obtain cooling rates in the order of 2×10^6 K/s (Heitor and Moreira, 1993 and Appendix D of Molina, 2002).

Another concern with the collection probe is that catalytic effects on the probe surface can affect the final gas concentration. In particular, NO can be reduced to N_2 when in contact with stainless steel at high temperatures. However, in the setup in Figure 2.5, the stainless steel is only in contact with the nitrogen oxide at low temperatures (< 373 K) since it is cooled by water (~288 K) over the entire length in contact with the gas.

2.3.3 Experimental Method

As stated in section 2.2.2, the experimental analysis had two main objectives. One to estimate the rate of NO destruction on the char surface and two, to evaluate the conversion of char nitrogen to nitrogen oxides under different experimental conditions. Different experiments were used to meet each of these objectives. This section describes these experiments.

2.3.3.1 Experiments under inert atmosphere

These experiments were designed to estimate the rate of NO reduction on the char surface. Jensen et al. (2000) suggested that, for some chars, the rate of NO reduction on the char surface suffers a strong deactivation with reaction time. This effect is manifest only for bituminous coal. Similar test for anthracite and a petroleum coke did not present the same effect (Jensen, 1999). To address possible char deactivation, the experiments were designed so that char was prepared in situ. Table 2.2 presents step by step the

methodology of the experiments. In Step 1, a mixture of NO/N_2/He with a specific NO concentration (750 ppm for most of the experiments) is added to the reactor until a steady state NO concentration is reached. 5 to 6 mg of solid is injected into this mixture and is deposited on the non-woven fabric inside the reactor. This represents time 0 of the experiment. After ~ 5 minutes, oxygen is allowed into the reactor to consume any remaining char. Figure 2.7 shows the profiles for CO_2, NO and CO for one of these experiments.

Table 2.2. Experimental method for evaluating the rate of NO reduction on the char surface

Step	Time (s)	Gases			Solid
		NO (ppm)	He	O_2	
1	Necessary to obtain equilibrium in NO concentration	0 - 750	Balance	0	
2	0	0 - 750	Balance	0	Injection
3	120 - 300	0	Balance	21%	

It is important to note in Figure 2.7 that when the solid injection occurs, the system is unchanged since the gas used to entrain the solid during the injection flows through the reactor during the entire experiment. The solids are elutriated from the feed tube by decreasing the distance from the hypodermic tube to the solid surface (Figure 2.8). Therefore the decrease in nitrogen oxide concentration is only due to the reduction of NO on the char surface. The production of CO is also evidence of this reaction. When oxygen is allowed into the reactor, CO_2 and CO are produced.

The injection of oxygen results in a dilution of the gases in the system. This is the reason why the NO concentration after the solid oxidation does not reach the same level it had before the solid injection. The constant increase in NO concentration with reaction time is due to a reduction on the mass of solid available for reaction

Experiments similar to the one illustrated in Figure 2.7 were performed at different temperatures, with different solid materials and at different NO concentrations. The detail analysis of the results is postponed for the next section. This section only illustrates the experimental method.

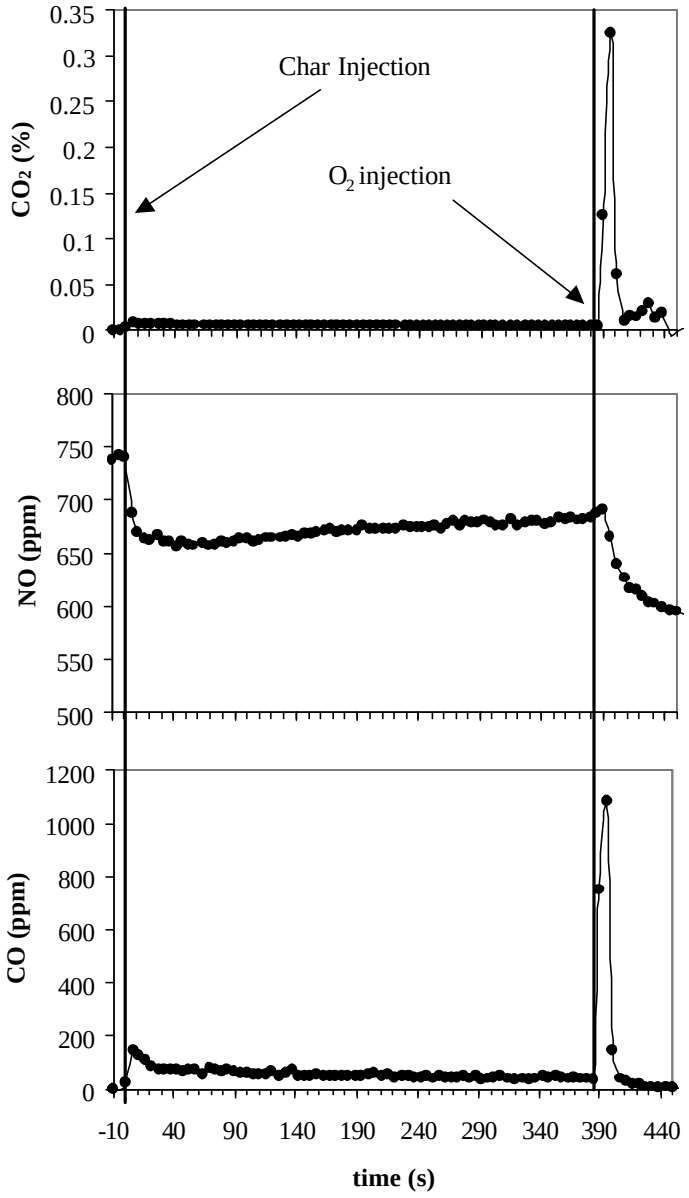

Figure 2.9. CO_2, NO and CO profiles in the inert atmosphere experiments.The solid is added to the reactor a time 0 to a mixture $He/N_2/NO$ (750 ppm).Oxygen (21%) enters the reactor at 480 (s). T = 1273 K, Char U Furnace

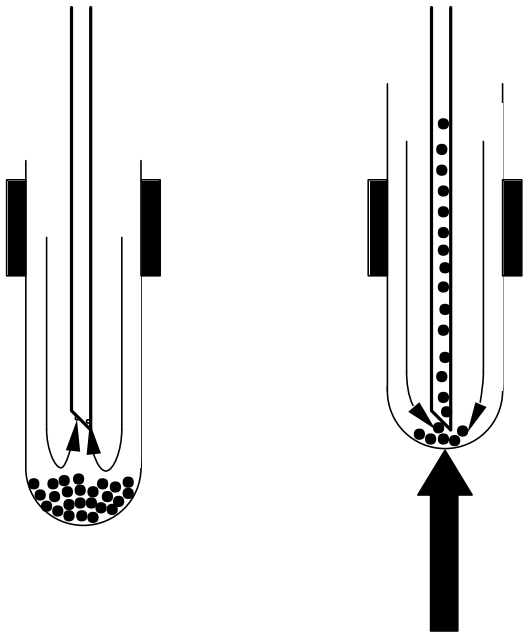

Figure 2.10. Process of solid injection. Left: Steady State, only gases flow through the hypodermic tube. Right: Injection; the test tube is moved upwards and the solids flow through the hypodermic tube into the reactor.

2.3.3.2 Experiments in the presence of oxygen

Two different types of experiment in the presence of oxygen were carried out in order to evaluate the conversion of char nitrogen to nitrogen oxides under different conditions.

2.3.3.2.1 Experiments with purge

The first set of experiments, or experiments with purge, is similar to the one described in Table 2.2. At the beginning of the experiments, the reactor is filled with He. At time 0, the solid is injected into the reactors, where it is collected on the non-woven fabric. After one minute of solid injection, O_2 is admitted into the system at a specific concentration. Figure 2.9 presents the concentration vs. time profiles for one of these experiments.

At time zero, when the solid, in this case chars prepared in the U-Furnace (see next section for a description in the solids used in this study), was injected into the reactor, CO is produced in considerable concentrations. CO_2 and NO are also produced, although in lower magnitude. The production of these species just by the addition of char into the system was unexpected since oxygen was not present in the system. The reason for this is examined in following sections. Besides NO and CO_2, other species as SO_2, HCN, and C_2H_2 were detected in the first part of the oxidizing/purge experiment. The presence of these species depended on the solid used and on the experimental conditions as will be discussed in the next sections. After oxygen addition, CO_2, NO and CO are produced in higher magnitudes.

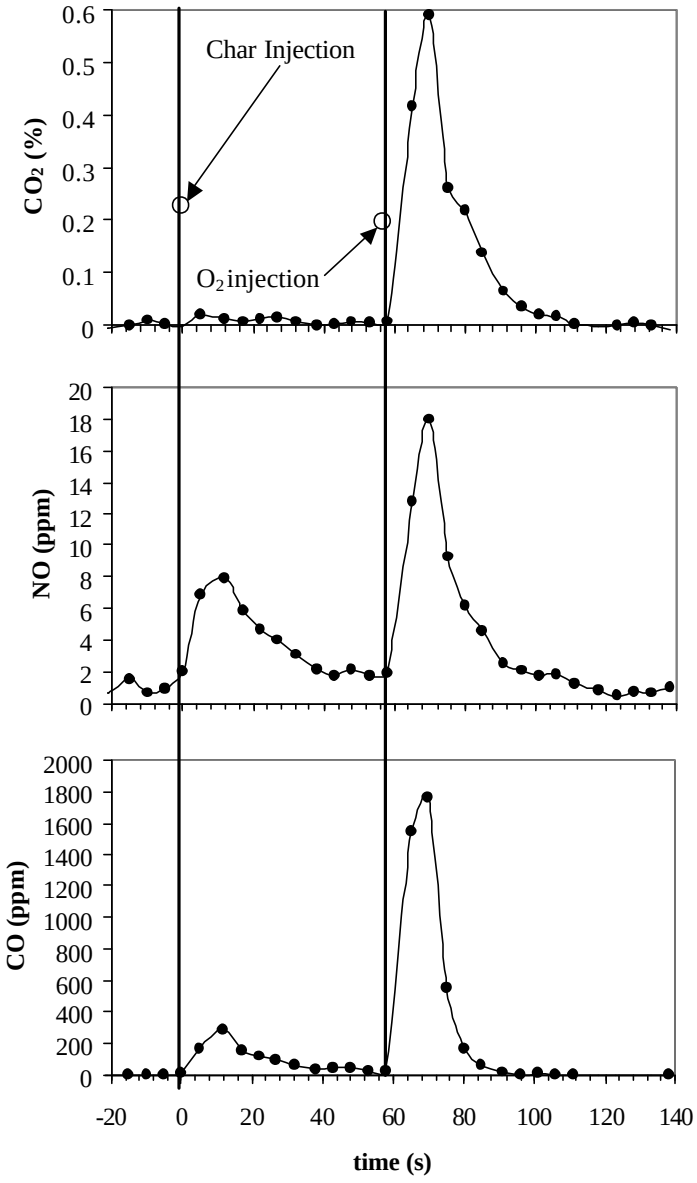

Figure 2.11. CO_2, NO and CO profiles in the oxidizing/purge experiments. The solid is added to the reactor that is under He purge at time 0. Oxygen (4%) enters the reactor after 60 seconds. T = 1698 K, U-Furnace char

2.3.3.2.2 Direct injection

In these experiments, the reacting solid was injected into a mixture of O_2/NO/He/N_2. Part of the reaction occurs while the solids fall in the reactor and the remaining char reacts on the non-woven fabric.

Two different oxygen concentrations (4 and 20%), five NO concentrations (0, ~250, ~500, ~750 ppm) and three different particle sizes (35, 58 and 118 μm) were used in these experiments. The results in Figure 2.6 are an example of the CO_2 and NO profiles obtained in this system. The CO profile is similar to the one of CO_2. However, the production of CO in this system was lower than in the purge experiments.

2.3.4 Characterization of Solid Samples

2.3.4.1 Ultimate and proximate analyses

One bituminous coal and one activated carbon were used in this study. Table 2.3 presents the ultimate and proximate analysis of the samples. Coal refers to the raw Illinois No. 6 coal. Char DT refers to char produced by injection of coal in a Drop Tube reactor without the presence of the non-woven fabric (continuous injection mode). U-Furnace char is char produced in a pulverized coal pilot scale furnace (Spinti, 1997) from Illinois No.6 coal under a self-sustained flame and typical pulverized combustor conditions. Activated carbon is the commercial activated carbon produced from coconut shell.

Table 2.3. Coal and Char analysis

	Proximate Analysis (%)				Ultimate Analysis daf (%)				
	Moist.	Ash	Volatile Matter	Fixed Carbon	C	H	N	S	O
Coal	6.91	5.56	46.38	41.15	80.67	5.30	1.87	0.98	11.19
Char DT	5.03	10.31	3.87	80.79	95.70	0.56	1.84	0.72	1.18
Char U-Furn.	0.89	17.85	N.A.	N.A.	92.63	1.48	1.96	0.62	3.31
Act. carbon	6.06	5.23	N.A.	N.A.	91.56	2.06	0.14	0.02	6.21

N.A. Not available

The data in Table 2.3 are from (Spinti, 1997), except for the data for Char DT that were obtained from Huffman Laboratories in Golden, Colorado. The data in Table 2.3 shows that the nitrogen content for the coal and the chars is very similar (~1.90 ± 0.06 %). The nitrogen content for the activated carbon is lower by one order of magnitude.

The differences in the elemental composition between the chars prepared in the drop tube and those prepared in the U-Furnace is due to different production techniques. The chars-DT were prepared by exposure to 1698 K of coal for residence times close to 1.4 s if completely developed laminar flow is assumed. The chars prepared in the U-furnace were submitted to temperatures close to 1500 K and residence times of the order of 0.3 s. These differences in temperature and residence time explain the higher carbon and lower hydrogen content of the chars prepared by injection in the drop tube.

The char was produced in order to provide the elemental and proximate analysis for the initial condition of the char in the in situ experiment explained in section 2.3.3.2.1. The difference in the residence time of the chars prepared in the drop tube (~1.5 s) and those prepared in section 2.3.3.2.1 (~1 min) represents a caveat in the use of the proximate and ultimate analysis of the first one when analyzing the conversion of char nitrogen to nitrogen oxides in the experiments with purge. Late devolatilization reactions

can occur during this minute and those are not considered in the elemental analysis. However, the difficulties associated to producing chars with only one-minute residence time inside the drop tube impose the use of an approximated elemental composition. The chars with 1.4 seconds residence time are therefore used for this approximation.

2.3.4.2 Particle size

All the samples used in this study were received as pulverized solid. Further sample preparation was limited to the use of sieves for the separation of particle size. For most of the experiments, a fraction +230 – 270 (63 – 53 μm) was used. This represents an average diameter of 58 μm. When the effect of particle size was studied, two additional sizes were considered +140 – 170 (108 – 88 μm) and +400 (<37μm). The first one represents an average particle diameter of 98 μm and the last one, particle size smaller than 37 μm.

Although the use of sieves for particle characterization presents numerous problems, particularly related to the discrete characteristic of the separation and difficulty on separating solids that as coal tend to agglomerate, this technique is sufficient to guarantee a relative uniform particle size and considerable differences between different size fractions to evaluate the influence of particle size on the production of nitrogen oxides.

2.3.4.3 Surface area

The surface area of the chars represents an additional parameter that is important for the evaluation of char reactivity. The BET surface area for the chars prepared in the U-furnace was 104.8 m^2/g. The one of the activated carbon is 1678 m^2/g. These data are from Spinti (1997).

2.4 REDUCTION OF NITRIC OXIDE ON THE CHAR SURFACE

2.4.1 Introduction

The most simplified approach to char nitrogen oxidation may be to consider that nitric oxide is the only product and to ignore the effect of diffusional restrictions and homogeneous reactions. In this case, the amount of char-nitrogen converted to nitric oxide depends on the difference between the reaction of nitric oxide formation (R 2.7) and destruction (R 2.8). According to this simplistic approach, if the ration between both rates is one, all the nitrogen oxide formed will be converted to N_2.

$$O_2 + -CN \xrightarrow{k_0} NO \qquad \text{R 2.7}$$

$$NO + -C \xrightarrow{k_{NO}} N_2 + -C(O) \qquad \text{R 2.8}$$

It is obvious that the real process of char-nitrogen conversion to nitric oxide is more complex that the simple scheme represented by R 2.7 and R 2.8. In particular, the time scales and surface areas in which both reactions occur are completely different. While it is more possible that R 2.7 occurs on the external area of the surface where the oxygen concentration is higher, R 2.8 can occur on all the internal surface area, where nitric oxide can diffuse.

Nevertheless, as a thought experiment, the ratio between the rates for reaction R 2.7 and R 2.8 can be used as an indicator of the amount of char-nitrogen converted to NO. E 2.2 represents an expression for this ratio. r_{CN-O} is the rate of char nitrogen oxidation to NO and r_{NO-C} the rate of NO destruction on the char surface. These two rates can be

characterized as the value of a kinetic constant k_i times the concentration of oxygen $\left(C_{O_2}\right)$ and nitric oxide $\left(C_{NO}\right)$ raised to the power of reaction orders a and ß respectively.

$$\frac{r_{CN-O}}{r_{NO-C}} = \frac{k_O C_{O_2}^{\alpha}}{k_{NO-C} C_{NO}^{\beta}} \qquad \text{E 2.2}$$

The value for the ratio between rates expressions is considerably sensitive to the units used for species concentration. Therefore, the following discussion assumes first order reactions. In this case, the factor for the ratio of concentration $\left(C_{O_2}^{\alpha} / C_{NO}^{\beta}\right)$ is 80 for a typical combustion system ($C_{O_2} \sim 0.04; C_{NO} \sim 5\times10^{-4}$ mol fraction units). At higher oxygen concentration this number increases to 420 (21 % O_2).

This implies, that under typical oxidation conditions, if the diffusion limitations and homogeneous reactions are not considered, and assuming first order reactions, there is a factor between one to two orders of magnitude that increases the possibilities of converting char-nitrogen to nitric oxide.

However, in E 2.2 there is an additional factor that relates the kinetic constants of both reactions $\left(k_{CN-O} / k_{NO-C}\right)$. This factor, combined to diffusion limitations determines the actual extent of char-nitrogen conversion to nitric oxide.

The fist term, k_{CN-O} that represents the rate of char nitrogen oxidation (R 2.2) can be assumed to be of the same order of the rate of char oxidation times the ratio of nitrogen to carbon atoms in the char. There is extensive literature on the rate of char oxidation (Shaddix, 2001 Hurt and Mitchell, 1992, Smith, 1982). Therefore, most of the emphasis on the evaluation of the selectivity towards nitric oxide is focused on the evaluation of the rate of NO destruction on the char surface, k_{NO-C}. This reaction has been extensively

studied. Aarna and Suuberg (1997) reviewed more than 20 different studies of this reaction for different carbonaceous materials and environmental conditions. They proposed an expression (E 2.3) that represented the rate of NO destruction at temperatures above 700 K within one order of magnitude.

$$k_{NO-C} = 5.5 \times 10^{6} \exp(-15939/T) \quad (g_{NO} m^{-2} h^{-1} atm_{NO}^{-1}) \qquad \text{E 2.3}$$

Molina et al. (2000) confirmed that expression E 2.3 represented within one order of magnitude the rates of NO/C reactions from different studies (Levy et al., 1981 - de Soete, 1990 Guo and Hecker, 1998). However, a recent study by Jensen et al. (2000) suggest that most of these kinetics under-predicted the rate of nitric oxide reduction on the char surface because of thermal deactivation of chars produced under inert atmospheres. These authors proposed an alternative expression (E 2.4) for the temperature range of 1123 – 1423 K that is according to Jensen et al (2000) a factor of 10 – 100 greater than the range of the literature data.

$$k_{NO-C} = 6 \times 10^{6} \exp(-14800/T) \quad (m^{3} kg\_C^{-1} s^{-1}) \qquad \text{E 2.4}$$

One main difference between E 2.3 and E 2.4 are the units used for normalization of the rate expression. While Aarna and Suuberg (1997) used the more classic approach of normalizing the reaction rate by the surface area of the solid (m^2/gm C), Jensen et al. (2000) chose the carbon density inside the reactor (kg C/m^3). Both rates expression can be converted to the units of the other if the carbon density and the surface area of the solid are known. Unfortunately, Jensen et al. (2000) did not report the surface area of the chars they used during their measurements. Nevertheless, as shown in Appendix E of

Molina (2002), when a reasonable value of surface area is applied to expression E 2.4, the results lie between one order of magnitude of those predicted by E 2.3.

Although the rate of NO reduction on the char surface reported by Jensen et al (2000) is probably not as high as the authors originally suggested, it is worthy to evaluate the effect of that char deactivation can have on this reaction. Illán-Gómez et al. (1995c), Aarna and Suuberg (1998), Guo and Hecker (1998) and Yamashita et al. (1993) have observed a similar effect, particularly at low temperatures (573 – 923 K). All these authors suggest that the accumulation of nitrogen in the initial stages of char gasification is the reason for this behavior. In fact, Guo and Hecker (1998) found a negative balance on nitrogen that suggests a build up of nitrogen complexes in this initial unsteady period. This process is first order with respect to nitric oxide concentration and tends to disappear as temperature increases (Aarna and Suuberg, 1998). Ashman et al. (1998) and Abbasi (1999) have also observed nitrogen accumulation during char oxidation. All this evidence suggests the existence of an adsorption-limited process that is more important at low temperatures when the char surface is not clean. At higher temperatures, the population of surface complexes is smaller and the reaction is no longer adsorption-limited, therefore the effect is lower.

The following section evaluates the effect of char deactivation on the reduction of nitric oxide on the char surface.

2.4.1.1 Influence of char in situ preparation on the rate of nitric oxide reduction on the char surface

Figure 2.10 to Figure 2.13 present the concentration profiles for CO_2, CO, NO and HCN for the injection of three different solids: *i.* Illinois No. 6 coal (coal), *ii.* Char from Illinois No. 6 formed in the U-Furnace (U-Furnace char) and *iii.* An activated carbon.

The gas temperature changes between figures. It is 1273 K for Figure 2.10, and 1415 K, 1556 K and 1698 K for Figure 2.11, Figure 2.12 and Figure 2.13 respectively.

At all temperatures there is a rapid increase of CO, CO_2 and HCN concentration as soon as the solids are injected. Simultaneously the NO concentration decreases. This increase in the concentration of CO, CO_2 and HCN as coal is injected is more pronounced for coal than for the other two solids, and this difference tends to reduce as the temperature increases. This peak corresponds to the release of volatiles. It is also observed in the char and the activated carbon since these two solids release some volatile compounds as product of secondary devolatilization reactions once injected into the drop tube reactor.

Although in Figure 2.10 to Figure 2.13 only HCN and to certain extent CO and CO_2, represent the evolution of volatiles during coal devolatilization or secondary devolatilization reactions, Molina (2002, Appendix F) shows evidence of the presence of some other light hydrocarbons (CH_4, C_2H_2 and C_2H_4) characteristic of devolatilization products at high temperatures. The analysis of the spectra by Molina (2002, Appendix F) suggests that the presence of these species is more evident at the lower temperatures (1273 K) since these species are converted to CO_2 inside the reactor at higher temperatures. The increase in the production of SO_2 with temperatures is also probably due to the oxidation of sulfur species. This reference also shows that the U-Furnace char also produced these volatiles species, although in considerably lower concentration than the one reported for the coal.

These results are also in agreement to those in Figure 2.10 to Figure 2.13. The increase in HCN relative concentration that occurs just after solid injection is considerable more pronounced at lower temperatures and for coal. It decreases with increasing temperature and is almost negligible for U-Furnace char and for the activated carbon. At the same time the peak for CO_2 increases with temperature.

In summary, the concentration vs. time profiles in Figure 2.10 to Figure 2.13 and the FTIR spectra reported by Molina (2002) show that there is release of volatiles during the

first few seconds after the injection of the solids in the reactor; that mainly these volatiles are produced during coal injection, though some small production of volatiles by the U-Furnace char and the activated carbon occurs. These volatiles are converted to CO_2 as the temperature increases.

It is important to remember that due to the large volume in the reactor, there is a relative broad Residence Time Distribution (see Appendix C of Molina, 2002) that transforms any instantaneous phenomenon inside the reactor into a 20 to 50 second event in the FTIR. This is the reason why, in Figure 2.10, where the coal is injected in the reactor at time 0, the corresponding production of volatiles appears to last 20 seconds, while the actual process should be in the order of a hundred milliseconds (Kobayashi et al., 1976).

The reason for the discussion of the detection of volatile compounds just after char addition is because they can have an influence in the evaluation of the rate of NO reduction on the char surface. Under rich conditions, the reduction of NO by natural gas is a well-known technique to reduce nitrogen oxide emissions in different combustion systems (Bilbao et al., 1995, Xu et al., 1999). Thus, it can be expected that at the temperatures in which the production of volatiles was higher (1273 K) the reduction of nitrogen oxide due to gas phase reaction is important and can affect the evaluation of the rate of nitric oxide reaction with the char surface. As temperature increases and the volatiles tend to form oxidized species such as CO_2 this effect should be lower. In the same way, this effect should be noticeable when coal is injected in the

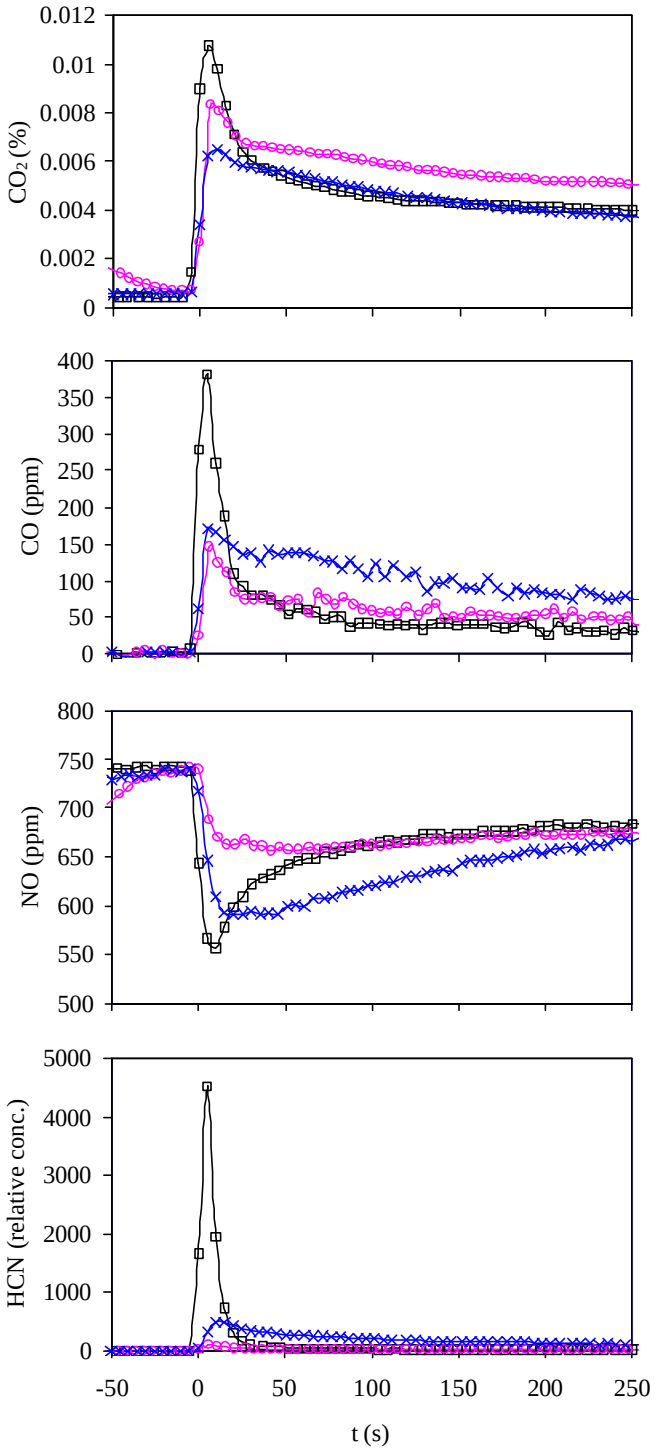

Figure 2.12. Profiles of CO_2, CO, NO and HCN vs. time during char reaction with a 750 NO / He stream. Solids are injected at time 0. T = 1273 KSample size = 5 mg. ? Coal, ? U-Furnace char, × Activated carbon

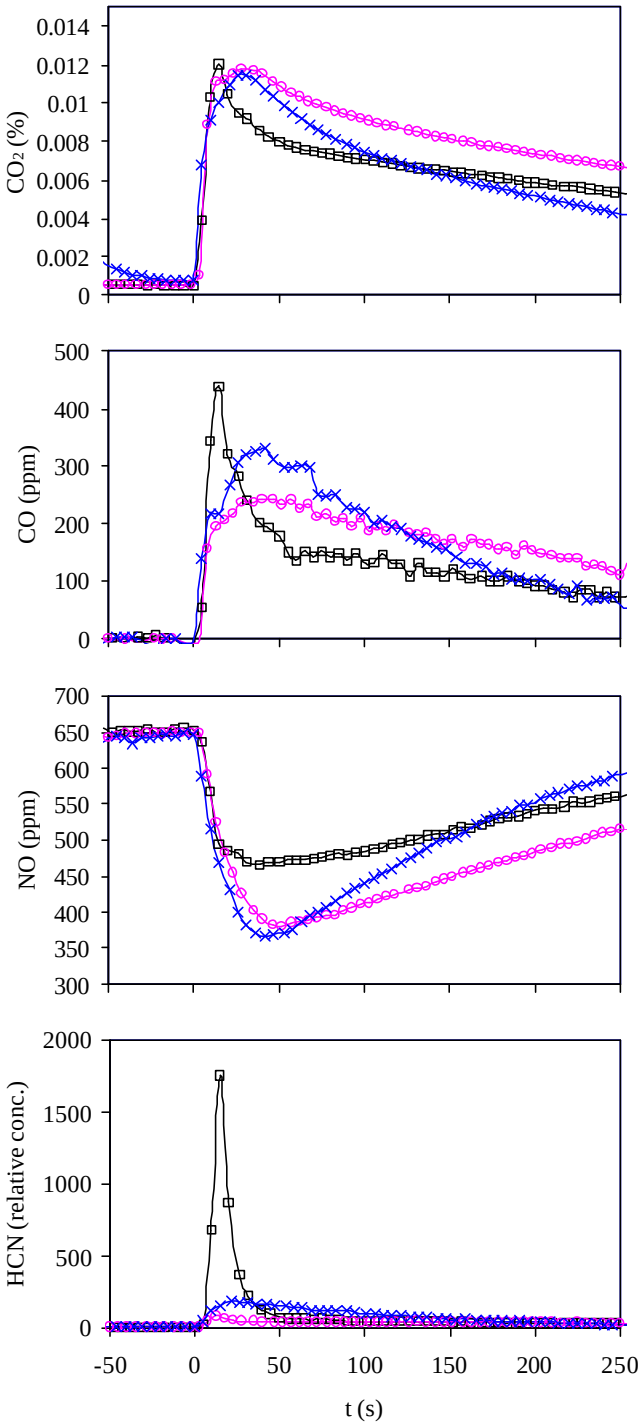

Figure 2.13. Profiles of CO_2, CO, NO and HCN vs. time during char reactionwith a 650 NO / He stream. Solids are injected at time 0. T = 1415 K Sample size = 5 mg. ? Coal, ? U-Furnace char, × Activated carbon

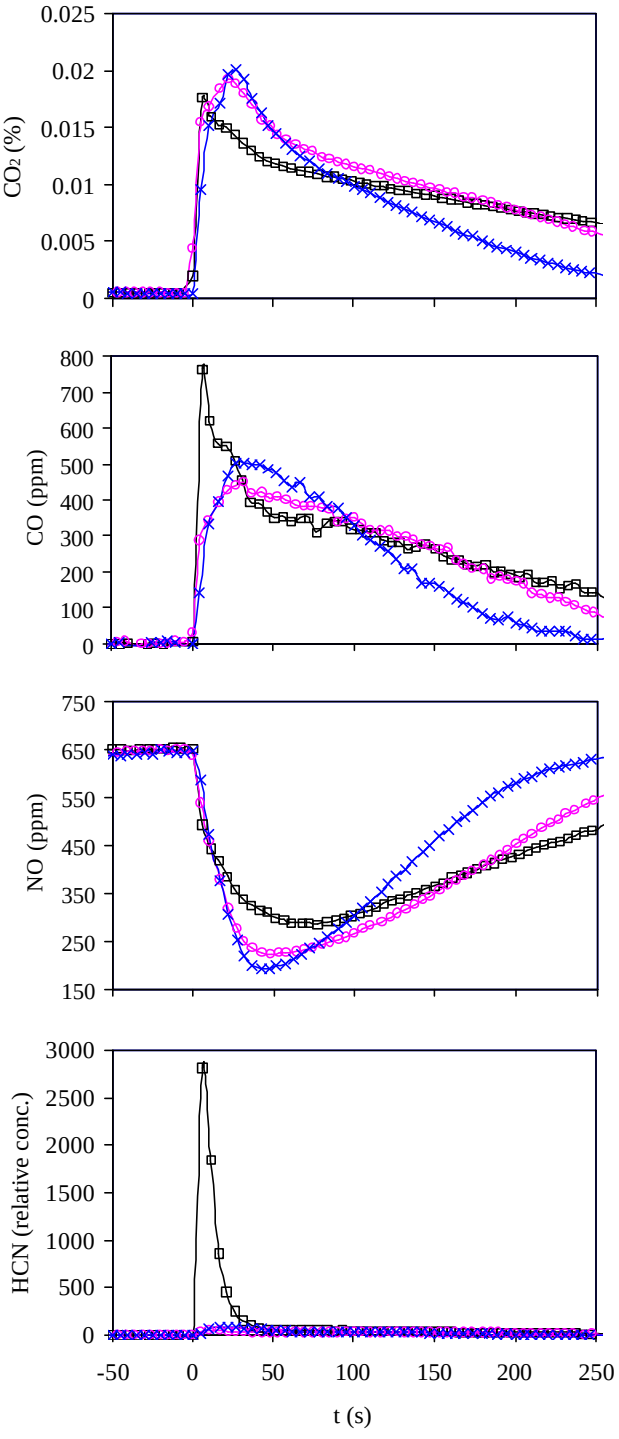

Figure 2.14. Profiles of CO_2, CO, NO and HCN vs. time during char reactionwith a 650 NO / He stream. Solids are injected at time 0. T = 1556 K Sample size = 5 mg. ? Coal, ? U-Furnace char, × Activated carbon

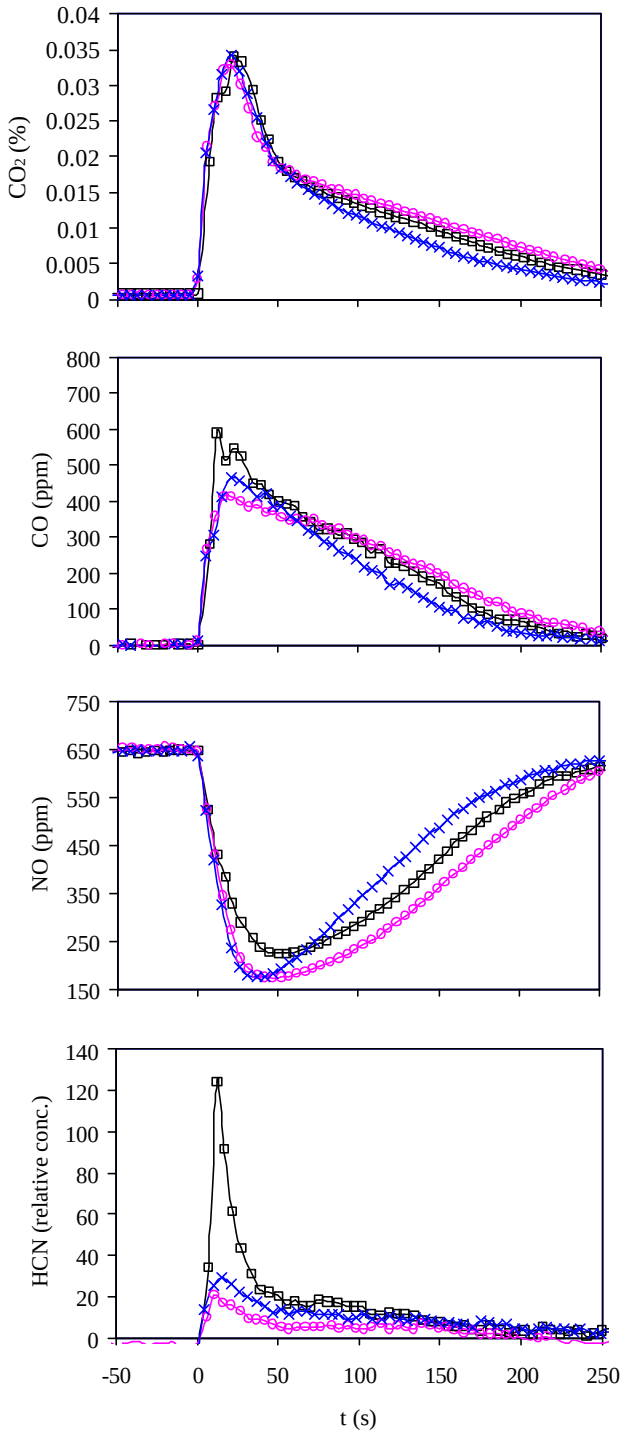

Figure 2.15. Profiles of CO_2, CO, NO and HCN vs. time during char reactionwith a 650 NO / He stream. Solids are injected at time 0. T = 1698 K Sample size = 5 mg. ? Coal, ? U-Furnace char, × Activated carbon

system, but smaller when U-Furnace char or activated carbon are injected since these solids tend to produce less volatiles.

All these observations occur in Figure 2.10 to Figure 2.13, for which at 1273 K (Figure 2.10), the reduction of nitric oxide after coal is steeper than for any of the other solids. At other temperatures (Figure 2.11 to Figure 2.13) this phenomenon is not observed.

This effect is easier to appreciate in Figure 2.14 where the reduction of NO as computed by E 2.5 is plotted as a function of time.

$$X_{NO} = \frac{[NO]_{in} - [NO]_{out}}{[NO]_{in}} \qquad \text{E 2.5}$$

Where $[NO]_{in}$ and $[NO]_{out}$ represent the nitric oxide concentration at the inlet and outlet of the droptube respectively. $X_{NO} = 1$ implies complete reduction of the incoming nitric oxide stream in the reactor.

Figure 2.14 shows an increase in the nitric oxide conversion when the solids are injected. For temperatures above 1273 K, this increase is slow and is followed by a slow decrease in conversion as the solid is consumed. The higher the temperature, the steeper this reduction since the reaction occurs faster. The difference in the onset of the peak between all the solids is almost negligible at these temperatures. It is important to notice that although the mass of carbonaceous materials injected in the reactor is always the same, the actual mass of the char reacting with the nitric oxide is different in every case since the amount of material devolatilized varies between solids. Therefore total nitric oxide conversion is not comparable between the different solids.

At 1273 K the plot looks different. The increase on char nitrogen reduction just after the injection of the solids is steeper when coal is injected than when any of the other two solids are injected. Two peaks are observed: One in the first 20 seconds and a second one, broader, that goes from 20 to 50 seconds. Both peaks superimpose to form one. They are observed in a better way in Figure 2.15 that shows the reduction of nitric oxide for

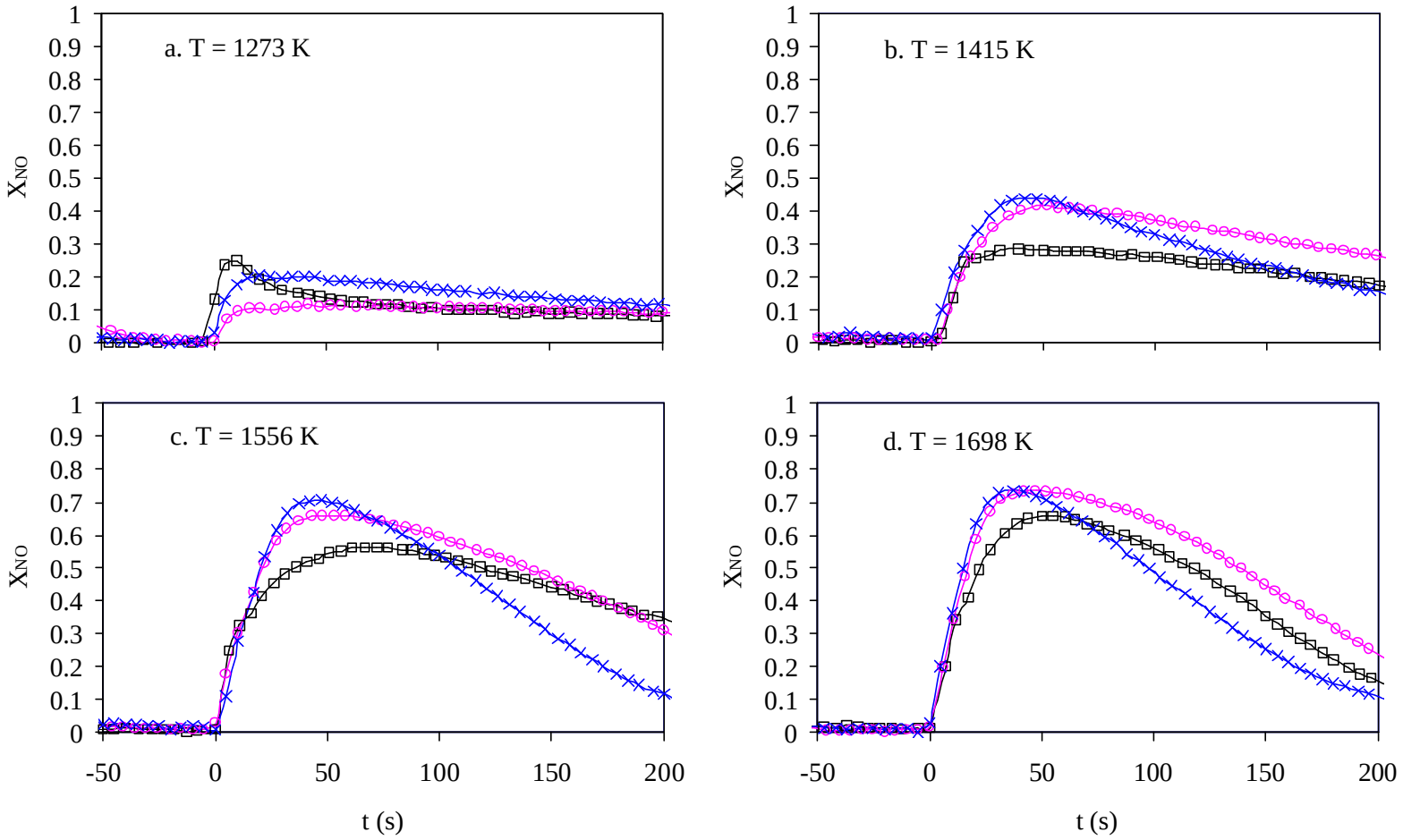

Figure 2.16. NO reduction after injection of carbonaceous materials into the drop tube. Solids are injected at time 0 into a 650 ppm NO/He stream. a. T = 1273 K, b. T = 1415 K, c. T = 1556 K,

d. T = 1698 K Sample size = 5 mg. ? Coal, ? U-Furnace char, × Activated carbon

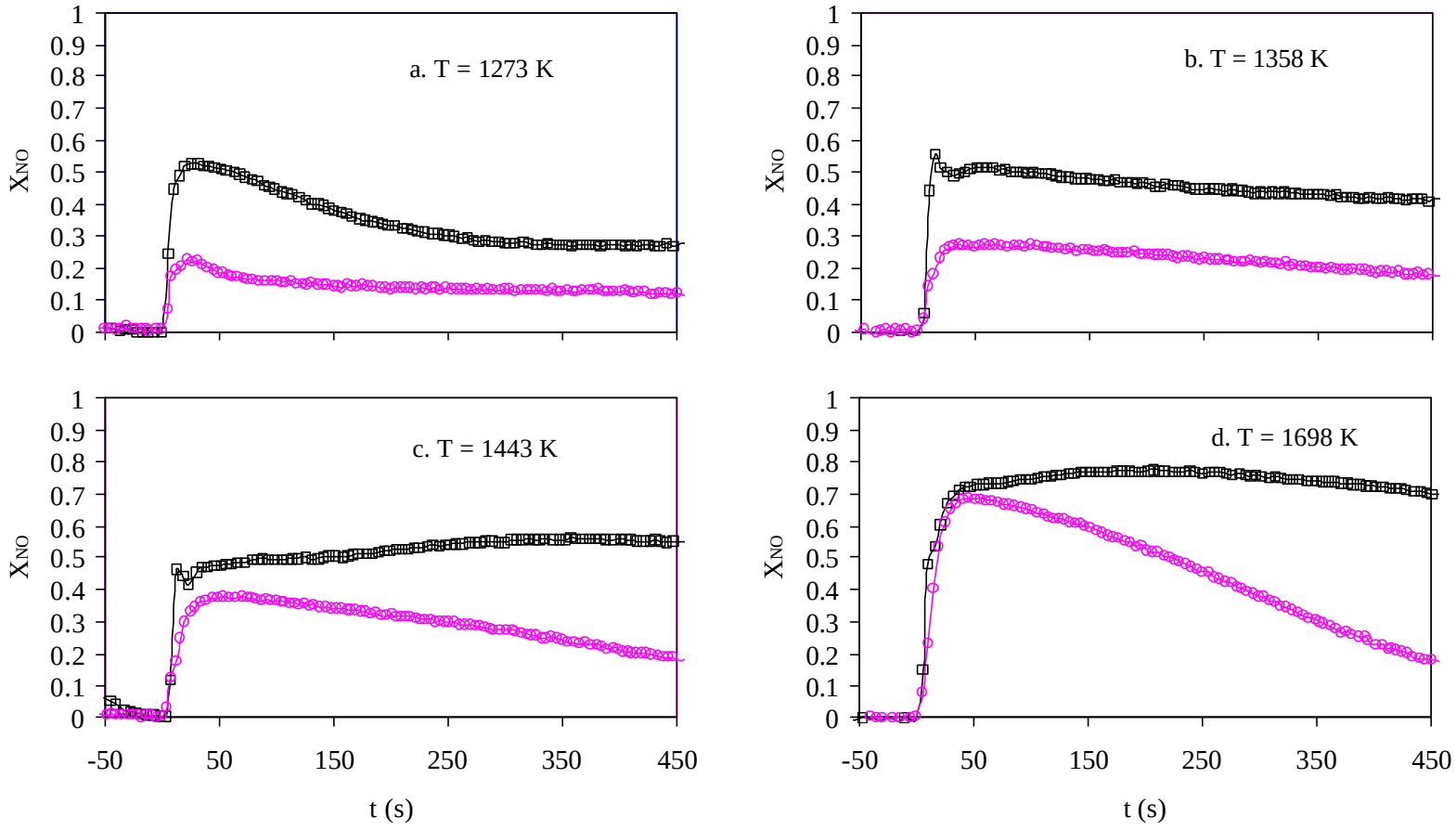

Figure 2.17. NO reduction after injection of carbonaceous materials into the drop tube. Solids are injected at time 0. a. T = 1273 K, b. T = 1353 K, c. T = 1443 K, d. T = 1698 K? Coal (15 mg), ? U-Furnace char (5 mg)

similar experiments when coal and U-Furnace char are injected into the reactor with a 250 ppm NO/He composition and for which the sample size for coal was 15 mg and for char 5 mg. At 1273 K, the steep increase in the conversion of nitric oxide just after coal injection is evident. A broader peak that extends from 20 to 250 seconds follows the first peak (15 – 20 s). After 250 seconds the conversion of nitric oxide stabilizes. For U-Furnace char at this same temperature, only the second broad peak is observable, although it only expands to 150 seconds approximately. For coal at 1353 K both peaks occur, although the second peak is not so evident. At 1443 K only the first peak is observed. These peaks occur in the first 20 seconds. At 1698 K no peak is observed, as it was the case in Figure 2.14 d.

It is also important to notice in Figure 2.17 that the difference in nitric oxide conversion between char and coal reduces as the temperature increases. The reason for this is that the amount of coal devolatilized increases with temperature (Kobayashi et al., 1976), and the difference between the masses of solid that reacts with nitric oxide decreases as temperature increases. It would be desirable to normalize the results by the mass of char actually reacting, but the numerous species released during devolatilization (Appengix G) prevent a good evaluation of the mass of carbon released by exclusive determination of the gaseous phase concentration. The use of proximate analysis of chars produced in the continuous injection mode at the temperatures of interest does not represent the actual mass of char in the reactor either since there is a considerable difference in residence times. In the next section, an alternative evaluation of the mass present in the reaction is used to determine the actual mass of carbonaceous material reacting with nitric oxide in order to estimate the rate of nitric oxide reduction on the char surface.

The last important observation in Figure 2.15 is that the results at 1698 K show that mass transfer limits the reaction of NO reduction for the coal in the first 400 seconds. The reduction of nitric oxide when coal is injected coincides with that of U-Furnace char in the first seconds after injection. Then the one of coal slightly increases, while the one of U-Furnace char decreases constantly. The one of coal finally decreases after 450 seconds.

The trend in X_{NO} with time for U-Furnace char corresponds to the decrease in the amount of char (and hence the rate of NO reduction) and it is a different mechanism from that leading to the decline of X_{NO} at 1273 K. The mass of char for the coal remaining after 450 seconds of reaction is more than twice that of the one of the U-Furnace char and this is the reason why the decrease in the nitric oxide reduction for the U-Furnace char is sharper. However, the two peaks coincide just after injection since mass transfer limits the reaction.

The following observations summarize the results in Figure 2.10 to Figure 2.15 and the spectra in Molina (2002, Appendix F):

1. Just after the injection of solids into the reactor there is a steep increase on the reduction on nitric oxide. This steep increase is only noticeable at the lower temperatures (T < 1450 K) (Figure 2.14 a. and Figure 2.15 a., b. and c) and coincides with volatiles evolution. It is observed only when coal is injected in the reactor, it does not occur when U-Furnace char or activated carbon are injected.

2. Following this peak, there is another one that expands beyond volatiles evolution. This peak is broader and only occurs at lower temperatures (Figure 2.14 a. and Figure 2.15 a. and b.) It is more pronounced at lower NO concentrations. It occurs for coal and to a lower extension for U-Furnace char.

3. After the occurrence of these two peaks, the extent of nitric oxide reduction constantly decreases with time, due to the reduction in char loading as a result of char oxidation by nitric oxide.

These observations and the analysis above suggest three different phenomena occurring during the process of nitric oxide reduction on chars produced in situ.

The first process corresponds to homogeneous reduction of nitric oxide by the volatiles produced just after the solids are injected in the reactor. The fact that this process occurs only when coal is the injected solid supports this conclusion. The evidence

found in Appendix F of Molina (2002), that at higher temperatures most of these volatiles species are oxidized to CO_2, explains why this peak is only present at low temperatures.

The second process corresponds to adsorption of nitrogen oxide complexes on the char surface. As described in the introduction, other groups (Illán-Gómez et al., 1995c, Aarna and Suuberg, 1998, Guo and Hecker, 1998, Yamashita et al., 1993) also observed this phenomenon. This process is characteristic of the nitric oxide – char reaction at low temperatures and has a first order dependence on the nitric oxide partial pressure (Aarna and Suuberg, 1998). The data in Figure 2.14 and Figure 2.15 shows that the appearance of the second broad peak only occurs at low temperatures, and it is more evident at low nitric oxide pressure. Also in Figure 2.14 a. and Figure 2.15 a. it is evident that after this process occurs, the rate of NO reduction on the char surface resumes at pseudo-steady state conditions.

The final process is the reaction of nitric oxide on the char surface. This occurs once the char surface has reached equilibrium between adsorption of nitric oxide to form nitrogen complexes on the char C(N) (R 2.1) and the reaction of these complexes with incoming NO to form N_2 (R 2.3). At high temperatures R 2.3 occurs at high enough rates that there is no nitrogen accumulation through R 2.1.

The decrease in the extent of the reduction of nitric oxide once the third process begins is only due to the reduction in the char mass available for NO reduction and is not a consequence of char deactivation. The decrease in the nitric oxide reduction that occurs after the end of the second process (Figure 2.15 a.) does not occur due to char deactivation but due to an activation of reaction R 2.3 as the char surface is covered with C(N) complexes. At higher temperatures, this process does not occur.

The next section presents a discussion on the actual effect that the first two processes can have on the evaluation of the rate of nitric oxide on the char surface.

2.4.2 Evaluation of the Rate of Nitric Oxide Reduction on the Char Surface

The previous section showed that for the experiments in this study, nitric oxide reduction on the char surface occurred through three different processes. The detection of these three phenomena is important in the understanding on the mechanism of nitric oxide reduction on the char surface. However, from the point of view of how much nitrogen oxides are actually produced during char combustion, it is more important to evaluate to what magnitude these phenomena contribute to the reduction of nitric oxide.

The first phenomenon is nitric oxide reduction by the volatiles produced after injection of the solids into the reactor. The influence of this process on the prediction of the conversion of char nitrogen to nitric oxide depends on the capacity to predict the amount and composition of the volatiles released and the reactions occurring in the gaseous phase. It is not the objective of this study to explore these two fields; detailed studies are available in the literature (Miller and Bowman, 1989, Glarborg et al., 1998, Perry et al., 2000Nevertheless, it is important to recognize that reaction of volatiles with nitric oxide can have an effect on the conversion of char nitrogen to nitric oxide under specific oxygen concentration and temperature.

The second process corresponds to an accumulation of the nitrogen on the char, possibly by the formation of C(N) complexes. The results in this study, as well as in others (Aarna and Suuberg, 1998, Guo and Hecker, 1998) suggest that this process is important at temperatures below 1300 K, in the range of fluidized bed combustion, but it may not be dominant at higher temperatures.

This process is more evident in chars produced just after devolatilization; its importance in reactions of NO with activated carbons and on chars produced under different conditions is almost negligible. One hypothesis to explain this behavior is that after coal devolatilization there is a population of sites that can form C(N) complexes. Not all these sites are active after devolatilization. Some of them need further exposure to high temperatures to react with NO to form C(N) complexes. Chars prepared before injection may have a smaller population of these sites, and therefore the formation of

C(N) complexes (R 2.1) and its reaction with nitric oxide to form N_2 is in equilibrium (R 2.3).

Although it is important to understand the mechanism of this process, it is also important to evaluate its magnitude. Even though it is complicated to determine reaction rates from the data in Figure 2.10 to Figure 2.15 since the evaluation of the mass of solid available for reaction at every time is difficult, it is possible to compare the relative reduction of nitric oxide by this phenomenon as compared to the reaction once pseudo-steady state is obtained.

Molina (2002, Appendix G) presents a description of the derivation of the expression for the rate of nitric oxide reduction on the char surface E 2.6.

$$K_{NO} = \frac{\nu}{W} \ln\left(\frac{[NO]_{in}}{[NO]_{out}}\right) \qquad \text{E 2.6}$$

If E 2.6 is applied to the process in Figure 2.10 when the process of formation of C(N) complexes is occurring (~10 s) and when the reaction is occurring at pseudo-steady state (~ 150 s) it is possible to obtain an approximation of the relative contribution of the process of C(N) formation on the reduction of nitric oxide on the char surface (E 2.7).

$$\frac{K_{NO}^{I}}{K_{NO}^{II}} = \frac{\frac{\nu^{I}}{W^{I}} \ln\left(\frac{[NO]_{in}}{[NO]_{out}^{I}}\right)}{\frac{\nu^{II}}{W^{II}} \ln\left(\frac{[NO]_{in}}{[NO]_{out}^{II}}\right)} = \frac{W^{II}}{W^{I}} \frac{\ln\left(\frac{[NO]_{in}}{[NO]_{out}^{I}}\right)}{\ln\left(\frac{[NO]_{in}}{[NO]_{out}^{II}}\right)} \qquad \text{E 2.7}$$

In E 2.7, superscript I represents the process of C(N) formation and superscript II the process when pseudo-steady state is obtained. E 2.7 recognizes that $\nu^{I} = \nu^{II}$. Since the values for nitric oxide concentrations are known, the only unknown is the ration between the mass of char at both times W^{II}/W^{I}. Since the reaction is more advanced at time II, W^{II}/W^{I} is always < 1. Therefore $W^{II}/W^{I} = 1$ in E 2.7 represents a maximum for K^{I}_{NO}/K^{II}_{NO}.

When the data in Figure 2.10 are applied to E 2.7, with $W^{II}/W^{I} = 1$, $K^{I}_{NO}/K^{II}_{NO} = 2.6$. For the data in Figure 2.15 d. $K^{I}_{NO}/K^{II}_{NO} = 2.7$. This implies that the process of C(N) formation produces an increase of the order of at most 2 to 3 times the rate at pseudo-steady state conditions. This number holds for the conditions of these experiments performed under inert atmosphere. When oxygen is present in the system, the population of active sites will be completely different and it is difficult to predict what the magnitude of this process on the rate of nitric oxide reduction will be.

To evaluate the rate for the third process, when char reacts with nitric oxide in pseudo-steady state, the experiment in Figure 2.10 was interrupted during the part when the slope of nitric oxide reduction was linear by injection of oxygen. Figure 2.16 presents the carbon dioxide evolution after oxygen injection to the system in Figure 2.10.

It is possible from CO_2 concentration to evaluate the total carbon mass in the reactor and through E 2.6 determine the rate of nitric oxide reduction on the char. Table 2.4 summarizes the results of this calculation for the three solids and compares this values to the one predicted by the correlations by Aarna and Suuberg (1997) and Jensen et al. (2000) (see Appendix E of Molina, 2002 for details of comparisons).

The experimental results show that the rates of nitric oxide reduction by the coal and the U-Furnace char are almost identical. This is in agreement with the fact that the CO_2 profiles for both solids as reported in Figure 2.16 are the same; therefore the mass inside the reactor is similar. At the same time the nitric oxide concentration for both solids is

also the same (Figure 2.10) therefore both rates should be equal. The rate for activated carbon is higher, since the mass is lower (Figure 2.16) but the nitric oxide concentration is a little bit lower than for coal and U-Furnace char. Since the surface area available for reaction in the activated carbon is one order of magnitude higher than the one for the char (see section 2.3.4.3) the higher reduction rate is not an unexpected result. Nevertheless, the difference between surface rates is not proportional to surface area, suggesting that not all the area is active for the reduction of nitric oxide.

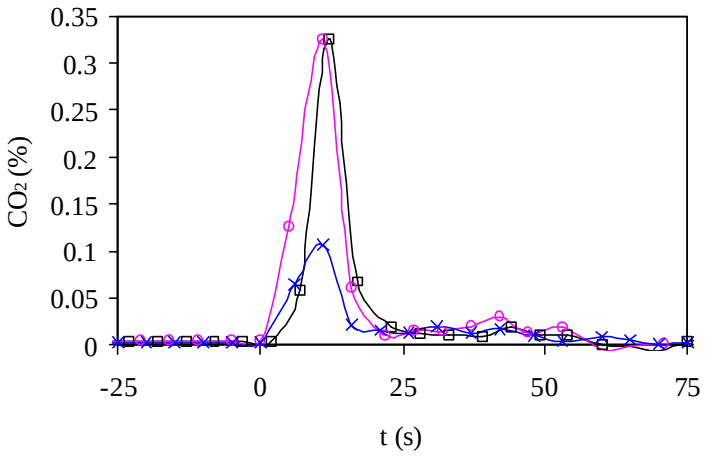

Figure 2.18. CO_2 evolution after the injection of oxygen to the drop tube when the solids where reacting with nitric oxide. T = 1273 K.? Coal, ? U-Furnace char, × Activated carbon

Table 2.4. Comparison of kinetic constants for the reaction of nitric oxide with char. Results from experiments and from two different values reportedin the literature

	K_{NO} (mol NO m^{-3} s^{-1})		
Solid	Present Study	Aarna and Suuberg (1997)	Jensen et al. (2000)
Coal	16.0	8.6	226.2
U-Furnace char	15.7	8.6	226.2
Activated Carbon	31.2	119.6	226.2

The comparison with the values reported by Aarna and Suuberg (1997) and Jensen et al. (2000) show that the expression by Aarna and Suuberg (1997) predicts kinetic reaction rates that differ by less than one order of magnitude from the results of the present study. The prediction for the coal and U-Furnace char are the same, since in the calculation it was assumed that both had similar surface areas. The predictions for the activated carbon are higher in a proportion to the difference in surface areas.

The expression for the kinetic reported by Jensen et al. (2000) over-predicts the experimental results by more than one order of magnitude. This expression does not predict any difference between the reactivity of coal, U-Furnace char or activated carbon since it does not consider the surface area available for reaction. The over-prediction on the experimental results can be related to the different coal used in the experiments by Jensen et al (2000) and to the fact that the rate expression reported by these authors was not normalized by char surface area, which makes it difficult to extend their results to different solids.

2.4.3 Summary

This section presented an evaluation of the rate of nitric oxide reduction on the char surface. In particularly, it addressed the claim that the rate for the destruction of nitric

oxide on the char surface has been under-predicted due to char deactivation in the process of char formation.

Experiments conducted with chars produced in situ, char previously produced at pulverized combustion conditions and with an activated carbon showed the existence of three phenomena during the reduction of nitric oxide. The first one represented the homogeneous reaction of the volatiles that evolved after the injection of the solid into the reaction with nitric oxide. The second one was related to the accumulation of nitric oxide on the char surface probably through the formation of C(N) complexes. The third one is the heterogeneous reaction of nitric oxide with char.

The results showed that at pulverized combustion conditions ($T > 1500$ K) the dominant process is the third one. The rate for nitric oxide reduction for this process was within one order of magnitude to the value predicted by the expression recommended by Aarna and Suuberg (1997).

At fluidized bed conditions ($T < 1300$ K) the second phenomenon may be important and the rate expressions such as those of Aarna and Suuberg (1997) may under-predict the nitric oxide conversion to N_2 when used at combustion conditions when the nitric oxide – char reactions begin immediately after char formation, before a pseudo-steady state is reached. For the solid used in this study, the increase in nitric oxide reduction due to formation of C(N) sites was a factor of 2 to 3.

2.5 CONVERSION OF FUEL NITROGEN TO NITRIC OXIDE AT PULVERIZED COMBUSTION CONDITIONS - EXPERIMENTAL RESULTS

2.5.1 Introduction

Section 2.4 suggested that by the use of one equation (E 2.2) that related the rates of NO production and destruction it was possible to evaluate in a simplified manner the relative conversion of char-nitrogen to nitric oxide during char combustion.

Section 2.4 also showed that the expression by Aarna and Suuberg (1997) for the reduction of nitric oxide on the char surface predicted the experimental results in this study within one order of magnitude. Given an expression for the rate of char oxidation and assuming that the formation of nitric oxide to be proportional to that of char oxidation it seems possible to use E 2.2 to evaluate the char-nitrogen conversion to NO.

However, there is still debate on the kinetic expressions for the rates of char oxidation (Shaddix, 2001, Hurt and Calo, 2001) and the conversion of char nitrogen to nitric oxide strongly depends on this value (Molina et al., 2000). Furthermore, the time scales for the reaction of nitric oxide formation and destruction are different. While the formation of nitric oxide occurs in the reaction front where char is oxidized, the nitric oxide formed in this front can diffuse inside the particle and react with the char to form N_2. E 2.2 does not describe this complex process. To obtain a better description, it is necessary to use experiments and more complex models.

This section presents the results of experiments designed to provide insight on the conversion of char nitrogen to nitric oxide at pulverized combustion conditions. The discussion of the models for the conversion of char-nitrogen to nitric oxide is deferred to the next section.

2.5.2 Variation of the Conversion of Fuel Nitrogen to Nitric Oxide with Background Nitric Oxide Concentration

The results in this section correspond to the experiments described in Section 2.3.3.2.2 in which a solid (either coal, U-Furnace char or activated carbon) is injected into the reactor at a 1698 K and 4% O_2/He. The nitric oxide concentration is varied between experiments.

As it was explained section 2.3 and Appendix C of Molina (2002), in these experiments an event that occurs in the order of a hundred milliseconds, appears as a wide peak of approximately 50 seconds due to the residence time distribution in the reactor and gas analysis system. Jensen et al. (2000) have shown the importance that the total mass concentration inside the reactor has on the conversion of char-nitrogen to nitric oxide. In particular, that the higher the sample size, the lower the conversion of char-nitrogen to nitric oxide, until an asymptote is reached at approximately 20 mg for the experiments of Jensen et al. (2000).

Therefore, extreme care was taken to ensure an adequate carbon mass balance and a constant sample size during the experiments. The first one guaranteed that despite the broad residence time distribution the complete process of char combustion was detected in the FTIR. Since N_2 was not measured, closure of the nitrogen balance was not possible. The constant sample size was important to avoid any effect on the sample size on the conversion of char-nitrogen to nitrogen oxides.

Table 2.5 presents the variation of the sample size, fixed carbon, carbon balance and the relative amount of CO_2 in the carbon balance $\left(\alpha_{CO_2}\right)$. The fixed carbon was computed as the sample size times the fixed carbon as reported from the proximate analysis for coal; or the sample size minus the amount of ash for the U-furnace char and the activated carbon. This number represents the amount of char actually injected in the reactor. Since the proximate analysis is performed at temperatures lower than the one used in this study, the actual mass of coal injected as char will be lower than the one presented in Table 2.5.

At the same time, some volatiles will be released due to secondary devolatilization reactions occurring in the U-Furnace char and activated carbon. Thus fur these two solids the mass injected as char may be lower than the one presented in Table 2.5. Nevertheless, the data in Table 2.5 suggests that the actual mass of char injected when U-Furnace char and activated carbon are injected into the reactor is higher than when coal is the fuel.

Table 2.5. Variation of the Sample Size, fixed Carbon, C balance and carbon conversion to CO_2 with background NO concentration. O_2 = 4%, 63 – 53 µm

Background NO (ppm)	Sample Size (mg)			Fixed Carbon (mg)		
	Coal	U-Furnace char	Activated Carbon	Coal	U-Furnace char	Activated Carbon
0	5.3	5.4	4.2	2.2	4.4	4.0
214	5.5	4.4	4.8	2.3	3.6	4.5
440	4.8	4.5	4.3	2.0	3.7	4.1
640	4.1	4.6	4.1	1.7	3.8	3.9
722	4.0	4.7	5.0	1.6	3.9	4.7
	C balance (%)			α_{CO_2}		
0	113.7	110.0	102.3	0.99	0.99	1.00
214	111.0	101.8	78.1	0.99	0.99	0.98
440	99.0	90.8	79.4	0.99	0.99	0.99
640	115.2	81.9	88.0	1.00	0.99	1.00
722	99.3	101.3	88.0	0.99	0.99	0.99

It was difficult to prepare such small size of perfectly constant weight, therefore the sample size varied between 4.0 and 5.5 mg (average = 4.6). However, there is not any specific trend on the sample size, carbon balance or conversion of carbon to CO_2 with the

variation of background nitric oxide or with the fuels. This suggests that any difference that results in the conversion of fuel-nitrogen to nitrogen oxides during fuel oxidation should be related to the variation in the nitric oxide background concentration and not on the mass of solid injected into the system.

Figure 2.17 to Figure 2.19 present the nitric oxide vs. time profiles that correspond to the results in Table 2.5. The figures show a transition from net nitric oxide production (at 0 ppm NO) to net nitric oxide reduction (at ~ 730 ppm NO). While the solids produced nitric oxide when there is no nitric oxide present in the background gas, their injection caused nitric oxide reduction when the nitric oxide concentration is high.

The effect is very similar for U-Furnace char (Figure 2.17) and coal (Figure 2.18). These two solids produce a peak of approximately 90 ppm nitric oxide after injection into a 4%O_2/He gas. The net emission of nitric oxide decreases as the background concentration increases and it becomes zero at ~ 400 ppm NO. With further increase in the background nitric oxide concentration, there is reduction in the nitric oxide concentration after solid injection. The maximum reduction of nitric oxide reached approximately 30 ppm for a background nitric oxide concentration of 725 ppm.

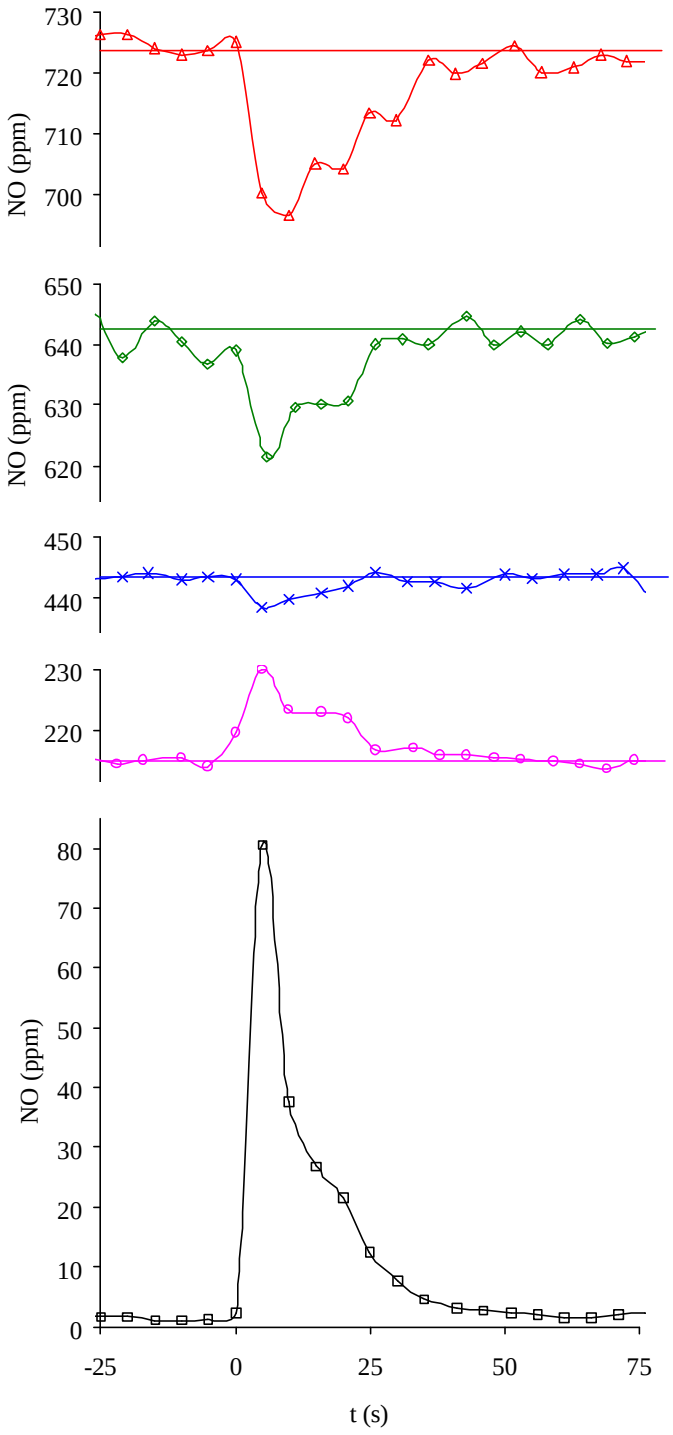

Figure 2.19 Profiles of nitric oxide vs. time. U-Furnace char injection at t = 0. NOconcentration in the background as parameter: ? 0 ppm; ? 217 ppm; × 445 ppm;? 643 ppm; ? 724 ppm O_2 = 4% / He, Tg = 1698 K, 63 – 53 µm

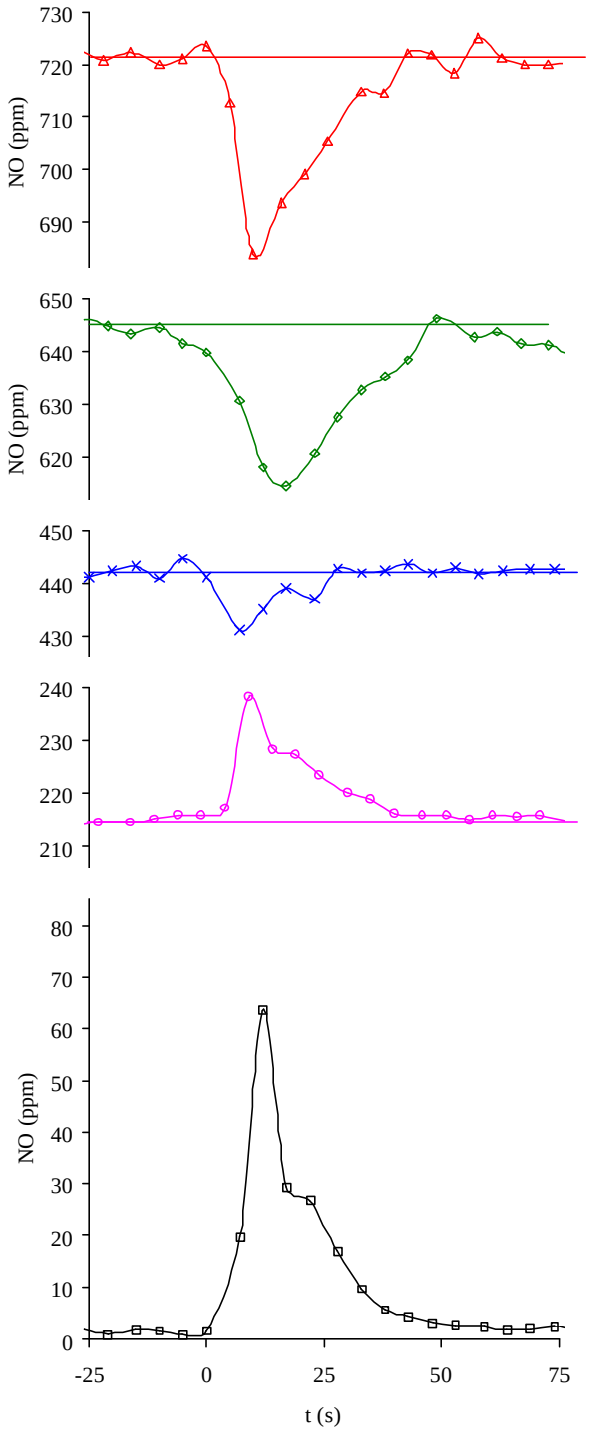

Figure 2.20. Profiles of nitric oxide vs. time. Coal injection at t = 0. NO concentrationin the background as parameter: ? 0 ppm; ? 217 ppm; × 445 ppm; ? 643 ppm; ? 722 ppm O_2 = 4% / He, Tg = 1698 K, 63 – 53 µm

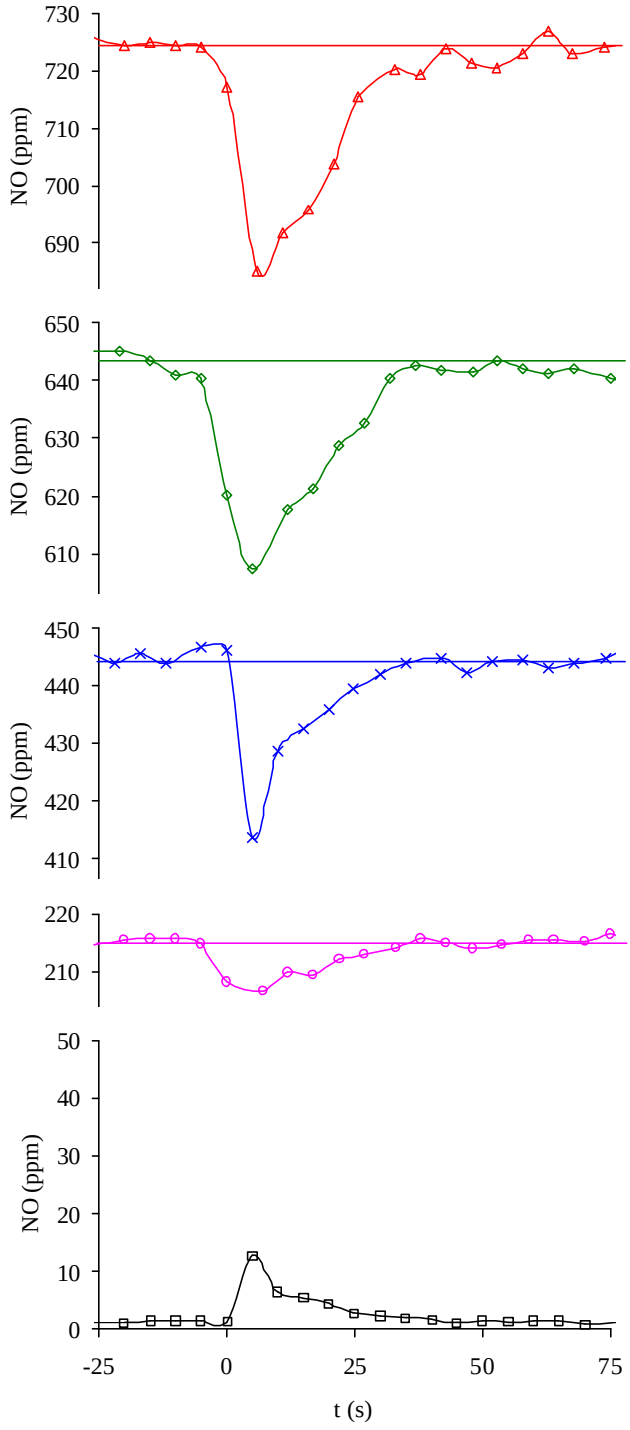

Figure 2.21. Profiles of nitric oxide vs. time. Activated carbon injection at t = 0. NO concentration in the background as parameter: ? 0 ppm; ? 217 ppm; × 445 ppm; ? 642 ppm; ? 726 ppm O_2 = 4% / He, Tg = 1698 K, 63 – 53 µm

For activated carbon (Figure 2.19) the production of nitric oxide is lower than for the other two solids. This is consistent with its lower nitrogen content (see Table 2.3). As in the cases of injection of coal and U-Furnace char a net reduction in the nitric oxide emissions occurs at high concentrations of background NO. However, the effect for activated carbon is more pronounced that for the other two solids. While a concentration of more than 400 ppm is necessary to begin nitric oxide reduction for the coal and the U-Furnace char, only 200 ppm is necessary when activated carbon is injected into the reactor.

Spinti (1997) observed the same phenomenon of reduction of char nitrogen conversion to nitric oxide as the background NO concentration is increased. Visona and Stanmore (1996), Coda et al. (1998) and Sarofim et al. (1999) have predicted the same effect from single particle calculations. Despite these studies, the exact mechanism by which this phenomenon occurs is not completely clear (Spinti, 1997). Therefore, the evaluation of this phenomenon at different conditions (oxygen concentration and particle size) can give additional insight on the conversion of char-nitrogen to nitrogen oxides.

The next two sections present the effect of an increase in the oxygen concentration and a variation in the particle size on the variation on the nitric oxide evolution with changes in background nitric oxide concentration. This section solely describes the experimental results. Their interpretation and explanation is deferred to the next section.

2.5.2.1 Effect of oxygen concentration

Experiments similar to the ones described before were carried out with an oxygen concentration of 20% instead of 4%. The sample size, carbon balance and conversion to CO_2 presented similar characteristics as described for the experiments at 4% O_2 (see Table 2.6). The main difference was the higher conversion of char to CO_2. As experienced at the lower oxygen concentration, no specific trend was observed in the profile for the concentration of carbon-containing species as the background nitric oxide concentration was varied.

Figure 2.20 to Figure 2.22 present the nitric oxide concentration profiles for the case when the oxygen concentration inside the reactor was 20%. Although experiments were conducted at five nitric oxide concentrations as in the experiments at 4% O_2, only three concentrations are presented here (additional data are given in Appendix H of Molina, 2002).

As occurred at 4% O_2, results for U-Furnace char (Figure 2.20) and coal (Figure 2.21) are very similar. There is a net production of nitric oxide when the background nitric oxide concentration is zero, and this net production decreases as the nitric oxide background concentration increases. The decrease in net production of nitric oxide with increases in background nitric oxide concentration is less pronounced at 20% oxygen than at 4% oxygen. For instance at a background concentration of 740 ppm, at 4% oxygen concentration there is actually a net reduction in the nitric oxide concentration, whereas at 20% there is almost no variation in nitric oxide concentration after the injection of the solid.

Table 2.6. Variation of the sample size, fixed Carbon, C balance and carbon conversion to CO_2 with background NO concentration. O_2 = 20%, 63 – 53 µm

Background NO (ppm)	Sample Size (mg)			Fixed Carbon (mg)		
	Coal	U-Furnace char	Activated Carbon	Coal	U-Furnace char	Activated Carbon
0	4.1	3.9	4.3	1.7	3.2	4.1
214	4.7	5.3	5.5	1.9	4.4	5.2
440	4.6	4.3	4.3	1.9	3.5	4.1
640	4.8	4.1	3.8	2.0	3.4	3.6
722	4.2	4.0	4.4	1.7	3.3	4.2
	C balance (%)			α_{CO_2}		
0	101.0	93.4	86.8	1.00	1.00	1.00
214	99.5	96.5	92.3	1.00	1.00	1.00
440	103.1	97.5	90.4	1.00	1.00	1.00
640	97.5	89.6	93.6	1.00	1.00	1.00
722	91.2	93.9	90.9	1.00	1.00	1.00

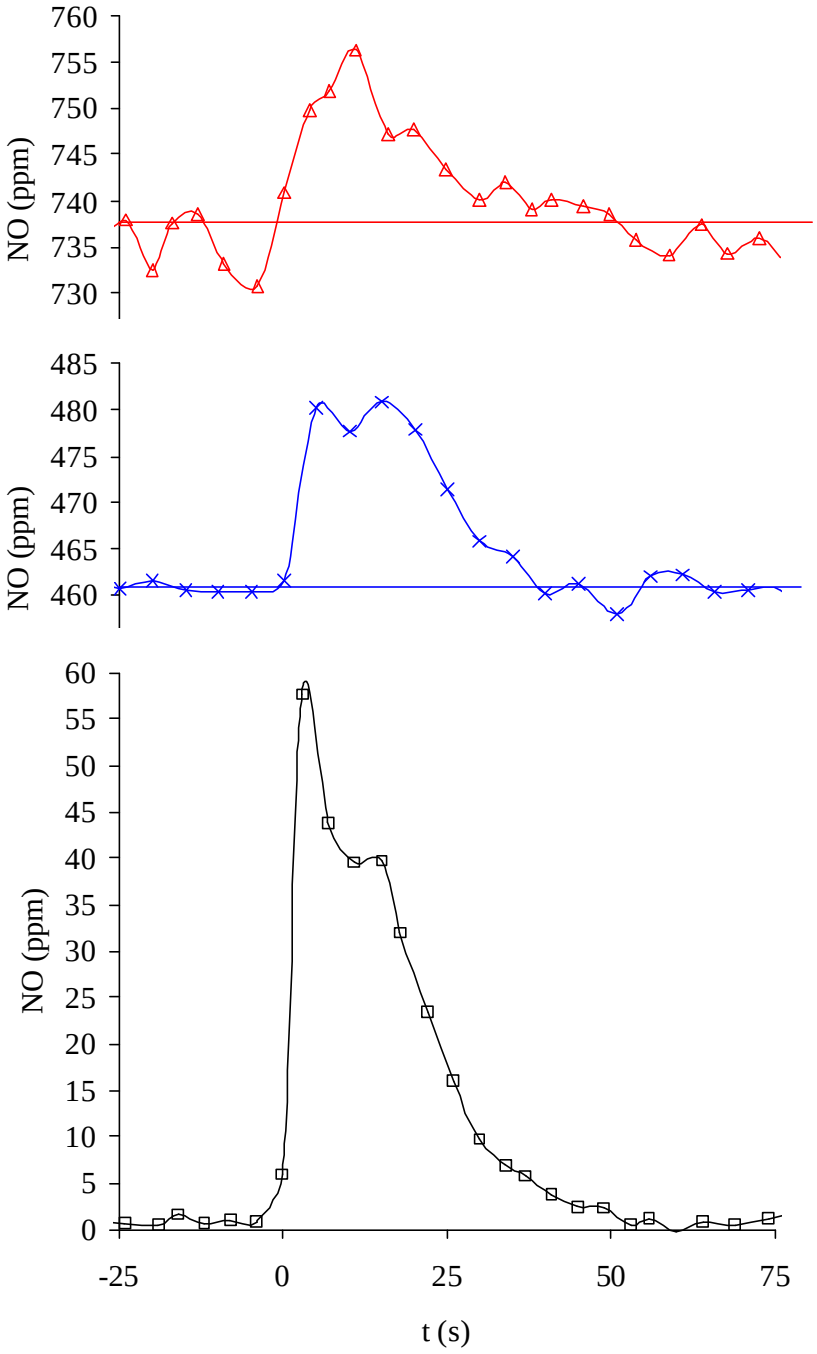

Figure 2.22 Profiles of nitric oxide vs. time. U-Furnace char injection at t = 0. NO concentration in the background as parameter: ? 0 ppm; × 460 ppm; ? 736 ppm O_2 = 20% / He, Tg = 1698 K, 63 – 53 µm

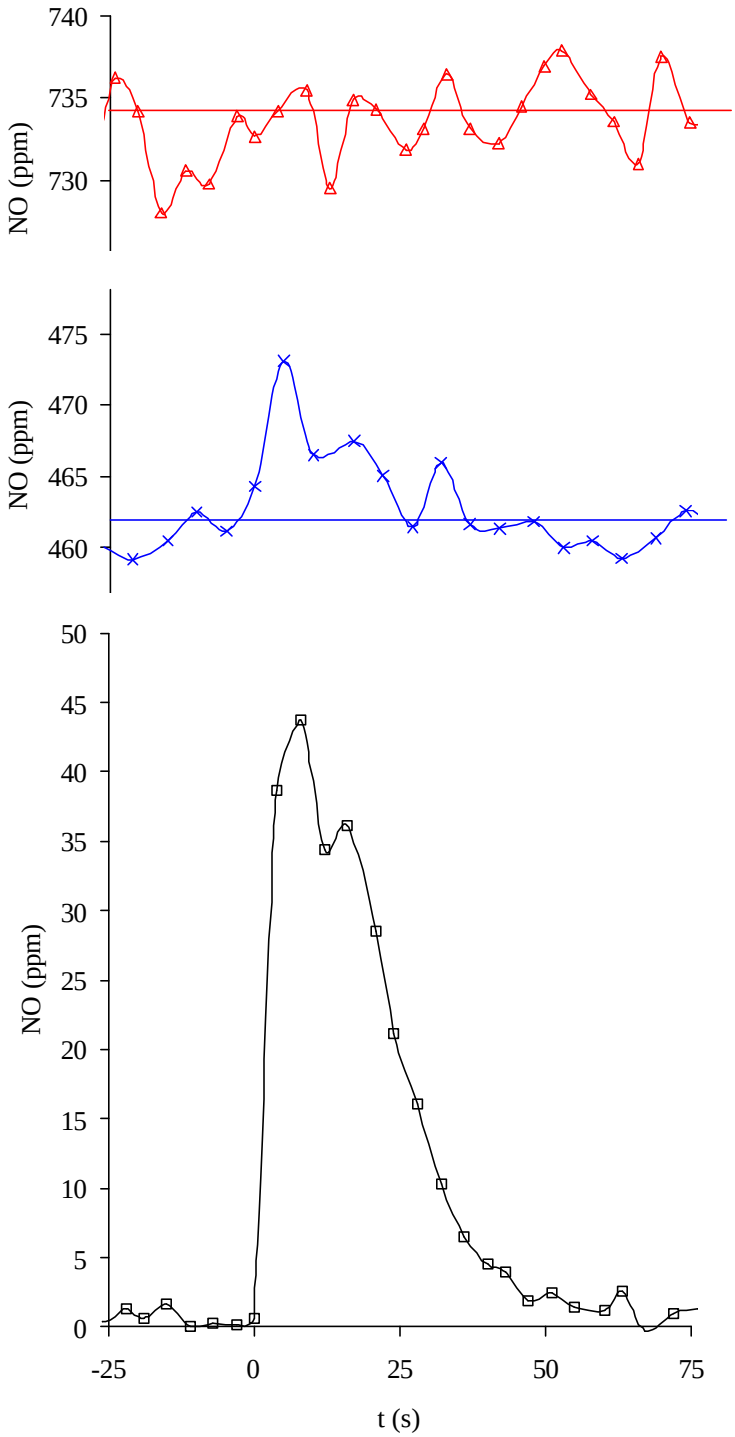

Figure 2.23 Profiles of nitric oxide vs. time. Coal injection at t = 0. NOconcentration in the background as parameter: ? 0 ppm; × 462 ppm; ? 736 ppm O_2 = 20% / He, Tg = 1698 K, 63 – 53 µm

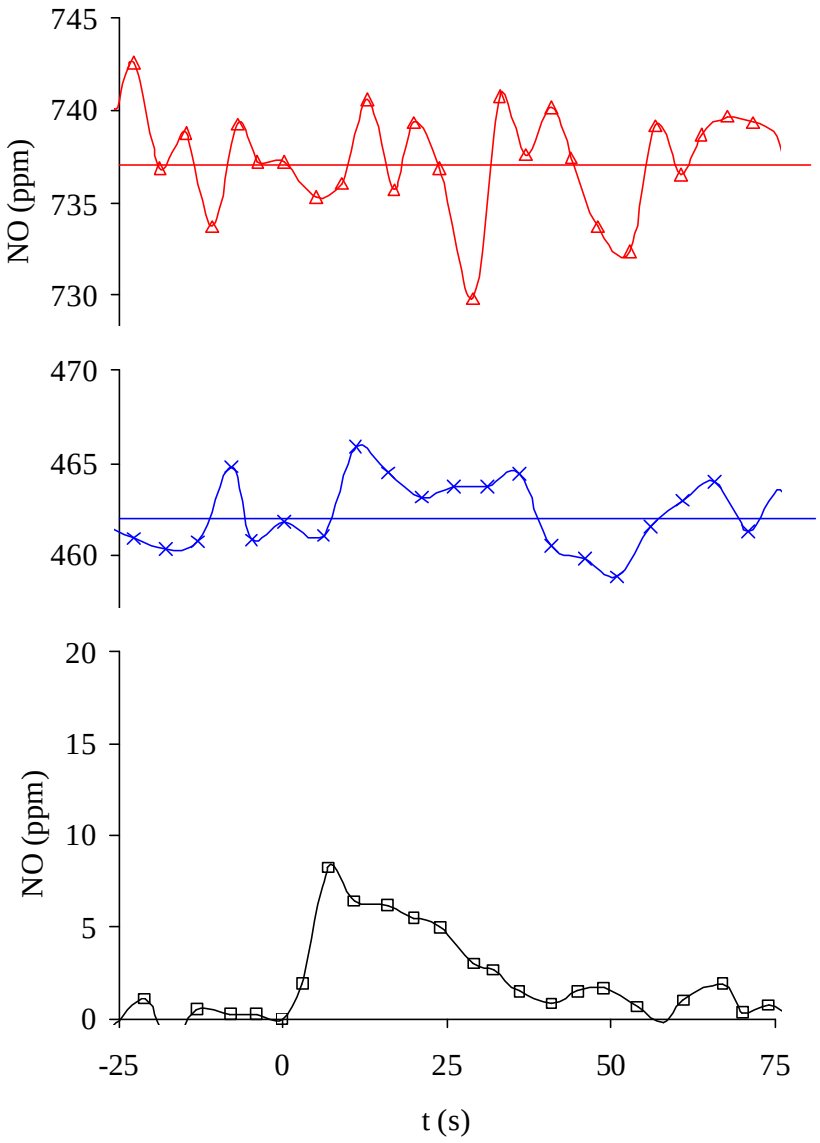

Figure 2.24 Profiles of nitric oxide vs. time. Activated carbon injection at t = 0. NO concentration in the background as parameter: ? 0 ppm; × 462 ppm; ? 736 ppm O_2 = 20% / He, Tg = 1698 K, 63 – 53 µm

For activated carbon (Figure 2.22) the reduction in nitric oxide production with an increase in the background nitric oxide concentration is more pronounced than those for the other two solids. Nevertheless, the effect is considerably less pronounced than that at 4% O_2 concentration.

It is conventional to present the net NO production at different NO background concentrations as a ratio to the amount of nitrogen present in the injected solid. For this purpose α_{NO} was defined as the cumulative conversion of nitrogen in the solid to nitric oxide.

$$\alpha_{NO} = \frac{\int_{t_1}^{t_2} \nu C_{NO} dt}{(N/C)_{solid} \int_{t_1}^{t_2} \nu (C_{CO} + C_{CO_2}) dt} \qquad \text{E 2.8}$$

Where: $t_2 - t_1$ is the experiment interval (sec); C_i the concentration of species i (mol/m^3); ν the volumetric flow (m^3/sec) and $(N/C)_{solid}$ the atomic ratio of nitrogen to carbon in the solid obtained from the elemental analysis.

Figure 2.23 presents the variation of α_{NO} with background nitric oxide concentration for the three solids and the two different oxygen concentrations. Each point in Figure 2.23 is obtained after integration of the CO_2, CO and NO vs. t profiles.

Figure 2.23 shows that α_{NO} decreases as the nitric oxide concentration increases. This reduction is very similar for coal and U-Furnace char, but it is different for activated carbon. It is more pronounce at 4% O_2 and it less steep at 20% O_2, in particular for activated carbon.

2.5.2.2 Effect of particle size

Figure 2.24 presents the results of the experiments for which two different particle sizes, 108 – 88 μm and < 37 μm were used. The results are presented as the variation of α_{NO} with background nitric oxide concentration. The figure also includes the curve for particles in the size range 63 – 53 μm that has already been presented in previous sections.

For the three solids and for the three particle-size fractions, the results are very similar. In fact, it is not possible to find a specific trend in the variation of α_{NO} with particle size.

The results in Figure 2.24 should be understood as if the experimental setup used in these experiments was not capable to determine any trend in the conversion of fuel nitrogen to nitric oxide for different particle size fractions. Figure 2.24 does not imply that a trend does not exist, but that it is not intense enough to be detected by the present experiments.

Detailed profiles of NO vs. time (similar to Figure 2.17 to Figure 2.22) and the results of the carbon mass balance (equivalent to Table 2.5 and Table 2.6) can be found in Appendix H of Molina (2002).

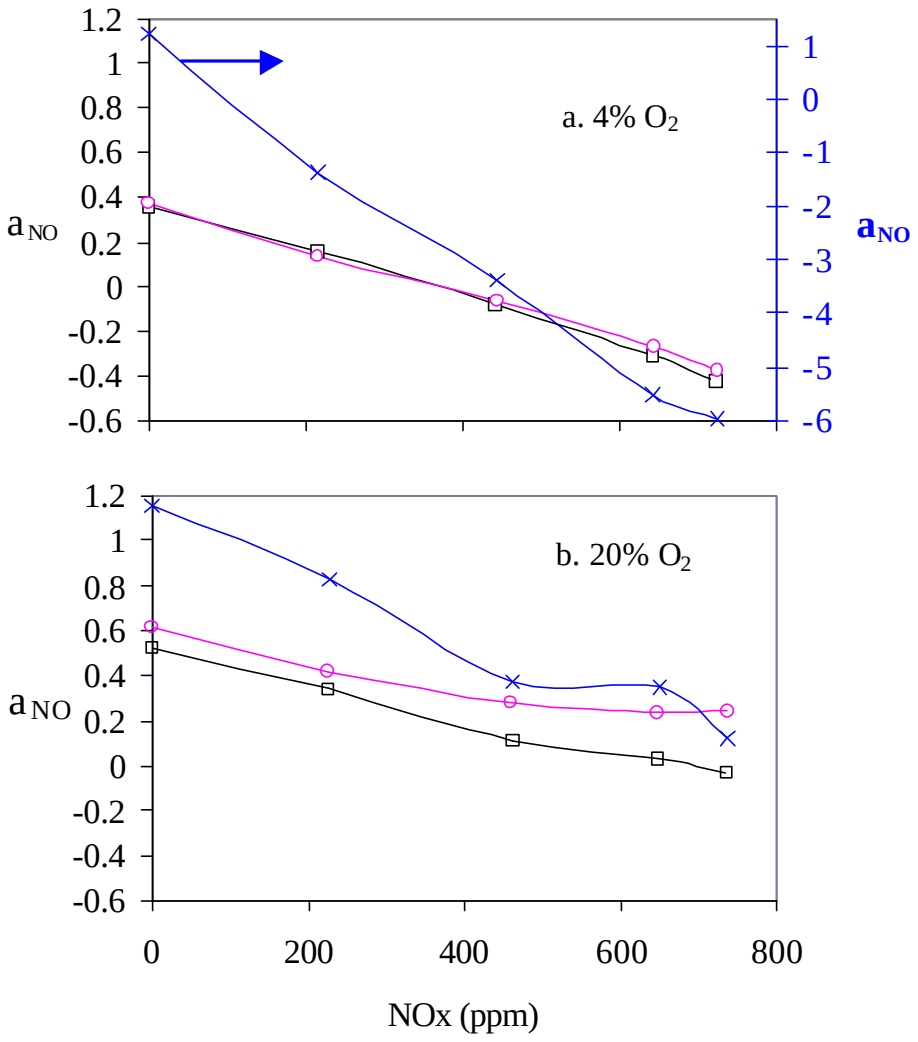

Figure 2.25. Variation of the conversion of char nitrogen to nitrogen oxide with NO concentration in the background for three different solids. ? Coal; ? U-Furnace char and × activated carbon. a. 4% O_2 / He, b. 20%O_2 / He. Tg = 1698 K, 63 – 53 µm

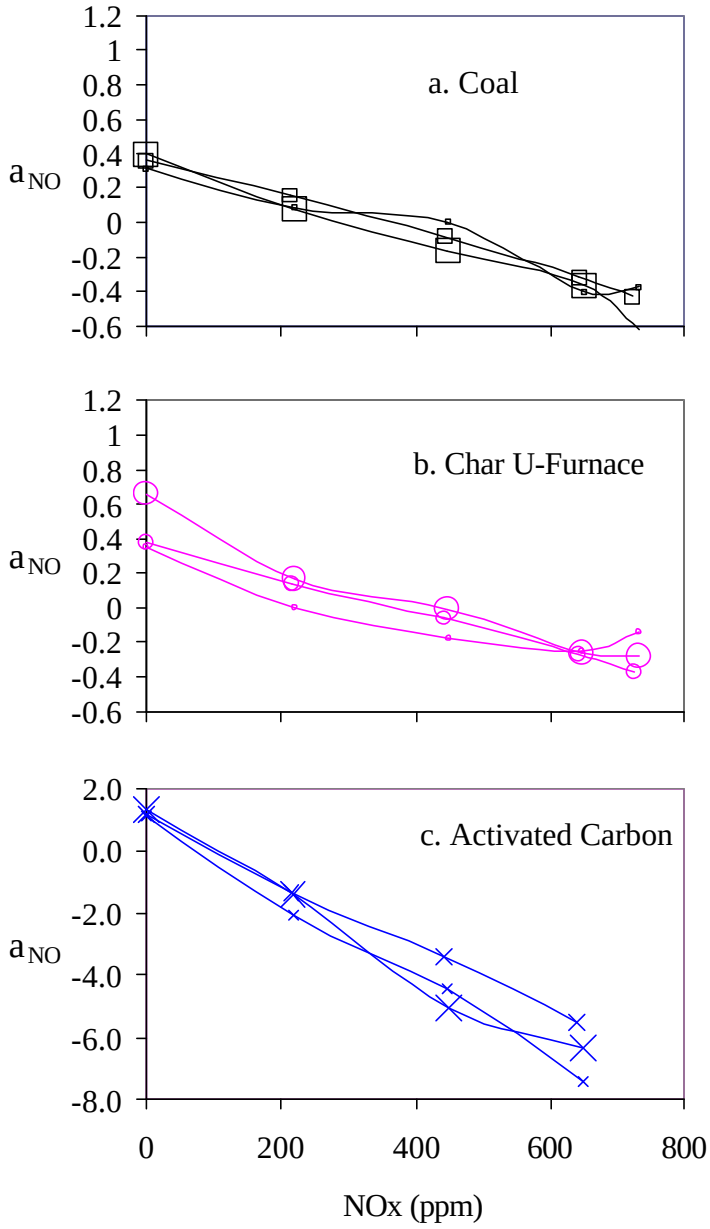

Figure 2.26. Variation of the conversion of char nitrogen to nitrogen oxide with NO concentration in the background for three different solids and three particle sizes 4% O_2 / He, Tg = 1698 K a. Coal: ? 108 – 88 µm, ? 63 – 53 µm, ? < 37 µm b. U-Furnace char: ? 108 – 88 µm, ? 63 – 53 µm, ? < 37 µm c. Activated carbon: × 108 – 88 µm, × 63 – 53 µm, × < 37 µm

2.5.3 Summary

This section presented experimental results on the variation of the conversion of fuel nitrogen to nitric oxide as the background nitric oxide concentration is varied from zero to 750 ppm.

For the three fuels used in the study (coal, U-Furnace char and activated carbon) there was a clear reduction on the conversion of fuel nitrogen to nitric oxides as the background nitric oxide concentrations increased. The effect of background nitric oxide concentration on the conversion of fuel nitrogen to nitric oxide is very similar for coal and U-Furnace char, but more pronounced for activated carbon.

An increase in oxygen concentration from 4% to 20% decreased the rate at which reduction in the conversion of fuel nitrogen to nitric oxide fell off as the background nitric oxide concentration increases.

The differences in the conversion of fuel-nitrogen to nitric oxide for three particle size fractions (108 – 88 μm, 63 – 53 μm and < 37 μm) was not measurable for the present experimental setup over the range of background concentrations studied, i.e. the variation in particle size did not produce any noticeable effect on the conversion of fuel nitrogen to nitric oxide.

2.6 CONVERSION OF FUEL NITROGEN TO NITRIC OXIDE AT PULVERIZED COMBUSTION CONDITIONS - ANALYSIS AND DISCUSSION

2.6.1 Introduction

There are several implications of the results described in section 2.5. The most obvious may be that as the nitric oxide concentration inside the boiler is reduced (e.g. to comply with stricter regulations) the contribution of char to the total nitric oxide produced during coal combustion becomes more important. This effect is stronger at lower oxygen concentration and does not seem to be highly affected by the particle size, at least in the 30 – 120 μm range.

Although this conclusion is significant, the analysis of the results in Section 2.5 should include a mechanism that explains the strong decrease on the conversion of char nitrogen to nitric oxide as the nitric oxide concentration in the background increases. When this mechanism is completely identified, it may be possible to take full advantage of the information obtained in Section 2.5, particularly by designing strategies to reduce the net conversion of char-nitrogen to nitrogen oxide.

Different approaches may be valid to infer the exact mechanism by which the nitric oxide formed during char oxidation is reduced to N_2. This study couples predictions made by theoretical models on char combustion to the experimental results in Section 2.5. Through the development of different models it is possible to understand the importance different mechanism have on the evolution of the char-nitrogen during combustion. This section describes different models and compares their predictions to the results in Section 2.5. Through this comparison it identifies the importance different mechanisms have in the conversion of char nitrogen to nitric oxide.

2.6.2 Simplified Single Particle Model (SSPM)

Beside the simplistic approach described in the introduction of section 2.4 that considers the conversion of char-nitrogen to nitric oxide as the ratio of nitric oxide formation to that of nitric oxide destruction; the simplest approach to understanding the results in Section 2.2.5 is to follow the pioneering work of Wendt and Schulze (1976). These authors used a single particle model to describe the process of char oxidation and to evaluate how much char nitrogen is oxidized to nitric oxide.

Several authors have used a similar method to study the conversion of char-nitrogen to nitrogen oxides at fluidized bed combustion conditions (e.g. Goel et al. 1994, Goel et al., 1996b) and at pulverized combustion conditions (e.g. Visona and Stanmore (1996), Visona and Stanmore, 1999 and Molina et al. (2000), Molina et al., 2001).

A detailed description of the SSPM can be found in Appendix I of Molina (2002). Basically, the SPPM consists of an analytical solution of the species mass conservation equation at constant temperature, for oxygen and nitric oxide inside a spherical char particle. The model uses an effective diffusivity and considers three reactions: carbon oxidation (R 2.9) and nitric oxide formation and destruction (R 2.7 and R 2.8 respectively).

Carbon oxidation:

$$-\mathrm{C} + 1/2\,\mathrm{O_2} \xrightarrow{k_{O_2}} \mathrm{CO} \qquad \text{R 2.9}$$

2.6.2.1 Rates of char oxidation and production and destruction of nitric oxide

From the simple approach described by E 2.2 it is possible to understand that the conversion of char-nitrogen to nitric oxide depends on the ratio of the nitric oxide

formation to that of nitric oxide destruction. Since it is reasonable to think that the rate of nitric oxide formation is proportional to that of char oxidation, it is important to guarantee that any model used to evaluate the net production of nitric oxide correctly predicts both the rate of char oxidation and that of NO destruction. An over-prediction on the rate of char oxidation relative to that of NO destruction will overestimate the conversion of char-nitrogen to nitric oxide. In contrast, if the rate of char oxidation is under-predicted relative to the reduction of nitric oxide on the char surface, the char-nitrogen conversion to nitric oxide will be underestimated.

As shown in detail by Molina (2002, Appendix I), the rate of char oxidation depends on the temperature and on the surface area of the char. To guarantee the correct evaluation of the rate of char oxidation, the surface area of the char particle was adjusted to give a value of time vs. char burnout that was in agreement with the experimental results.

The experimental results of Hurt (1993) for Illinois No. 6 coal were used for comparison. The data of Hurt (1993) relate char burnout to time and particle temperature for two different oxygen concentrations. Since the SSPM assumes a constant temperature, the mean temperature for every experiment reported by Hurt (1993) was used. With a value of surface area of 10 $m^2\ g^{-1}$, good agreement was obtained between Hurt's measurements and model predictions as presented in Figure 2.25.

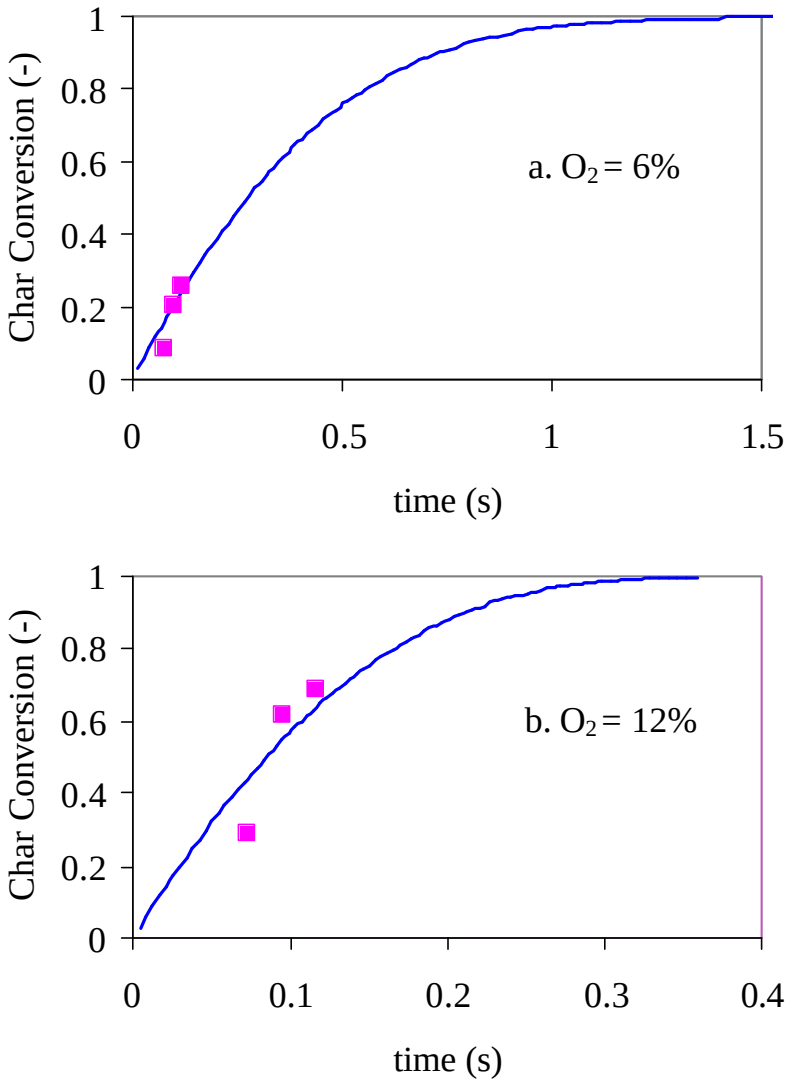

Figure 2.27. Comparison of the conversion of the burnout as predicted by the SSPM (lines) and by the experiments of Hurt (1993) (symbols). Illinois No. 6, 125 – 106 μm. a. O_2 = 6% Tg = 1700 K, b. O_2 = 12%, Tg = 1850 K

Although the data by Hurt (1993) only represents few points in the complete char oxidation domain, Figure 2.25 shows that the rate of char oxidation used in the SSPM predicts burnout profiles that are similar to those obtained in the experiments. This guarantees that the influence of the rate of char oxidation on the conversion of char-nitrogen to nitric oxide predicted by the SSPM should be consistent to the actual situation in the experiments.

The additional parameters used in the generation of the data in Figure 2.25 were ρ_p = 700 kg m^{-3} (particle density) and ε = 0.41 (porosity).

Given that the model estimates in a reasonable way the rate of char oxidation, the next step is to choose the rate of nitric oxide production. In this case it was assumed to be proportional to the rate of char oxidation, with N/C, the atomic ratio of nitrogen to carbon atoms in the char, as a proportionality constant. This has been found to be a good approximation at these high temperatures (Ashman et al. 1998, Molina et al., 2000).

The expression of Aarna and Suuberg (1997) was used for the rate of nitric oxide reduction on the char surface. According to section 2.2.4, this expression predicts this rate for the experiments in this study within one order of magnitude.

2.6.2.2 Comparison to experimental results

Figure 2.26 presents the comparison of the experimental values of char-nitrogen conversion to nitric oxide, (α_{NO}) as a function of background NO concentration to that predicted with the SSPM for the U-Furnace char and the activated carbon at two different oxygen concentrations. Since the model constantly predicts high char nitrogen conversion to nitric oxide when the original expression of Aarna and Suuberg (1997) for nitric oxide

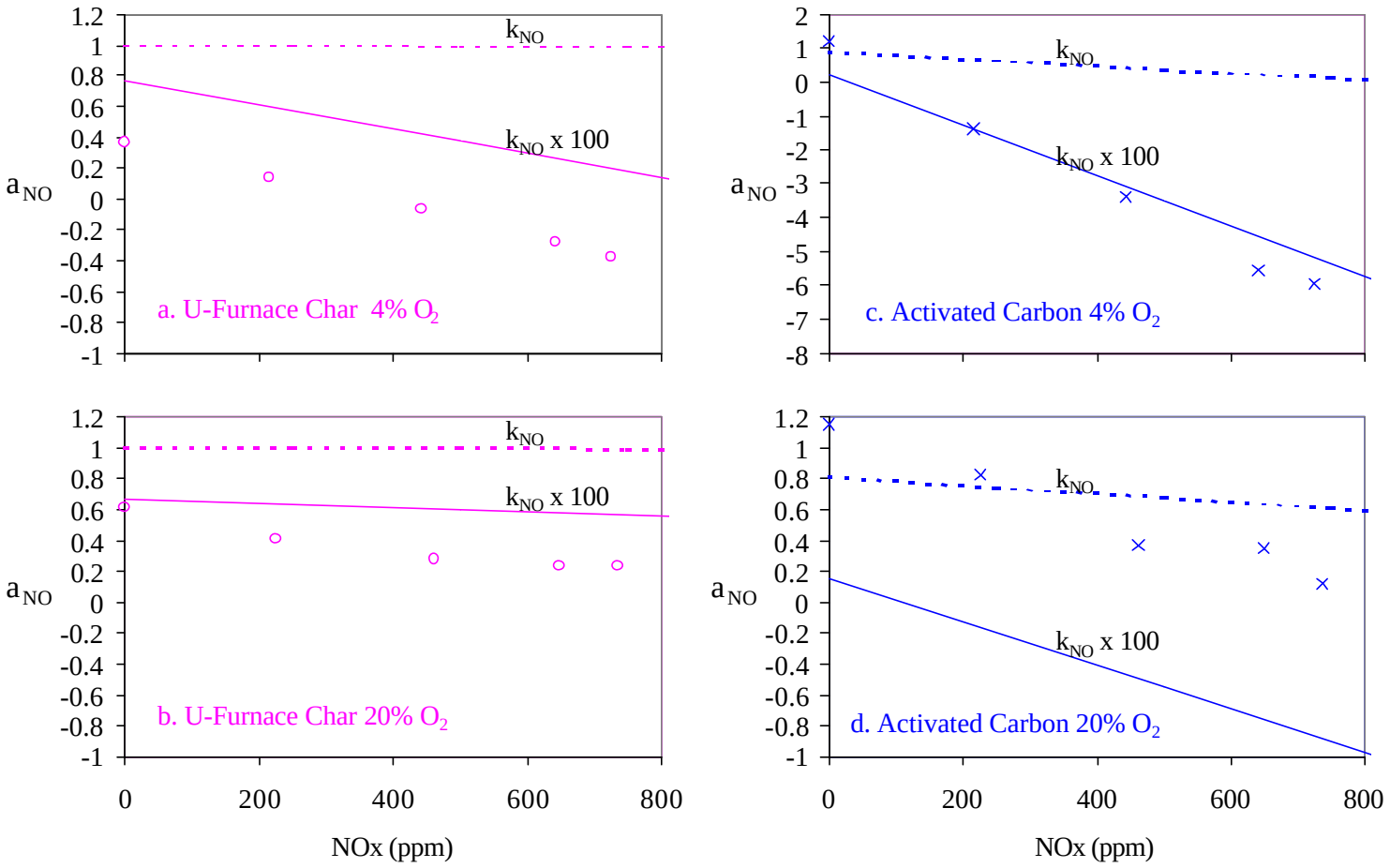

Figure 2.28. Comparison of the variation of the conversion of char-nitrogen to NO with increasing NO in the background for the experiments (symbols) and the predictions by SSPM for two values of k_{NO} (Aarna and Suuberg 1997): Dashed line: k_{NO}; Bold line k_{NO} x 100. T_g = 1698 K, 63 – 53μm. U-Furnace char: a. 4% O_2; b. 20% O_2; Activated Carbon c. 4% O_2; d. 20% O_2

reduction on the char surface (k_{NO}) was used, the simulation was also carried out with a value two orders of magnitude higher (k_{NO} x 100) than the one reported by Aarna and Suuberg (1997).

The surface area used for the U-Furnace char during the simulation was 10 $m^2\ g^{-1}$ since this value was the one that gave good agreement with the experimental data of Hurt (1993) as was explained above. This number is one order of magnitude lower than the one determined by BET experiment (see section 3.4.4). However, it is known that during char oxidation not all the char surface is active for reaction, and a value of 10 is possible. For activated carbon, a surface area of 1000 $m^2\ g^{-1}$ represented the higher surface area according to the BET analysis.

Figure 2.26 shows that the SSPM predicts a decrease in the conversion of char-nitrogen to nitric oxide as the nitric oxide concentration is increased. However, the slope of the line of α_{NO} vs. background nitric oxide concentration predicted by the model is low compared to that for the experimental results.

For U-Furnace char, after multiplying the rate of nitric oxide formation by 100 one obtains values of α_{NO} that are still high relative to the experimental values.

For activated carbon k_{NO} x 100 predicts the results in a correct way at 4% O_2, but it underestimates α_{NO} at 20%O_2. Nevertheless, the model correctly predicts a steeper slope for the plot α_{NO} vs. background NO concentration for the case at 4% O_2. The predictions by the SSPM for α_{NO} can be affected by the fact that the kinetics of char oxidation was not calibrated to experimental results. Thus, the results predictions for this fuel are analyzed more regarding the good prediction of the trends that on the exact determination of the quantity.

Figure 2.27 presents again the comparison between the model predictions and the experimental results, this time for different particle sizes. The SSPM predicts a lower α_{NO} for chars with larger particle size. The reason for this is that a larger particle

presents more surface area available for NO reduction to N_2 inside the particle. This effect is almost negligible for U-Furnace char at the original value of k_{NO} and more noticeable for k_{NO} x 100.

In contrast, the effect for activated carbon is more noticeable for the original k_{NO} that for the case when k_{NO} x 100 was used. This occurs because for a very high surface area (m^2 g^{-1}), as the one of the activated carbon in the model, the effect of an increase in the carbon mass (g) available for reaction is not as significant as when the surface area is low. Furthermore, when the rate is extremely high, the SSPM predicts that the destruction of nitric oxide on the char surface is limited by the diffusion of nitric oxide from the boundary layer. In this case, the effect of a larger surface area for nitric oxide reduction in the bigger particles is partially neutralized by its lower mass transfer coefficient in the boundary layer.

From the results in Figure 2.26 and Figure 2.27 it seems that a model that exclusively considers the heterogeneous reactions (R 2.7 to R 2.9) implemented in the SSPM tends to overestimate the conversion of char-nitrogen to nitrogen oxide when a typical value of the constant of nitric oxide reduction over char is used.

If the model uses a value for this rate two orders of magnitude higher than the one traditionally reported in the literature, the predictions are in better agreement with the experimental results.

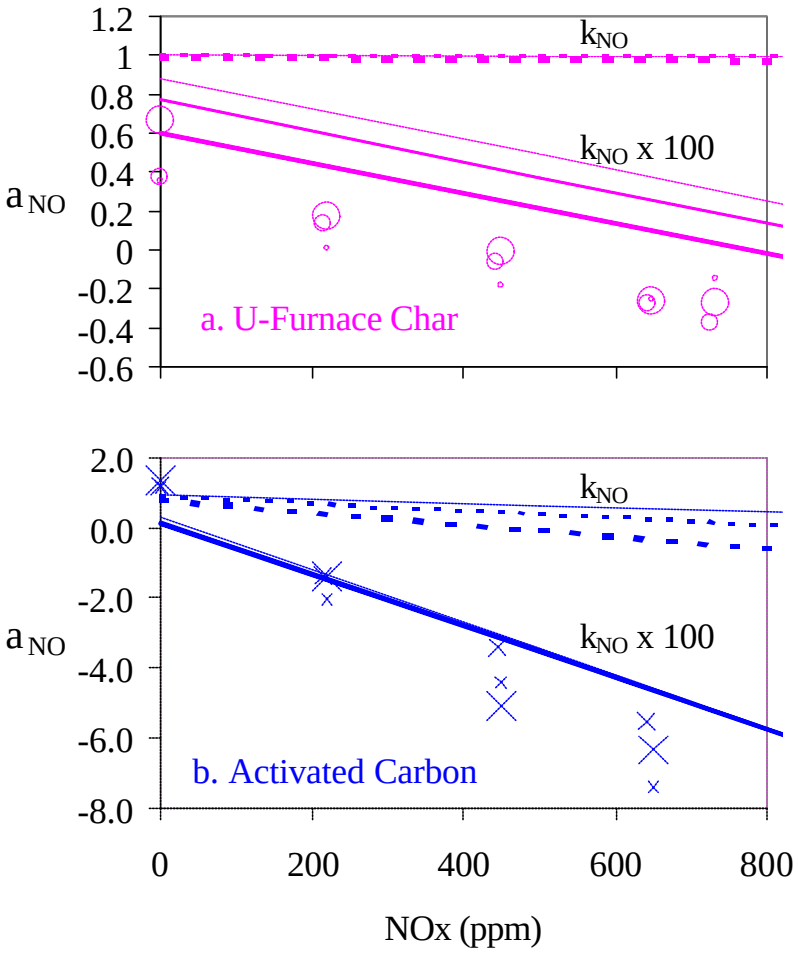

Figure 2.29. Comparison of the variation of the conversion of char-nitrogen to NO with NO in the background for the experiments (symbols) and the predictions by SSPM for twovalues of k_{NO} (Aarna and Suuberg 1997): Dashed line: k_{NO}; Bold line k_{NO} x 100. T_g = 1698 K, 4% O_2.a. U-Furnace char: 108 – 88 µm: ? , ----, - - 63 – 53 µm: ?, ----, - - < 37 µm: ?, ----, - - b. Activated carbon: 108 – 88 µm: ×, ----, - - 63 – 53 µm: ×, ----, - - < 37 µm: ×, ----, - -

An apparent contradiction is evident since the kinetics for NO reduction need to be increased two orders of magnitude to fit the data obtained under experimental conditions but can predict the rate of nitric oxide reduction on the char surface for these same fuels under inert conditions within less than one order of magnitude (section 2.2.4). The next section examines this contradiction.

2.6.2.3 Factors affecting the rate of NO reduction on the char surface

Among the phenomena that can cause an increase in the rate of nitric oxide reduction on the char surface, in particular two occur during char oxidation at the conditions of the experiments in this study. The first one is that most of the rates of nitric oxide reduction have been evaluated under oxygen-free conditions and oxygen increases this rate. The second possibility is the reaction of nitric oxide with carbon monoxide on the char surface (R 2.10). During char oxidation, it is obvious that oxygen is present in the system and that there is simultaneous presence of carbon monoxide and nitric oxide inside the particle, therefore both phenomena can increase the rate of nitric oxide destruction on the char surface above the values found under oxygen-free conditions.

$$NO + CO \rightarrow 1/2\, N_2 + CO_2 \qquad \text{R 2.10}$$

2.6.2.3.1 Oxygen

Different studies report that the reduction of nitric oxide on the char surface is considerable increased in the presence of oxygen. Tomita (2001) has found that the N_2 formation rate during char oxidation by nitric oxide is "significantly increased" in the presence of oxygen. Although Tomita did not quantify the magnitude of this enhancement, the rate increased by a factor of 4 after the oxygen concentration was

varied from 0% to 0.4 % at 1123 K and a NO concentration of 500 ppm for chars produced from phenol formaldehyde resin. The mechanism for the increase on nitric oxide reduction as the oxygen concentration is increased was not conclusively identified by Tomita and coworkers (1998b, 2001) but they suggested that oxygen activates the C(N) complexes originated after nitrogen oxide dissociative chemisorption on the char (R 2.1).

Although it is difficult to extrapolate the results of Tomita and coworkers from 1123 K up to 1698 K, the experimental results by Ashman et al. (1998) suggest that the importance of the population of C(N) complexes at high temperatures is lower than at 1123 K.

Jensen et al. (2000) also reported an increase in the rate of nitric oxide reduction on the char, but as it is explained in section 2.2.4 and Appendix E of Molina (2002), this effect seems to be more related to nitrogen adsorption on the initial stages of carbon oxidation and to a misrepresentation of the surface area available to reaction. Since at the temperatures of the experiments in this study the influence of nitrogen chemisorption is low and the surface area was set according to experimental results on the rates of char oxidation, it does not seem very possible that a similar effect occurs in the present setup.

2.6.2.3.2 Carbon Monoxide

Levy et al. (1981) and Chan et al. (1983) studied the effect of carbon monoxide in the nitric oxide reduction on the char surface. Both concluded that carbon monoxide increases the conversion of nitric oxide on the char surface. They found that the effect was less pronounced at high temperatures and proposed an oxide striping reaction (R 2.11) as the mechanism by which carbon monoxide enhances the reduction of nitric oxide on the char. The C(O) complexes were proposed to inhibit the reduction of nitric oxide on the char surface. Furusawa et al. (1985) obtained similar experimental results and proposed the same mechanism.

$$CO + C(O) \rightarrow CO_2 + C() \qquad \text{R } 2.11$$

More recently, Aarna and Suuberg (1999) questioned R 2.11 as the reason for the enhancement of the reduction of nitric oxide on the char surface and suggested a zero order expression with respect to CO for R 2.10. Their study was at 1073 K.

The effect of CO on the prediction of the conversion of char-nitrogen to nitric oxide during char oxidation has been examined by Visona and Stanmore (1996) and Molina et al. (Molina et al., 2001) at pulverized coal conditions. The first authors used the Langmuir-Hinshelwood expression for the enhancement of the reduction of nitric oxide reported by Chan et al. (1983). Although Visona and Stanmore (1996) do not present the value of nitric oxide conversion they state that the results were unsatisfactory.

Molina et al. (2001) used the rate expression determined by Aarna and Suuberg (1999) for R 2.11 and found that although there is a reduction of the conversion of char-nitrogen to nitric oxide when R 2.11 is included in the model, this reduction is minimum.

In summary, it seems unlikely that the presence of CO in the system can increase the rate of nitric oxide reduction on the char surface to the values necessary to obtain a correct prediction of the conversion of char-nitrogen to nitric oxide during char combustion. In particular at the temperatures at which this experiments were carried out the effect of CO was found to be minor (Levy et al., 1981). However, the effect of oxygen in the reduction of nitric oxide is more obscure, and can increase the value of k_{NO} to values for which the rate of NO reduction on the char surface can become important.

2.6.2.4 Summary of the comparison of the predictions of the SSPM to the experimental results

The following are the main conclusions obtained from the comparison of the predictions by the SSPM and the results in Section 2.2.5:

1. A simplified single particle model that only considers three reactions (R 2.7 to R 2.9) predicts a decrease in the conversion of char-nitrogen to nitric oxide as the background nitric oxide concentration is increased. This is in agreement with experimental results. However, the slope for the plot of char-nitrogen conversion to nitric oxide (α_{NO}) vs. background nitric oxide is too low if a value for the rate of nitric oxide reduction on the char surface (k_{NO}) traditionally reported in the literature is used.

2. If the same model is modified by multiplying k_{NO} by 100, model predictions are closer to experimental results.

3. The model predicts a steeper slope for the α_{NO} vs. background nitric oxide concentration for an oxygen concentration of 4% than for 20%. This is in agreement with the experimental results.

4. The model predicts that as the particle size increases, the conversion of char-nitrogen to nitric oxide decreases. However, the uncertainty in the experimental measurement prevents a comparison of these predictions with the experimental results. For large surface areas, as the one presented by the activated carbon, this effect is less pronounced.

5. The effect of oxygen was identified as the most possible cause for an increase in the rate of nitric oxide reduction on the char surface. However, the experimental data obtained in this study as well as in the literature are not sufficient to quantify the real magnitude of this effect.

The comparison of the predictions by the SSPM with the experimental results suggests that a heterogeneous model than only considers R 2.7 to R 2.9 does not predict the experimental trends reported in Section 2.2.5, unless the rate for reduction of nitric oxide in the char surface is a value two orders of magnitude higher than the one traditionally reported in the literature. Considering the results in Section 2.2.4, this high value on the k_{NO} seems unrealistic unless the presence of oxygen in the system causes an increase in k_{NO}.

In the case that the high value of k_{NO} is correct, the SSPM predicts the most important trends on the conversion of char nitrogen to nitric oxide when the background nitric oxide concentration increases, however the exact magnitude of the process is not correctly predicted.

Taking into account that the results with the SSPM are not completely satisfactory it is advisable to explore other mechanisms that can contribute to the conversion of char-nitrogen to nitric oxide during char oxidation. The next sections discuss two of these mechanisms: the interaction of nitric oxide with other particles present in the reactor and the effect of homogeneous reactions.

2.6.3 Effect of Sample Size

Jensen et al. (2000) showed that as the sample size increases, the conversion of char-nitrogen to nitric oxide decreases (e.g. for a bituminous coal char at 1473 K the conversion of char nitrogen to nitric oxide is ~0.9 for a 0.5 mg sample, but ~ 0.05 for a 6 mg sample.) These authors considered that the effect of a larger sample size was that the nitric oxide formed by one particle, was reduced by the surrounding particles. The larger the sample size the higher the area available for nitric oxide reduction.

Figure 2.28 presents results from the present study of the variation on the conversion of char-nitrogen to nitric oxide with sample size when U-Furnace chars are injected into

the reactor at 20% O_2 and 1698 K. The figure also presents the carbon balance. Figure 2.28 shows that the conversion of char-nitrogen to nitric oxide decreases as the sample size increases. Although the curves for α_{NO} and carbon balance follow a similar trend, the variation in the carbon balance is lower (96.5 to 103.6%) compared to the one for α_{NO} (0.47 to 0.55). Furthermore, an overestimation of the carbon balance would occur when the denominator in E 2.8 is too high, and this would produce a reduction in α_{NO} and not an increase as occurs in Figure 2.28. Therefore, the variation of α_{NO} with sample size seems related to the sample size and not to the process of evaluation of α_{NO}.

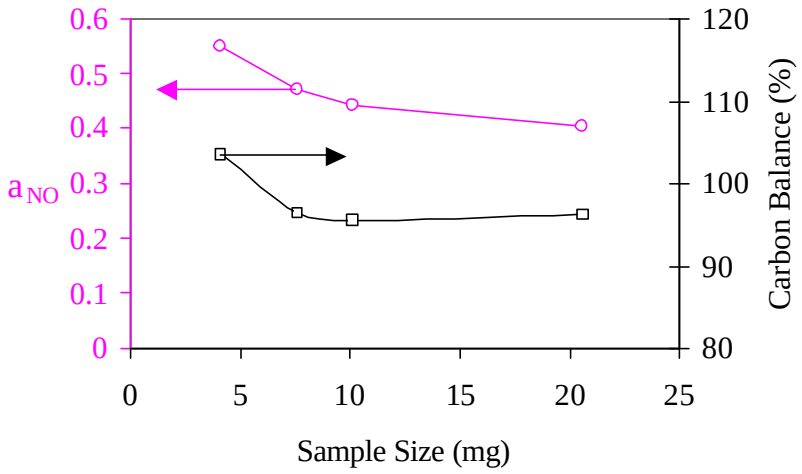

Figure 2.30. Variation of the conversion of char-nitrogen to nitric oxide and carbon balance with sample size. Injection of U-furnace char into the droptube at 20%O_2 Tg = 1698 K, 63 – 53 µm

According to the results in Figure 2.28 and the previous experience of Jensen et al. (2000) it seems possible that in the experiments presented in Section 2.2.5 the surrounding particles reduce the nitric oxide produced by one particle. Therefore, the value of char nitrogen conversion to nitric oxide evaluated from the experiments is lower

than the actual one occurred in the experiment. This would explain why the predictions by the SSPM overestimated α_{NO}.

As sound as the previous conclusion seems, it is in disagreement with the results in Section 2.2.5. Table 2.5 and Table 2.6 show that when a similar sample size of coal and U-Furnace char is injected into the reactor, as was the case in the experiments in Section 2.2.5, the actual amount of char mass introduced when coal is injected into the reactor is approximately half the amount of when U-Furnace char is injected. This occurs since approximately half of the mass of the coal is released as volatiles after injection into the reactor. The amount released for U-Furnace char has to be lower.

If the reduction of nitric oxide by surrounding particles was as determinant on the evaluation of the conversion of char-nitrogen to nitric oxide as Figure 2.28 and previous studies (Jensen et al., 2000) suggest, α_{NO} should be lower when char is injected into the reactor than when coal is injected into the reactor. But as Figure 2.23 shows, this is not the case. In Figure 2.23 a., when the oxygen concentration is 4%, the values of α_{NO} for coal and U-Furnace char are practically the same. Moreover, in Figure 2.23 b. (20% O_2) α_{NO} is always higher for char than for coal, in total contradiction to what an effect on char sample size suggest.

It could be argued, though, that the conversion of the nitrogen in the volatiles to nitric oxide during coal oxidation is such that when it is added to the conversion of char-nitrogen to nitric oxide it gives the same number for α_{NO} as when U-Furnace char is injected in the reactor. This seems however an unlikely event. In particular, if this needs to be the case for all five experiments at different background nitric oxide concentrations.

To sum up, the experimental evidence suggests that although an increase in the sample size tends to reduce the conversion of char-nitrogen to nitric oxide, this reduction is not originated by variations in the actual mass of char injected into the reactor and therefore the influence of the reduction of nitric oxide from other particles in the present

experimental setup is negligible. Next sections discuss an alternative hypothesis that explains why α_{NO} decreases with sample size.

2.6.4 Experiments with Purge

This section presents results for the experiments described in section 2.2.3.3.2.1 where the solid is injected into the reactor under inert atmosphere, and after a one-minute purge, oxygen is admitted into the reactor (see Figure 2.9). These experiments differ from those in Section 2.2.5 in which the solid is injected when oxygen is already present in the reactor.

Figure 2.29 shows the variation of the conversion of char-nitrogen to nitric oxide (α_{NO}) and the carbon balance with the sample sizes for three different experiments. The first case (squares) is for experiments with purge in which the collection probe is placed immediately after the char. The second case (crosses) is also for experiments with purge but this time the collection probe was placed 8 cm downstream for the non-woven fabric that holds the char. This gives an additional residence time of ~ 0.36 s. The third case corresponds to the results already presented in Figure 2.28, that are included for comparison.

In the results in Figure 2.29, α_{NO} was calculated by E 2.8 from the concentration profiles after oxygen injection (see Figure 2.9). The carbon balance represents a comparison between the amount of carbon injected and the amount of carbon detected as CO and CO_2 in the period after oxygen was injected.

As Figure 2.9 shows, immediately after injection, there is release of CO and CO_2; therefore it is not surprising that in Figure 2.29 the carbon balance for the purge experiments is lower than the one for the direct injection experiments. What is unexpected is the considerably lower conversion of char-nitrogen to nitric oxide for the experiments with purge. The conversion is lower by a factor of almost four and it is lower

for the experiments in which the collection probe was placed further downstream in the reactor. To explain this behavior, it is convenient to review the definition of α_{NO}.

E 2.8 shows that α_{NO} depends on the profile of gas concentration of NO, CO and CO_2 and on the atomic ratio of nitrogen to carbon (N/C) in the solid. Where N/C is evaluated from the elemental analysis of the solid injected into the reactor. Although α_{NO} reveals any effect that the purge time prior to oxygen injection can have on the release of CO, CO_2 and NO, it is insensitive to any variations on N/C, since this value is computed from the elemental analysis of the solid prior injection into the reactor.

In the injection experiments in which the solid immediately reacts with oxygen, the value of N/C calculated from the elemental analysis is a correct representation of the ratio of nitrogen to carbon in the char when oxidation begins. However, in the

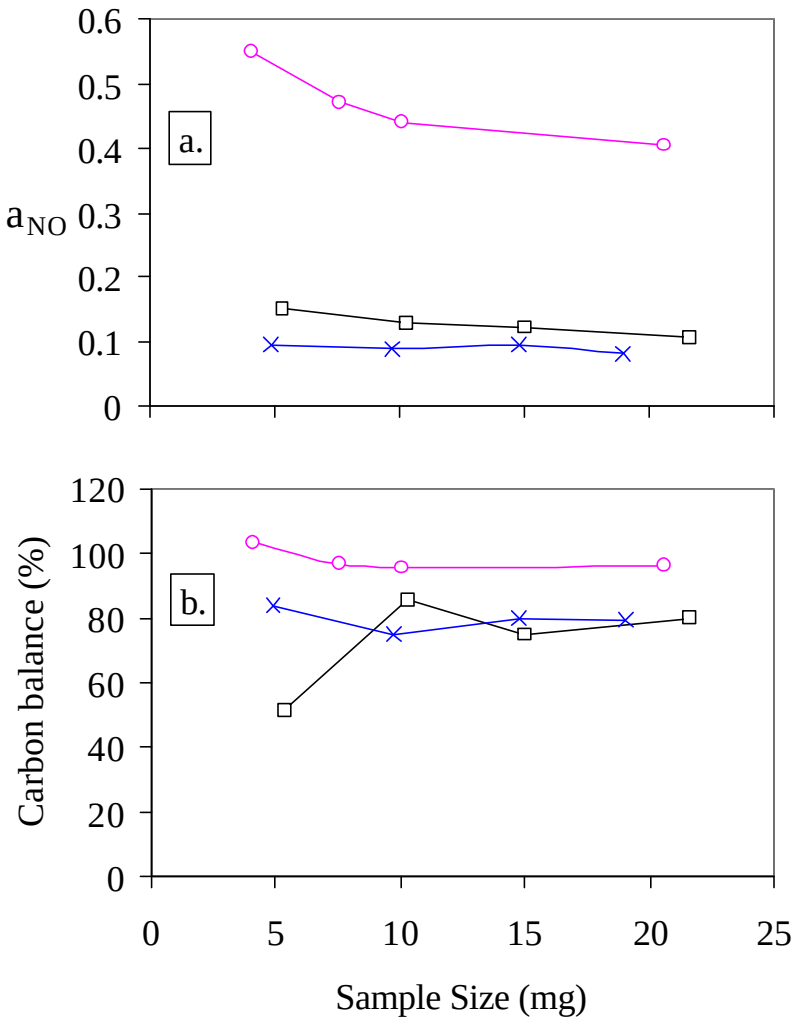

Figure 2.31. Variation of the conversion of char-nitrogen to nitric oxide (a.) and carbon balance (b.) with sample size for three different experiments: ? Purge experiment, probe at 0 cm × Purge experiment, probe at 8 cm. ? Direct injection; 20%O_2/He, Tg 1698 K, 63 – 53 µm

experiments with purge, the solids can experience additional devolatilization that can alter the value of N/C as evaluated from the elemental analysis.

A reduction of N/C during the purge period can explain why α_{NO} is lower for the experiments with purge. In this case, the actual mass fraction of nitrogen in the char would be lower than the one in the elemental analysis of the char prior injection.

The lower value of α_{NO} for the experiments with purge is not enough evidence to conclude that there is released of nitrogen during the period the char is in purge. Since the U-Furnace chars were prepared at conditions that resembled pulverized coal combustion (Spinti, 1997) one would expect a minimum amount of material released after exposure to high temperature. A one-minute residence time is far from the long residence times (~1 hr) required for complete depletion of nitrogen under inert atmosphere reported by Pohl and Sarofim (1976). However, the analysis of the FTIR spectra of the exhaust gases during the purge time shows evidence of the presence of HCN (Figure 2.30) and NO (Figure 2.31).

Figure 2.30 presents the spectra of the exhaust gases produced during the purge period after injection of U-Furnace char into the reactor. The spectra are compared to a standard for HCN. Figure 2.30 shows the presence a peak characteristic of HCN concentration during the purge experiments at high sample sizes. As the sample size decreases from 40 to 5 mg the peak disappears. This is evidence that during the purge experiments, the chars release HCN. The amount of HCN released is low, and only detectable for high sample sizes.

Figure 2.31 shows FTIR peaks related to nitric oxide during the experiments with purge (the spectrum of an H_2O standard is presented so that the peaks for NO can be separated from those of H_2O). The production of nitric oxide probably occurs from the oxidation of HCN. The fact that as the sample size decreases the peak for nitric oxide do not decrease but that it increases for some cases suggests that after the injection of the U-Furnace char into the reactor, the amount of oxygen in the reactor is enough to oxidize all

the HCN released to NO when the sample size is low. At higher sample sizes, some HCN escapes oxidation and it is detected by the FTIR (Figure 2.30).

In other words, the lower the mass of carbon injected, the higher the possibility that the species released from the char are oxidized. As the sample size increases, the atmosphere becomes more reducing and species as HCN that in the presence of O_2 at 1698 K are rapidly oxidized to NO can survive until detection.

If the height of the peak for nitric oxide presented in Figure 2.31 is normalized by the mass of char injected into the reactor, this number increases as the sample size decreases (see Figure 2.32). This further supports the conclusion that higher sample sizes promote a reducing atmosphere where HCN is not oxidized to NO.

The previous discussion suggests that homogeneous reactions can have an effect on the conversion of char-nitrogen to nitric oxide and that can explain the variation of α_{NO} with the sample size, as observed in Figure 2.28 and Figure 2.29. The higher the sample size, the more reducing the atmosphere.

One additional way to measure the magnitude of the carbon oxidation occurring in the reactor is to evaluate the ratio CO_2/CO. At these high temperatures, CO is the main product of char oxidation (Tognotti et al., 1990). Therefore, the rate CO_2/CO gives information on the extent of carbon oxidation in the homogeneous phase. If CO_2/CO is zero, there is no oxidation of CO. A high value of CO_2/CO implies that CO is oxidized by homogeneous reactions and suggests a more oxidizing atmosphere.

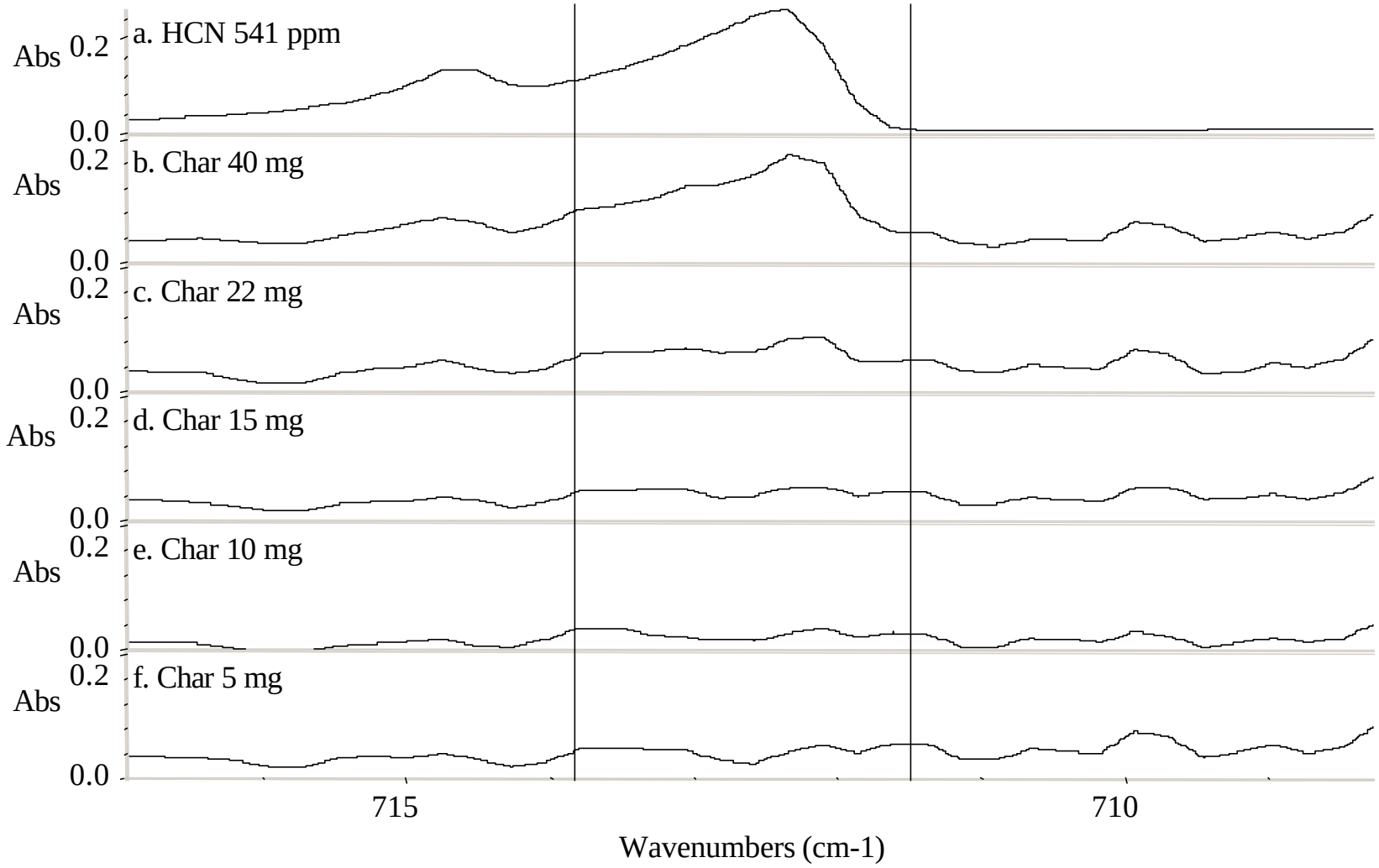

Figure 2.32. FTIR spectra of the exhaust gases in the purge experiments after U-Furnace char injection into the reactora. HCN standard. b. 40 mg, c. 22 mg; d. 15 mg; e. 10 mg and f. 5 mg. Tg = 1698 K 63 – 53 µm

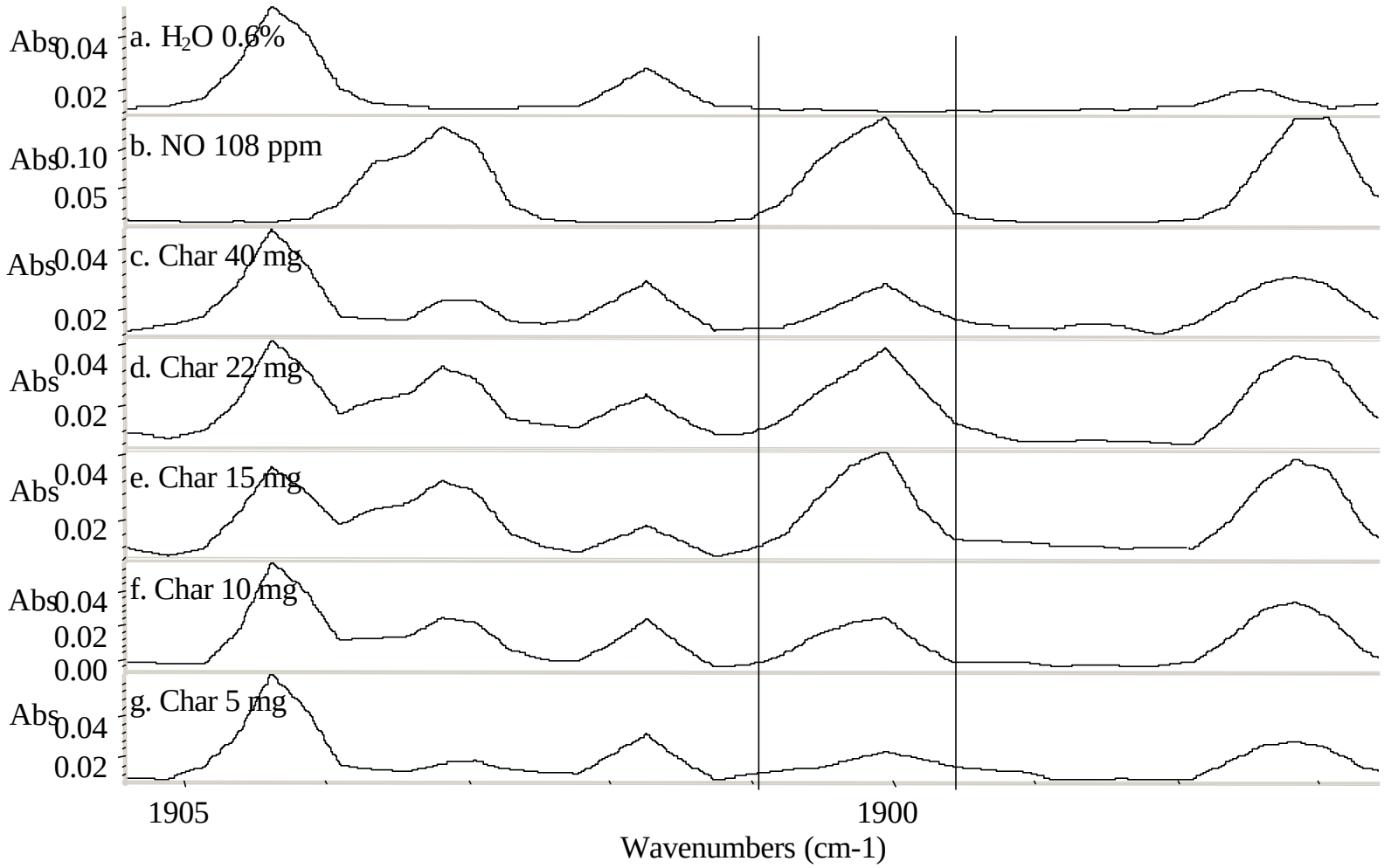

Figure 2.33. FTIR spectra of the exhaust gases in the purge experiments after U-Furnace char injection into the reactora. H_2O standard. b. NO standard. c. 40 mg, d. 22 mg; e. 15 mg; f. 10 mg and g. 5 mg. Tg = 1698 K 63 – 53 µm

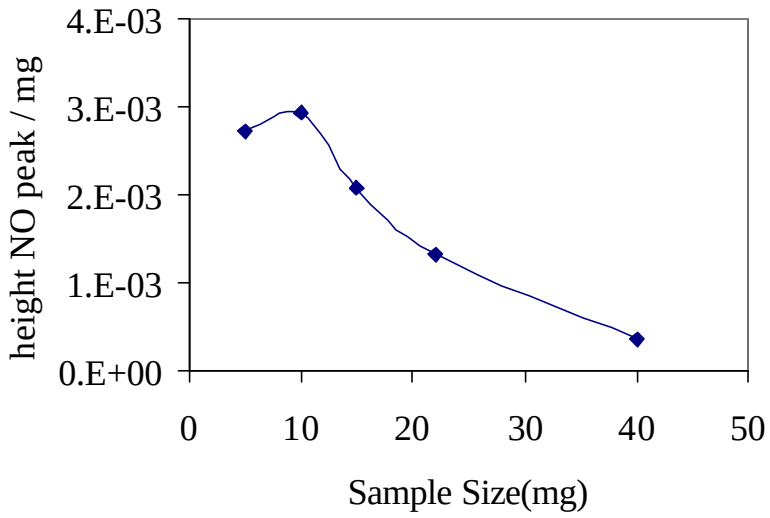

Figure 2.34. Variation of the height of the nitric oxide peak in Figure 2.31 normalized by the sample size injected into the reactor with the sample size U-Furnace Char. Tg = 1698, 63 – 53 µm

In the experiments of direct injection, almost all CO is converted to CO_2 and the ratio CO_2/CO does not give additional information on the magnitude of reduction in the homogeneous phase. However, in the experiments with purge before oxygen injection, the concentration of CO in the exhaust gases is significant and the ratio CO_2/CO can be used to quantify the magnitude of carbon oxidation in the gaseous phase.

Figure 2.33 presents this ratio for the experiments presented in Figure 2.29 when U-Furnace char is injected in the system. It also includes data when coal was injected into the reactor. The figure shows that ratio CO_2/CO is considerably lower for coal than for U-Furnace char and that it increases as the sample size decreases.

The amount of carbon-containing species released from volatiles after the injection of coal has to be higher than the one of char. The data of Molina (2002, Appendix J) show that during this period, acetylene, ethylene, methane and HCN are detected in the reactor. For char, only HCN was detected. This explain why the ratio CO_2/CO is higher

for the char since the higher the amount of carbon-containing material in the gaseous phase, the more reducing the atmosphere surrounding the particle and less CO will be oxidized.

In the same way, the higher the sample size, the higher the mass of gaseous material, released after the injection of the solid. This explains why the ratio CO_2/CO decreases as the sample size increases.

In summary, this section presented additional experimental data on the conversion of char-nitrogen to nitric oxide following an experimental procedure in which oxygen is injected into the reactor after the solids have been in purge in the reactor for one-minute. The results show that the conversion of char-nitrogen to nitric oxides decreases as the sample size increases and that it is considerably lower for the experiments with purge than for those in which char is directly injected into a He/O_2 stream.

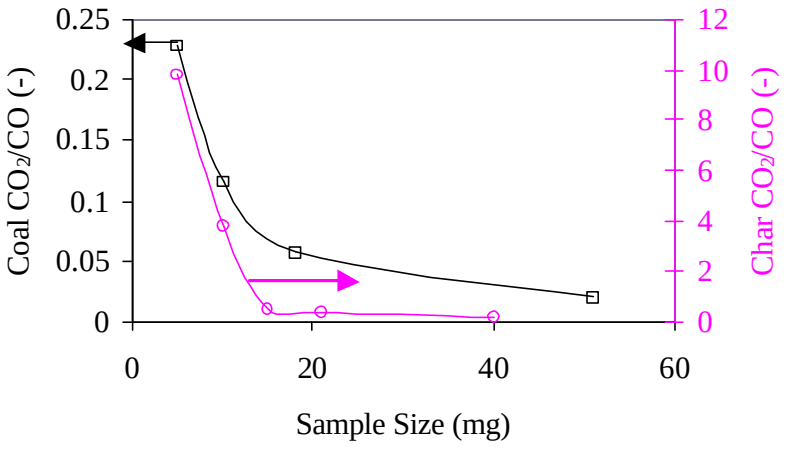

Figure 2.35. Variation of the CO_2/CO ratio with the sample size during the purge period for ? Coal and ? U-Furnace char, Tg = 1698 K, 63 – 53 µm

A detailed analysis of the FTIR spectra of the exhaust gases produced during the purge period after the injection of coal and char shows that HCN is produced in measurable amounts for large sample sizes. However, as the sample size decreases, HCN is oxidized to NO.

A decrease in the ratio CO_2/CO as the sample size increases and when more volatiles are releases supports the conclusion that a bigger sample size contributes to a more reducing atmosphere, in which not all the HCN released from the char is oxidized to NO.

The reason why these chars release HCN after injection may be related to the fact that the activation energy of the volatile released is a distributed function. Some unstable nitrogen-containing polyaromatic compounds may condense in the char matrix during char production, particularly under the conditions at which the U-Furnace chars were produced (exposure to high temperatures at low residence times). These compounds, once exposed to high temperatures can be released as HCN. Furthermore, the presence of O_2 in the system, as the production of CO and CO_2 suggests, can produce the disruption of the char matrix and nitrogen-containing species, such as HCN, can be released.

2.6.5 Effect of Homogeneous Reactions

At this point it seems proper to evaluate if the influence of homogeneous reactions can explain the behavior observed in the different experimental results presented in Section 2.2.5 and in the previous section.

As shown in Figure 2.30 and Appendix J of Molina (2002), HCN is released just after the injection of coal and U-Furnace char in the reactor. Some of this HCN is oxidized to nitric oxide by the oxygen present in the system. As the sample size increases, the amount of HCN that is oxidized to nitric oxide decreases.

The higher presence of HCN as the sample size increases suggests that the reduction on the conversion of nitric oxide as the sample size increases can originate from the

influence that homogeneous reactions can have on the conversion the nitrogen-containing species released after the solids are injected into the reactor. In this way, when the sample size is low, the atmosphere surrounding the injected solid is more oxidizing and tends to favor NO production. As the sample size increases, the atmosphere becomes more reducing and the favored species is N_2.

The effect of homogeneous reactions can also explain the decrease on the conversion of fuel-nitrogen to nitric oxide as the background nitric oxide concentration increases (Figure 2.17 to Figure 2.24). Any HCN released after the injection of the solid into the reactor, can react with the nitric oxide produced by the particle and in the background to produce N_2. The higher the concentration of background nitric oxide, the higher the amount of HCN converted to N_2. This effect has to be more pronounced at low oxygen concentrations and almost independent of particle size. All of this is in agreement to the results in Figure 2.23 and Figure 2.24.

Furthermore, if the reduction on α_{NO} as the background nitric oxide concentration increases occurs due to the destruction of NO with the HCN released from the particle, one can expect a similar slope for the plot of α_{NO} vs. background NO for the coal and the U-Furnace char since in both cases the effective amount of NO reduced will depend on the presence of HCN in the gaseous phase. The FTIR results in Figure 2.30 and in Appendix J of Molina (2002) show that HCN is released from both solids. Figure 2.23 a shows that the conversion of fuel-nitrogen to nitric oxide is the same for coal and U-Furnace char at 4% O_2. At 20% O_2 where there is a higher possibility of HCN oxidation to NO that at 4%, the solid that produces a more reducing atmosphere will present a lower value of α_{NO}. And this is the case in Figure 2.23 b., where the conversion of fuel-nitrogen to nitric oxide for coal is always lower than the conversion of char-nitrogen for the U-Furnace char.

The effect of homogeneous reactions can also explain why α_{NO} is lower in the experiments with purge (Figure 2.29). Not only the value of N/C decreases because of

the release of HCN after the injection of solids in the system, but also when HCN is released into a gaseous stream that already contains oxygen, the conversion to nitric oxide should be higher than when HCN is released into the reactor when oxygen is just been injected into the system. In addition, the lower value of α_{NO} when the residence time is higher (collection probe at 8 cm in Figure 2.29) supports a homogeneous process, in which the nitrogen produced from the char is reduced to N_2.

The existence of this parallel mechanism for NO reduction on the homogeneous phase can also explain why the SSPM that only considered heterogeneous reactions overestimated the conversion of char-nitrogen to nitric oxide when kinetic parameters for the reduction of nitric oxide on the char surface that are traditionally reported in the literature were used.

Although the experimental evidence support that homogeneous reactions affect the conversion of char-nitrogen to nitric oxide, it is necessary to understand if a theoretical treatment that considers homogeneous reactions explains the experimental results of Section 2.2.5 and section 2.6.4. Furthermore, previous studies (Pohl and Sarofim, 1976, Kobayashi et al. (1976) and Gibbins and Williamson (1998) have shown that the release of the nitrogen present in the char by exposure to a constant high temperature is minimal in the time frame of char oxidation at pulverized combustion conditions. Therefore, the release of char-nitrogen as HCN has to be promoted by the presence of oxygen in the system. However, at the temperature and oxygen concentration typical of pulverized coal combustion the conversion of char-nitrogen to nitric oxide seems more possible than to HCN.

The next section presents a comparison of the predictions of a model that couples homogeneous and heterogeneous reactions to the experimental results presented in this study. This comparison presents information that helps to understand the relative importance that a homogeneous mechanism can have in the conversion of char-nitrogen to nitrogen oxides.

2.6.6 Model with Homogeneous Reactions

Any HCN released from the char after injection in the reactor can react in the homogeneous phase in the char boundary layer or in the bulk, before the gas temperature is low enough to freeze the chemistry of the system.

This section examines the homogeneous reactions that HCN can undergo in the boundary layer and in the bulk.

2.6.6.1 Reactions in the boundary layer

Different authors have examined the homogeneous reactions occurring in the boundary layer of the char. Mitchell et al (1990) coupled the heterogeneous reactions occurring in the char with homogeneous reactions occurring in the boundary layer and studied the extent of conversion of CO to CO_2. Their model predicted that in the boundary layer at 6 and 12% O_2 the conversion of CO to CO_2 is minimum. Lee et al. (1995) developed a robust transient numerical model for carbon particle ignition and oxidation that coupled heterogeneous and homogeneous reactions in the boundary. Goel et al. (1996a) used a similar model and compared the predictions to data obtained from experiments in an electrodynamic balance (Tognotti et al., 1990) and to study the reactions of N-containing species in the boundary layer at fluidized bed conditions (Goel et al., 2001). They concluded that the reaction of HCN and other cyanide-like compounds in the boundary layer with NO can produce N_2O.

The present study uses a model that couples reactions in the boundary layer with a detailed description of the heterogeneous chemistry that occurs during char oxidation with an approach similar to those described above. This program is Skippy (Ashman et al., 1999) (Surface Kinetics In Porous Particles).

2.6.6.1.1 Model Description

Skippy, originally developed within the Department of Chemical Engineering at The University of Sydney, calculates species and temperature profiles for the reaction of a porous solid in a reacting gaseous environment at pseudo-steady state. The Skippy code employs data and subroutines from CHEMKIN package (Kee et al., 1989), the SURFACE CHEMKIN package (Coltrin et al., 1990) and the Sandia transport packages. (Kee et al, 1986).

Skippy solves the mass conservation equation, the energy equation, and the species conservation equation by considering a multicomponent diffusion system and mass convection. A more detailed explanation of the structure of Skippy is presented in reference (Haynes, 2001) and in Appendix K of Molina (2002).

Among the different inputs required in Skippy, the mechanism for the gas and surface chemistry may be the most important. For the gas phase the GRI-Mech 3.0 (Smith et al.) was used. GRI-Mech 3.0 is optimized for the combustion of methane and natural gas under the limits of 1000 to 2500 K, 1.3 to 1013.3 kPa and equivalence ratio from 0.1 to 5. These limits for pressure and temperature are within the conditions occurring in the boundary layer during char oxidation. Since the main fuel oxidized during the combustion of the char is CO and since the oxidation of CO is a fundamental step during methane oxidation, it was assumed that GRI-Mech 3.0 represents the homogeneous phase reactions occurring in the boundary layer. In fact the targets for the GRI Mech 3.0 included the prediction of CO oxidation at 1700 – 1900 K and at equivalence ratios from 0.04 to 6. This is the rage were more of the simulations in the present study were performed.

The heterogeneous mechanism used in Skippy has to follow a detailed scheme that conserves surfaces complexes and active sites. However, it can be simplified by the global reactions presented in Table 2.7. A more detailed description of the heterogeneous mechanism and kinetic parameters used in the system are presented in Appendix K of Molina (2002).

R 2.12 to R 2.13 represent the heterogeneous formation of CO and CO_2 from the char surface. The rate parameters were taken from reference (Muris and Haynes, 2001) in which the ratio CO/CO_2 was defined to satisfy the experimental data by Tognotti et al. (Tognotti et al., 1990).

R 2.14 and R 2.15 represent the formation and destruction of nitric oxide respectively. The rate of nitric oxide formation was considered to be proportional to the rate of carbon monoxide formation from char oxidation (R 2.12). The rate expression for nitric oxide reduction on the char surface by Jensen et al. (2000) was used in R 2.15.

Table 2.7. Summary of heterogeneous mechanism used in Skippy

No.	Reaction
R 2.12	$-C+\frac{1}{2}O_2 \rightarrow CO$
R 2.13	$-C+O_2 \rightarrow CO_2$
R 2.14	$-N+\frac{1}{2}O_2 \rightarrow NO$
R 2.15	$-C+NO \rightarrow \frac{1}{2}N_2+CO$
R 2.16	$-HCN \xrightarrow{O_2} HCN$

An additional reaction was added to simulate any HCN released to the gaseous phase (R 2.16). The proportion of HCN to NO released could be varied as input parameter. The condition was that the fraction converted to HCN plus the one converted to NO was the mass fraction of nitrogen in the char. Note that the mechanism in Table 2.7 assumes that HCN is released at a rate proportional to the one for char oxidation. This is done since previous studies (Krammer and Sarofim, 1994) showed that oxygen is necessary to release the nitrogen in the char at the temperatures and time scale typical of char oxidation.

2.6.6.1.2 Calibration for the rate of char oxidation

As explained in section 2.6.2.1, the rate of char oxidation is fundamental in the evaluation of the conversion of char-nitrogen to nitric oxide. In section 2.6.2.1 the SSPM was calibrated to the experimental data obtained by Hurt (1993) for char conversion. The same process was done for Skippy. Figure 2.34 presents the comparison of the experimental results by Hurt (1993) and Skippy's predictions when a surface area of 5 $m^2 g^{-1}$ is used.

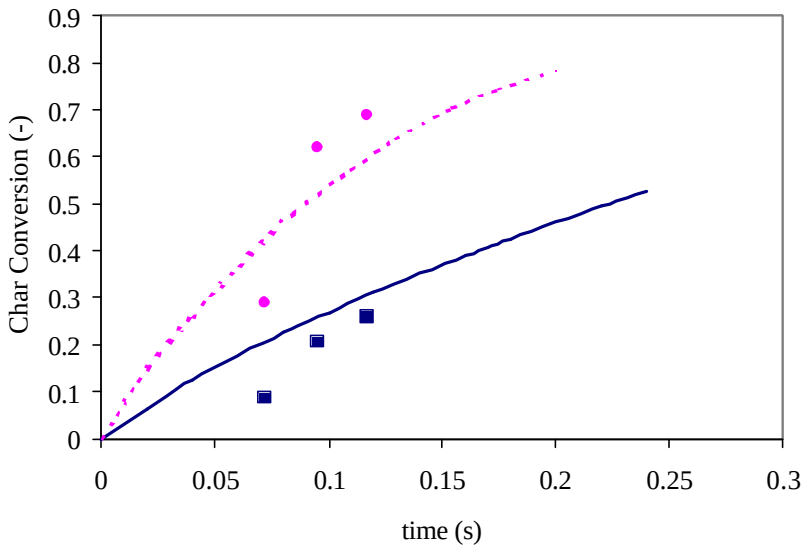

Figure 2.36. Comparison of the char burnout as predicted by Skippy (symbols) and by experiments (Hurt, 1993) (lines). Illinois No. 6, 125 – 106 μm. ? (experiment) - - - (model) at 6% O_2 ? (experiment) ------- (model) at 12% O_2

Although the agreement between experiments and prediction is not perfect, it is considered enough to guarantee that the model estimates in a reasonable way the char burnout. If the char surface area is increased from 5 m^2 g^{-1} char reactivity will be overestimated and this affects the conversion of char-nitrogen to nitric oxide as it is discussed later.

2.6.6.1.3 Predictions when all char-nitrogen is converted to nitric oxide

Figure 2.35 presents the comparison of the predictions by Skippy and the experimental results presented in Section 2.2.5 assuming that all char-nitrogen is converted to nitric oxide. As it was the case in Figure 2.26 and Figure 2.27 when the predictions by the SSPM were compared to the experimental results, two values of k_{NO} were used. The first one (k_{NO}) , corresponds to the kinetic expression by Jensen et al. (2000). The second one is the same number multiplied by 100 (k_{NO} x 100).

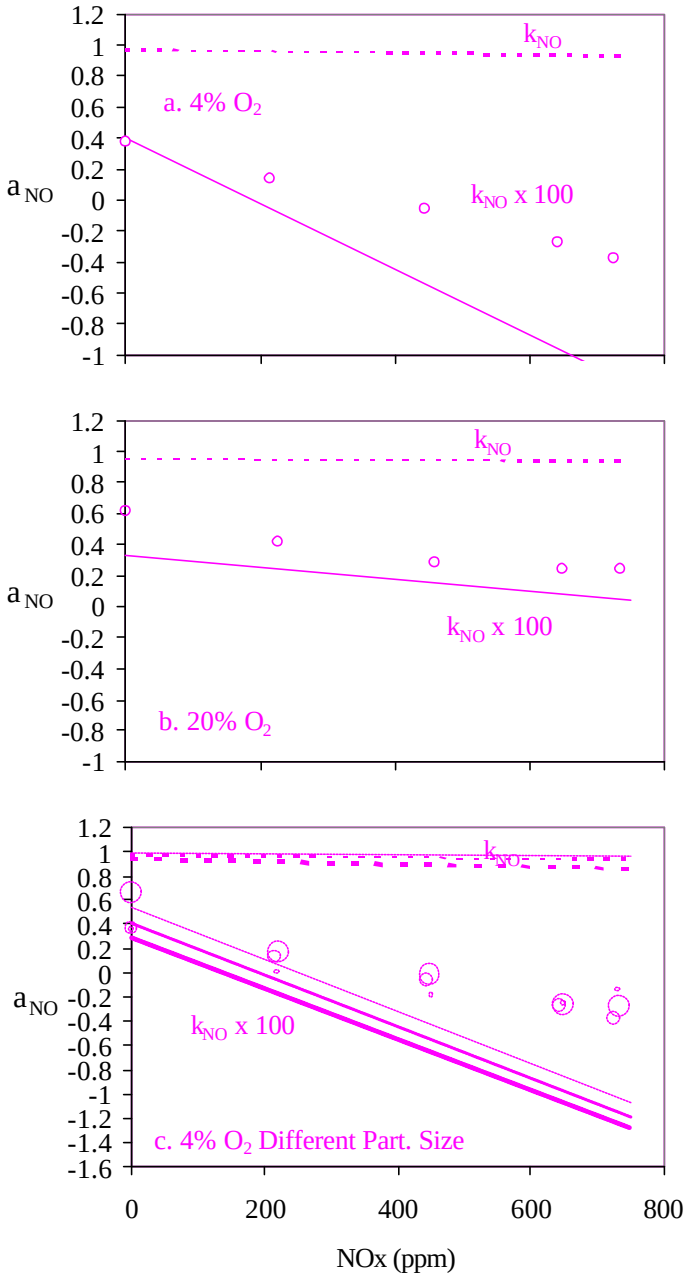

Figure 2.37. Comparison of the variation of the conversion of char-nitrogen to NO with NO in the background for the experiments (symbols) and the predictions by Skippy for two values of k_{NO} (Aarna and Suuberg 1997): Dashed line: k_{NO}; Bold line k_{NO} x 100. T_g = 1698 K, U-Furnace Char. a. 4% O_2, 63 – 53 µm; b. 20 % O_2 63 – 53 µm. c. Different Particle sizes: 108 – 88 µm: ? , ----, - - ; 63 – 53 µm: ? , ----, - - < 37 µm:?, ----, - -

The predictions obtained from Skippy are very similar to the ones by the SSPM (Figure 2.26 and Figure 2.27). The main difference is that Skippy with a value of k_{NO} x 100 underestimates α_{NO} while the SSPM slightly overestimates it. The reason for this is that Skippy uses the kinetic of Jensen et al. (2000) by assuming that the surface area in those experiments was 10 $m^2\ g^{-1}$ (see Appendix K of Molina, 2002). With this value, the rate of reduction of nitric oxide on the char surface is approximately one order of magnitude higher than the one by Aarna and Suuberg (1997) used in the SSPM (see section 2.6.2). In this case, Skippy predicts a lower conversion of char-nitrogen to nitric oxide.

The results in Figure 2.35 suggest that an increase in the rate of nitric oxide reduction on the char surface is required to predict the total conversion of char-nitrogen to nitric oxide. In Figure 2.35, k_{NO} was increased by multiplying the original expression by 100. However, this is not the only way to increase k_{NO}. Since an increase in surface area increases the rate available for destruction, it seems right to assume that the higher the surface area the lower the conversion of char-nitrogen to nitric oxide. However, an increase in surface area also increases the rate of char oxidation. And this effect competes with any increase in the reduction of NO on the char surface.

Figure 2.36 presents the effect of an increase in surface area from 5 to 50 $m^2\ g^{-1}$ for the radial profile of oxygen (a.), the char burnout vs. time (b.) and the variation of the conversion of char-nitrogen to nitric oxide (c.) and nitrogen (d.) as predicted by Skippy for the oxidation of U-Furnace char at 4%O_2

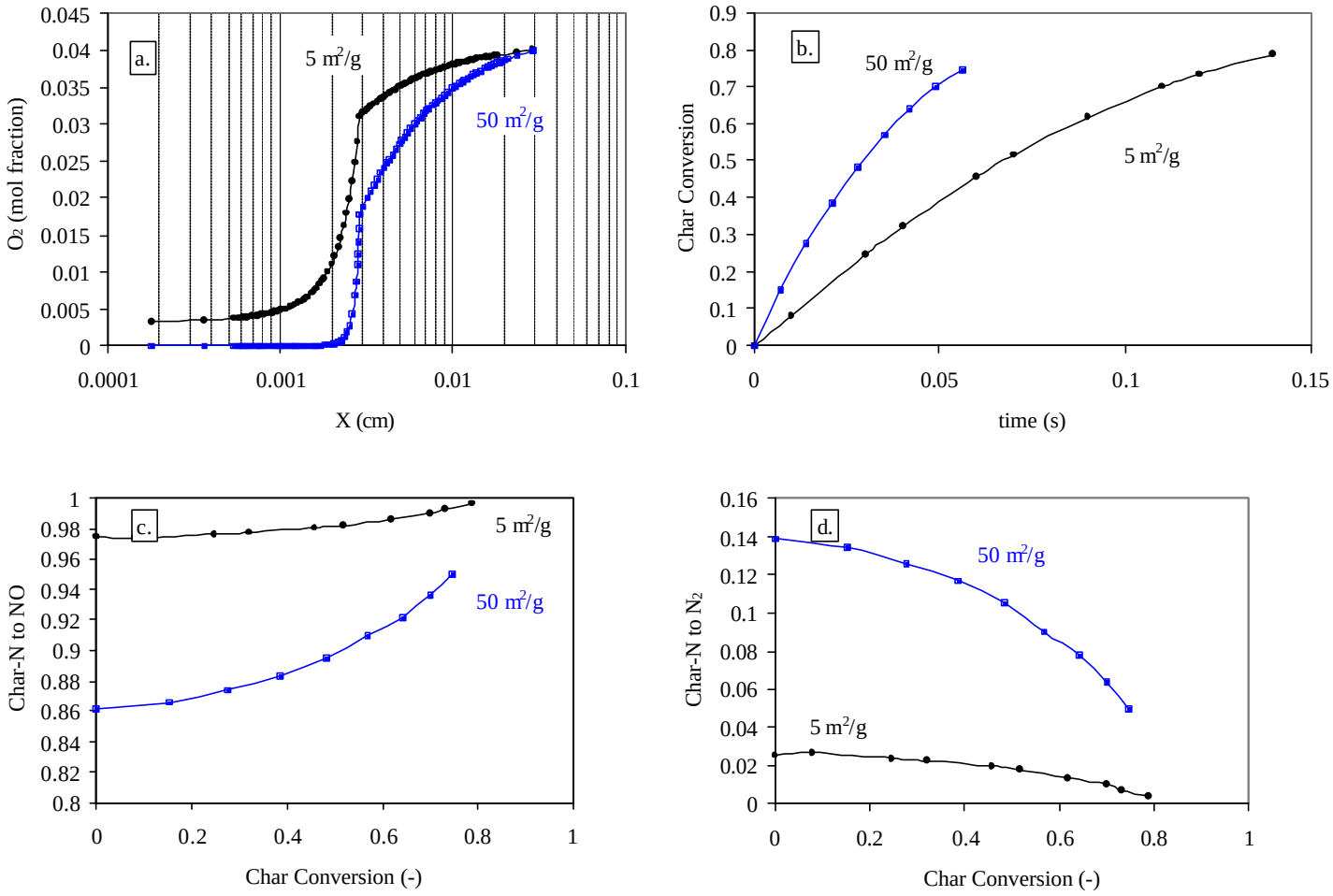

Figure 2.38 Predictions by Skippy for: a. O_2 profile inside the particle vs. particle radius at the initial step of the reaction; b. Char conversion; c. Char-N conversion to NO; d. Char-N conversion to N_2. U-Furnace char. Tg = 1698 K, 56µm, 4% O_2 for two different surface areas: ?: 5 m^2 g^{-1}; ?: 50 m^2 g^{-1}

Figure 2.36 shows that as char conversion advances, the conversion of char-nitrogen increases. This is in agreement with results at fluidized bed conditions (Goel et al., 1994) and is due to a reduction on the area available for NO reduction.

Figure 2.36 also shows, that a larger surface area reduces the conversion of char-nitrogen to nitric oxide. For instance at a burnout of zero the conversion of char-nitrogen to nitric oxide reduces from 0.98 to 0.86 when the char surface area increases from 5 to 50 $m^2 g^{-1}$.

Although this seems an improvement in the predictions presented in Figure 2.35, it has one additional effect, a considerable increase in the char reactivity (Figure 2.36 b.) The time for 60% char conversion reduces from 100 ms to 40 ms. Given the fact that the model was calibrated to predict the experimental data of Hurt (1993) for char oxidation (see Figure 2.34) this increase seems unrealistic. Furthermore, the improvement on the prediction of the conversion of char-nitrogen to nitric oxide is minimum (from 0.98 to 0.86) when the experimental result is ~ 0.4 (Figure 2.23). All this evidence suggests that an underestimation on the surface area available for reaction is not the reason why Skippy over-predicts the conversion of char-nitrogen to nitric oxide.

One final observation from Figure 2.36 is that although the total conversion of char-nitrogen to nitric oxide increases with char burnout, the change is not steep, particularly at the beginning of the char oxidation. According to this, the conversion of char-nitrogen to nitric oxide at the beginning of the reaction is a good indicator of the total conversion of char-nitrogen to nitric oxide.

The next simulations with Skippy present the results at the beginning of the char conversion. Therefore the results will slightly underestimate the conversion of char-nitrogen to nitric oxide compared to that if the complete burnout is computed. However, this effect is minor and it should not effect the evaluation of trends. The high computational demand of the evaluation of a complete char oxidation profile provides the basis for this assumption.

To end this section, Figure 2.37 presents the comparison of the predictions by Skippy to the experimental data for the oxidation of active carbon at (4% O_2). The simulation used a surface area of 100 m^2 g^{-1} and the elemental composition in Table 2.3. For this high surface area, the profile close to the reaction front is really steep (see Figure 2.36 a.) and the solution of Skippy becomes difficult. This prevented obtaining a solution for higher surface area or higher oxygen concentrations. For these cases it is necessary to use a simplified version of the homogeneous mechanism. However, this was considered beyond the scope of this study.

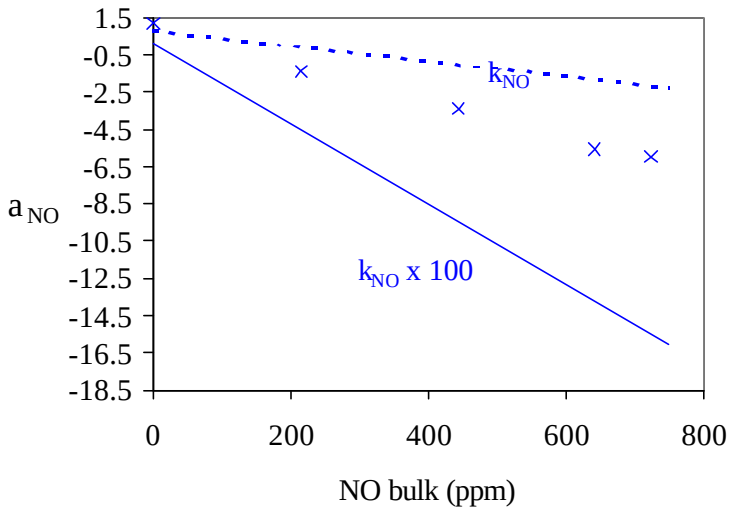

Figure 2.39. Comparison of the variation of the conversion of char-nitrogen to NO withNO in the background for the experiments (symbols) and the predictions by Skippy for two values of k_{NO} (Aarna and Suuberg 1997): Dashed line: k_{NO}; Bold line k_{NO} x 100. T_g = 1698 K, Activated Carbon 4% O_2, 63 – 53 µm

As it happened with the U-Furnace char (Figure 2.35), Figure 2.37 shows that Skippy overestimates α_{NO} when k_{NO} is used and it underestimates it for k_{NO} x 100. However, the predictions with k_{NO} for activated carbon are closer to the experimental results than those for U-Furnace char. The higher surface area and carbon content of the activated carbon are the reason for this.

2.6.6.1.4 Extent of the reactions in the boundary layer

Up to this point, the predictions obtained from Skippy are very similar to the ones obtained from the SSPM. This is not surprising since both considered the same heterogeneous reactions.

However, the purpose behind the use of Skippy was to understand the magnitude of the reactions in the boundary layer. To do this, the extent of the conversion in the boundary layer of carbon to CO and CO_2 and of char-N to different N-containing compounds in the event that all the char-nitrogen was released as HCN was studied. This value was arbitrarily set to one to facilitate the study of the reactions of HCN in the boundary layer.

Figure 2.38 presents the predictions by Skippy for the oxidation of U-Furnace char and for five different cases in which the location of the boundary layer expressed as the ratio of the boundary layer to the particle diameter (R_{BL}/R_{char}) was varied from 1 to 75 (cases A to D). In all the cases it was assumed that all the char-N was converted to HCN and that the bulk concentration was 4% O_2/He, except for case E where 1 % H_2O was included. This case was added because results from previous studies (Lee et al., 1995, Goel et al., 1996a) have shown that H_2O is required to obtain the oxidation of CO in the boundary layer.

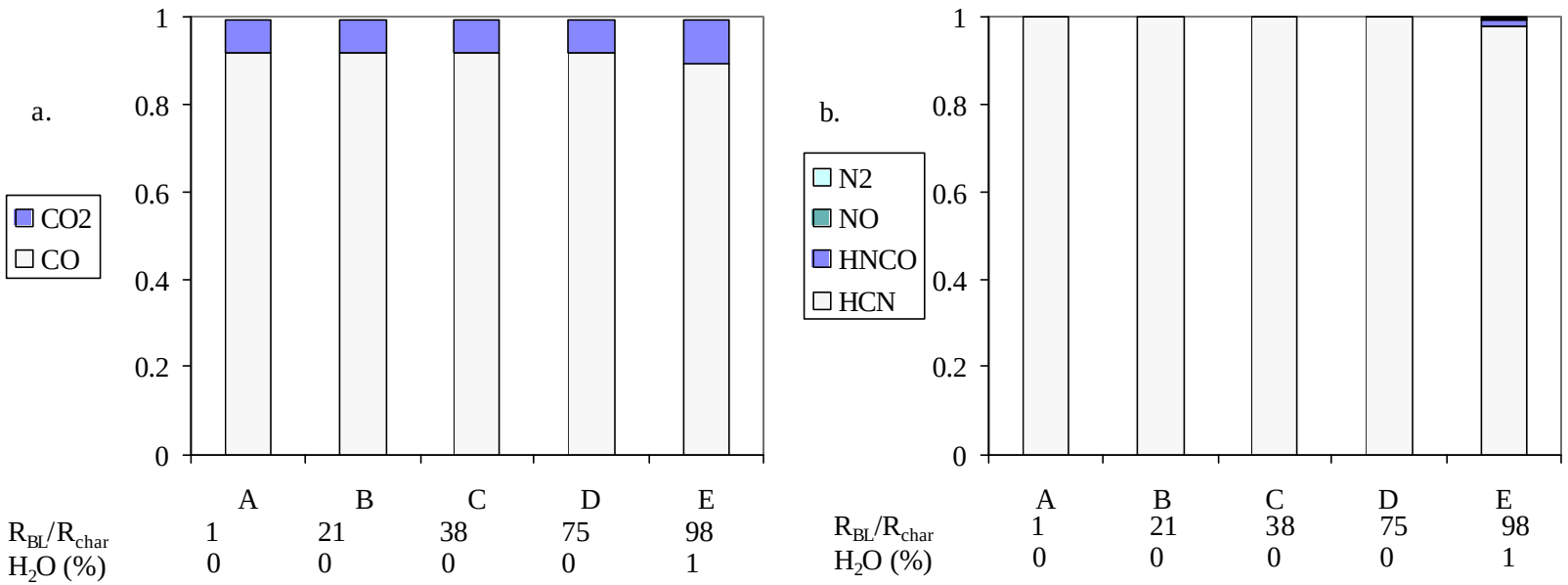

Figure 2.40. Skippy's prediction for the conversion of a. Char-carbon and b. Char-nitrogen for the combustion of U-Furnace char at 1698 K, 58μm, and 4% O_2. All cases with k_{NO} from Jensen et al. (2000) and assuming 100% conversion of char-nitrogen to HCN. The size of the boundary layer (R_{BL}/R_{char}) changes between cases: A: 1; B: 21; C: 38; D: 75. Case E is at R_{BL}/R_{char} = 98 and with 1% H_2O in the background

Figure 2.38 shows that under the conditions of the simulations CO and HCN do not undergo any considerable transformation in the boundary layer. Not even with a ratio R_{BL}/R_{char} as high as 98 it was possible to obtain any reactions in the boundary layer. With the addition of 1% H_2O the activity in the boundary layer increases, but not in a considerable way. Since a boundary layer of more than 100 times the particle size is unrealistic for the experimental conditions of this system, the simulation suggest that for the oxidation of the U-Furnace char, any homogeneous reactions should occur in the bulk and not in the boundary layer.

Since Goel et al. (2001), using a similar model, found that the conversion of HCN in the boundary layer at fluidized bed conditions was minimum if NO was not present; some simulations with Skippy were run with a variation in the nitric oxide in the background. Figure 2.39 presents the conversion of carbon to CO and CO_2 and of nitrogen to NO, HCN, NO_2 and N_2 for the oxidation U-Furnace char (cases A to B) and activated carbon (cases C to H). The nitric oxide concentration in the background changes between cases, and for the last two cases (I and H), the boundary layer is longer.

The results on the conversion of the carbon in the fuel to CO and CO_2 are similar to those in Figure 2.38. For all the cases, the oxidation of CO in the boundary layer is negligible. This is in agreement with previous results by Mitchell et al. (1990).

The results for the conversion of char-nitrogen to different nitrogen-containing species (Figure 2.39 b.) show that HCN does not react in the boundary layer. For all the cases, the conversion of char-nitrogen to HCN is one. Not even in case H in which the boundary layer was extended to $R_{BL}/R_{CH} = 95$ HCN reacts in the boundary layer.

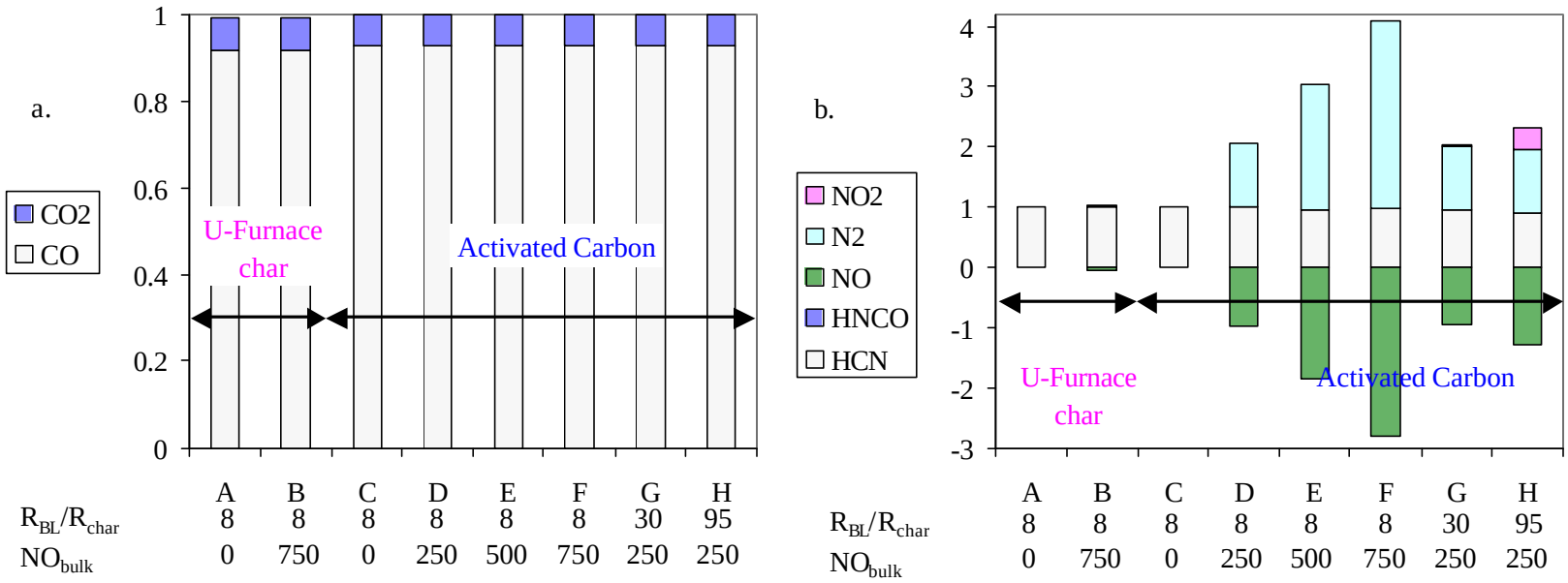

Figure 2.41. Skippy's prediction for the conversion of a. Char-carbon and b. Char-nitrogen for the combustion of U-Furnace char and activated carbon at 1698 K, 58μm, and 4% O_2.All cases with k_{NO} from Jensen et al. (2000) and assuming 100% conversion of char-nitrogen to HCN. The nitric oxide in the bulk and the size of the boundary layer (R_{BL}/R_{char}) change between cases as indicated in the figure.

Figure 2.39 b also gives additional information on the process of nitric oxide reduction on the activated carbon. The results for case C where the background concentration is zero show that all char-N is converted to HCN. However, as the nitric oxide increases to 750 ppm, the production of N_2 is considerable. This occurs because of the destruction of nitric oxide on the char surface. Since the results in Figure 2.39 b are normalized by the amount of char-nitrogen in the char, the conversion of char-nitrogen to nitric oxide can get negative values higher than –1. In the same way the conversion of char-nitrogen to N_2 can get values of more than one. This effect is more noticeable for a fuel like the activated carbon for which the nitrogen content is low and the surface area available for nitric oxide reaction is high. In this way, a conversion of char-nitrogen to N_2 of ~3.0 (as in case F) means that the amount of N_2 produced is three times the one that would have been produced if all the nitrogen produced in the char was converted to nitrogen.

In contrast to the results in Figure 2.38 and Figure 2.39, the experimental evidence shows that almost all the carbon monoxide produced during char oxidation is converted to carbon dioxide before reaching the gas analyzers. Therefore, additional reactions in the bulk should occur. The next section examines the influence of these reactions on the conversion of char-nitrogen to nitric oxide.

2.6.6.2 Reactions in the bulk

If CO and HCN do not react in the boundary layer; they should react in the bulk, before the reactions in the gaseous phase cease in the collection probe. The estimated residence time for the exhaust gases from the char surface to the collection probe is 0.13 s at 1698 K and for the gas flow of the experiments. Since the collection probe has a relative high cooling rate (see Appendix D of Molina, 2002), most of the reactions should occur within this section.

To simulate the reactions occurring in this region, the output of the gaseous phases obtained from Skippy at the different cases studied was used as input to SENKIN (Lutz et al., 1988), a program that computes the time evolution of a homogeneous reacting system. The homogeneous reaction mechanism was GRI Mech 3.0 (Smith et al.). The simulations were performed assuming constant temperature (1698 K) and a residence time of 0.13 s. In this case the evaluation of the conversion of char-nitrogen to nitric oxide is not as straightforward as with Skippy, since the data available to compute α_{NO} outputs are mole fractions and not molar flows. In this case α_{NO} was calculated according to E 2.9.

$$\alpha_{NO} = \frac{[NO]_{OUT} + [NO_2]_{OUT} - [NO]_{IN}}{[NO]_{IN\,CHAR}} \qquad \text{E 2.9}$$

Where $[NO]_{IN}$ represents the mol fraction of nitric oxide in the input obtained from the simulation by Skippy. This value is a few ppm lower than the nitric oxide in the background because some nitric oxide is reduced by the particle. It is important to note that the input obtained from Skippy corresponds to the species concentration at a radius eight times the particle radius, and before the end of the boundary layer. This is done because the gas concentration at the end of the boundary layer corresponds to the boundary condition of the problem.

$[NO]_{OUT}$ and $[NO_2]_{OUT}$ are the nitric oxide and nitrogen dioxide concentration predicted by SENKIN after a residence time of 0.13 seconds. Since some NO is oxidized to NO_2 it is necessary to account for both during the evaluation of α_{NO}. $[NO]_{IN\ CHAR}$ represents the amount of nitric oxide that would be produced if all char-nitrogen were converted to NO. It is computed as the fraction of nitrogen in the input obtained from Skippy when the background nitric oxide concentration is zero.

E 2.9 represents the apparent conversion of char-nitrogen to nitric oxide when it is assumed that all char-nitrogen is converted to HCN. In the cases when the conversion of char-nitrogen to HCN is less than one, E 2.9 has to be corrected by taking into account the amount of char-nitrogen already converted to nitric oxide in the input, as

$$\alpha_{NO} = \frac{[NO]_{OUT} + [NO_2]_{OUT} - [NO]_{IN} + [NO]_{NO=0}}{[NO]_{IN\,CHAR}} \qquad \text{E 2.10}$$

Where $[NO]_{NO=0}$ represents the mol fraction of nitric oxide in the boundary layer, when the background nitric oxide concentration is zero. For example for a background nitric oxide concentration of 250 ppm, when the conversion of char-nitrogen to HCN is 0.5, $[NO]_{IN}$ will be few ppm higher than 250 (e.g. 255 ppm) because of the contribution of the char-nitrogen to NO (5 ppm in this case). If all the HCN is converted to N_2, $[NO]_{OUT} + [NO_2]_{OUT}$ will be 255 ppm and $[NO]_{OUT} + [NO_2]_{OUT} - [NO]_{in}$ is zero. According to E 2.9, α_{NO} is zero, however some char-nitrogen (5 ppm) was already converted to nitric oxide and this is the reason why it is necessary to add $[NO]_{NO=0}$ in the denominator of E 2.10.

Figure 2.40 presents the results for the variation of α_{NO} with variations in the background NO during the oxidation of U-Furnace char and activated carbon when the inputs obtained from Skippy are used. There is no comparison at 20% O_2 for activated carbon, since as it was mentioned above, it was not possible to obtain a solution for the system with Skippy. Two different cases are considered. One in which all the char-nitrogen is assumed to be released as HCN (α_{HCN} = 1) and a second one for α_{HCN} = 0.5. It is important to remember that during these simulations, the release of HCN and NO was assumed proportional to char oxidation; i.e., HCN is released due to the presence of oxygen in the system.

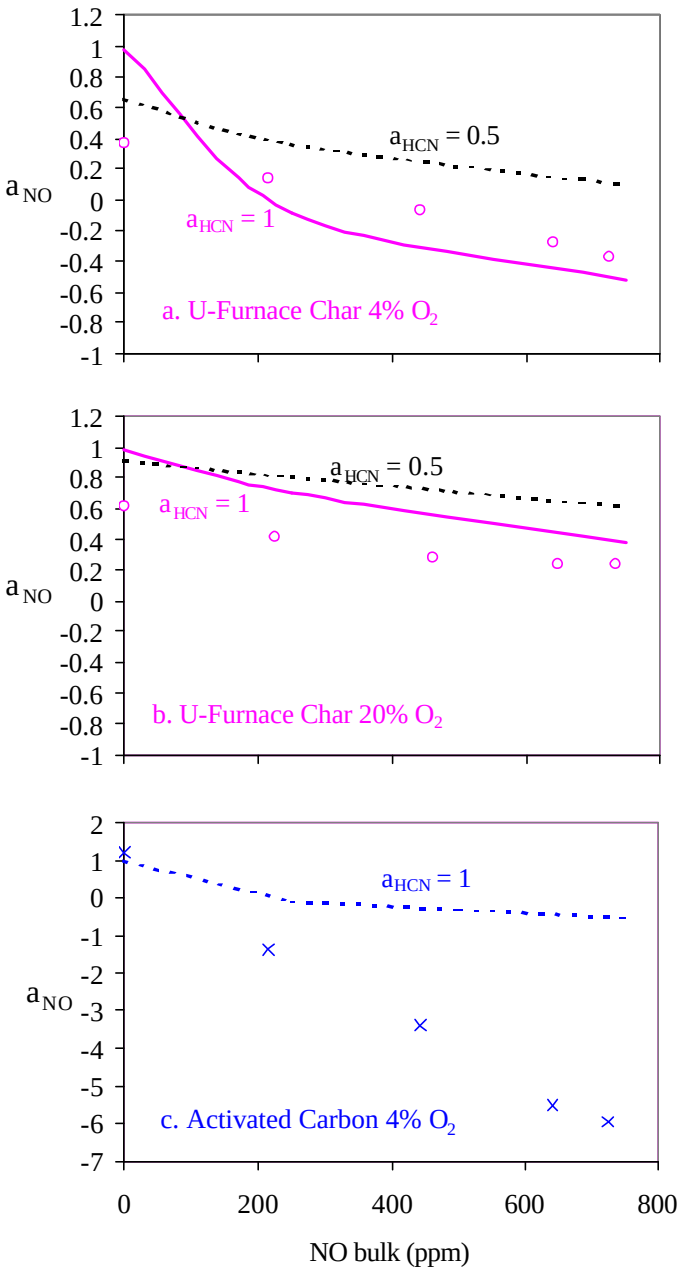

Figure 2.42. Comparison of the variation of the conversion of char-nitrogen to NO with NO in the background for the experiments (symbols) and the predictions after the reactions in the bulk are considered. T_g = 1698 K, Res. time = 0.13 s. 63 – 53μm a. U funrance char 4% O_2, - - : a_{HCN} = 1; ----: a_{HCN} = 0.5 and NO = 80 at NO_{bulk} = 0 b. U-furnace char 20% O_2 - - : a_{HCN} = 1; ----: a_{HCN} = 0.5 and NO = 45 at NO_{bulk} = 0 c. Activated Carbon 4% O_2

For all the cases in Figure 2.40, all the HCN was either reduced to N_2 or oxidized to NO and NO_2. Also the conversion of char-C to CO_2 was always higher than 0.6 at 4% O_2 and .98 at 20 % O_2. A higher residence time increases the conversion to CO_2 but has no influence on the conversion of char-nitrogen to different species. This shows supports the conclusion that the conversion of CO and HCN occurs in the bulk and not in the boundary layer.

When α_{HCN} is one, the predictions are very close to experimental results for U-Furnace char when the nitric oxide background concentration is not zero. It is important to remember that in this simulation there is no fitted parameter. The reduction of nitric oxide occurs from the reaction of HCN with the NO in the background. The more oxidizing the atmosphere surrounding the particle, the higher the oxidation of HCN to NO. Therefore the predicted value of α_{NO} is lower at 4% than at 20 %, again in agreement with the experimental results.

Despite the correspondence between model predictions and experimental results when $\alpha_{HCN} = 1$, the predicted value for α_{NO} is considerable different from the experimental results when the background nitric oxide concentration is zero. This occurs because if there is no nitric oxide in the gaseous phase, HCN is oxidized to NO.

In order to explain this disagreement it is possible to consider the case in which α_{HCN} is less than one. In that case (for instance at $\alpha_{HCN} = 0.5$) the background nitric oxide concentration will not be zero, even if there is not addition of nitric oxide to the gaseous stream. In fact, Figure 2.17 and Figure 2.20 show an average concentration for nitric oxide concentration in the bulk when the background nitric oxide concentration is zero of 80 and 45 ppm at 4 and 20 % O_2 respectively. If the simulation are repeated assuming $\alpha_{HCN} = 0.5$ and a background concentration of 80 and 45 ppm when there is no injection of nitric oxide into the reactor, the predicted value of α_{NO} gets closer to the experimental results at background NO concentration of 0.

In contrast to the relative agreement between the predictions obtained when the reactions of HCN in the boundary layer are considered for the U-Furnace char and the experimental results, the predictions for the activated carbon considerable differ the experimental results. The reason for this that α_{NO} cannot be less than -1 if the nitric oxide is only reduced by the reaction with HCN; i.e., if every atom of char-nitrogen is converted to HCN and then reacts with NO to produce N_2, α_{NO} will be -1. This is different for the case where NO can react with the char surface. In this case the limit on the amount of nitric oxide that can be reduced by the char will be the mass of char, and this number is considerably higher than the nitrogen in the char.

2.6.7 Final Discussion

This objective of this chapter was to explain the why the conversion of fuel-nitrogen to nitric oxide decreased as the background nitric oxide concentration decrease. A first approach to explain this result was by a single particle model that only considered heterogeneous reactions occurring on the char surface. This model predicted the correct trend for the decrease in the conversion of char-nitrogen to nitric oxide. It also predicted more conversion of char-nitrogen at 20% O_2 and lower at 4% O_2 and a low dependence on particle size. However, the magnitude for the reduction of nitric oxide production from the char as the background nitric oxide concentration increases was only predicted correctly, when the rate of nitric oxide reduction on the char surface was two orders of magnitude higher than the results predicted in the literature and found experimentally in the present study.

An alternative model that considered homogeneous reactions in the boundary layer predicted a similar conversion of char-nitrogen to nitric oxide than the SSPM when all the char-nitrogen was assumed converted to nitric oxide. The use of kinetic parameters for the rate of nitric oxide reduction on the char slightly higher than the one used in the SSPM made that the predictions for the activated carbon were closer to experimental

results. However, the predictions for the U-Furnace char were considerably different from the experimental results, unless the rate was increased by two orders of magnitude.

The same model suggested that the reactions in the boundary layer at the conditions of these experiments do not affect the conversion of char-nitrogen to nitric oxide. However, the conversion in the bulk, before the reactions are suppressed in the collection probe has a strong influence in the system.

In particular, if the char-nitrogen is converted to nitric oxide and HCN, the reactions in the bulk can explain the constant decrease of the conversion of char-nitrogen to nitric oxide when the background nitric oxide concentration increases for the U-furnace char. They also explain the reduction on the conversion of char-nitrogen to nitric oxide as the sample size increases.

The comparison of the model predictions with the experimental results suggests that the release of HCN from the particle has an important role on the conversion of char-nitrogen to nitric oxide; in particular for chars with relative low surface area and high nitrogen content. The evidence collected shows that the exclusive heterogeneous reduction of nitric oxide on the char surface cannot account for the steep reduction on the conversion of char-nitrogen to nitric oxide as the background nitric oxide concentration is increased for the U-furnace char, unless the rate of nitric oxide reduction is considerable higher than the one found experimentally. For an activated carbon with low nitrogen content and high surface area, the heterogeneous process can be dominant, but for the U-furnace char the influence of the homogeneous reactions in the bulk is significant.

This suggests that some of the char-nitrogen is released as HCN after char oxidation begins. The experimental evidence and the simulations are not enough to conclude what is the amount of char-nitrogen converted to HCN by direct oxidation of the char. But this number is probably less than one, since when there is not nitric oxide injected in the background the amount of char-nitrogen to nitric oxide is not one as would occur if all the char-nitrogen was released as HCN.

One could expect therefore that some of the nitrogen present in the char will be converted to nitric oxide after direct attack of oxygen to the particle, while other fraction of nitrogen, present in more labile functionalities, is released as HCN and further react in the bulk.

A single particle model that aims to predict the conversion of char-nitrogen to nitric oxide should therefore allow for the conversion of char-nitrogen to HCN. The extent of the HCN conversion to NO or N_2 will depend on the composition of the atmosphere surrounding the particle.

For some chars, as the activated carbon in this case, the heterogeneous destruction of nitric oxide on the char surface is important, therefore this process should also be included in a single particle model. Under certain conditions, where the oxygen concentration is too low to produce the released of HCN from the particle, this mechanism will dominate over the homogeneous reactions of HCN with nitric oxide.

3 PILOT-SCALE STUDIES: INITIAL MEASUREMENTS OF MULTIBURNER FIRING

3.1 INTRODUCTION

In general, low NOx burner development and optimization is performed with a single burner in pilot-scale and commercial-scale test facilities. These burners are subsequently installed in multiple burner arrays in boiler applications and the optimization can thus be invalidated. To assess the impact of switching from single-burner firing to multiple-burner firing, the University of Utah pilot-scale pulverized coal test facility was modified to operate with a three-burner configuration.

Two pilot-scale testing campaigns were carried out to evaluate the impact of multiburner firing of pulverized coal on NOx emissions. In addition, extensive data was collected under a separate Department of Energy program (Combustion 2000 - Low Emission Boiler System - LEBS), using a single pulverized-coal (PC) burner (Eddings, et al. 2000). A range of multiburner operating conditions were explored that were compatible with the single-burner data, and emission trends as a function of air staging, burner swirl and other parameters were studied and will be described below. In addition, a number of burner-to-burner operational variations were explored that provided interesting insight on their potential impact on NOx emissions. Some of these variations include: running one burner very fuel rich while running the others fuel lean; varying the swirl of a single burner while holding others constant; increasing the firing rate of a single burner while decreasing the others.

3.2 EXPERIMENTAL

3.2.1 Pilot-Scale Facility

The University of Utah pilot-scale combustion test furnace referred to as the “L1500” is a nominal 5 MMBtu/hr pilot-scale pulverized-coal-fired furnace designed to simulate commercial combustion conditions. A major objective of this combustion

facility is to study pollutant formation and control, carbon utilization, and ash management in a system which operates similar to commercial boilers. Therefore, the L1500 pilot-scale furnace has the following characteristics:

- Simulates the range of time/temperature histories that are found in commercial units.
- Includes both the ability to fire single or multiple gas burners and/or coal burners.
- Has the provision for evaluating different slag screen designs for improved ash management.
- Has the capability to test different reburning and burnout air injection locations and velocities for emissions control.
- Provides simulated waterwall area (if desired) for deposition studies.
- Has a nominal firing rate of 5 MMBtu/hr with coal.
- Permits multiple locations for coal injection such that coal and/or gas can be used as reburning fuels independent of main firing burner.
- Has adequate sample/observation ports for measuring all inputs and outputs as well as ports to allow detailed species and temperature profiles to be obtained.
- Has a completely instrumented control room adjacent to the facility to control the operation of the furnace and to record and analyze data.

Figure 3.1 is a schematic diagram of the L1500 combustor. The horizontal-fired combustor is 1.1 m x 1.1 m square and nearly 12.5 meters long. The walls have multiple-layered insulation to reduce the temperature from about 1925 K on the fire-side to below 330 K on the shell-side. The combustor is modular in design with numerous access ports and optional cooling panels in each section. This allows the flue gas temperature profile to be adjusted to better simulate commercial equipment. The access ports are used for visual observations, fuel and/or air injection, and product sampling.

The overall combustion facility includes the air supply system, water supply and cooling system, L1500 combustor, fuel supply systems (either gas or coal or both), a flue-

gas cooling chamber, scrubber, and induced-draft fan and a stack. The facility meets all environmental regulations.

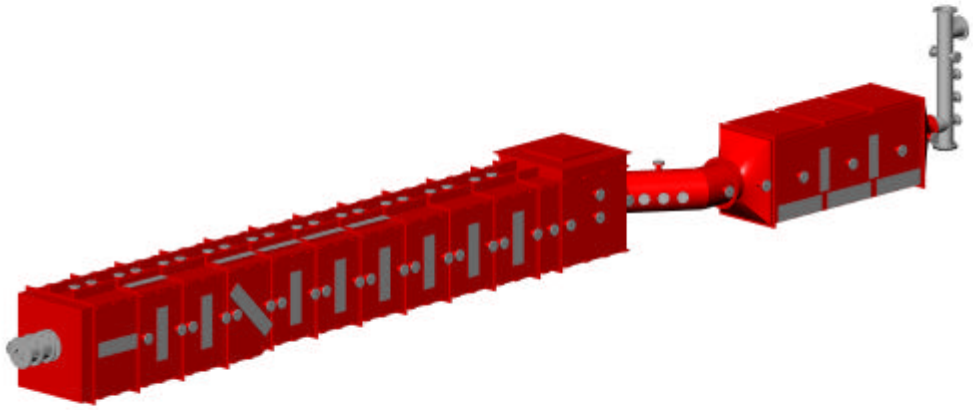

Figure 3.1. The 5 MMBtu/hr multi-fuel combustion test facility at the University of Utah referred to as the L1500 Furnace.

3.2.2 Burner Design

Four 1.5 MMBtu/hr dual swirl block burners (Figure 3.2) were designed to fit on the L1500 Furnace at the University of Utah. This burner design is patterned after an existing 5 MMBtu/hr burner. Each burner has the ability to independently vary the swirl of the secondary and tertiary air from a swirl number (Ratio of tangential momentum to axial momentum) of 0-2 with the use of swirl blocks. The design parameters are described in Table 3.1.

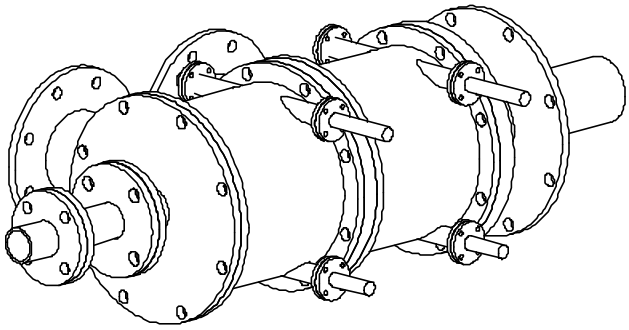

Figure 3.2. Sketch of the dual-register, swirl-block low NOx burner.

Table 3.1. Burner Design Parameters

Nominal Firing Rate	**1.5**	**MMBtu/hr**
Primary Air Stoichiometric Ratio	**0.15**	
Primary Air Velocity	**80**	**ft/sec**
Primary Air Temperature	**150**	**F**
Secondary Air/Tertiary Air Ratio	**33%/66%**	
Secondary Air Swirl Numbers	**0-2**	
Secondary Air Velocity	**85**	**ft/sec**
Secondary Air Temperature	**600**	**F**
Tertiary Air Swirl Numbers	**0-2**	
Tertiary Air Velocity	**115**	**ft/sec**

Each register contains a set of stationary and moveable blocks. Figure 3.3 and Figure 3.4 show how the air can be shifted from an axial direction (no swirl) to a tangential direction (full swirl) by changing the moveable blocks.

At any given time, three burners (top, middle, and bottom) can be in operation. By choosing three burners, the middle burner will be shielded from wall effects and thus give a better indication of the effects of burner-to-burner interaction. Burner wall effects can be determined using the outer two burners.

In an effort to determine the effect of swirl direction, three burners were designed with a clockwise swirl and a fourth burner was designed with a counter-clockwise swirl. The opposite swirl burner can be installed in any of the three positions.

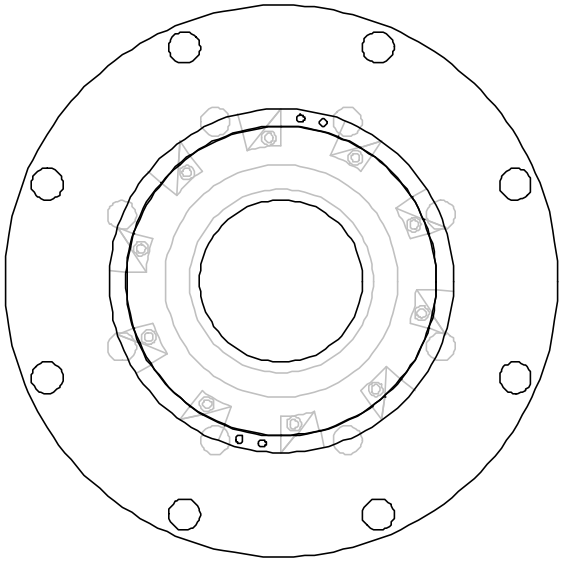

Figure 3.3. Burner swirl blocks in the no swirl position.

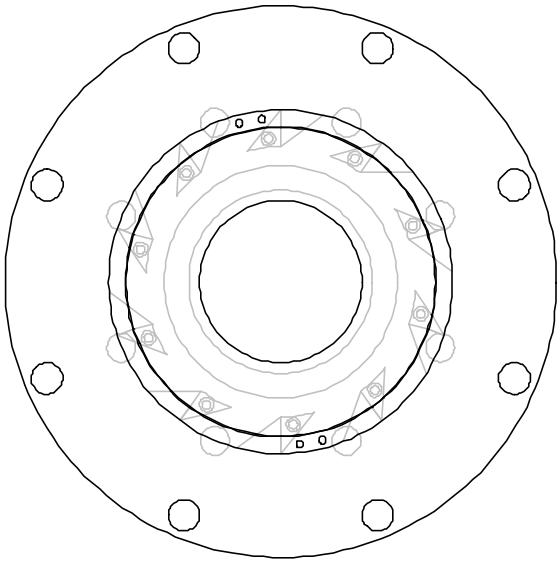

Figure 3.4. Burner swirl blocks in the full swirl position.

Figure 3.5 shows a comparison between the single-burner and three-burner firing configurations. The single 5 million BTU/hr burner is shown on the left, and the three 1.5 million BTU/hr burners are shown on the right. All burners are based on the same low NOx burner design, and scaling to the smaller, multiple burners was performed by matching velocities. The burners are dual-air-register burners, and the innermost air annulus is termed the secondary air stream while the outermost air annulus is termed the tertiary air stream. For most conditions in these tests, 33% of the combustion air was introduced in the secondary and 67% was introduced in the tertiary. An additional amount of air (15% of stoichiometric requirement) was utilized in the primary air stream to convey the pulverized coal.

The coal pipe runs down the center of the burner and has a bluff body along its centerline, resulting in the coal being introduced in an annular region. A small annulus for natural gas injection is located on the periphery of the coal pipe, and unless otherwise indicated a small amount of natural gas (~5% of thermal input) was introduced at this location to assist with flame attachment. The burner swirl is generated by the use of IFRF-type swirl blocks, and there is separate swirl control for the secondary and tertiary air streams. Unless otherwise specified, all tests were performed at a firing rate of 4.5

million BTU/hr with exhaust conditions of 15% excess air. Tests involving burner staging used staging air introduced into section 3 of the L1500, providing a staged residence time of approximately 1 second.

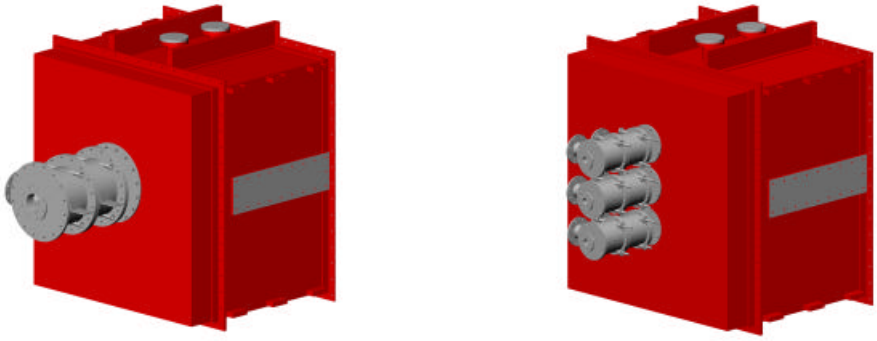

Figure 3.5. Two different firing configurations for the L1500. A single 5 MMBtu/hr burner is shown on the left, and three 1.5 MMBtu/hr burners are shown on the right.

As the burners were being fabricated, the design for the installation and operation of the multiple burners was started. A vertical arrangement of three burners was decided to be the desired configuration for the burners (Figure 3.5b). In this arrangement, there will be both mixing from burner to burner and buoyancy effects. The burner centerlines were spaced on the same distance as the L1500 sample ports. This spacing will provide the best opportunity to obtain centerline emissions profiles along the length of the furnace to determine the mixing characteristics. The burner quarl was designed with a 35^{o} half angle and an L/D=1 to be consistent with the single burner design. Each burner has two one-inch access holes in the quarl angled from the outside of the shell to the quarl for UV peepers and ignition sparkers. An additional peeper was placed down the barrel of each burner for use with gas flames during furnace heat-up and overnight conditions.

Each burner has primary air, secondary air, tertiary air, natural gas, and coal streams which are measured and controlled independently from the other burners. The secondary and tertiary air inputs are independently controlled for both flow and preheat temperature. The flows are measured by V-Cones and are controlled by control valves. The temperatures are controlled with electric heaters and SCR's. The natural gas streams are

controlled by mass flow controllers, which were sized to control the flow for low stabilization gas flows as well as heat-up and overnight conditions. Primary air streams are measured with V-Cones and controlled by control valves before going through an eductor to carry the pulverized coal to the burner. The coal is fed into the eductors with screws from loss-in-weight feeders.

The L1500 furnace previously had only one coal feeder and an associated hopper. In order to accurately control additional coal streams, two additional loss-in-weight feeders were purchased. In addition, new hoppers and slide valves were designed and purchased. The location of the new feed system made for some interesting design problems. The pulverized coal is loaded into the hoppers from bulk solids bags using the building crane. However, the crane stops short of the hoppers, and therefore a trolley was designed to bring the hoppers to the crane (Figure 3.6). When a hopper is empty, the hopper will be disconnected from the feeder, through a soft connection, and rolled out to where the crane can fill the hopper from a new coal bag.

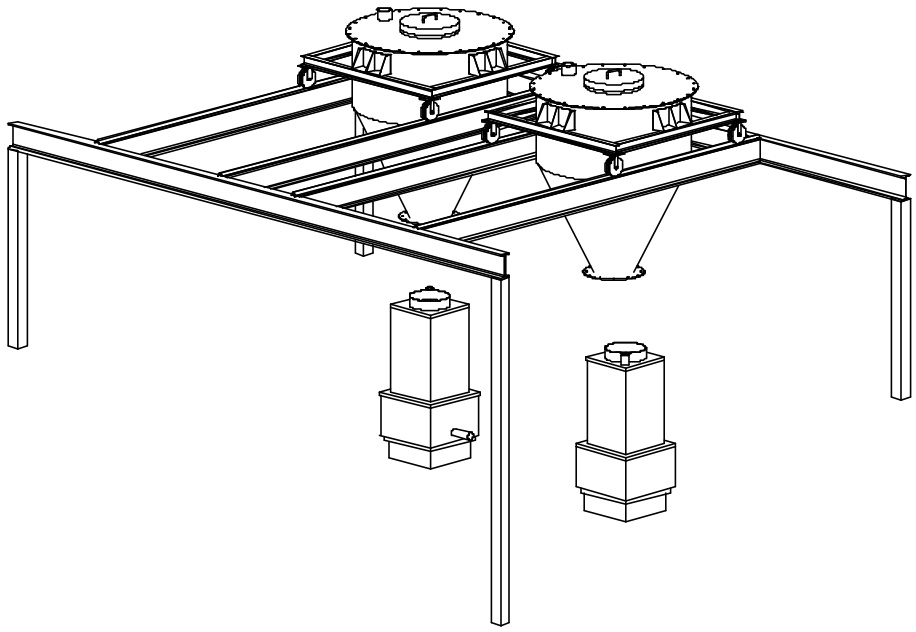

Figure 3.6. New coal feed system with moveable hoppers and feeders.

3.3 RESULTS & DISCUSSION

3.3.1 Effect of Burner Swirl

An initial comparison was made between the two firing conditions under unstaged conditions, and the major firing parameter varied was burner swirl. The results, shown in Figure 3.7, indicate higher NOx emissions for the multiburner scenario. The swirl setting axis refers to a percentage of maximum swirl achievable with the IFRF-type swirl blocks used with these burners. The 100% swirl setting corresponds to a theoretical swirl number of 2. Note that under the condition of totally axial flow (swirl setting of 0%), that both firing configurations yield similar NOx emissions; however, this condition represents optimized burner operation (reflected by the high NOx levels) and does not represent how these burners would be utilized in practice. No combustion air preheat was used for these swirl comparisons; therefore, all flame attachment (and thus NO reduction) was due to the interaction of the swirl setting and the burner quarl geometry.

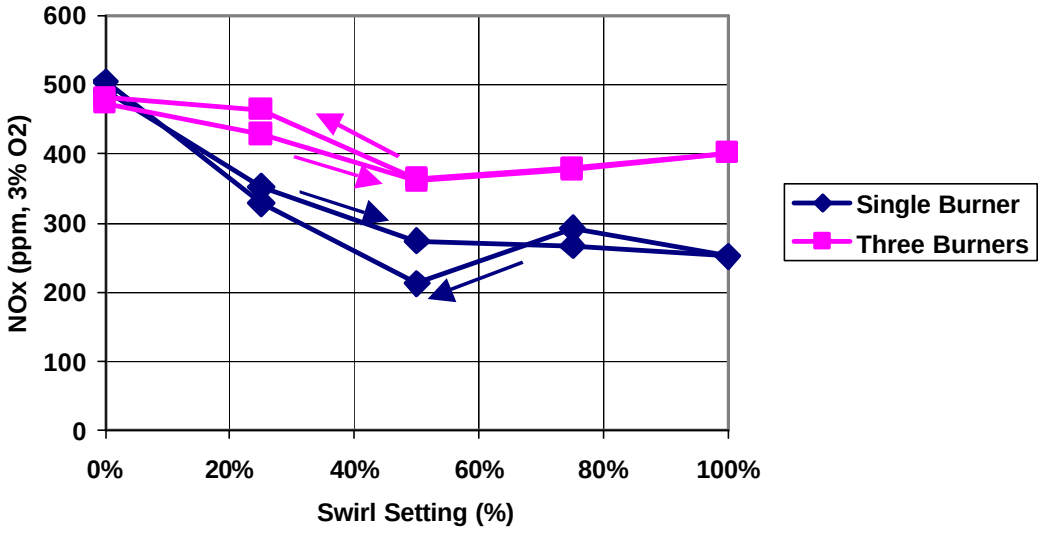

Figure 3.7. Comparison of the effect of burner swirl on single and multiburner firing scenarios under unstaged conditions.

3.3.2 Effect of Air Staging

Both firing configurations were tested under staged conditions to see how the two conditions compared as increasing lower burner zone stoichiometries. The results are shown in Figure 3.8, where it is clear that again the multiburner firing condition yielded higher NOx except at very low burner stoichiometries.

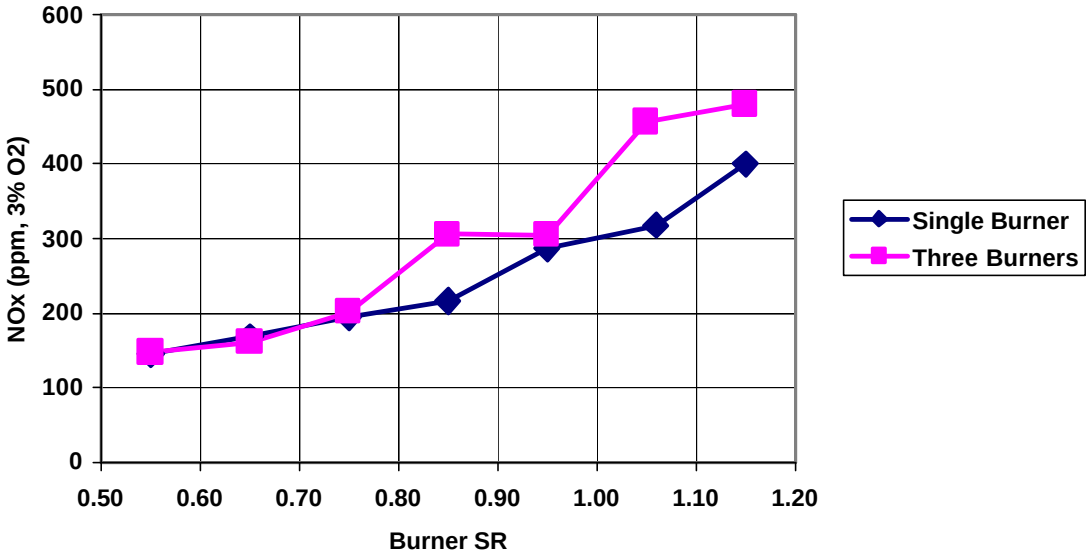

Figure 3.8. Comparison of the effect of air staging on single and multiburner firing scenarios. Burner swirl was set at 25%.

At very fuel rich burner stoichiometries (SR < 0.75), the difference between multiple and single burners became indistinguishable. This result is consistent with previous single-burner data (Eddings et al, 2000) that showed that at very rich stoichiometries the NOx emissions became independent of burner settings such as air distributions, velocities and burner swirl. The explanation of this independence is the removal of large quantities of air from the burner zone to be later introduced downstream for air staging. Once the air flow rates have been reduced substantially, the burner aerodynamics become less significant with respect to NOx formation behavior. The oxidation of fuel nitrogen species such as HCN and NH3 in the burner zone, will be controlled by the level of oxygen entrained into the fuel rich core created by this burner design. An unattached

flame or significant shear layer mixing between the primary and secondary streams can both increase the amount of oxygen in the fuel rich core early in the flame. Typically, low NOx pulverized-coal burners are designed to minimize the possibility of these two phenomena, thereby providing the greatest opportunity for fuel nitrogen decay to N2 in the hot, rich regions of the coal flame. As more and more air is removed from the burner, the probability for flame detachment or significant secondary/primary shear layer mixing is minimized.

3.3.3 Effect of Mismatched Firing Rates

3.3.3.1 Preserving burner stoichiometry

To identify whether a burner mismatch has advantageous or deleterious effects on NOx emissions, a staging curve was run for widely varied firing rates as shown in Figure 3.9. For the mismatched firing rate data, the center burner was operated at 3X the firing rate of the other two, yielding firing rates of (from top to bottom burner) 0.9MM BTU/hr, 2.7 MM BTU/hr and 0.9 MM Btu/hr. The increases and decreases in firing rate were accomplished by increasing both fuel and air flow rates; therefore, the burner stoichiometries were held constant relative to each other. As shown in the figure, the burner mismatch provided similar NOx levels for most burner stoichiometries. The 3X middle firing rate case appeared to be slightly lower under most conditions, but there was a fair amount of scatter in the uniform curve. There was no attempt to optimize the burners during these tests, as the burner swirl settings were held constant. As noted with the single versus multiburner comparison, the differences at very low stoichiometries are even less than at higher stoichiometries due to the large amount of air that has been removed from the burners.

For the unstaged condition (SR=1.15), it appeared that NOx emissions were slightly higher with a burner mismatch, even though the staged cases appeared to yield slightly lower values. Additional data were taken to further explore this behavior using both a 2X and a 3X increase in middle burner firing rate, as shown in Figure 3.10. Each condition was run under a range of swirl settings to try and obtain optimal burner conditions for

stability and low NOx. Also, the overall firing rate was held constant at 4.5 MM BTU/hr for all three data sets. As shown, a factor of 2 mismatch in burner firing rates did not provide a significant increase in NOx emissions under unstaged conditions; however, a factor of 3 mismatch resulted in a very notable increase in NOx emissions.

Recall that the experimental conditions for Figure 3.9 and Figure 3.10 involved preserving burner stoichiometries when firing rates were varied. Thus, even though mixing in regions between burners would vary due to increases in air velocity in the center burner, the overall stoichiometry in the core of each flame was unlikely to be changed significantly until much further downstream. This change would occur downstream since the core flame conditions at the exit of the coal pipe were the same for all three burners initially and would only vary further downstream due to the increased shear mixing between burners with the center burner firing at a higher rate.

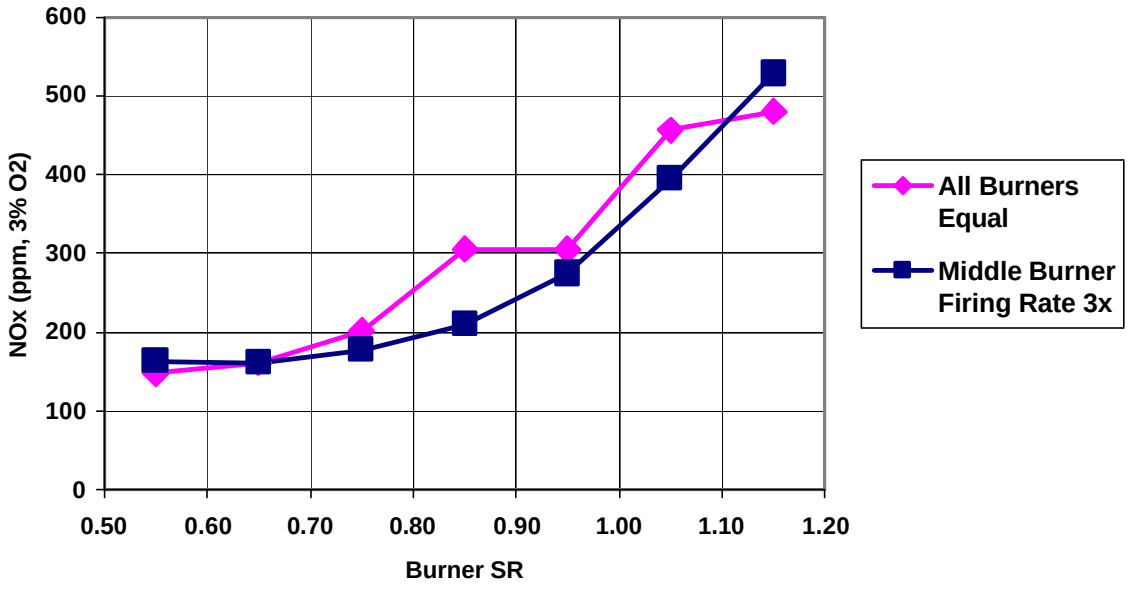

Figure 3.9. Effect of mismatched firing rates on NOx emissions over a range of burner stoichiometries.

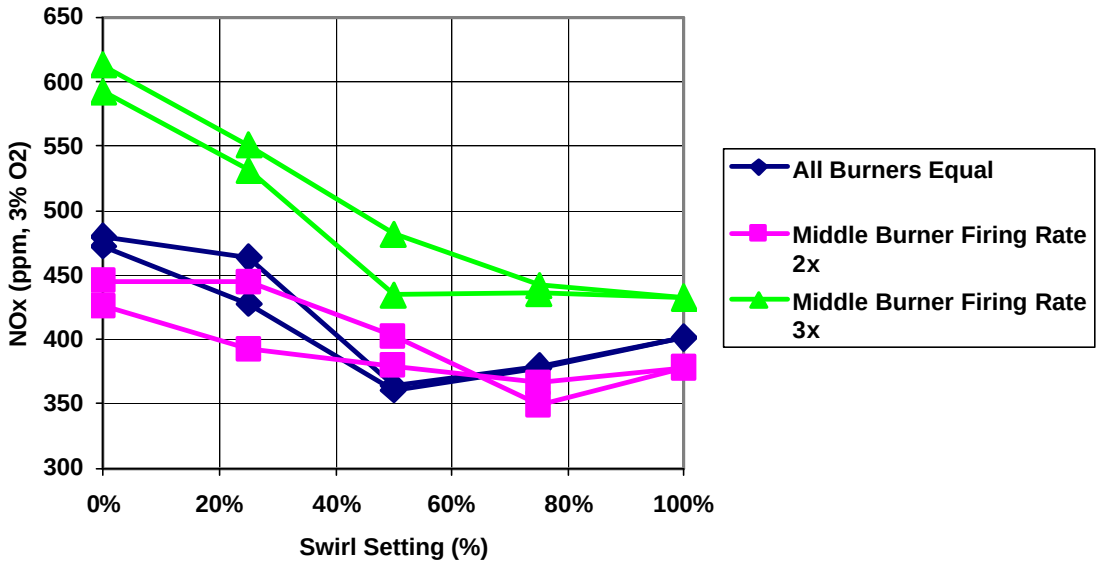

Figure 3.10. Effect of mismatched firing rates on NOx emissions using constant burner stoichiometries under unstaged (SR=1.15) conditions.

3.3.3.2 Variable burner stoichiometry

Additional tests were carried out on the effect of mismatched firing rates under conditions were the burner stoichiometry was not preserved. In practice, burner mismatch in a boiler is more likely to occur due to an increase or decrease in coal flow rate, with the air flow rate to individual burners remaining relatively constant. Since different elevations of burners are typically fed from different pulverizers, it is not uncommon to have some variations in fuel feed rate in the vertical direction. In the previous tests, the air flowrates were changed to match changes in the coal feedrate to preserve burner stoichiometry. Thus, additional tests were performed where the air to each of the three burners remained evenly distributed between them, and the coal feed rate was increased in the center burner with corresponding decreases in the top and bottom burners. These tests were carried out under staged (SR=0.90) and unstaged (SR=1.15) burner conditions, and the results are shown in Figure 3.11and Figure 3.12. The swirl setting for all three burners was varied as the independent parameter for a given firing configuration, to identify the optimal setting for lowest NOx.

As shown in the figures, there is a clear trend of increasing NOx with an increase in coal feed to the center burner. This trend was evident for both the unstaged and staged configurations. Also, higher swirl settings appeared to yield lower NOx for the multiburner configuration, and for the quarl and burner designs utilized in this facility.

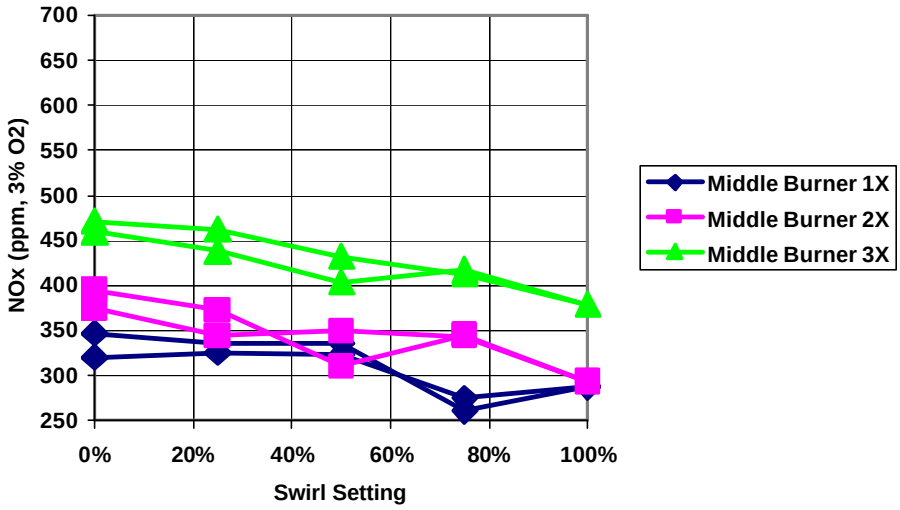

Figure 3.11. Effect of mismatched firing rates on NOx emissions using variable burner stoichiometries for staged (SR=0.90) conditions.

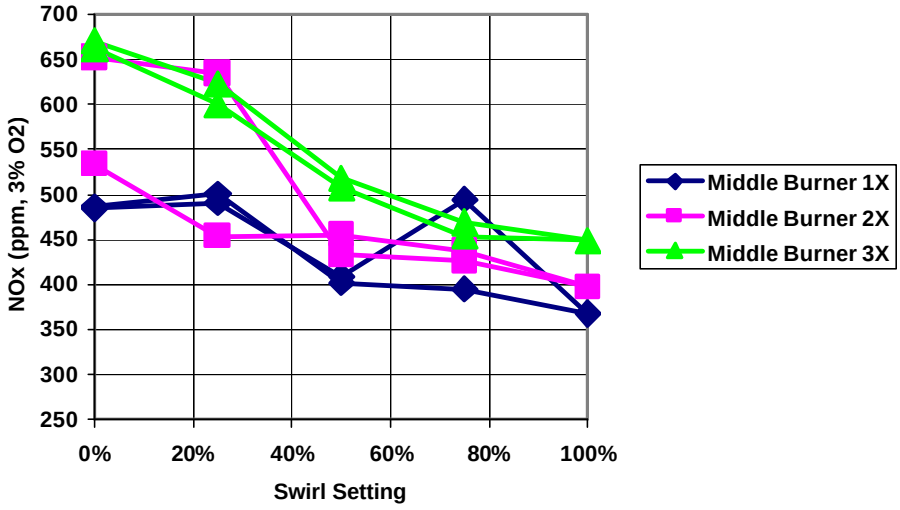

Figure 3.12. Effect of mismatched firing rates on NOx emissions using variable burner stoichiometries for unstaged (SR=1.15) conditions.

3.3.4 Effect of Burner Biasing

The previous set of experiments described the effect of varying the coal feedrate between the different burners, resulting in a firing rate mismatch. This section describes experiments in which the coal feedrate was constant, thus preserving individual burner firing rates, but the combustion air flowrates were varied. The use of burner biasing, where some burners are operated fuel rich and others are operated fuel lean, represents a condition that could have potential for NOx reductions. In practice, one would envision operating lower levels of burners in a boiler under fuel rich conditions, and bias the additional air to upper levels of burners yielding an effectively staged system (in the absence of overfire air). To explore this possibility, tests were performed using two different biasing scenarios. The overall burner zone stoichiometry was held constant at 1.15 (thus no overfire air was used), with the center burner being operated fuel rich and the upper and lower burners being operated fuel lean. The first scenario represented mild biasing, with the middle burner operating at SR=0.95 and the outer burners operating at SR=1.25. The second scenario represented very severe biasing, with the middle burner operating at SR=0.65 and the outer burners operating at SR=1.40. The results, shown in Figure 3.13, indicate a minimal impact using the mild biasing scenario (middle burner SR=0.95). The severe biasing scenario, however, shows some promise for NOx reductions. There is a significant amount of spread in the data at low levels of swirl, indicating the highly unstable flames produced with the biasing. However, at high levels of swirl the spread in the data is minimal and the severe biasing configuration provides consistently lower NOx.

There are some differences between this pilot-scale evaluation and a commercial application; most notably, the ability to bias in the direction of flow. Thus, although very rich stoichiometries were required in the middle burner to demonstrate a reduction, it is anticipated that in practice the application of biasing would prove effective with less severe disparities between burners. The ability to operate with lower burner levels fuel rich followed by very lean upper burners should provide significant NOx reduction. Such biasing has been shown to provide some degree of NOx reduction in Cyclone-fired coal boilers, although it was proven to be less effective than actual staging with overfire air

use (Adams, et al. 1999). This difference is likely due to the difference in rich zone residence time. Thus, large boilers with many levels of burners may be able to achieve greater NOx reductions using biasing due to the ability of maintaining a fuel rich zone for longer residence times.

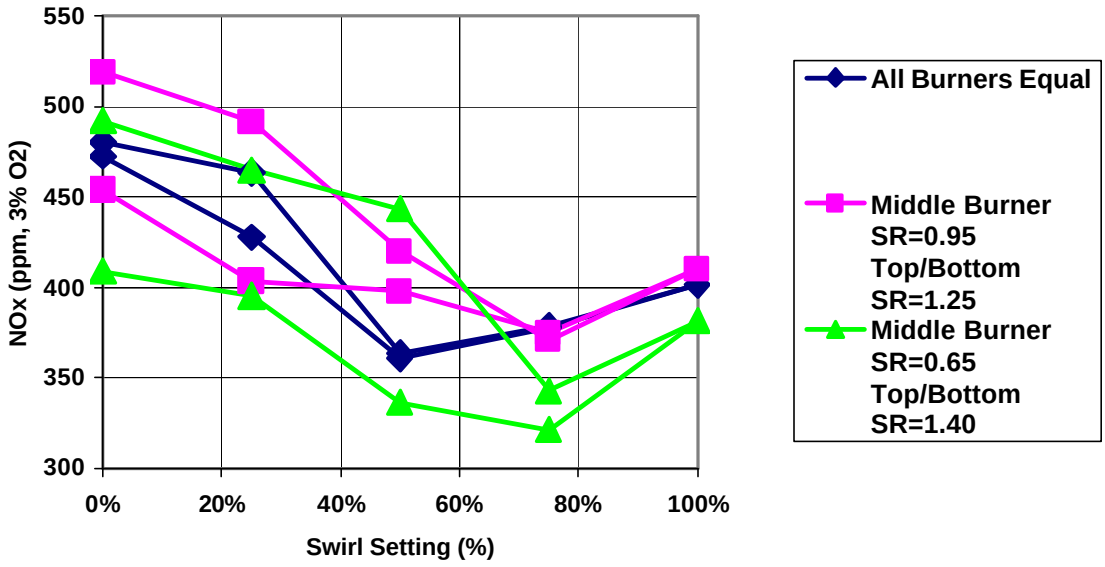

Figure 3.13. Effect of burner biasing on NOx emissions. Burner firing rates were held constant (same coal mass flow) while air flow rates were varied.

3.4 CONCLUSIONS & RECOMMENDATIONS

A pilot-scale testing campaign was carried out to evaluate the impact of multiburner firing on NOx emissions. Extensive data had been previously collected using a single pulverized-coal (PC) burner, and this data was thus available for comparison with NOx emissions obtained while firing three burners at the same overall load and operating conditions. A range of operating conditions were explored that were compatible with the single-burner data, and the emission trends as a function of air staging, burner swirl and other parameters were compared. In addition, a number of burner-to-burner operational variations were explored to provide insight on their potential impact on NOx emissions.

In general, the results indicated that multiburner firing yielded higher NOx emissions than single burner firing at the same fuel rate and excess air. At very fuel rich burner stoichiometries (SR < 0.75), the difference between multiple and single burners became indistinguishable. This result is consistent with previous single-burner data that showed that at very rich stoichiometries the NOx emissions became independent of burner settings such as air distributions, velocities and burner swirl (Eddings et al., 2000).

Comparisons were made exploring a mismatch in individual burner firing rates to identify any positive or negative impact. Two different approaches to firing rate mismatch were used: 1) where individual burner stoichiometries were held constant (changing both coal and air flowrates); and 2) where individual burner stoichiometries were varied (changing coal feedrate only). In both approaches, the center burner firing rate was increased up to as high as 3X that of baseline, and the upper and lower burner firing rates were decreased to maintain an overall constant firing rate. In general, a 3X increase in firing rate in the center burner resulted in a notable increase in NOx emissions for both staged and unstaged conditions. This effect was observed for both constant and variable burner stoichiometry conditions. Note that a 2X increase in firing rate in the center burner resulted in minimal differences from uniform operation.

Some conditions were identified where NOx emissions could be reduced in a multiburner firing scenario; specifically, through the use of burner biasing. If the middle burner was operated very fuel rich, with the outer burners operated at high excess air levels to compensate, the overall NOx emissions were lower than when all burners were operated with equal air/fuel flow rates. Burner parameters such as swirl had to be optimized, however, to achieve stable operation. This approach yielded NOx emissions that were slightly lower than the single burner data under unstaged conditions; however, the application of such severe biasing should be evaluated in the context of corrosion, deposition, or other potential adverse affects in the near burner region. A commercial application would be likely to demonstrate a greater effectiveness at less severe biasing due to the ability to bias in the direction of gas flow. In other words, a vertical staging effect could be accomplished without the use of overfire air.

4 COMPUTATIONAL MODELING

4.1 APPLICATION OF COMPREHENSIVE MODELING

A comprehensive combustion code was used to simulate the reacting flow of the pilot scale pulverized coal facility and a 500 MW utility opposed wall fired boiler.

4.1.1 Computational Tool

The computational tools used in this study were developed to address the operational and design considerations of a wide range of combustion systems including, but not restricted to, utility boilers. The current models simulate reacting flows and particles, including gaseous diffusion flames, pulverized-coal flames, liquid sprays, coal slurries, injected sorbents, and other oxidation/reduction systems. In particular, emphasis has been placed on simulating coal combustion and pollutant formation. *GLACIER*, a three dimensional, two-phase reacting flow code includes several capabilities necessary for accurate simulation of coal-fired boilers. These capabilities include turbulent, particle transport with full coupling of particle and gas phase mass and momentum; coal reaction processes such as devolatilization, char oxidation and gas-particle interchange; NOx formation/reduction chemistry; particle convection and radiation with absorption, emission and anisotropic scattering; full coupling of gas-particle energy exchange; and ash deposition. In addition, boiler-side waterwall and radiant panel surface temperatures can be predicted as part of the computation, given a back-side (i.e., steam) temperature and surface resistance (from the deposit thickness and thermal conductivity, for example).

4.1.2 Pilot Scale Furnace Modeling

The pilot scale furnace of the University of Utah, known as the L1500 furnace, was simulated. The facility, described in the previous section of this report, was configured to fire coal using three burners at 1.5 MM Btu/hr each. The impact of the direction of burner swirl was investigated. Two arrangements were modeled:

Arrangement 1 had all three burners rotating clockwise looking from the burners toward the exit.

Arrangement 2 had all two burners rotating clockwise and the center burner rotating counterclockwise looking from the burners toward the exit.

The operating conditions are given in Table 4.1. The agreement between the measured and predicted axial temperature profiles (Figure 4.1) is good. The predicted results are shown in Figure 4.2 through Figure 4.4. All these figures show contours in the vertical plane passing through the burner centerlines. Figure 4.2 through Figure 4.4 show the gas temperature, oxygen, and CO distributions, respectively. Comparison of Figure 4.2, Figure 4.4 and Figure 4.5 demonstrates that the flame shapes have been well simulated. The flames shown are well attached.

The flames all look similar with all the burners having equal direction of swirl. The effect of changing the sense of the center burner swirl is seen in Figure 4.2 through Figure 4.4. The opposite direction of swirl in the center burner causes the bottom two flames to move slightly downward.

Table 4.2 gives the predicted effluent results. The temperatures, oxygen and NOx are in reasonable agreement with the measured data. Changing the direction of swirl of the center burner reduced the NOx by about 7.5%. The exit temperature, O_2, and CO where essentially unchanged. This reduction in NOx, though small, is the effect of changes in mixing between the burners.

4.1.3 Utility Furnace Modeling

The unit modeled is a 500 MWe opposed-wall-fired furnace with 24 burners, three rows and four columns on each wall. Prior to a low-NOx retrofit, the unit was fitted with Intervane burners. During the retrofit the burners were replaced by low NOx burners. In addition, an advanced overfire air (OFA) system was installed. This consists of an independent wind box for improved penetration/control of OFA injection through 8

directly opposed ports above each column of burners, and 4 underfire air ports at the level of the bottom burner row near the walls. After retrofit, NOx emissions from this unit were decreased but there was a significant increase in the level of unburned carbon.

The test conditions that were used for the pre- and post-retrofit simulations are presented in Table 5. The proximate and ultimate analyses for the coal used for the simulations are shown in Tables 6 and 7, respectively. The coal size distribution for the pre-retrofit case was 64% through 200 mesh and 97.6% through 50 mesh. The corresponding percentages for the post-retrofit conditions were 72.6% and 99%, respectively.

Ten variations from the post-retrofit conditions were modeled:

1 Base Case - actual test conditions including non-uniform secondary air distribution and non-uniform coal distribution at coal pipe exit (post-retrofit conditions).

2 Top-row Classified - in order to remove large particles from the worst burners with the least investment, the particle size distribution typical of a rotary classifier was used on coal supplied to the upper row of burners.

3 Top-row Intervanes - burner coal distribution nozzles based on the intervane design were considered for the upper burner row on both walls.

4 Reversed Outer Burners - coal pipe inlets in the outer columns were flipped 180° to direct the heavier particle loading towards the interior of the furnace in order to avoid a large number of particles in the side wall/wing wall gap.

5 60/40 SA (secondary air) - the secondary air split was changed to 60/40 between the outer and inner burner columns. (The split was 55/45 in the base case).

6 MFA (midfire air port) Ports - a midfire air port near the side wall between the middle and upper burner rows was added.

7 Front MFA Ports - a midfire air port near the side wall between the middle and upper burner rows (front wall only) was added.

8 No OFA - the OFA ports were removed and the air was redistributed to all the burners and underfire air ports.

9 No OFA or UFA (underfire air) - the overfire air ports and underfire air ports were removed with redistribution of the air to all the burners.

10 High UFA - a 50% increase in the front wall underfire air port flow was made with air taken from the twelve burners on the front wall.

Case 2 contemplated the removal of the split flame coal pipe with an intervane coal pipe without modifying the burner throat or air registers. In Case 3 the coal distribution was changed so that the higher loading was toward the center of the furnace. The intent of this modification was to reduce the coal particle density in the region close to the side wall. In the baseline 55 % of the secondary went to the outer columns and 45% to the inner. In Case 4 this bias was increased to 60% in the outer columns and 40% in the inner. Cases 5 and 6 contemplated the addition of air ports between the middle and upper burner rows adjacent to the side wall. Case 5 added ports on the front and rear walls, but only the front ports are open in case 6. In both cases the overall air flow is constant and the midair ports draw air from the overfire air. Cases 7 and 8 investigated different staged air scenarios. In Case 7 the OFA was eliminated and the air redistributed to the burners and the underfire air (UFA) ports. Finally, in Case 9 the UFA flow was increased by 50%.

The results of these simulations are summarized in Table 5 which the lists predicted NOx emissions.

The objective of this study was to determine the effect burner interactions of the different scenarios, all at a constant overall excess oxygen level of 3.1%, would have on NOx emissions. Carbon-in-ash was also evaluated. From Table 8, two cases showed significant increase in NOx emissions, Case 2 and Case 8, as might be expected.

Case 2 changed the coal pipe on the upper row of burners improving the initial coal/air mixing, increasing NOx emissions and reducing carbon-in-ash somewhat. Therefore, it can be concluded that increasing the mixing in the top burners to reduce LOI elevates NOx that cannot be compensated from low NOx burners below.

Reversing swirl of the outer burners (Case 3) had essentially no effect on the NOx. Case 4 addressed the interaction from increasing the air bias between columns of burners. A slight reduction was predicted in the NOx emissions with this increase in bias. The further staging of the inner burners more than compensates for the reduction in staging in the outer burners. This is one of the more promising approaches for this furnace as the carbon-in-ash was significantly reduced.

Adding midfire air ports (MFA) (Cases 5 and 6) slightly increased NOx even though the burner belt stoichiometry was lower. High Underfire air (UFA) flow (Case 9) produces only minor variations in NOx but also improves carbon-in-ash.

Eliminating both the OFA and UFA (Cases 7 and 8) increased NOx as expected. However, the simulations suggest that a 50% reduction compared to the pre-retrofit (not presented) is possible with low-NOx burners; but OFA can give a further significant reduction of approximately 25%.

Combinations of the two approaches of Cases 4 and 9 could prove to be most effective. They are also, potentially low-cost options with little to no capital expenditures required.

4.2 CPD MODEL IMPLEMENTATION/APPLICATION

The Chemical Percolation Devolatilization (CPD) Model (Genetti, 1999) has been incorporated into *GLACIER* and has been used to predict coal particle volatile yields as compared to those of the original two-step devolatilization model of *GLACIER* (Kobayashi et al., 1976) for a simple simulation with Illinois #6 coal. Particle temperatures input to the CPD model are predicted by *GLACIER*. Volatile yields

predicted by the CPD model are not coupled back into *GLACIER*, since *GLACIER* accounts for only one reacting volatile stream and the CPD model distinguishes between two streams, tar and light gas.

A reacting flow simulation was performed with Illinois #6 coal. A sample CPD input file for Illinois #6 coal file provided inputs required by the model. Coal properties for Illinois #6 coal, compiled by Fletcher and Hardesty (1992a) and tabulated in Table 4.3, were used in the simulation. The two-step coal devolatilization rate parameters of Ubhayakar et al. (1976) were used by G*LACIER.*

The simulation was performed with 60 μm coal particles in a 10 cm square tube of 1.0 m. length. Coal particles entered the tube at 350 K. and tube walls were held at a constant temperature of 800 K. Air entered the tube at a mass flow rate of 0.01 kg/s and a temperature of 700 K. The simulation was performed at a stoichiometry of 1.9.

Comparisons of volatile yield predicted by the CPD model and by *GLACIER* are shown in Figure 4.6. The times of onset of devolatilization and the overall volatile yields predicted by the two models are comparable. However, the initial devolatilization rate predicted by the CPD model is steeper than that predicted by *GLACIER* and the duration of devolatilization is longer.

4.3 SOOT MODEL IMPLEMENTATION/APPLICATION

The soot model for coal-fired system developed by Brown et al. (1998) has been implemented into *GLACIER* and applied to a pilot-scale test furnace at the University of Utah Combustion Research Laboratory. The soot model is made of three transport equations for tar mass fraction, soot mass fraction, and the number of soot particles per unit mass. Tar evolution is calculated from the CPD model (Fletcher et al., 1992b).

Utah coal was fired at a firing rate of 4.1 MMBtu/hr in the pilot-scale test furnace equipped with a dual-swirl coal-fired burner. Burner and overall stoichiometries were 0.86 and 1.1, respectively. The mass mean particle size was 68.0 μm, coal feeding rate

was 152.4 kg/hr, primary air rate was 205.5 kg/hr, secondary air rate was 327.2 kg/hr, tertiary air rate was 653.9 kg/hr, and staging air rate was 349.0 kg/hr. The staging air port was located at 3.25 meter from the burner exit. Utah coal is a bituminous coal and its proximate and ultimate analysis results are shown in Table 4.4.

The selected simulation results at a middle cross-section of the test furnace are shown in Figure 4.7. Tar starts to form from coal devolatilization close to the burner as shown in Figure 4.7-a. At the same location, soot volume fraction and number density increase as tar is being converted to soot. Soot volume fraction, then, decreases due to oxidation. Soot number density also decreases due to oxidation and agglomeration of soot particles. Upon additional air introduction at the staging port, complete soot oxidation occurs. Figure 4.8 shows average soot volume fraction and oxygen concentration as a function of distance from burner exit. At close to burner, oxygen is rapidly consumed by coal combustion. Soot oxidation starts at around 1 meter from the burner exit and this further decrease oxygen level. Additional air input at staging port completes soot oxidation.

According to the work of Veranth (2000), about 0.2 ~ 0.6% of fuel carbon forms soot (or small size char) for low-NOx burner conditions with bituminous coal. Soot volume fraction before staging air, then, is about $1.0 \times 10^{-7} \sim 3.1 \times 10^{-7}$. Estimated average soot volume fraction before the staging port from *GLACIER/SOOT* is about 1.2×10^{-7}.

Table 4.1. Operating Conditions

	lb/hr
Coal Carrier Air	450
Secondary Air	1100
Tertiary Air	2200
Natural Gas	10.8
Coal	318
S.R.	1.15

Table 4.2. Model Effluent Results

	Arrangement 1	Arrangement 2
Exit Gas Temp., K	1427	1423
Exit CO, dry ppm	15	16
Exit O2, %	3.0	3.0
Exit NOx, dry ppm	421	390
Exit NOx, ppm@3% O_2	421	390

Table 4.3. Illinois #6 Coal Properties

(Fletcher and Hardesty, 1992a)

	Mass Weight
C	59.98 %
H	3.78 %
O	7.38 %
N	1.15 %
S	4.51 %
ash	13.77 %
moisture	9.43 %
HHV	10,835 Btu/lb

Table 4.4. Properties of Utah Coal (As received)

	wt%		wt%
Fixed Carbon	45.46	C	69.65
Volatile Matter	39.42	H	4.42
Moisture	4.68	O	9.16
Ash	10.44	N	1.25

		S	0.40
HHV	12,303 Btu/lb	ash	10.44
		Moisture	4.68

Table 4.5. Summary of Utility Furnace Operating Conditions

Component	Pre-Retrofit	Post-Retrofit
Coal	42.5 kg/s	44.8 kg/s
Primary Air	113.4 kg/s	105.4 kg/s
Total Secondary Air	393.3 kg/s	408.5 kg/s
Secondary Burner Air		269.3 kg/s
Overfire Air		106.8 kg/s
Underfire Air		32.4 kg/s
Excess Oxygen	1.90%	3.10%
Burner Stoichiometric Ratio	1.1	1.18

Table 4.6. Proximate Analysis of the Coal Used in Utility Furnace

Component	Mass Percent
Fixed Carbon	51.70%
Volatile Matter	33.10%
Ash	9.10%
Moisture	6.10%

Table 4.7. Ultimate Analysis of the Coal Used in Utility Furnace

Species	Mass Percent
C	71.40%
H	4.70%
O	5.80%
N	1.40%
S	1.70%

Table 4.8. Summary of Parametric Cases

Case	NO, ppm	Burner Belt Stoichiometry
1 - Base	351	0.87
2 - Top row intervane coal pipe	421	0.87
3 - Coal pipe inlets reversed in outer burners	350	0.87
4 - 60/40 secondary air split	345	0.87
5 - MFA port on front and rear walls	354	0.8
6 - MFA port on front wall only	362	0.83
7 - No OFA port	380	0.92
8 - No OFA port and UFA port	447	1.19
9 - High UFA ports	376	0.83

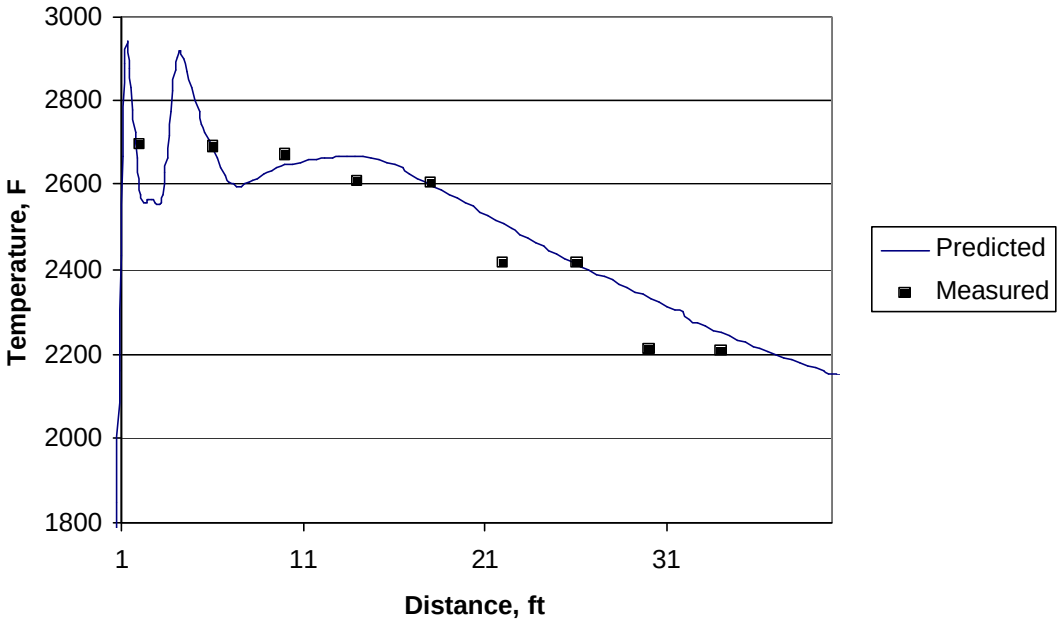

Figure 4.1. Comparison of Predicted and Measured Axial Temperature Profile.

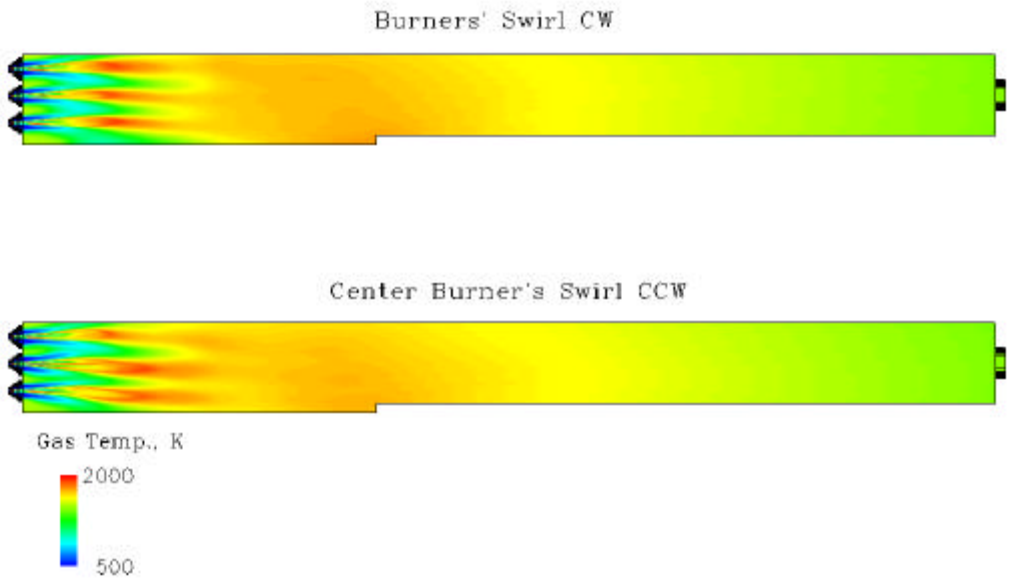

Figure 4.2. Predicted gas temperature distribution.

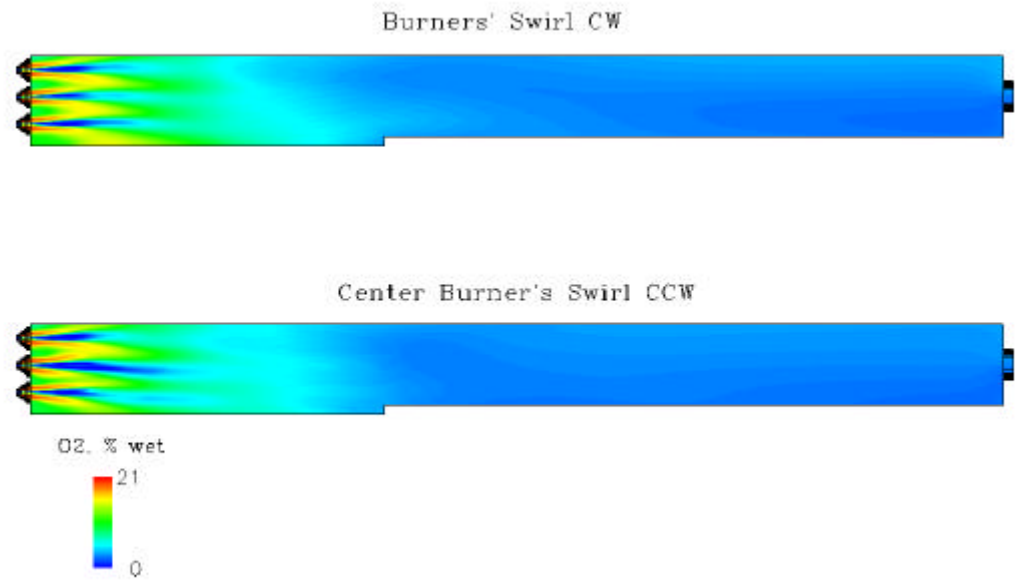

Figure 4.3. Predicted Oxygen concentration distribution.

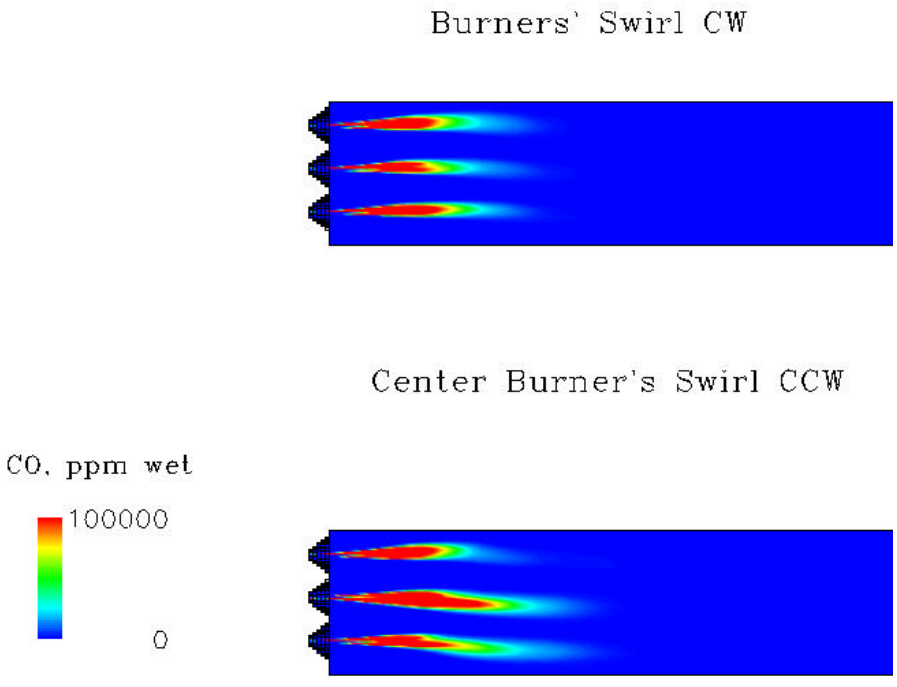

Figure 4.4. Predicted CO distribution.

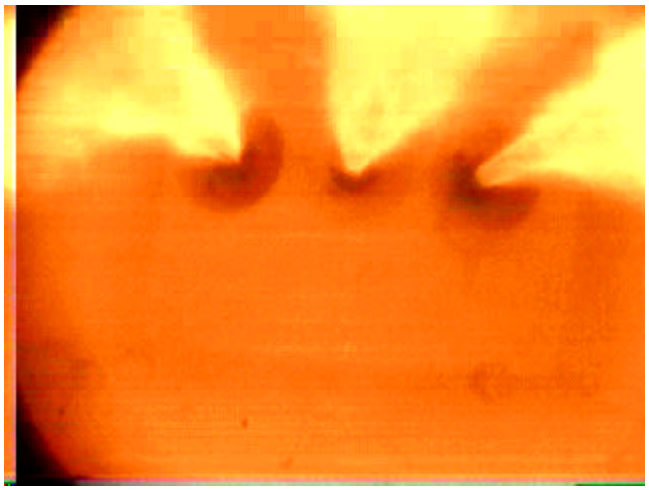

Figure 4.5. Flame images taken with all burners at full load, 1.5 MM Btu / hr.

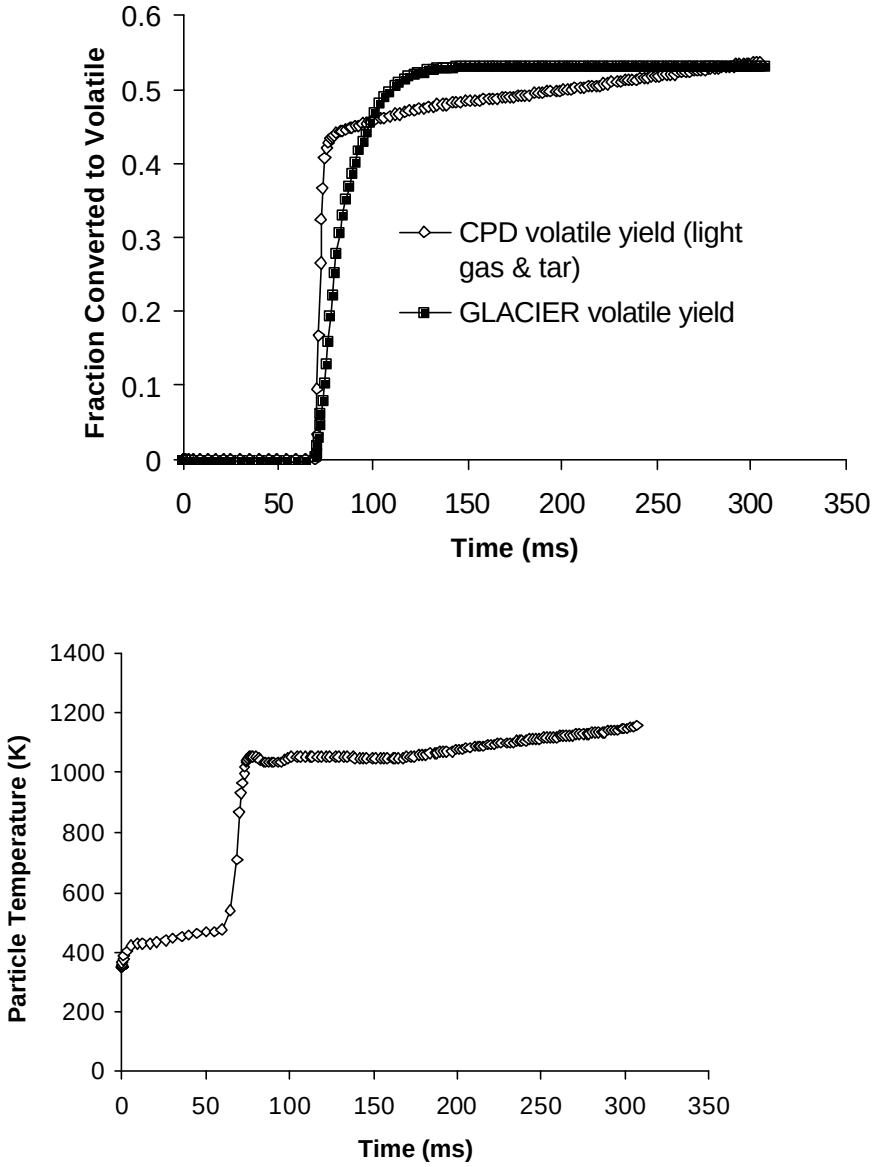

Figure 4.6. Volatile yields and particle temperature as a function of residence time.

a) Tar mass fraction

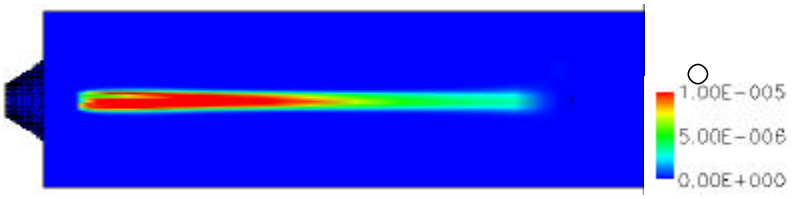

b) Soot volume fraction

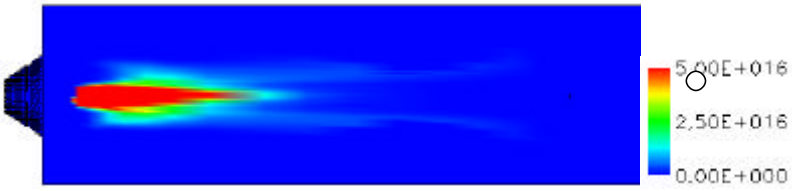

c) Soot number density [particles/m^3]

Figure 4.7. Selected *GLACIER/SOOT* simulation results at a middle cross-section of the test furnace: a) Tar mass fraction, b) soot volume fraction, c) soot number density, and d) O_2 concentration (Vol %). Staging air port is marked with a circle.

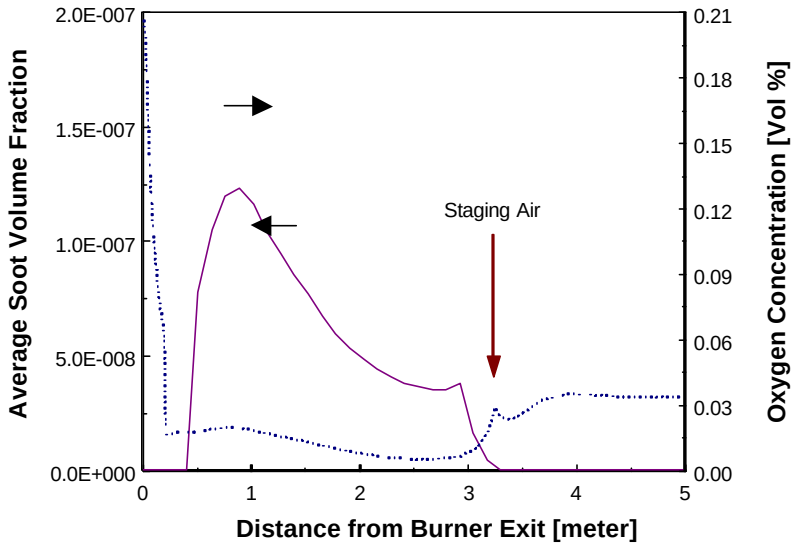

Figure 4.8. Average soot volume fraction and volumetric oxygen concentration as a function of distance from burner exit.

5 REFERENCES

Aarna, I, and Suuberg, E.M. Energy & Fuels 1999, 13, 1145

Aarna, I. and Suuberg, E. Fuel 1997, 76, 475

Aarna, I. and Suuberg, E. Twenty-seventh Symposium (International) on Combustion/ The Combustion Institute 1998, 3061

Abbasi, M., "Mechanistic and Kinetic Aspects of Nitrogen Oxides Formation in Coal Char and Model Char Oxidation Processes", Ph. D. Thesis. University of Utah, 1999

Adams, B. M. Heap, R. Shah, D. O'Connor, W. Bakker, "Computational Evaluation of NOx Reduction and Associated Operational Impacts in Cyclone-Fired Boilers," proceedings of the Joint EPRI/EPA/DOE Combined Utility Air Pollutant Control Symposium, Atlanta, GA, Aug. 16-20, 1999.

Aho, M. J., J. P. Hamalainen, and J. L. Tummavuori, "Conversion of Peat and Coal Nitrogen through HCN and NH3 to Nitrogen Oxides at 800oC." Fuel 72: 837-841 (1993).

Alzueta, M., Bilbao, R., Millera, A., Glarborg, P., Østberg, M. and Dam-Johansen, K. Energy & Fuels 1998, 12, 329 - 338

Åmand, L.-E. and Leckner, B. Energy & Fuels 1993, 7, 1097-1107

Ashman, P.J., Haynes, B.S., Buckley, A.N. and Nelson, P.F. Proceedings of the Combustion Institute 1998, 27, 3069-3075

Ashman, P.J., Haynes, B.S., Nelson, P.F., Nancarrow, P.C., Bus, J., Nicholls, P.M., Prokopiuk, T., Buckey, A.R., and Li, C.Z., "Improved Techniques for the Prediction of NOx Formation from Char Nitrogen", ACARP Report No. C4065, 1999

Ashman, P.J., Haynes, B.S., Nicholls, P.M. and Nelson, P.F. Proceedings of the Combustion Institute 2000, 28, 2171 - 2179

Austin, J., "Revised Comprehensive Reaction Mechanism for CO/H2/O2 kinetics." (1999), World Wide Web Homepage through http://web.galcit.caltech.edu/EDL/mechanisms/library/library.html

Axworthy, A. E., V. H. Dayan and G. B. Marin, "Reactions of Fuel-Nitrogen Compounds under Conditions of Inert Pyrolysis." Fuel 57: 29-35 (1978).

Badger, G. M., J. K. Donnelly and T. M. Spotswood, "The Formation of Aromatic Hydrocarbons at High Temperatures XXIII The Pyrolysis of Anthracene." Australian Journal of Chemistry. 17: 1147-1156 (1964).

Bassilakis, R., Y. Zhao, P. R. Solomon and M. A. Serio, “Sulfur and Nitrogen Evolution in the Argonne Coals: Experiment and Modeling.” Energy & Fuels 7: 710-720 (1993).

Baxter, L. L., R. E. Mitchell, T. H. Fletcher and R. H. Hurt, “Nitrogen Release during Coal Combustion.” Energy & Fuels 10: 188-196 (1996).

Baxter, L., Mitchell, R., Fletcher, T. and Hurt, R. Energy & Fuels 1996, 10, 188 -196

Bilbao, R., Alzueta, M.U., Millera, A. and Duarte, M. Ind. Eng. Chem. Res. 1995, 34, 4540 - 4548

Bird, R., Stewart, W. and Lightfoot, E. Transport Phenomena. John Wiley & Sons: New York 1960, 780 p

Bittner, J. D. and J. B. Howard, "Composition Profiles and Reaction Mechanisms in a Near-Sooting Premixed Benzene/Oxygen/Argon Flames." 18th Symposium (International) on Combustion 18: 1105-1116 (1981).

Blair, D. W., J. O. L. Wendt and W. Bartok, "Evolution of Nitrogen and Other Species during Controlled Pyrolysis of Coal." 16th Symposium (International) on Combustion 16: 475-489 (1976).

Breton, H., "Multi-Component Analysis Using Established Techniques." Proceedings of SPIE 1717: 76-91 (1992).

Brill, T. B., P. J. Brush, K. J. James, J. E. Shepherd and K. J. Pfeiffer, “T-Jump/FTIR Spectroscopy: A New Entry into the Rapid, Isothermal Pyrolysis Chemistry of Solids and Liquids.” Applied Spectroscopy 46: 900-911 (1992).

Brown, A. L. and T. H. Fletcher, “Modeling Soot Derived from Pulverized Coal.” Energy & Fuels 12: 745-757 (1998).

Brown, A.L.; Fletcher, T.H. *Energy Fuels*, 12, 745-757 (1998).

Cai, H. Y., A. J. Guell, D. R. Dugwell and R. Kandiyoti, “Heteroatom Distribution in Pyrolysis Products as a Function of Heating Rate and Pressure.” Fuel 72: 321-327 (1992).

Carabineiro, S., Silva, I. and Fernandes, F. Proceedings ICCS '97. Ed. by Ziegler et al. 1997, 1103

Chambrion, P., Kyotani, T. and Tomita, A. Energy & Fuels 1998, 12, 416

Chambrion, P., Kyotani, T. and Tomita, A. Twenty-seventh Symposium (International) on Combustion/ The Combustion Institute 1998, 3053

Chambrion, P., Orikasa, H., Kyotani, T. and Tomita, A. Prepr. -Am. Chem. Soc., Div. Fuel Chem. 1996, 41 (1), 170

Chambrion, P., Orikasa, H., Suzuki, T., Kyotani, T. and Tomita, A. Fuel 1997, 76, 493

Chambrion, P., Suzuki, T., Zhang, Z., Kyotani, T. and Tomita, A. Energy & Fuels 1997, 11, 681

Chan, L., Sarofim, A. and Béer, J. Combustion and Flame 1983, 52, 37

Chen, J. C. and S. Niksa, "Coal Devolatilization during Rapid Transient Heating 1. Primary Devolatilization." Energy & Fuels 6: 254-264 (1992a).

Chen, J. C. and S. Niksa, "Suppressed Nitrogen Evolution from Coal-Derived Soot and Low-Volatility Coal Chars." 24th Symposium (International) on Combustion 24: 1269-1276 (1992b).

Chen, J. C., "Effects of Secondary Reactions on Product Distribution and Nitrogen Evolution from Rapid Coal Pyrolysis", Ph. D. Dissertation, Mechanical Engineering Department, Stanford University, Stanford, CA (1991).

Chen, N. and Yang, R. T. J. Phys. Chem. A. 1998, 102, 6348 - 6356

Chen, S. L., J. A. Cole, J.C. Kramlich, J. M. McCarthy and D. W. Pershing, "Advanced NOx Reduction Process using -NH and -CN Compounds in Conjunction with Staged Air Addition." 22nd Symposium (International) on Combustion 22: 1135-1145 (1988).

Chu, Xi. And Schmidt, L.D. Ind. Eng. Chem. Res. 1993, 32, 1359

Ciambelli, P., Palma, V., Russo, P. and Vaccaro, S. Mediterranean Combustion Symposium, Antalya - Turkey 1999

Cliff, D. I., K. R. Doolan, J. C. Mackie and R. J. Tyler, "Products from Rapid Heating of a Brown Coal in the Temperature range 400-2300oC." Fuel 63: 394-400 (1984).

Coda, B., Kluger, F., Förtsch, D., Spliethoff, H., Hein, K.R.G. and Tognotti, L. Energy & Fuels 1998, 12, 1322-1327

Coltrin, M.E., Kee, R.J. and Rupley, F.M., "Surface Chemkin (Version 3.7): A Fortran Package for Analyzing Heterogeneous Chemical Kinetics at a Solid-Surface-Gas-Phase Interface", Sandia National Laboratories CA, Report No. SAND90-8003, 1990

Compton, S. V. and D. A. C. Compton, Practical Sampling Techniques for Infrared Analysis, Chapter 8: Quantitative Analysis-Avoiding Common Pitfalls. CRC Press, Ann Arbor, MI (1993).

de Soete, G. G. Proceedings of the Fifth International Workshop on Nitrous Oxide Emissions; NIRE/IFP/EPA/SCEJ: Tsukuba 1992, P Kl-4-1

de Soete, G. G., Croiset, E. and Richard, J.R. Combustion and Flame 1999, 117, 140

de Soete, G. Proceedings of the Combustion Institute 1975, 18, 1093

de Soete, G. Proceedings of the Combustion Institute 1990, 23, 1257

Domino, S.P and Smith, P.J. Proceedings of the ASME Heat Transfer Division HTD-Vol. 364-2 1999, 2, 395-403

Doolan, K. R., J. C. Mackie, R. J. Tyler, "Coal Flash Pyrolysis: Secondary Cracking of Tar Vapours in the Range 870-2000 K." Fuel 66: 572-578 (1986).

Duncan, J.B. and Torr, H.L. AIChE Journal 1962, 8, 38-41

Eddings, E., Smith, P., Heap, M., Pershing, D. and Sarofim, A. Coal-Blending and Switching of Low-Sulfur Western Coals, ASME 1994, 169

Eddings, E.G., Djurisic, Z.M., Okerlund, R., Wachenhausen, M., and D.W. Pershing, "Combustion 2000 Low Emission Boiler System (LEBS)," Final DOE Technical Report to D.B. Riley, Inc., Project Number DE-AC22-92PC92158, June, 2000.

Epple, B., Schneider, R., Schnell, U. and Hein, K. Combust. Sci. and Tech. 1995, 108, 383

Evans, A.B., Pont, J.N., Moyeda, D.K., England, G.C., Moyeda, D.K. and England, G.C. Western State Section/ The Combustion Institute 1993 Srping Meeting University of Utah 1993, Paper 93S-33

Fenimore, C. P., "Studies of Fuel-Nitrogen Species in Rich Flame Gases." 17th Symposium (International) on Combustion, 17: 661-670 (1979).

Field, M., Gill, D., Morgan, B. and Hawksley, Combustion of Pulverized Fuel, Brit. Coal Util. Res. Assoc. Surrey, 1967, 413 p.

Fiveland, W. and Wessel, R. Journal of the Institute of Energy 1991, 64, 41

Fletcher, T. H. and Hardesty, D. R., Compilation of Sandia Coal Devolatilization Data: Milestone Report Sandia Technical Report, (1992a).

Fletcher, T.H.;Kerstein, A.R.;Pugmire, R.J.;Solum, M.S.;Grant, D.M. *Energy Fuels*, 6, 414-431 (1992b).

Fletcher, T. H., A. R. Kerstein, R. J. Pugmire, M. S. Solum and D. M. Grant, "A Chemical Model of Coal Devolatilization 3. Direct Use of 13C NMR Data to Predict Effects of Coal Type." Energy & Fuels 6: 414 (1992c).

Fletcher, T. H., J. Ma, J. R. Rigby, A. L. Brown and B. W. Webb, “Soot in Coal Combustion Systems.” Progress in Energy and Combustion Science 23: 283-301 (1997).

Fletcher, T. H., M. S. Solum, D. M. Grant, S. Critchfield and R. J. Pugmire, “Solid State 13C and 1H NMR Studies of the Evolution of the Chemical Structures of Coal Char and Tar during Devolatilization.” 23rd Symposium (International) on Combustion 23: 1231-1237 (1990).

Folger, H.S., Elements of Chemical Reaction Engineering 3rd Ed., Prentice Hall International, New York 2000, 967 p

Frank-Kamenetskii, D.A., Diffusion and Heat Transfer in Chemical Kinetics, 2nd Ed. Plenum Press, New York, 1969, 574 p.

Freihaut, J. D. and D. J. Seery, “An Investigation of Yields and Characteristics of Tars Released During the Thermal Decomposition of Coal.” ACS Division of Fuel Chemistry, Preprints 26(2): 133-149 (1981).

Freihaut, J. D., W. M. Proscia and D. J. Seery, “Chemical Characteristics of Tars Produced in a Novel Low-Severity, Entrained-Flow Reactor.” Energy & Fuels 3: 692-703 (1989).

Freihaut, J. D., W. M. Proscia and J. C. Mackie, “Chemical and Thermochemical Properties of Heavy Molecular Weight Hydrocarbons Evolved During Rapid Heating of Coal of Varying Rank Characteristics.” Comb ustion Science and Technology 93: 323-347 (1993).

Frenklach, M. and H. Wang, "Detailed Modeling of Soot Particle Nucleation and Growth." 23rd Symposium (International) on Combustion 23: 1559-1566 (1990).

Frenklach, M., D. W. Clary, W. C. Gardiner and S. E. Stein, "Effect of Fuel Structure on Pathways to Soot." 21st Symposium (International) on Combustion 21: 1067-1076 (1986).

Friebel, J. and R. F. W. Kopsel, “The Fate of Nitrogen during Pyrolysis of German Low Rank Coals- A Parameter Study.” Fuel 78: 923-932 (1999).

Furusawa, T., Kuni, D., Oruma., A. and Yamada, N. Int. Chem. Eng. 1980, 20, 239

Furusawa, T., Tsunoda, M., Tsujimura, M. and Adschiri, T. Fuel 1985, 64, 1306

García-García, A., Illán-Gómez, M. J., Linares-Solano, A. and Salinas-Martínez de Lecea, C. Energy & Fuels 1999, 13, 499

García-García, A., Illán-Gómez, M. J., Linares-Solano, A. and Salinas-Martínez de Lecea, C. Fuel 1997, 76, 499

Genetti, D. and Fletcher, T.H. Energy & Fuels 1999, 13, 1082

Genetti, D. B., "An Advanced Model of Coal Devolatilization Based on Chemical Structure", M. S. Thesis, Department of Chemical Engineering, Brigham Young University, Provo, UT (1999).

Genetti, D., "An Advanced Model of Coal Devolatilization Based on Chemical Structure," M.S. Thesis, Brigham Young University, Provo, Utah (1999).

Genetti, D.B., "An Advanced Model of Coal Devolatilization Based on Chemical Structure", MSc. Thesis, Brigham Youhg University, 1999

Gibbins, J. and Williamson, J. Proc. Instn. Mech. Engrs. 1998, 212 A, 13

Glarborg, P. and J. A. Miller, "Mechanism and Modeling of Hydrogen Cyanide Oxidation in A Flow Reactor." Combustion and Flame 99: 475-483 (1994).

Glarborg, P., Alzueta, M.U., Dam-Johansen, K. and Miller, J.A. Combustion and Flame 1998, 115, 1-27

Glassman, I., "Soot Formation in Combustion Processes." 22nd Symposium (International) on Combustion 22: 295-311 (1988).

Glassman, I., Chapter 8: Environmental Combustion Considerations, Combustion, 3rd edition. Academic Press, Inc., New York (2000).

Goel, S., Lee, C.H., Longwell, J.P. and Sarofim, A.F. Energy & Fuels 1996, 10, 1091-1098

Goel, S., Molina, A. and Sarofim, A.F. Energy & Fuels 2001, Submitted for publication

Goel, S., Morihara, A., Tullin, C. and Sarofim, A. Proceedings of the Combustion Institute 1994, 25, 1051-1059

Goel, S., Sarofim, A. and Lu, J. Proceedings of the Combustion Institute 1996, 26, 3127

Goel, S., Zhang, B. and Sarofim, A. Combustion and Flame 1996, 104, 213-217

Graham, K., "Submicron Ash froamtion and interaction with sulfur oxides during pulverized coal combustion", Ph.D. Thesis, Massachusetts Institute of Technology, 1991

Guo, F. and Hecker, W. Proceedings of the Combustion Institute 1998, 27, 3085 - 3092

Guo, F. and Hecker, W. Twenty-Sixth Symposium (International) on Combustion/ The Combustion Institute 1996, 2251

Hambly, E. M., "The Chemical Structure of Coal Tar and Char During Devolatilization", M. S. Thesis, Department of Chemical Engineering, Brigham Young University, Provo, UT (1998).

Hanst, P. L., QASoft User's Mannual. Anaheim, CA, Infrared Analysis, Inc. (1999a).

Hanst, P. L., QASOFT Version-32. Anaheim, CA, Infrared Analysis, Inc (1999b).

Haussmann, G. J. and C. H. Kruger, "Evolution and Reaction of Fuel Nitrogen During Rapid Coal Pyrolysis and Combustion." Presented at the Spring meeting of the Western State Section of The Combustion Institute, Livermore, CA. (1989).

Hayashi, J., K. Nakagawa, K. Kusakabe and S. Morooka, “Change in Molecular Structure of Flash Pyrolysis Tar by Secondary Reaction in a Fluidized Bed Reactor.” Fuel Processing Technology 30: 237-248 (1992).

Haynes, B. S., Chapter 5: Soot and Hydrocarbons in Combustion, Fossil Fuel Combustion. Editor: W. Bartok and A. F. Sarofim, John Wiley & Sons, Inc., New York. (1991).

Haynes, B.S. Combustion and Flame 2001, 126, 1421-1432

Heitor, M.V. and Moreira, A.L.N. Prog. Energy Combust. Sci. 1993, 19, 259

Homann, K. H. and H. G. Wagner, "Some New Aspects of The Mechanism of Carbon Formation in Premixed Flames." 11th Symposium (International) on Combustion 11: 371-379 (1967).

Homann, K. H., "Formation of Large Molecules, Particulates and Ions in Premixed Hydrocarbon Flames; Progress and Unresolved Questions." 20th Symposium (International) on Combustion 20: 857-870 (1984).

Hurt, R. and Mitchell, R. Proceedings of the Combustion Institute 1992, 24, 1233

Hurt, R. Energy & Fuels 1993, 7, 721

Hurt, R.H. and Calo, J.M. Combustion and Flame 2001, 125, 1138-1149

Illán-Gómez, M., Linares-Solano, A., Radovic, L. and Salinas-Martínez de Lecea, C. Energy & Fuels 1995, 9, 104

Illán-Gómez, M., Linares-Solano, A., Radovic, L. and Salinas-Martínez de Lecea, C. Energy & Fuels 1995, 9, 112

Illán-Gómez, M., Linares-Solano, A., Radovic, L. and Salinas-Martínez de Lecea, C. Energy & Fuels 1995, 9, 97

Illán-Gómez, M., Linares-Solano, A., Salinas-Martínez de Lecea, C. and Calo. J. Energy & Fuels 1993, 7, 146

Illán-Gómez, M.J., Linares-Solano, A., Radovic, L. R. and Salinas-Martínez de Lecea, C. Energy & Fuels 1996, 10, 158

Illán-Gómez, M.J., Salinas-Martínez de Lecea, C., Linares-Solano, A. and Radovic, L. R. Energy & Fuels 1998, 12, 1256

Illán-Gómez, M.J., Salinas-Martínez de Lecea, C., Linares-Solano, A., Philips, J. and Radovic, L. R. Prepr. -Am. Chem. Soc., Div. Fuel Chem. 1996, 41, 174

Incropera, F.P. and DeWitt, D.P. John Wiley & Sons, New York 1996, 886 p.

Ingle, J. D., Jr. and S. R. Crouch, Spectrochemical Analysis Prentice Hall, New Jersey, (1988).

Jang, D. and Acharya, S. Journal of Energy Resources Technology 1991, 113, 117

Jensen, L.S., "NOx from cement production - Reduction by Primary Measures", Ph.D. Thesis, Technical University of Denmark. 1999

Jensen, L.S., Jannerup, H.E., Glarborg, P., Jensen, A. and Dam-Johansen, K. Proc. Combust. Inst. 2000, 28, 2271 - 2278

Jones, J. M., Zhu, Q., Thomas, K.M. Carbon 1999, 37, 1123

Jones, J.M., Harding, A.W., Brown, S.D. and Thomas, K.M. Carbon 1995, 33, 833

Jones, J.M., Patterson, P.M., Pourkashanian, M. ans Williams, A. Carbon 1999, 37, 1545-1552

Kallonen, R., "Smoke Gas Analysis by FTIR Method, Preliminary Investigation." Journal of Fire Science 8: 343-360 (1990).

Kambara, S., T. Takarada, M. Toyoshima and K. Kato, "Relations Between Functional Forms of Coal Nitrogen and NOx Emissions from Pulverized Coal Combustion." Fuel 74: 1247-1253 (1995).

Kambara, S., Takarada, T., Yamamoto, Y. and Kato, K. Energy & Fuels 1993, 7, 1013

Kassman, H., M. Abul-Milh and L. E. Amand, "Measurement of NH3 and HCN Concentrations in a CFB Boiler, A Comparison Between A Conventional Absorption and FTIR Technique." 13th International Conference on Fluidized Bed Combustion 2: 1447-1454 (1995).

Kee, R. J., J. F. Grcar, M. D. Smooke and J. A. Miller, "A Fortran Program for Modeling Steady Laminar One-Dimensional Premixed Flame", Sandia Report SAND85-8240 (1985).

Kee, R. J., Rupley, F. M., Miller, J. A., Coltrin, M. E., Grcar, J. F., Meeks, E., Moffat, H. K., Lutz, A. E., Dixon-Lewis, G., Smooke, M. D., Warnatz, J., Evans, G. H., Larson, R. S., Mitchell, R. E., Petzold, L. R., Reynolds, W. C., Caracotsios, M., Stewart, W. E. and Glarborg, P., " CHEMKIN Collection", Release 3.5, Reaction Design, Inc., San Diego, CA 1999

Kee, R.J., Dixon-Lewis, G., Warnatz, J., Coltrim, M.E., Miller, J.A., "A Fortran Computer Code Package for The Evaluation of Gas-Phase, Multicomponent Transport Properties", Sandia National Laboratories CA, Report No. SAND 86-8246, 1986

Kee, R.J., Rupley, F.M. and Miller, J.A., "CHEMKIN II: A Fortran Chemical Kinetics Package for the Analysis of Gas-Phase Chemical Kinetics", Sandia National Laboratories CA, Report No. SAND 89-8009, 1989

Kelemen, S. R., M. L. Gorbaty, P. J. Kwiatek, T. H. Fletcher, M. Watt, M. S. Solum and R. J. Pugmire, "Nitrogen Transformations in Coal During Pyrolysis." Energy & Fuels 12: 159-173 (1998).

Kelemen, S. R., M. L. Gorbaty, S. N. Vaughn and P. J. Kwiatek, "Quantification of Nitrogen Forms in Argonne Premium Coals." ACS Division of Fuel Chemistry Preprint 384-392 (1993).

Kelemen, S. R., M. L. Gorbaty, S. N. Vaughn and P. J. Kwiatek, "Quantification of Nitrogen Forms in Argonne Premium Coals." Energy & Fuels 8: 896-906 (1994).

Kelemen, S., Gorbaty, M., Kwiatek,P., Fletcher, T., Watt., M., Solum, M. and Pugmire, R. Energy & Fuels 1998, 12, 159

Kelemen, S.R., Freund, H., Gorbaty, M.L. and Kwiatek, P.J. Energy & Fuels 1999, 13, 529

Kelemen, S.R., Gorbatay, M.L., and Kwistek, P.J. Energy & Fuels 1994, 8, 896

Kilpinen, P., Glarborg, P. and Hupa, M. 31, 1477-1490, (1992) Industrial & Engineering Chemistry Research 1992, 31, 1477 - 1490

Kilpinen, P., Kallio, S., Konttinen, J. and Forssen, M. Fuel Chemistry Division Preprints 2001, 46, 167 - 169

Ko, G. H., D. M. Sanchez, W. A. Peters and J. B. Howard, "Correlations for Effects of Coal Type and Pressure on Tar Yields from Rapid Devolatilization." 22nd Symposium (International) on Combustion 22: 115-124 (1988).

Kobayashi, H., Howard, J.B. and Sarofim, A.F. Proceedings of the Combustion Institute 1976, 411-425

Kramlich, J.C., Cole, J.A., McCarthy, J.M., Lanier, W.S. and McSorley, J.A. Combustion and Flame 1989, 77, 375-384

Krammer, G.F. and Sarofim, A.F., Combustion and Flame 97:118-124, 1994

Kremer, H. and W. Schulz, "Influence of Temperature on the Formation of NOx during Pulverized Coal Combustion." 21st Symposium (International) on Combustion 21: 1217-1222 (1986).

Kyotani, T. and Tomita, A. The Journal of Physical Chemistry B 1999, 103, 3434

Laskin, A. and A. Lifshitz, "Isomerization and Decomposition of Indole. Experimental Results and Kinetic Modeling." Journal of Physical Chemsitry 101(A): 7787-7801 (1997).

Laskin, A. and A. Lifshitz, "Thermal Decomposition of Quinoline and Isoquinoline. The Role of 1-Indene Imine Radical." Journal of Physical Chemistry 102(A): 928-946 (1998).

Ledesma, E. B., "Investigation of the Rates of Evolution and Distribution of Products During the Pyrolysis and Combustion of Coal Volatiles," Ph. D. Dissertation, Department of Physical and Theoretical Chemistry, University of Sydney, Sydney, Australia (1998).

Ledesma, E. B., C. Z. Li, P. F. Nelson and J. C. Mackie, "Release of HCN, NH3, and HNCO from the Thermal Gas-Phase Cracking of Coal Pyrolysis Tars." Energy & Fuels 12: 536-541 (1998).

Lee, J.C., Yetter, R.A. and Dryer, F.L. Combustion and Flame 1995, 101, 387-398

Leppalahti, J. and T. Koljonen, "Nitrogen Evolution from Coal, Peat and Wood during Gasification: Literature Review." Fuel Processing Technology 43: 1-45 (1995).

Leppalahti, J., "Formation of NH3 and HCN in slow-heating-rate Inert Pyrolysis of Peat, Coal and Bark." Fuel 74: 1363-1368 (1995).

Levy, J., Chan, A., Sarofim, A., and Beér, J. Eighteenth Symposium (International) on Combustion/The Combustion Institute 1981, 111

Li, C. Z., A. N. Buckley and P. F. Nelson, "Effects of Temperature and Molecular Mass on the Nitrogen Functionality of Tars Produced under High Heating Rate Conditions." Fuel 77: 157-164 (1997).

Li, C. Z., P. F. Nelson, E. B. Ledesma and J. C. Mackie, “An Experimental Study of the Release of Nitrogen from Coals Pyrolyzed in Fluidized-Bed Reactors.” 26th Symposium (International) on Combustion 26: 3205-3211 (1996).

Li, Y.H., Lu, G.Q. and Rudolp, V. Chemical Engineering Science 1998, 53, 1

Lizzio, A. A., DeBarr, J.A. and Kruse, C.W. Energy & Fuels 1997, 11, 250

Lockwood, F. and Romo-Millares, C. Journal of the Institute of Energy 1992, 65, 144

Lutz, A.E., Kee, R.J. and Miller, J.A. “SENKIN: A Fortran Program for Predicting Homogeneous Phase Chemical Kinetics” Sandia National Laboratories Report No. SAND87-8248, Livermore, CA, 1988

Ma, J., "Soot Formation From Coal Pyrolysis," Ph. D. Dissertation, Department of Chemical Engineering, Brigham Young University, Provo, UT (1996).

Mackie, J. C., M. B. Colket and P. Nelson, “Shock Tube Pyrolysis of Pyridine.” Journal of Physical Chemistry 94: 4009-4106 (1990).

Mackie, J. C., M. B. Colket, P. Nelson and M. Esler, “Shock Tube Pyrolysis of Pyrrole and Kinetic Modeling.” International Journal of Chemical Kinetics 23: 733-760 (1991).

Madley, D.G. and Strickland-Constable, R.F. Trans. Faraday Soc. 1953, 49, 1312

Man, C. K., N. V. Russell, J. R. Gibbins and J. Williamson, "A Kinetic Study of Secondary Volatile Nitrogen Release from Coal." ACS Division of Fuel Chemistry 43(3): 1139-1142 (1998).

McBride, B.J. and Gordon, S. “Computer Program for Calculation of Complex Chemical Equilibrium Compositions and Applications ”, NASA Reference Publication 1311, 1996

McLean, W. J., D. R. Hardesty and J. H. Phol, "Direct Observations of Devolatilizing Pulverized Coal Particles in a Combustion Environment." 18th Symposium (International) on Combustion 18: 1239-1248 (1981).

Miettinen, H. Energy & Fuels 1996, 10, 197-202

Miettinen, H., Paulsson, M. and Strömberg, D. Energy & Fuels 1995, 9, 10-19

Miettinen. H. and Abul-Milh, M. Energy & Fuels 1996, 10, 421-424

Miller, J. A. and C. T. Bowman, “Mechanism and Modeling of Nitrogen Chemistry in Combustion.” Progress in Energy and Combustion Science 15: 287-338 (1989).

Miller, J. A. and P. Glarborg, Springer Series Physical Chemistry 61: 318 (1996).

Miller, J. and Bowman, C. Prog. Energy Combust. Sci. 1989, 15, 287

Mithchell, R.A., Kee, R.J., Glarborg, P. and Coltrin, M.E. Proceedings of the Combustion Institute 1990, 23, 1169-116

Molina, A., Eddings, E.G., Pershing, D.W. and Sarofim, A.F. Proceedings of the Joint Meeting of the US Sections of the Combustion Institute 2001, 2, Paper 210

Molina, A., Eddings, E.G., Pershing, D.W. and Sarofim, A.F. Prog. Energy Combust. Sci. 2000, 26, 507 - 531

Molina, A., Ph.D. Dissertation, Dept. of Chemical and Fuels Engineering, University of Utah, 2002.

Molina, A., Sarofim, A.F., Ren, W., Lu, J., Yue, G., Beér, J.M. and Haynes, B.S. Proceedings of the Mediterranean Combustion Symposium 2002, 2, In press

Montoya, A and Truong, T.H. Submitted for publication, 2001

Montoya, A., Mondragón, F. and Truong, T.N. Fuel Chemistry Division Preprints 2001, 46, 217

Montoya, A., Truong, T.N. and Sarofim, A.F. J. Phys. Chem. A 2000, 104, 8409

Moulijn, J. A. and Kapteijn, F. Carbon 1995, 33, 1155 - 1165

Mullins, O. C., S. Mitra-Kirtley, J. V. Elp and S. P. Cramer, "Molecular Structure of Nitrogen in Coal from XANES Spectroscopy." Applied Spectroscopy 47: 1268-1275 (1993).

Muris, S. and Haynes B.S. To be published

Nelson, P. F. and R. J. Tyler, "Formation of Light Gases and Aromatic Species During the Rapid Pyrolysis of Coal." 21st Symposium (International) on Combustion 21: 427-435 (1986).

Nelson, P. F., A. N. Buchley and M. D. Kelly, "Functional Forms of Nitrogen in Coals and the Release of Coal Nitrogen as NOx Precursors (HCN and NH3)." 24th Symposium (International) on Combustion 24: 1259-1267 (1992).

Nelson, P. F., I. W. Smith, R. J. Tyler and J. C. Mackie, "Pyrolysis of Coal at High Temperatures." Energy & Fuels 2: 391-400 (1988).

Nelson, P. F., M. D. Kelly and M. J. Wornat, "Conversion of Fuel Nitrogen in Coal Volatiles to NOx Precursors Under Rapid Heating Conditions." Fuel 70: 403-407 (1990).

Nenniger, R. D., "Aerosols Produced From Coal Pyrolysis." Ph. D. Dissertation, Department of Chemical Engineering, MIT, Cambridge, MA (1986).

Niksa, S. and S. Cho, “Conversion of Fuel-Nitrogen in the Primary Zones of Pulverized Coal Flames.” Energy & Fuels 10: 463-473 (1996).

Niksa, S., "Predicting the Evolution of Fuel Nitrogen from Various Coals." 25th Symposium (International) on Combustion 25: 537-544 (1994).

Niksa, S., “FLASHCHAIN Theory for Rapid Coal Devolatilization Kinetics. 6. Predicting the Evolution of Fuel Nitrogen from Various Coals.” Energy & Fuels 9: 467-478 (1995).

Niksa, S., and Kerstein, A.R. Energy & Fuels 1991, 5, 647-665

Noda, K., Chambrion, P., Kyotani, T. and Tomita, A. Energy & Fuels 1999, 13, 941

Orikasa, H., Suzuki, T., Kyotani, T., Tomita, A. and Martin, R. 22nd Biennal International Conference on Carbon, San Diego 1995, 626

Peck, R. E., K. C. Midkiff and R. A. Altenkirch, "The Evolution of Nitrogen from Pulverized Subbituminous Coal Burnt in a One-Dimensional Flames." 20th Symposium (International) on Combustion 20: 1373-1380 (1984).

Pels, J. R., Kapeteijn, F., Moulijn, J.A., Zhu, Q. and Thomas, K.M. Carbon 1995, 33, 1641

Pels, J., Wójtowicz, M. and Moulijn, J. Fuel 1993, 72, 373

Perry, S. T., "A Global Free-Radical Mechanism for Nitrogen Release during Coal Devolatilization Based on Chemical Structure.", Ph. D. Dissertation, Department of Chemical Engineering, Brigham Young University, Provo, UT (1999).

Perry, S.T., Fletcher, T.H., Solum, M.S. and Pugmire, R.J. Energy & Fuels 2000, 14, 1094 - 1102

Pershing, D. W. and J. O. Wendt, "Pulverized Coal Combustion: The Influence of Flame Temperature and Coal Composition on Thermal and Fuel NOx." 16th Symposium (International) on Combustion 16: 389-399 (1977).

Phong-Anant, D., L. J. Wibberley and T. F. Wall, “Nitrogen Oxide Formation from Australian Coals.” Combustion and Flame 62: 21-30 (1985).

Pohl, J. and Sarofim, A. Proceedings of the Combustion Institute 1976, 16, 491-501

Pohl, J. H. and A. F. Sarofim, "Devolatilization and Oxidation of Coal Nitrogen.", 16th Symposium (International) on Combustion 16: 491-501 (1977).

Pugmire, R. J., M. S. Solum, D. M. Grant, S. Critchfield and T. H. Fletcher, “Structural Evolution of Matched Tar-Char Pairs in Rapid Pyrolysis Experiments.” Fuel 70: 414-423 (1990).

Pugmire, R. J., Personal Communication, (1999).

Rees, D. P., L. D. Smoot and P. O. Hedman, "Nitrogen Oxide Formation Inside A Laboratory Pulverized Coal Combustor." 18th Symposium (International) on Combustion 18: 1305-1311 (1981).

Ren, W., Lu, J., Yue, G., Beér, J.M, Molina, A. and Sarofim, A.F. CFB7: 7th International Conference on Circulating Fluidized Beds, Niagara Falls, Canada 2002, In Press

Rigby, J. R., "Experimentally Determined Optical Properties and Chemical Compositions of Coal-Derived Soot.", Ph. D. Dissertation, Department of Mechanical Engineering, Brigham Young University, Provo, UT (1996).

Rodriguez-Mirasol, J., Ooms, A., Pels, J., Kapteijn, F. and Moulijn, J. Combustion and Flame 1994, 99, 499

Rubel, A.M., Stewart, M.L. and Stencel, J.M. In: Reduction of Nitrogen Oxide Emissions, ACS Symposium Series 587. Ozkan, U.S., Agarwal, S. K. and Marcelin, G. Eds. American Chemical Society, Washington D.C. 1995, 208

Rudiger, H., U. Greul, H. Spliethoff and K. R. G. Hein, “Distribution of Fuel Nitrogen in Pyrolysis Products Used for Reburning.” Fuel 76: 201-205 (1997).

Sarofim, A.F., Pershing, D.W., Eddings, E.G. and Molina, A. Proceedings of the Mediterranean Combustion Symposium 1999, 1, 72 - 83

Satterfield, C.N., Heterogeneous Catalysis in Industrial Practice 2nd Ed. McGraw-Hill, Inc.1991, 554 p.

Satterfield, C.N., Mass Transfer in Heterogeneous Catalysis MIT PRESS, Massachusetts, 1970, 267 p.

Schafer, S. and B. Bonn “Hydrolysis of HCN as An Important Step in Nitrogen Oxide Formation in Fluidized Combustion. Part 1. Homogeneous Reactions.” Fuel 79: 1239-1246 (2000).

Schuler, J., Baumann, H. and Klein,J. 1987 International Conference on Coal Science, edited by J.A. Moulijn et al. 1987, 857

Seeker, W. R., G. S. Samuelsen, M. P. Heap and J. D. Trolinger, "The Thermal Decomposition of Pulverized Coal Particles.", 18th Symposium (International) on Combustion 18: 1213-1226 (1981).

Serio, M. A., W. A. Peters and J. B. Howard, “Kinetics of Vapor-Phase Secondary Reactions of Prompt Coal Pyrolysis Tars.” Ind. Eng. Chem. Res. 26: 1831-1838 (1987).

Shaddix, C.R. Joint US Sections/CI 2001, Paper 20

Shimizu, T., Sazawa, Y., Adshiri, T. and Furusawa, T. Fuel 1992, 71, 361

Sirdeshpande, A.R., “Incineration for Resource Recovery in a Regenerative Life-Support System: Flue Gas Treatment”, Ph.D. Thesis, University of Utah 1999

Smith, G.P., Golden, S.D., Frenklach, M., Moriarty, N.W., Eitener, B., Goldenberg, M., Bowman, C.T., Hanson, R.K., Song, S., Gardiner, W.C., Lissianski, V.V. and Qin, Z., “GRI-MECH 3.0”, http://www.me.berkeley.edu/gri_mech/

Smith, I. Fuel 1978, 57, 409

Smith, I.W. Proceedings of the Combustion Institute 1982, 1045

Smith, J., Hill, S. and Smoot, D. Proceedings of the Combustion Institute 1982, 1263

Smith, J.M., Chemical Engineering Kinetics 3rd Ed., Mc Graw Hill, Boston 1981, 676 p

Smith, K. L., L. D. Smoot, T. H. Fletcher and R. J. Pugmire, The Structure and Reaction Processes of Coal. Plenum Press, New York (1994).

Smith, K., Smoot, L. and Fletcher, T. In: "Fundamentals Of Coal Combustion, For Clean and Efficient Use" (Ed. Smoot, L.). Elsevier, Amserdam 1993, 131

Smith, P., Eddings, E., Heap, M., Pershing, D. and Sarofim, A. 1993 Joint Symposium on Stationary Combustion NOx Control, Miami Beach, FL, May. 24-27, 1993

Smith, R., Swinehart, J. and Lesnini, D. J. Phys. Chem. 1959, 63, 544

Smoot, D., Boardman, R., Brewter, B., Hill, S. and Foli, A. Energy & Fuels 1993, 7, 786

Smoot, L. D., Editor, Fundamentals of Coal Combustion for Clean and Efficient Use. Elsevier, New York (1993).

Solomon, P. R. and M. B. Colket, “Evolution of Fuel Nitrogen in Coal Devolatilization.” Fuel 57: 749-755 (1978).

Solomon, P. R., D. G. Hamblen, R. M. Carangelo, M. A. Serio and G. V. Deshpande, “General Model of Coal Devolatilization.” Energy & Fuels 2: 405-422 (1988).

Solomon, P. R., M. A. Serio and E. M. Suuberg, “Coal Pyrolysis: Experiments, Kinetic Rates and Mechanisms.” Progress in Energy and Combustion Science 18: 133-220 (1992).

Solomon, P. R., M. A. Serio, R. M. Carangelo and R. Bassilakis, "Analysis of the Argonne Premium Coal Samples by Thermogravimetirc Fourier Transform Infrared Spectroscopy." Energy & Fuels: 319-333 (1990).

Solomon, P.R., Hamblen, D.G., Carangelo, R.M., Serio, M.A. and Deshpande, G.V. Energy & Fuels 1988, 2, 405-422

Solum, M. S., A. Sarofim, R. J. Pugmire, T. H. Fletcher and H. Zhang, "C-13 NMR Analysis of Soot Produced from Model Compounds and A Coal." In Press (2000).

Solum, M. S., R. J. Pugmire and D. M. Grant, "13C Solid-State NMR of Argonne Premium Coals." Energy & Fuels 3: 187-193 (1999).

Song, Y., Beér, J. and Sarofim, A. Combustion Science and Technology 1981, 25, 237

Spinti, J. "An Experimental Study of the Fate of Char Nitrogen in Pulverized Coal Flames", Ph.D. Thesis, University of Utah 1997, ,

Stanczyk, K. Energy & Fuels 1999, 13, 82

Stanmore B. and Jung, K. Trans. IChemE. 1980, 58, 66

Stanmore B.R. Combustion and Flame 1991, 83, 221

Suuberg, E., Teng, H. and Aarna, I. Prepr. -Am. Chem. Soc., Div. Fuel Chem. 1996, 41 (1), 160

Suzuki, T., Kyotani, T. and Tomita, K. Ind. Eng. Chem. Res. 1994, 33, 2840

Takagi, H., T. Isoda, K. Kusakabe and S. Morooka, "Effects of Coal Structures on Denitrogenation during Flash Pyrolysis." Energy & Fuels 13: 934-940 (1999).

Taylor, R. and Krishna, R., Multicomponent Mass Transfer, John Wiley & sons, Inc. 1993, 579 p.

Teng, H. and Suuberg, E. Ind. Eng. Chem. Res. 1993, 32, 416

Teng, H. and Suuberg, E. J. Phys. Chem. 1993, 97, 478

Teng, H., Suuberg, E. and Calo, J. Energy & Fuels 1992, 6, 398

Teng. H., Lin, H. and Hsieh, Y. Ind. Eng. Chem. Res. 1997, 36, 523

Terentis, A., A. Doughty and J. C. Mackie, "Kinetics of Pyrolysis of A Coal Model Compound, 2-Picoline, the Nitrogen Heteroaromatic Analogue of Toluene. 1. Product Distributions." Journal of Physical Chemistry 96: 10334-10339 (1992).

Thomas, K. Fuel 1997, 76, 457

Tine, G., Gas Sampling and Chemical Analysis in Combustion Processes, Pergamon Press, New York, 1961, 94 p

Tognotti, L., Longwell, J. and Sarofim, A. Proceedings of the Combustion Institute 1990, 23, 1207

Tomita, A. Fuel Processing Technology 2001, 71, 53-70

Tullin, C., "Emissions of N2O and NO from Single Particles of Coal under Fluidising Bed Combustion Conditions", Ph.D. Thesis, University of Göteborg, 1995

Tullin, C., Goel, S., Morihara, A., Sarofim, A. and Beér, J.M. Energy & Fuels 1993, 7, 796-802

Tullin, C., Sarofim, A. and Beér, J.M. Journal of the Institute of Energy 1993, 66, 207-215

Tyler, R. J., "Flash Pyrolysis of Coals. Devolatilization of Bituminous Coals in a Small Fluidized-Bed Reactor." Fuel 59: 218-226 (1979).

Ubhayakar, S.K., Stickler, D.B, Von Rosenberg, C.W., and Gannon, R.E., "Rapid Devolatilization of Pulverized Coal in Hot Combustion Gases," *16th Symposium (International) on Combustion*, The Combustion Institute, Pittsburg, PA, p. 427, (1976).

Van der Lans, R. P., P. Glarborg and K. Dam-Johansen, "Influence of Process Parameters on Nitrogen Oxide Formation in Pulverized Coal Burners." Progress in Energy and Combustion Science 23: 349-377 (1997).

Veranth, J. M., T. H. Fletcher, D. W. Pershing and A. F. Sarofim, "Measurements of Soot and Char in Pulverized Coal Fly Ash.", Fuel 79: 1067-1075 (2000).

Veranth, J., *Fuel*, 79, 1067-1075 (2000).

Visona, S. and Stanmore, B. Combustion and Flame 1996, 106, 207

Visona, S.P. and Stanmore, B.R. Chemical Engineering Science 1998, 53, 2013

Visona, S.P. and Stanmore, B.R. Combustion and Flame 1999, 118, 61 - 75

Walker, P.L. Jr., Taylor, R.L. and Ranish, J.M Journal of Physical Chemistry 1991, 29, 411 - 121

Watt, M., "The Chemical Structure of Coal During Devolatilization.", M. S. Thesis, Brigham Young University, Provo, UT (1996).

Watt, M., T. H. Fletcher, S. Bai, M. S. Solum and R. J. Pugmire, "Chemical Structure of Coal Tar during Devolatilization.", 26th Symposium (International) on Combustion 26: 3153-3160 (1996).

Wen, C.Y. and Fan, L.T. Models for Flow Systems and Chemical Reactors, Marcel Dekker, Inc. New York, 1975, 570 p

Wendt, J. and Schulze, O. AIChE Journal 1976, 22, 102

Wheeler, A. Advan. Catalysis 1951, III, 249

White, J. U., “Long Optical Paths of Large Aperture.” J. Opt. Soc. Amer. 32: 285-289 (1942).

Williams, A., Pourkashanian, M., Jones, J.M and Rowlands, L. Journal of the Institute of Energy 1997, 70, 102-113

Winter, F., Löffler, G., Wartha, C., Hofbauer, H., Preto, F. and Anthony, E. The Canadian Journal of Chemical Engineering 1999, 77, 275

Winter, F., Warth, C., Loffler, G. and Höfbauer, H. Proceedings of the Combustion Institute 1996, 26, 3325-3334

Wójtowicz, M.A., Pels, J.R. and Moulijn, J.A. Fuel 1995, 74, 507

Wójtowicz, M.A., Pels, J.R. and Moulijn, J.A. Fuel Processing Technology 1993, 34, 1 - 71

Wornat, M. J., A. F. Sarofim and J. P. Longwell, "Pyrolysis-Induced Changes in the Ring Number Composition of Polycyclic Aromatic Compounds form a High Volatile Bituminous Coal.", 22nd Symposium (International) on Combustion, 22: 135-143 (1988a).

Wornat, M. J., A. F. Sarofim, J. P. Longwell and A. L. Lafleur, “Effect of Pyrolysis Conditions on the Composition of Nitrogen-Containing Polycyclic Aromatic Compounds from a Bituminous Coal.” Energy & Fuels: 775-782 (1988b).

Xia, B., Phillips, J., Chen, C., Radovic, L,R., Silva, I,F. and Menéndez, J.A. Energy & Fuels 1999, 13, 903

Xu, H., Smoot, L.D. and Hill, S.C. Energy & Fuels 1999, 13, 411 - 420

Xu, M., Azevedo, J.L.T. and Carbalho, M.G. Fuel 2000, 79, 1611-1619

Xu, W. C. and A. Tomita, “Effect of Coal Type on the Flash Pyrolysis of Various Coals.” Fuel 66: 627-636 (1986).

Xu, W. C. and A. Tomita, “The Effects of Temperature and Residence Time on the Secondary Reactions of Volatiles from Coal Pyrolysis.” Fuel Processing Technology 21: 25-37 (1989).

Yamashita, H., Tomita, A., Yamada, H., Kyotani, T. and Radovic, L. Energy & Fuels 1993, 7, 85 - 89

Yetter, R. A., F. L. Dryer and H. Rabits, “A Comprehensive Reaction Mechanism for Carbon Monoxide/Hydrogen/Oxygen Kinetics.” Combustion Science and Technology 79: 97-128 (1991).

Yu, L. E., L. M. Hildemann and S. Niksa, “Characteristics of Nitrogen-Containing Aromatic Compounds in Coal Tars during Secondary Pyrolysis.” Fuel 78: 377-385 (1999).

Zhang, H. “Nitrogen Evolution and Soot Formation During Secondary Pyrolysis,” Ph.D. Dissertation, Brigham Young University, Provo, UT (2001).

Zhang, H. and T. H. Fletcher, "Nitrogen Transformations during Secondary Coal Pyrolysis", ACERC Annual Report 1999, ACERC, Brigham Young University, Provo, UT (1999).

Zhang, H., "Nitrogen Release during Secondary Coal Pyrolysis", ACERC Annual Report 1998, ACERC, Brigham Young University, Provo, UT (1998).

Zhonghua, Z., Lu, G.Q., Zhuang, Y. and Shen, D. Energy & Fuels 1999, 13, 763